Theoretical and observational aspects of physical processes in the field of compact objects

Kateřina Klimovičová

DISSERTATION

SLEZSKÁ UNIVERZITA V OPAVĚ
Filozoficko-přírodovědecká fakulta

Theoretical and observational aspects of physical processes in the field of compact objects

Kateřina Klimovičová

Supervisor: doc. RNDr. Gabriel Török, Ph.D.

DISSERTATION OPAVA 2021

Acknowledgments

At this point, I would like to thank my current supervisor Gabriel Török and my former supervisor Zdeněk Stuchlík. I also thank my colleagues, especially Pavel Bakala, Eva šrámková and Evariste Boj, for the endless help they gave me that cannot be listed here because of its large extent. Furthermore, I thank Stanislav Hledík, whose Latex class was used to compile this work. Last but not least, I would like to thank my parents and all my family. They supported me during my more than ten years of study at different university stages.

Poděkování

Na tomto místě bych především chtěla poděkovat svému aktuálnímu školiteli doc. RNDr. Gabrielu Törökovi, Ph.D. a předchozímu školiteli prof. RNDr. Zdeňku Stuchlíkovi CSc. Dále svým kolegům a kolegyním, speciálně RNDr. Pavlu Bakalovi, Ph.D., RNDr. Evě Šrámkové, Ph.D. a Mgr. Evaristu Bojovi, za pomoc nesčetněkrát poskytnutou a zde nevyjmenovatelnou. Také bych chtěla podekovat doc. RNDr. Stanislavu Hledíkovi, Ph.D. za poskytnutí Latexové třídy s jejímž využitím je tato práce sepsána. V neposlední řadě bych chtěla poděkovat svým rodičům a vůbec celé rodině, že mě podporovali během mého více jak desetiletého studia na různých univerzitních stupních.

Contents

„Cílem vzdělání a moudrosti je, aby člověk viděl před sebou jasnou cestu života, po ní opatrně vykračoval, pamatoval na minulost, znal přítomnost a předvídal budoucnost.“

Jan Ámos Komenský

Preface

In the form of a collection of annotated papers, the present dissertation represents an outcome of my study at the Institute of Physics of the Silesian University in Opava.

During my studies, I encountered several different tasks some of which I will attempt to summarize in the following lines. Despite their fragmented nature, they have one thing in common. They are all related to the effort of explaining the quasi-periodic oscillations (QPOs) present in the power density spectra of some low-mass X-ray binaries. The first chapter is devoted to a summary of the main features of this phenomenon.

The chapter that follows is dedicated to a description of different models of QPOs. These among others include several models that were proposed by our group in the papers (see references in the second chapter).

The third chapter presents an analysis of the QPO data from twelve different sources. For data fitting, we used models mentioned in Chapter 2. Some of the results presented in the third chapter were taken from the literature. The majority were, however, obtained solely for the purpose of this thesis.

The fourth chapter is devoted to simulations that should lead to a better understanding of predictions of some QPO models described in the second chapter.

The eight selected papers annotated within the above four chapters are listed below. Their full text is presented within Part II of this work. During my study, I collaborated on nine more papers that I will not describe here. In two of them, including one Letter to the editor, I was the main author. These are included within a separate list. Moreover, I was a co-author of about a dozen of proceeding papers.

The list of annotated papers[1]:

- TÖRÖK, G.; BAKALA, P.; ŠRÁMKOVÁ, E.; STUCHLÍK, Z.; URBANEC, M. & GOLUCHOVÁ, K.: Mass-Angular-momentum Relations Implied by Models of Twin Peak Quasi-periodic Oscillations. *The Astrophysical Journal*, **760**, 138, 2012, 1408.4220.

- STUCHLÍK, Z.; KOTRLOVÁ, A.; TÖRÖK, G. & GOLUCHOVÁ, K.: Test of the Resonant Switch Model by Fitting the Data of Twin-Peak HF QPOs in the Atoll Source 4U 1636-53. *Acta Astronomica*, **64**, 45–64, 2014.

[1] Most articles were published under my maiden surname Goluchová.

- BAKALA, P.; GOLUCHOVÁ, K.; TÖRÖK, G.; ŠRÁMKOVÁ, E.; ABRAMOWICZ, M. A.; VINCENT, F. H. & MAZUR, G. P.: Twin peak high-frequency quasi-periodic oscillations as a spectral imprint of dual oscillation modes of accretion tori. *Astronomy & Astrophysics*, **581**, A35, 2015, 1505.06673.

- STUCHLÍK, Z.; URBANEC, M.; KOTRLOVÁ, A.; TÖRÖK, G. & GOLUCHOVÁ, K.: Equations of State in the Hartle-Thorne Model of Neutron Stars Selecting Acceptable Variants of the Resonant Switch Model of Twin HF QPOs in the Atoll Source 4U 1636-53. *Acta Astronomica*, **65**, 169–195, 2015, 1507.00373.

- TÖRÖK, G.; GOLUCHOVÁ, K.; URBANEC, M.; ŠRÁMKOVÁ, E.; ADÁMEK, K.; URBANCOVÁ, G.; PECHÁČEK, T.; BAKALA, P.; STUCHLÍK, Z.; HORÁK, J. & JURYŠEK, J.: Constraining Models of Twin-Peak Quasi-periodic Oscillations with Realistic Neutron Star Equations of State. *The Astrophysical Journal*, **833**, 273, 2016, 1611.06087.

- TÖRÖK, G.; GOLUCHOVÁ, K.; HORÁK, J.; ŠRÁMKOVÁ, E.; URBANEC, M.; PECHÁČEK, T. & BAKALA, P.: Twin peak quasi-periodic oscillations as signature of oscillating cusp torus. *Monthly Notices of the Royal Astronomical Society: Letters*, **457**, L19–L23, 2016, 1512.03841.

- TÖRÖK, G.; GOLUCHOVÁ, K.; ŠRÁMKOVÁ, E.; HORÁK, J.; BAKALA, P. & URBANEC, M.: On one-parametric formula relating the frequencies of twin-peak quasi-periodic oscillations. *Monthly Notices of the Royal Astronomical Society*, **473**, L136–L140, 2018, 1710.10901.

- TÖRÖK, G.; KOTRLOVÁ, A.; MATUSZKOVÁ, M.; KLIMOVIČOVÁ, K.; LANČOVÁ, D.; URBANCOVÁ, G. & ŠRÁMKOVÁ, E.: Simple analytic formula relating the mass and spin of accreting compact objects to their rapid X-ray variability. *Submitted to The Astrophysical Journal*.

The list of other papers published in refereed journals:

- BAKALA, P.; TÖRÖK, G.; KARAS, V.; DOVČIAK, M.; WILDNER, M.; WZIENTEK, D.; ŠRÁMKOVÁ, E.; ABRAMOWICZ, M.; GOLUCHOVÁ, K.; MAZUR, G. P. & VINCENT, F. H.: Power density spectra of modes of orbital motion in strongly curved space-time: obtaining the observable signal. *Monthly Notices of the Royal Astronomical Society*, **439**, 1933–1939, 2014, 1401.4468.

- ŠRÁMKOVÁ, E.; TÖRÖK, G.; KOTRLOVÁ, A.; BAKALA, P.; ABRAMOWICZ, M. A.; STUCHLÍK, Z.; GOLUCHOVÁ, K. & KLUZNIAK, W.: Black hole spin inferred from 3:2 epicyclic resonance model of high-frequency quasi-periodic oscillations. *Astronomy & Astrophysics*, **578**, A90, 2015, 1505.02712.

- GOLUCHOVÁ, K.; KULCZYCKI, K.; VIEIRA, R. S. S.; STUCHLÍK, Z.; KLUZNIAK, W. &

ABRAMOWICZ, M.: Hořava's quantum gravity illustrated by embedding diagrams of the Kehagias-Sfetsos spacetimes. *General Relativity and Gravitation*, **47**, 132, 2015, 1511.01345.

- KOTRLOVÁ, A.; ŠRÁMKOVÁ, E.; TÖRÖK, G.; STUCHLÍK, Z. & GOLUCHOVÁ , K.: Super-spinning compact objects and models of high-frequency quasi-periodic oscillations observed in Galactic microquasars. II. Forced resonances. *Astronomy & Astrophysics*, **607**, A69, 2017, 1708.04300.

- KOTRLOVÁ, A.; ŠRÁMKOVÁ, E.; TÖRÖK, G.; GOLUCHOVÁ, K.; HORÁK, J. & STRAUB, O.: Non-geodesic corrections to mass-spin estimates for Galactic microquasars implied by quasiperiodic oscillation models. *Astronomische Nachrichten*, **340**, 112–115, 2019.

- GOLUCHOVÁ, K.; TÖRÖK, G.; ŠRÁMKOVÁ, E.; ABRAMOWICZ, M. A.; STUCHLÍK, Z. & HORÁK, J.: Mass of the active galactic nucleus black hole XMMUJ134736.6+173403. *Astronomy & Astrophysics*, **622**, L8, 2019, 1901.05419.

- TÖRÖK, G.; GOLUCHOVÁ, K.; ŠRÁMKOVÁ, E.; URBANEC, M. & STRAUB, O.: Time-scale of twin-peak quasi-periodic oscillations and mass of accreting neutron stars. *Monthly Notices of the Royal Astronomical Society*, **488**, 3896–3903, 2019, 1907.05174.

- BAKALA, P.; DE FALCO, V.; BATTISTA, E.; GOLUCHOVÁ, K.; LALČOVÁ, D.; FALANGA, M. & STELLA, L.: Three-dimensional general relativistic Poynting-Robertson effect. II. Radiation field from a rigidly rotating spherical source. *Physical Review D*, **100**, 104053, 2019, 1911.00540.

- KOTRLOVÁ, A.; ŠRÁMKOVÁ, E.; TÖRÖK, G.; GOLUCHOVÁ, K.; HORÁK, J.; STRAUB, O.; LALČOVÁ, D.; STUCHLÍK, Z. & ABRAMOWICZ, M. A.: Models of high-frequency quasi-periodic oscillations and black hole spin estimates in Galactic microquasars. *Astronomy & Astrophysics*, **643**, A31, 2020, 2008. 12963.

Part I

Overview

Chapter 1

Low mass X-ray binaries

At the beginning of the twentieth century, German physicist Wilhelm Conrad Röntgen, during his experiments, discovered a new type of radiation which he called X-rays. The medical benefits of the discovery are so crucial that there can be no doubt about its utility. We had to wait till the sixties of the last century for a more extensive use in astronomy. Then, the boom of balloons, rockets, and satellite technologies allowed people-created devices to be placed sufficiently long to a sufficient height for a systematic observation of the cosmos in the X-ray spectra.

In 1962, nearly sixty years ago, the rocket Aerobee 150 targeted its detectors to space to measure Sun's X-rays reflected by the Moon. The possibility of a significant amount of X-rays coming from places out of our Solar system was considered highly unlikely. However, X-rays reflected by the Moon were overshadowed by another source that was unknown at that time. This way, the first X-ray source from a place out of our Solar system was found in the constellation of the Scorpion [1]. A frantic search in a new spectral band has started. There were found thousands of surprisingly strong X-ray sources. Rockets, which could measure X-rays just for a short time, were replaced in the 1970s by satellites or more noble X-ray observatories placed on orbits high above the Earth's surface.

The X-ray sources can be expected in the universe. Even our Sun emits this type of radiation because of the high temperatures in the Solar corona. However, how to explain the existence of the sources which are a thousand times brighter than our Sun? One of the proposed mechanisms of X-ray generation assumes that the source is a binary system consisting of two components. One of them is some compact object (a neutron star or a black hole). The second one can be a main-sequence star, a red giant, or a white dwarf. The compact object's counterpart must have less mass than the compact object itself. Material from the companion component fills Roche's lobe and is moved. The material does not fall directly towards the compact object, but an accretion disk is created. Due to friction, the material loses its angular momentum and spirals down the compact object. The disk is heated to high temperatures and is bright in the X-ray spectrum. Such configurations were called Low Mass X-ray Binaries (LMXBs). It is not the only X-ray emission mechanism known today[1]. Nevertheless, about others, we will not talk

[1] For example, some X-ray sources are so-called high mass X-ray binaries. The emission principle is similar to that of LMXBs. However, the material of a more massive companion star does not overcome the critical closed equipotential, but the accretion takes place due to stellar wind.

here.

Unlike radiation in the visible field, X-ray radiation comes from areas close to a compact object where the gravitational field is strong enough. It is not possible to describe this area by Newtonian theory. It is necessary to use the results of General relativity[2]. By the discovery of LMXBs, astrophysicists received an excellent opportunity to verify the predictions of this theory.

In 1983, observatory EXOSAT (The European X-ray Observatory SATellite) was launched to orbit Earth. When analyzing the measured light curves of the source GX-5, it turned out that X-rays are changing with specific, time-varying frequencies on the order of dozens of hertz [2]. The effect was called the quasi-periodic oscillations. Until the year 1986, thanks to the satellite EXOSAT, QPOs were also detected in other LMXBs.

1.1. High frequency quasi-periodic oscillations

Parameters of the EXOSAT Observatory allowed measurements of radiation changes with frequencies in the order of dozens of hertz. Modern Rossi X-Ray Timing Explorer (RXTE), launched in 1995, can measure even faster variability in the order of hundreds of hertz. It turned out that incoming radiation varies with frequencies ranging from thousandths (10^{-3}) to hundreds (10^{2}) of hertz.

It seems that the most interesting are the so-called high frequency (HF) QPOs, typically in the range of hundreds of hertz. This is because the frequency of orbital motion in the vicinity of a compact object is just in the order of hundreds of hertz. It brought physicists to the idea that X-ray variabilities called HF QPOs are due to oscillatory motions of some structures in the vicinity of the compact object. If it is so, then analysis of this phenomenon can bring new information about strong gravity areas.

HF QPOs are observed in both kinds of LMXBs. The one which involves a neutron star or the one with a black hole. HF QPOs occurring in systems that we assume contain a black hole have many features common to neutron star systems. However, there is no unity in the community regarding whether or not the HF QPOs have the same origin in these two kinds of LMXBs. We will not talk about black hole systems here. Let us say that the HF QPOs were observed in four (or three) black hole LMXBs (see, e.g., [3]). A power spectrum of the two LMXBs which contain black hole candidates can be seen in Figure 1.1.

1.2. High frequency quasi-periodic oscillations in neutron star Low mass X-ray binaries

In the case of neutron star LMXBs, HF QPOs are characteristic by two sharp peaks in the power density spectra (PDS). The peaks can be detected simultaneously or each peak separately. In

[2] In this work, we assume that General relativity is the correct theory.

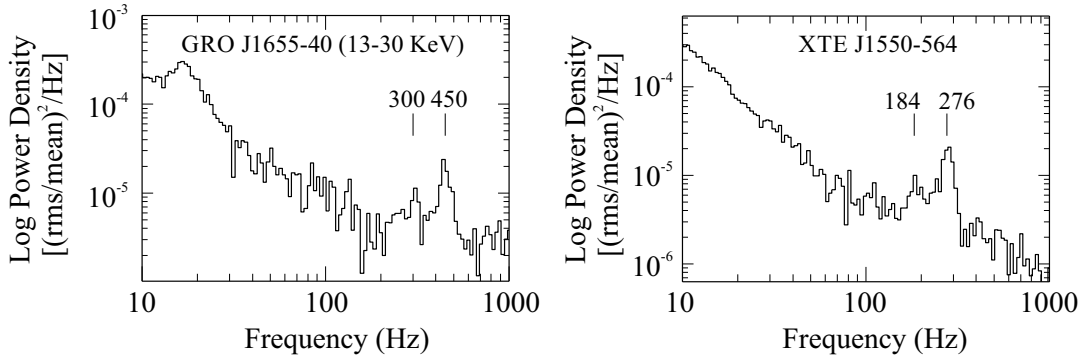

Figure 1.1. HF QPOs in two black hole binary systems (adopted from [3]). The peaks positions do not change with time in black hole systems. The ratios of oscillation frequencies are always close to 3 to 2. On the contrary, in neutron star systems, the position of the peaks does change with time.

Figure 1.2 can be seen PDS of one of the neutron star LMXBs[3]. If both peaks are present in PDS simultaneously, then the phenomenon is called the twin-peak HF QPOs[4]. The peaks have their features. One peak was called lower QPOs peak with frequency ν_L and the second upper QPOs peak with frequency ν_U. This naming is justified by the fact that if they are present together, it applies $\nu_L < \nu_U$. Despite the fact that $\nu_L < \nu_U$ the peaks position is changing with time. Figure 1.2 also shows frequency pairs ν_L, ν_U for twelve sources used in our papers [4–15]. For more information about this phenomenon see e. g. [16, 17].

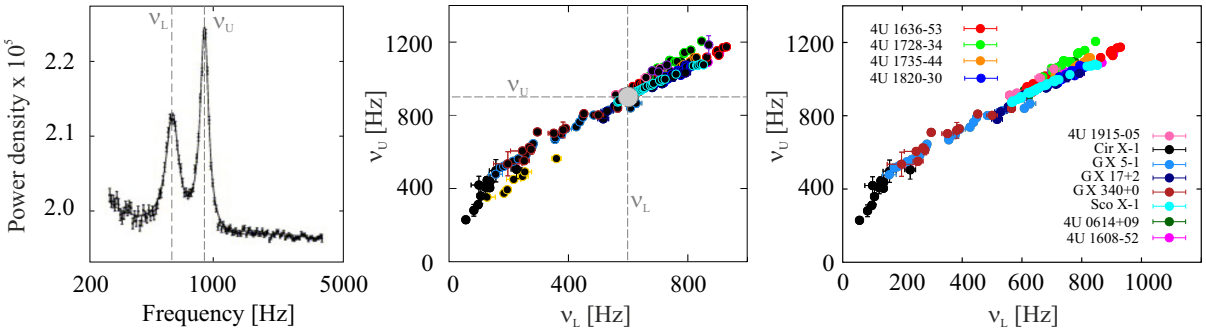

Figure 1.2. QPOs in neutron star sources. The left: PDS of one of the QPO sources (adopted from [18]). Middle: Frequency of peaks from the left panel together with QPO frequencies of the other sources. Right: QPOs in twelve systems that contain neutron stars (see Table 1.2).

In the following chapters, we will work with a group of QPOs frequency pairs observed in the PDS spectrum of twelve LMXBs. Table 1.2 shows a list of the LMXBs together with the numbers of reported QPOs frequency pairs and references.

[3] Here after we will talk about neutron stars or black holes, although we cannot be sure that this is not another object.

[4] From now on, we will use the term „QPOs“ as a synonym for twin-peak HF QPOs.

Table 1.1. List of neutron star LMXBs that we use in papers ([4–14]) and that we will deal with in next chapters of this work[5] . There is also information about number of frequency pairs ν_U, ν_L given from observations (second and fifth column) together with references.

Source	Data	Ref.	Source	Data	Ref.
4U 1608-52	25	[19–23]	4U 1636-53	91	[19, 19–21, 24–29]
4U 1735-44	11	[19–21, 30]	4U 1915-05	5	[31]
GX 17+2	18	[32, 33]	Sco X-1	51	[25, 34–36]
Cir X-1	11	[37]	4U 1728-34	63	[19–21, 38–42]
4U 0614+09	77	[19–21, 43–45]	4U 1820-30	28	[19–21, 38]
GX 340+0	12	[46]	GX 5-1	21	[47]

[5] In papers [4–14], we use fourteen sources, but for two of them, we do not have suitable data for our analysis.

Chapter 2

QPO models

We proceed to the description of some often used models of QPOs which we have used in [4–14, 48–52]. The list does not contain all the QPO models that were proposed in a few decades of the QPO research (see for example [53–70]). We take into consideration the models which connect QPOs with orbital motion of some objects in the inner parts of accretion disks. Typically, these models connect frequencies of QPOs with some combinations of the orbital (Ω_K), radial (ω_R) and vertical (ω_Θ) epicyclic frequencies of a free test particle orbiting in the vicinity of compact objects.

In Kerr geometry and Boyer-Lindquist coordinates, one can express the frequencies in the form (see e.g. [71, 72])

$$\Omega_K = \frac{c^3}{2\pi GM}\frac{1}{j+r^{3/2}}, \tag{2.1}$$

$$\omega_R = \Omega_K\sqrt{\frac{-3j^2+8j\sqrt{r}+(-6+r)\,r}{r^2}}, \tag{2.2}$$

$$\omega_\Theta = \Omega_K\sqrt{1+\frac{j\,(3j-4\sqrt{r})}{r^2}}, \tag{2.3}$$

where M, j are the mass and the spin of the compact object.

In the Hartle-Thorne geometry (H-T), which describes the vicinity of a slowly rotating neutron star with mass M, spin j and quadrupole moment q (see, e.g., [73]), the orbital Ω_K, radial ω_R and vertical ω_Θ epicyclic frequencies of a free test particle can be expressed as [74, 75]

$$\Omega_K = \frac{GM}{c^2}\frac{1}{r^{3/2}}\left[1-\frac{j}{r^{3/2}}+j^2F_1(r)+qF_2(r)\right], \tag{2.4}$$

$$\nu_R^2 = \left(\frac{GM}{c^2}\right)^2\frac{(r-6)}{r^4}[1+jH_1(r)-j^2H_2(r)-qH_3(r)], \tag{2.5}$$

$$\nu_\Theta^2 = \frac{GM}{c^2}\frac{1}{r^3}[1-jG_1(r)+j^2G_2(r)+qG_3(r)], \tag{2.6}$$

where $F_1(r), F_2(r), H_1(r), H_2(r), H_3(r), C(r), G_1(r), G_2(r), G_3(r), B(r)$ can be found in [74, 75].

For a space-time description around slowly rotating neutron stars, it is in general necessary to use the H-T geometry. However, Kerr geometry can be used for slowly rotating neutron stars with a sufficiently high mass (see, e.g., [4]).

As one can see in Figures 2.1 and 2.2, the frequency profiles (Ω_K, ω_R, ω_Θ) depend on the characteristics of the central compact object. Therefore, orbital models of QPOs can bring information about the parameters of the central compact object.

In the following text, we will describe the main features of some of the most used models of the QPOs, which deal with orbital motion in the close vicinity of compact objects.

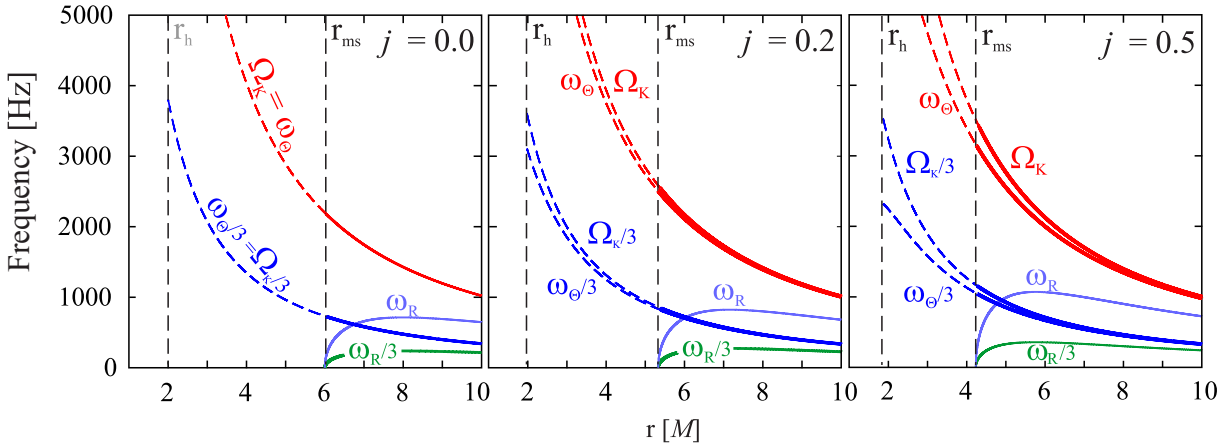

Figure 2.1. Radial profiles of orbital (Ω_K), radial (ω_R), and vertical (ω_Θ) epicyclic frequency of a free test particle in Kerr geometry. The frequencies are drawn for one solar mass (Ω_K, ω_R, ω_Θ) and three solar masses ($\Omega_K/3$, $\omega_R/3$, $\omega_\Theta/3$). r_{ms} is the marginally stable circular orbit, r_h indicates the position of the black hole horizon.

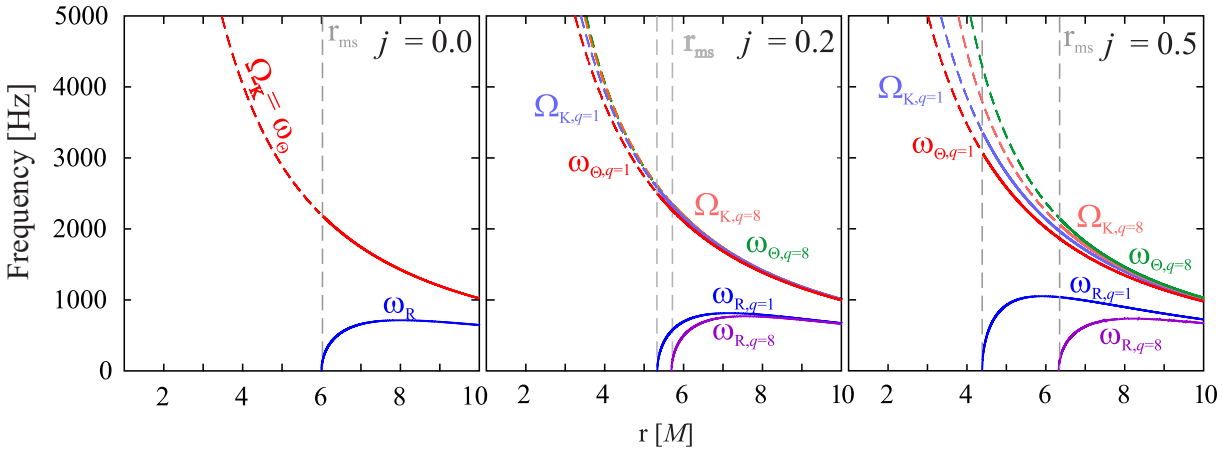

Figure 2.2. Radial profiles of orbital (Ω_K), radial (ω_R), and vertical (ω_Θ) epicyclic frequency of free test particles in the H-T geometry. The frequencies are drawn for a unit mass and two different values of quadruple momentum q.

2.1. Relativistic precession model

The Relativistic precession model (RP model) was introduced by Stella and his collaborators at the end of the last century in a series of works [76–80]. The authors explain the emission of QPOs as a result of orbiting hot spots in the inner parts of the accretion disk (see Fig. 2.3). According to this model, the frequency of the lower peak should correspond to the periastron precession frequency of a free test particle ($\nu_L = \omega_P = \Omega_K - \omega_R$) and the frequency of the upper peak should correspond to the frequency of the orbital motion of the particle ($\nu_U = \omega_K$).

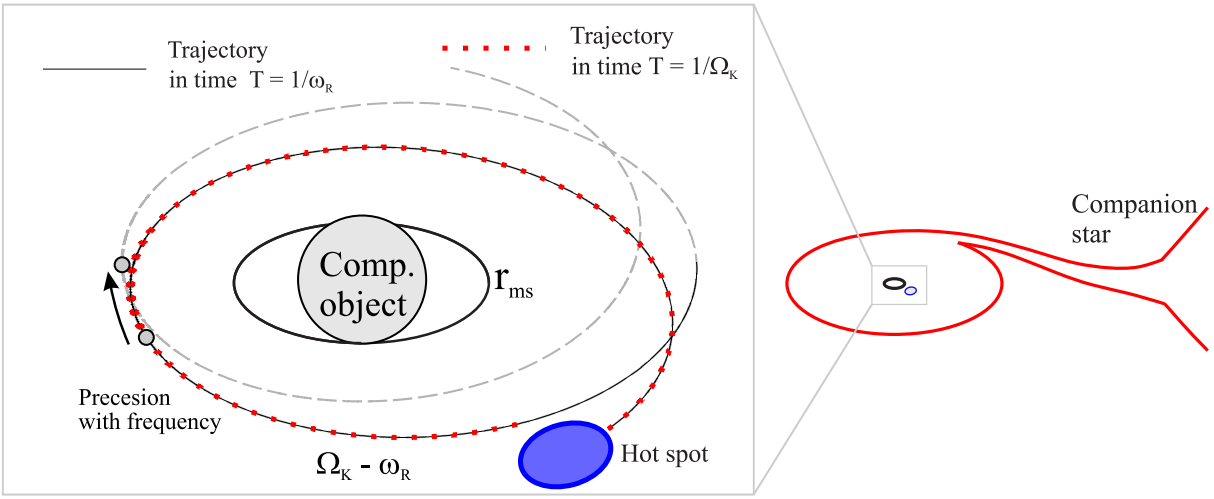

Figure 2.3. Illustration of the RP model. In the case of the RP model, the frequency of the upper QPO peak correspond to the frequency of the orbital motion of a free test particle. The lower frequency corresponds to the radial epicyclic frequency of the particle. If the compact object is a neutron star, then r_{ms} can be below the surface.

2.2. Tidal disruption model

The Tidal disruption model (TD model) was proposed a few years ago by a predominantly Slovenian group in the works [68, 81, 82]. The model assumes a cluster of material squeezed by tidal forces when it orbits around a black hole (or, in our case, around a neutron star). The cluster is squeezed along the trajectory (see Fig. 2.4). Oscillations of such an object are then responsible for the observed X-ray variability. Frequency of the lower QPO peak corresponds to the Keplerian frequency, $\nu_L = \Omega_K$, the upper peak frequency corresponds to the sum of the orbital and radial epicyclic frequencies of a free test particle ($\nu_U = \Omega_K + \omega_R$).

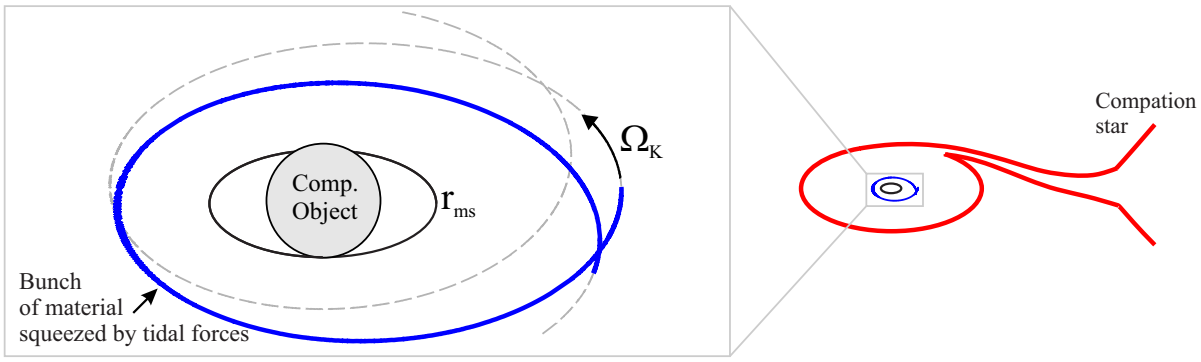

Figure 2.4. Illustration of the TD model. An initially spherical cluster of material is squeezed along the trajectory because of tidal forces. Such an object then orbits a central compact object.

2.3. Resonant disk-oscillation models

Resonant-disk oscillation models are based on the effort to explain the reason for the clustering of QPO frequencies ratios around ratios of small natural numbers.

The Epicyclic resonance model (ER model) was proposed by [59, 64, 83, 84]. It connects the excitation of QPOs with axially symmetric modes of disk oscillations. The model assumes that emissions are driven by a radially and vertically oscillating accretion torus in the vicinity of a resonant radius (radius, where radial and vertical frequencies are in a ratio of small natural numbers). Figure 2.5 shows such an oscillating torus. According to the model lower and upper QPO peaks corresponds to the radial ($\nu_L = \nu_R$) and the vertical ($\nu_U = \nu_\Theta$) epicyclic frequency, respectively.

Another model from the class of resonant models is the *Warped disk* model (WD model). The model was proposed by Kato [85–87]. Unlike ER model, it assumes non-axially symmetric modes. The model connects the lower QPO frequency to $\nu_L = 2(\nu_K - \nu_R)$ and the upper to $\nu_U = 2\nu_K - \nu_R$.

The *RP1* model was proposed by [67] and is also classified as a resonant model. The model assumes the QPOs as a manifestation of an oscillating torus as it was in the ER model. However, in this case, the frequency of the lower QPO peak should correspond to the precession frequency, $\nu_L = \omega_P = \Omega_K - \omega_R$, and the upper frequency corresponds to the vertical epicyclic frequency, $\nu_U = \omega_\Theta$. In the Schwarzschild geometry with zero spin, the RP1 model merges with the RP model. Figure 2.5 shows a torus oscillating as it is assumed by the RP1 model.

The last resonant-disk oscillation model is the *RP2* model proposed by [88, 89]. The behaviour of the torus can be seen in Figure 2.5. The lower frequency should correspond to the precession frequency ($\nu_L = \nu_K - \nu_R$) and the upper QPO frequency should correspond to a difference between the double of the Keplerian frequency and the vertical epicyclic frequency ($\nu_U = 2\nu_K - \nu_\Theta$). As in the previous case, the model matches the RP model in Schwarzschild geometry.

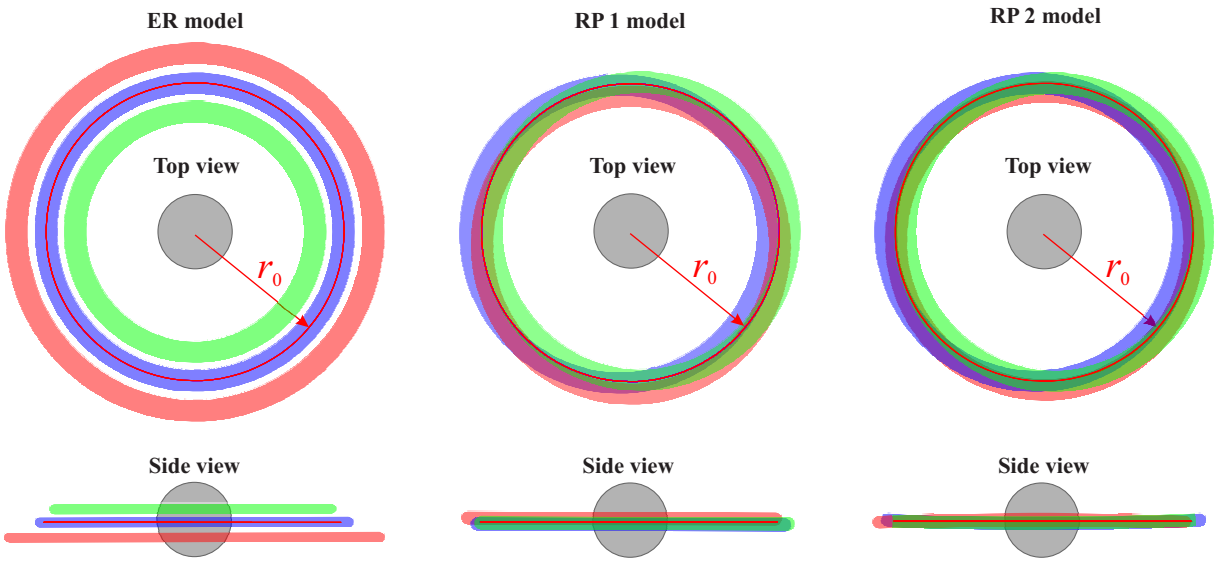

Figure 2.5. Oscillating torus schemes for the ER (Left), RP1 (middle) and RP2 (righ) model. The colours symbolize torus positions in different parts of the oscillation period. The bottom row corresponds to the side view. The top row corresponds to the top view.

2.4. Cusp torus model

Above, we have described several models, some of which assumed that QPOs are emitted because of the accretion torus oscillating in the inner parts of the accretion disk. So far, the torus was approximated by an infinitely thin ring. The structure oscillated with frequencies that correspond to the oscillation frequencies of free test particles.

If one considers a slightly non-slender torus, the oscillation frequencies will be modified. The pressure correction on the radial and vertical oscillating frequencies of an accretion torus with non zero (but still small) thickness were computed in [90, 91]. For their complexity, we will not specify them here.

Figure 2.6 shows equipotentials around the compact object in the vicinity of which, at the radial coordinate r_0, is an axially symmetric torus in hydrostatic equilibrium. The torus is made by perfect fluid whose own gravity is negligible (see for example [92–94]). The material of the accretion disk fills closed equipotentials. There is a critical (last) closed equipotential[1]. Oscillations of such a critical torus are responsible for QPOs emission according to the Cusp torus model (CT model). Different QPOs are excited by oscillations of the torus on different central radial coordinates (r_0).

Such a torus can oscillate in different modes. The CT model assumes that one of the QPOs frequencies corresponds to a Keplerian frequency at the torus centre[2]. The second frequency

[1] The situation is similar to Roche's lobe in the theory of binary stars.

[2] As you can see, for example, in [92–94], the material in the torus centre orbits with the frequency of free test particles.

corresponds to the modified (by pressure correction) precession frequency of a free test particle (see Figure 2.6). The CT model was proposed in paper [8] thatis included in the list of papers in Chapter II. The expression for the lower QPO frequency is complicated. However, there is no need to adopt a new parameter. The frequency is given by the features of the central the compact object[3].

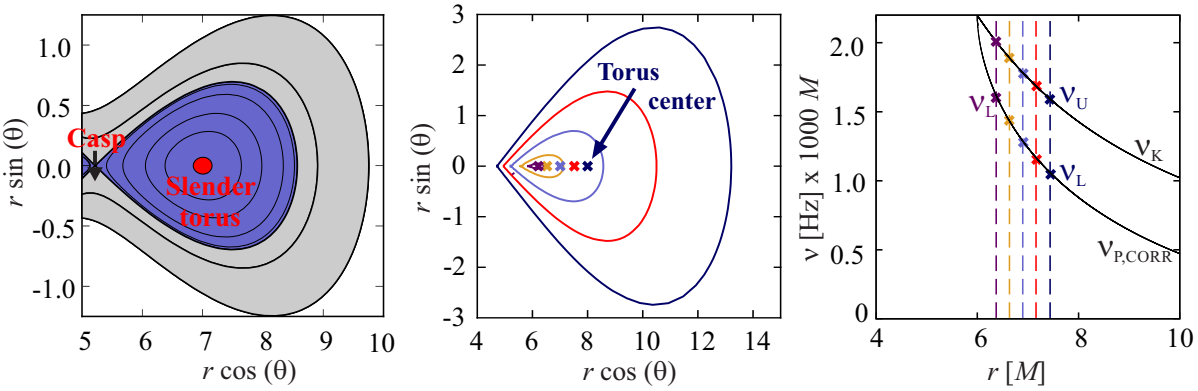

Figure 2.6. A Cusp torus model illustration. Left panel: Torus configuration. The black lines indicate torus equipotentials. Closed torus always fills one of the closed equipotentials. The red colour indicates the critical (maximal) closed torus. The smallest torus, which is marked by green colour, is the torus with which work models described in the last Chapter 2.3. A neutron star surface is chosen randomly but appropriately. Middle and right panel: Explanation of CT model predictions. Every couple of QPO frequencies correspond to oscillation frequencies of a torus on some radial coordinate which filled critical closed equipotential. In the middle panel, there are tori for different central radial coordinate r_0. In the right panel, there are corresponding QPO frequencies predicted by the CT model.

2.5. One-parameter and two-parametric relation

Abramowicz and his colaborators noted in 2005 ([95, 96]) that parameters a, b resulting from fitting of QPOs of six LMXB's by the linear relation

$$\nu_U = a\nu_L + b \tag{2.7}$$

are corellated and that the quality of the fits is quite good. For the rest of the eight sources it was done in [9]. It led to an idea, that there should be a good fitting model of QPOs with just one parameter. In [4] we find out that fitting the source 4U 1636-53 by the relation

$$\nu_L = \nu_U \left(1 - 0.8\sqrt{1-(\nu_U/\nu_0)^{2/3}}\right), \tag{2.8}$$

[3] In Schwarzschild geometry, it is just mass of the compact object.

gives good results. In the formula $\nu_{ISCO} = \frac{1}{6^{3/2}} \frac{c^3}{2\pi G} \frac{1}{\mathscr{M}}$, is the orbital frequency of a free test particle on the innermost stable circular orbit. The fenomenological model turns out to be suitable also for some other sources (see [9]). For the purposes of this work, we will call it a one-parameter relation.

Physical meaning of the one-parameter relation will be clear if we will look at the RP model within the Schwarzschild geometry with the radial epicyclic frequency modified by a factor of 0.8 with respect to the epicyclic frequency of free test particles

$$\nu_U = \nu_K = \frac{1}{r^{3/2}} \frac{c^3}{2\pi G} \frac{1}{\mathscr{M}}, \Rightarrow r = \left(\frac{1}{\nu_U} \frac{c^3}{2\pi G} \frac{1}{\mathscr{M}} \right)^{2/3} \tag{2.9}$$

$$\begin{aligned} \nu_L &= \nu_K - 0.8\nu_R = \frac{1}{r^{3/2}} \frac{c^3}{2\pi G} \frac{1}{\mathscr{M}} \left(1 - 0.8\sqrt{1 - \frac{6}{r}} \right) \\ &= \nu_U \left(1 - 0.8\sqrt{1 - (\nu_U/\nu_0)^{2/3}} \right). \end{aligned} \tag{2.10}$$

Modification of the radial epicyclic frequency can be produced either by the influence of magnetic field or something not yet known.

As we can see in [9], for five sources we do not have good fits for this one-parameter relation. It leads to the idea of introducing some a new parameter, lets call it $\mathscr{B}$, which will express the modification of the radial epicyclic frequency with respect to the epicyclic frequency of a free test particle. We will call this new relation the two-parametric relation

$$\nu_L = \nu_U \left(1 - \mathscr{B}\sqrt{1 - (\nu_U/\nu_0)^{2/3}} \right). \tag{2.11}$$

2.6. Models modifications

We should mention a few modifications of the above-described models:

The **Total precession model (TP model)** was created by [97]. The model connect the lower and the upper QPO frequencies to the total precession frequency ($\nu_L = \nu_\Theta - \nu_R$) and the vertical epicyclic frequency ($\nu_U = \nu_\Theta$).

The **TP1 model** is a modification of the TP model. It connects the lower QPO frequency to total precession frequency ($\nu_L = \nu_\Theta - \nu_R$) and the upper to the Keplerian frequency ($\nu_U = \nu_K$).

The **TPB model** is another modification of the TP model. It connects the lower frequency to the total precession frequency ($\nu_L = \nu_\Theta - \nu_R$) and the upper to the sum of the vertical and the radial epicyclic frequency, $\nu_U = \nu_\Theta + \nu_R$.

2.7. Resonant switch model

The Resonant switch model (RS model) was introduced in the series of works [5, 70]. It assumes that a pair of the oscillation modes (corresponding to a model of QPOs described above) switches to a different pair due to non-linear resonant phenomena at some resonant point. In other words, QPOs generation is explained by the combination of two models. This model has so far been used for fitting the data of 4U 1636-53 (see [5, 6, 70]).

2.8. Summary

Summary of the models mentioned above and frequency identifications can be seen in Table 2.1.

Table 2.1. The models summary. The list of models is completed with the corresponding frequency identification and references.

Model	ν_L	ν_U	Ref.	Model	ν_L	ν_U	Ref.
RP	$\Omega_K - \omega_R$	Ω_K	[76–80]	TD	Ω_K	$\Omega_K + \omega_R$	[68, 81, 82]
WD	$2\,(\Omega_K - \omega_R)$	$2\Omega_K - \omega_R$	[85–87]	ER	ω_R	ω_Θ	[59, 64, 83, 84]
RP1	$\Omega_K - \omega_R$	ω_Θ	[67]	RP2	$\Omega_K - \omega_r$	$2\Omega_K - \Omega_\Theta$	[88, 89]
CT	$\nu_{r,m=-1}$	Ω_K	[8]	one-par.	see eq. (2.8)		[9]
two-par.	see eq. (2.11)		[9]	TP	$\omega_\Theta - \omega_R$	ω_Θ	[97]
TP1	$\omega_\Theta - \omega_R$	ω_Θ	[97]	TPB	$\omega_\Theta - \omega_R$	$\omega_\Theta + \omega_R$	[97]

Chapter 3

QPOs in low mass X-ray binaries and compact object parameters estimations

The last chapter is devoted to basic information about selected orbital models of QPOs. Some of the papers attached to this thesis ([4–9, 15]) have one thing in common - an effort to obtain information about compact objects by applying the models on the observed data.

In what follows, I will focus on the topics discussed in the following papers:

- *Mass-Angular-momentum Relations Implied by Models of Twin Peak Quasi-periodic Oscillations* [4] - In [89] authors find out that fitting QPO data from a group of sources with low QPO frequencies by RP model in Kerr geometry leads to a relation between mass and spin rather than a specific combination of these parameters. In our paper [4] this finding is also expanded to sources with high QPO frequencies and other models. We also derived a relationship between the upper and lower QPO frequencies in RP (and TD) models. In this article, we have shown how to get a specific combination of mass and spin if we consider the NS equations of state. Last but not least, we discussed how much the RP model would have to be modified to fit the QPO data of high-frequency sources well.

- *Test of the Resonant Switch Model by Fitting the Data of Twin-Peak QPOs in the Atoll Source 4U 1636-53* [5] - This article is similar to [4] but this time, we used the resonant switch model described in 2.7. In the resonant switch model, we get a combination of mass and spin instead of a relation between these parameters.

- *Equations of State in the Hartle-Thorne Model of Neutron Stars Selecting Acceptable Variants of the Resonant Switch Model of Twin QPOs in the Atoll Source 4U 1636-53* [6] - In this article, there are results of [5] compared with predictions of NS equations of states.

- *Twin peak quasi-periodic oscillations as signature of oscillating cusp torus* [8] - the Casp torus model was proposed in the article (see Section 2.4).

- *Constraining Models of Twin-Peak Quasi-periodic Oscillations with Realistic Neutron Star Equations of State* [7] - It is another extension of the article [4]. This time we are considering the NS equations of states. In this article, we work in the Hartle-Thorne geometry. We use

the fact that the rotational frequency of NS in 4U 1636-53 is known from independent observations. We verify which combinations of an equation of state and QPO models are compatible.

- *A one-parameter formula relating the frequencies of twin-peak quasi-periodic oscillation* [9] - This article finds and investigates a simple relation with one parameter which reproduces the correlations between QPO frequencies of several sources (see Section 2.5 of this thesis). The article also shows that if we add another parameter to the relation, the relation interprets all fourteen examined resources well. We discuss the physical meaning of the parameters and deal with the proofs of the orbital origin of the QPOs.

- *Simple analytic formula relating the mass and spin of accreting compact objects to their rapid X-ray variability [15]* The paper was just submitted to The Astrophysical Journal. A well-fitting one-parameter relation derived in [9] was found as a good approximation of the CT model in the Schwarzschild geometry. In this article, we found something similar but within the Kerr and the Hartle-Thorne geometry. This relation can be helpful for the fast estimation of NS parameters.

In this chapter, we will focus on the estimations of parameters of the NS, which are present in twelve LMXB's. Figure 3.1 shows a map of the X-ray sky with a position of all the sources. Example power spectra of the sources can be seen in Figure 3.2.

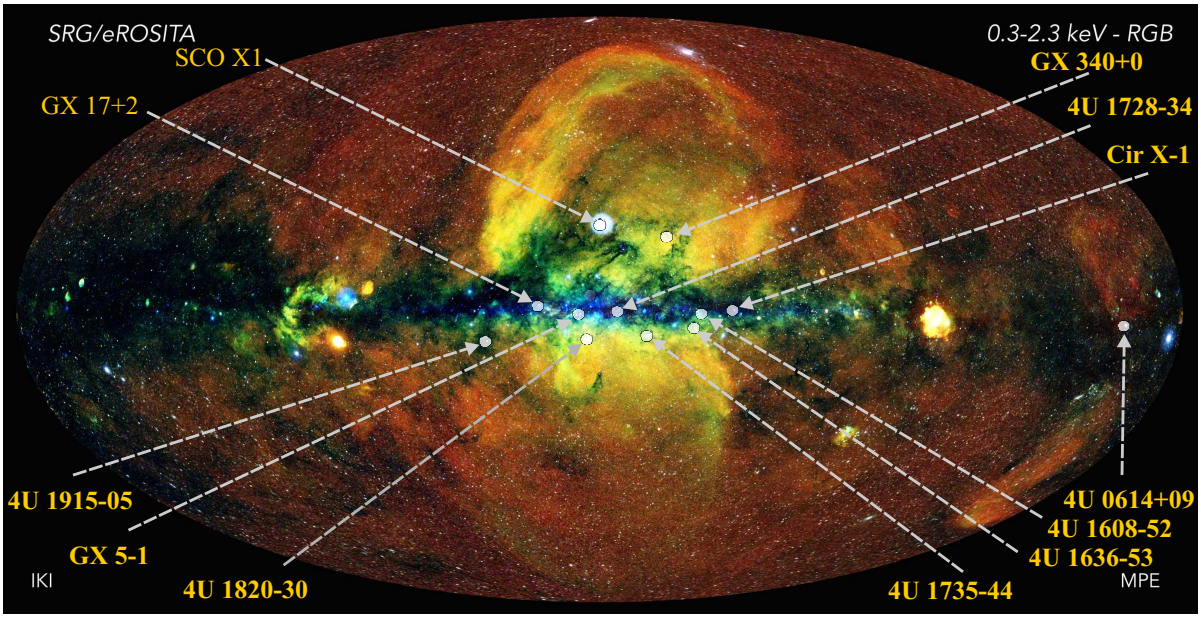

Figure 3.1. The X-ray sky with source positions. The sky map comes from [98].

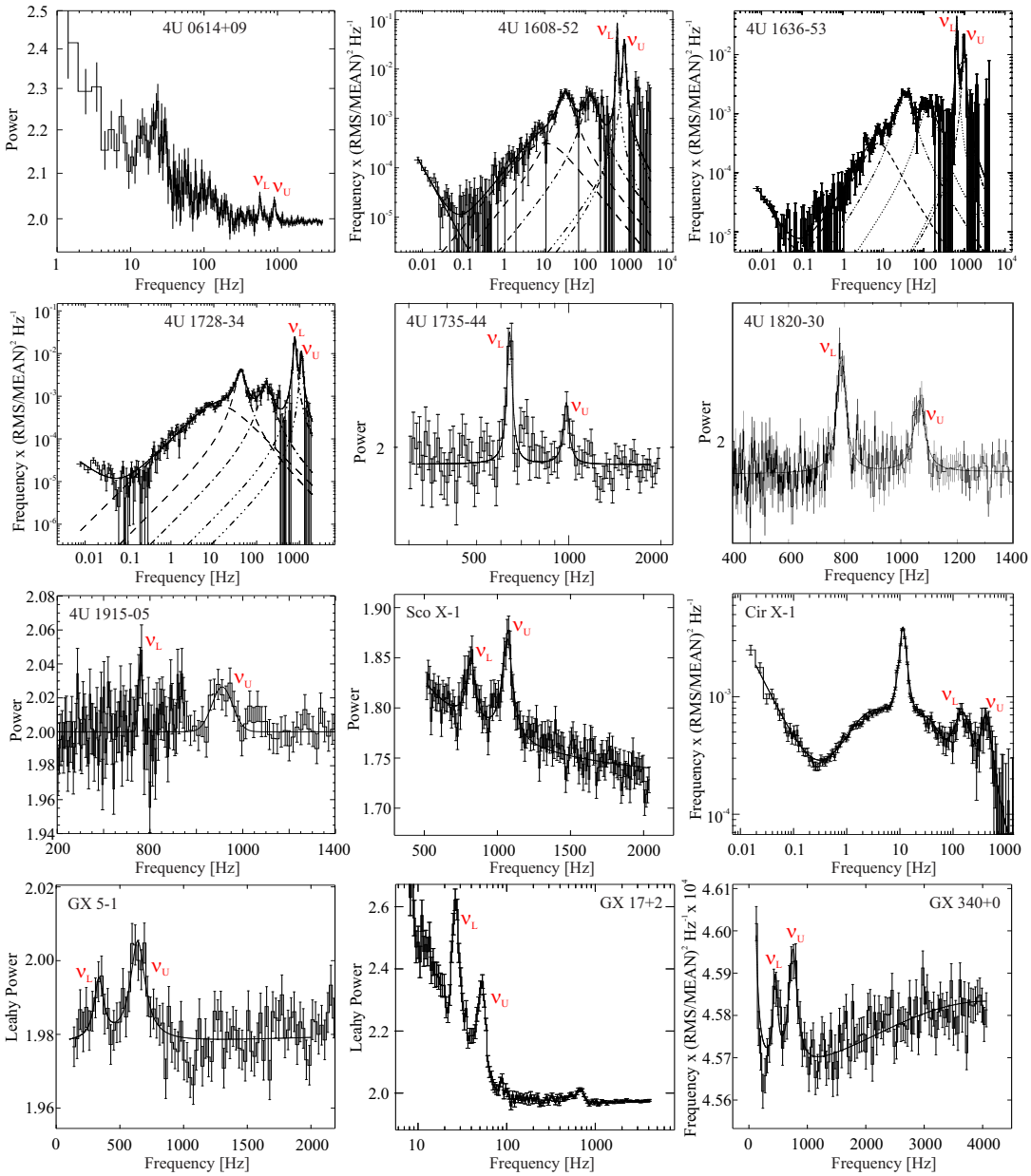

Figure 3.2. Examples of the power spectra. All information can be found in papers [23, 26, 30, 33, 36, 39, 43, 99–102] from which this plot is taken.

In the above mentioned articles, we, among other things, performed an analysis of the observational data leading to the estimation of parameters of compact objects. I have always had concerns whether our results were not affected by the fact that we only took into account a limited amount of data. I wanted to perform the same analysis for all the twelve sources as was done in the papers, but this time utilizing all the data reported by different authors. The authors in general use different procedures for obtaining the data using different parts of the light curves, so it could be interesting to see how this influences the parameters estimations.

However, finding all the available data (i.e. going through thousands of papers) and analysing

them seemed too time-consuming for a regular article. At the same time, it was clear that in the best case (i.e. when the conclusion is that there is no distortion), this work would not lead to any new result.

The opportunity to analyse such a huge number of data came to me while working on this dissertation. Comparison between the data commonly used by us in the papers [4–9] and all data reported over the years by various authors is displayed in Figure 3.3.

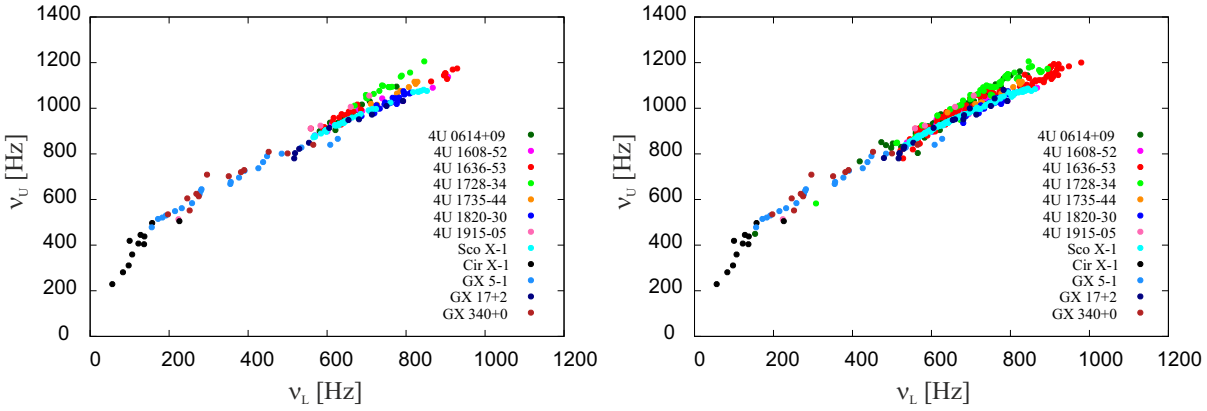

Figure 3.3. Frequencies of the QPOs found in the power spectra. Left: the data we use in papers [4–9]. Right: data avaliable in the literature.

Now, I use models described in Chapter 2 for parameters estimation and compare them across data from different authors. In part, such an analysis was performed by other authors whose list can be found in our publications [4–9, 15]. Here, I only mention publications [25, 103].

In Figures (3.17 - 3.16), we can see the best fits made for all the models and data.

Let us now talk about the quality of the fits. It can be seen from the right panel of Figure 3.3 that a "simple" relation should be able to well approximate the dependency of ν_U on ν_L. However, reduced χ^2 will be high for all simple models (because of scattering of the points).

Therefore, let us explore properties of another quantity ε defined as

$$\varepsilon = ((\nu_L - \nu_{L,\text{theoretical}})^2 + (\nu_U - \nu_{U,\text{theoretical}})^2)^{1/2}. \tag{3.1}$$

In Equation 3.1, ν_L, ν_U are frequencies of the QPO peaks (a point in the right panel in Figure 3.3) and $[\nu_{L,\text{theoretical}}, \nu_{U,\text{theoretical}}]$ are coordinates of the nearest point on the curve corresponding to the best fit of the model. If we consider a given model to be potentially good, ε should be a random variable (the points should by randomly scatterred arround the curve). The correlation between ε and ν_L is on the following lines quantified by the Pearson's correlation coefficient p ([104]).

First, I focus on models that were only taken from the literature (i.e. the linear, quadratic, square-root, RP, TD and WD models - see Section 3.1). Later, I will use our own proposed models (i.e., the one-parameter and two-parametric relations, and the CT model - see Section 3.2.).

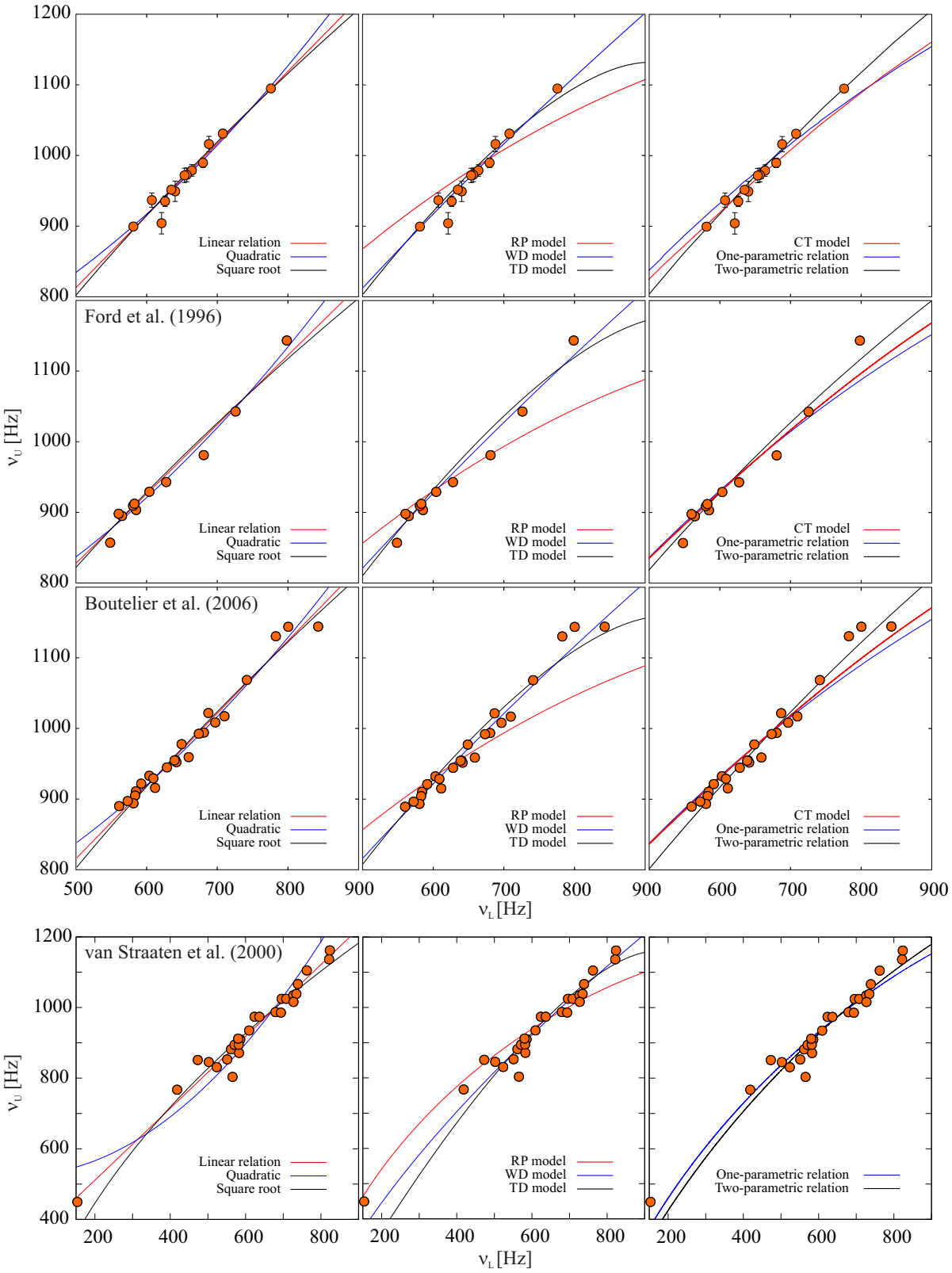

Figure 3.4. Frequencies of the upper ν_U and lower ν_L QPOs of the binary star 4U-0614+09 together with best fits by the models.

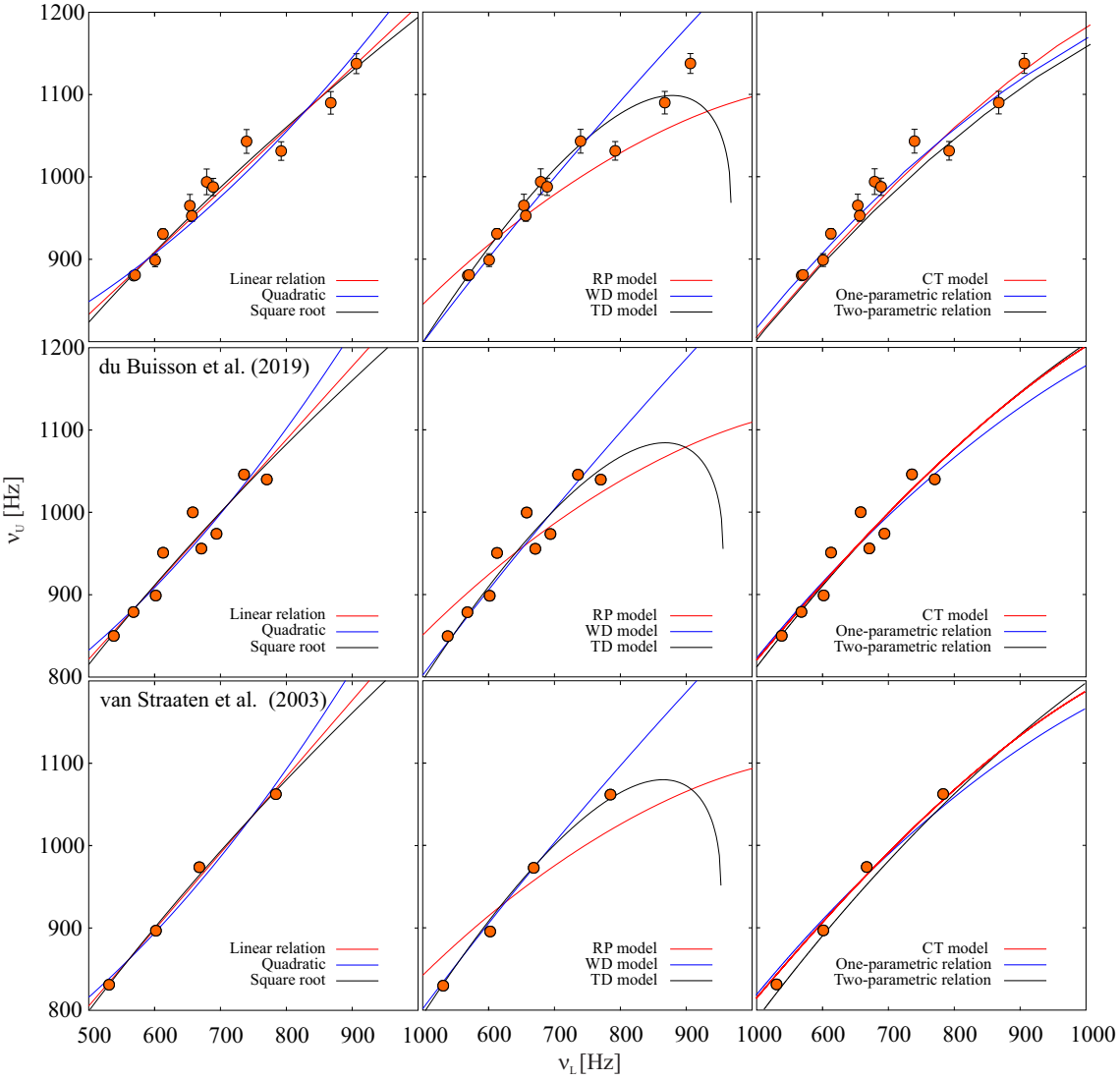

Figure 3.5. The same as in 3.4 but for 4U 1608-52.

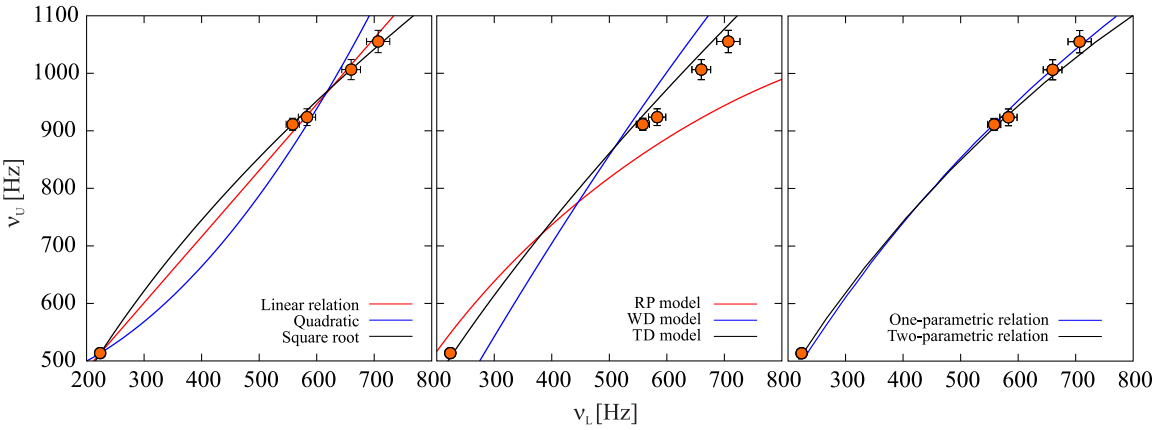

Figure 3.6. The same as in 3.4 but for 4U 1915-05.

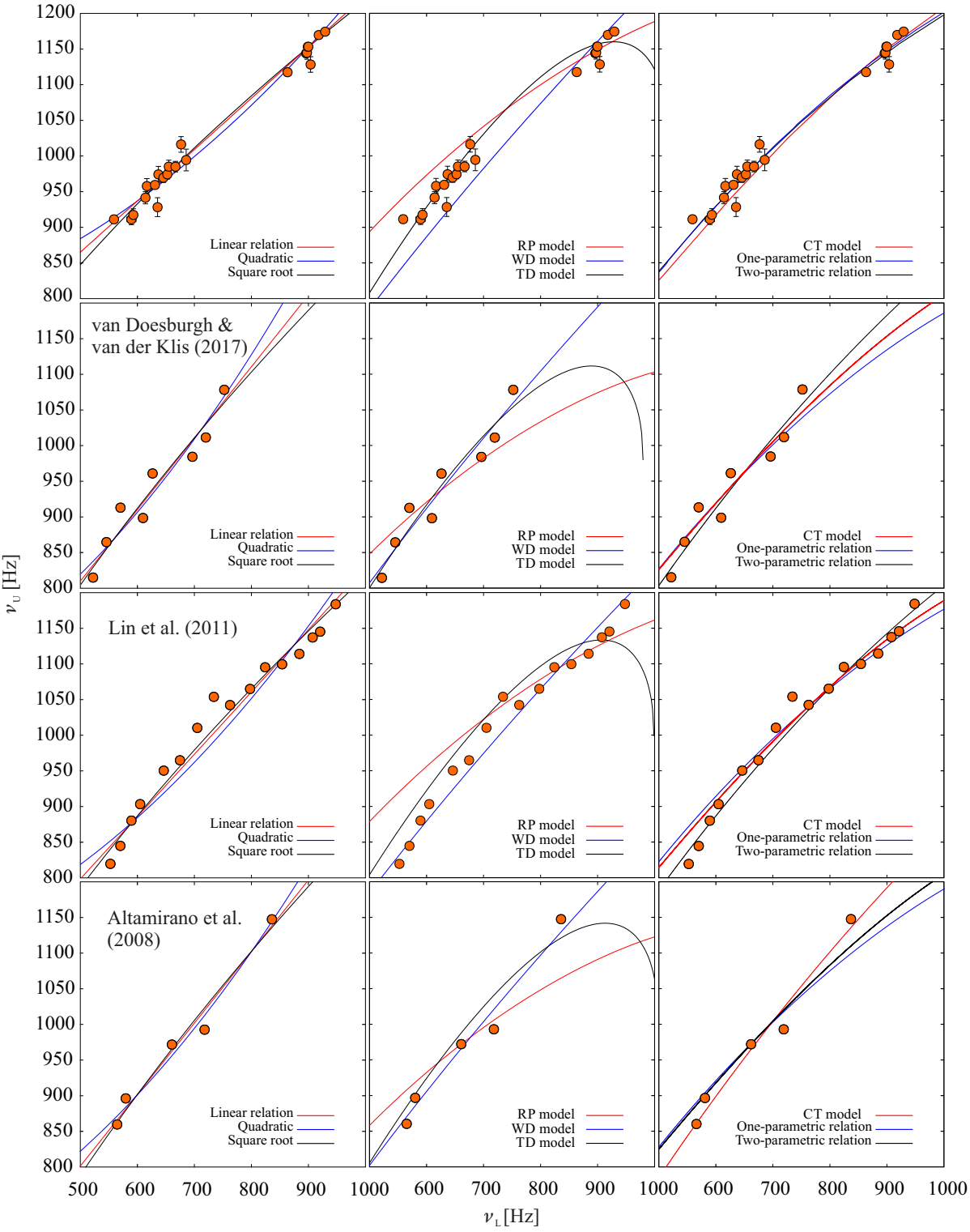

Figure 3.7. The same as in 3.4 but for 4U 1636-53 - the first part.

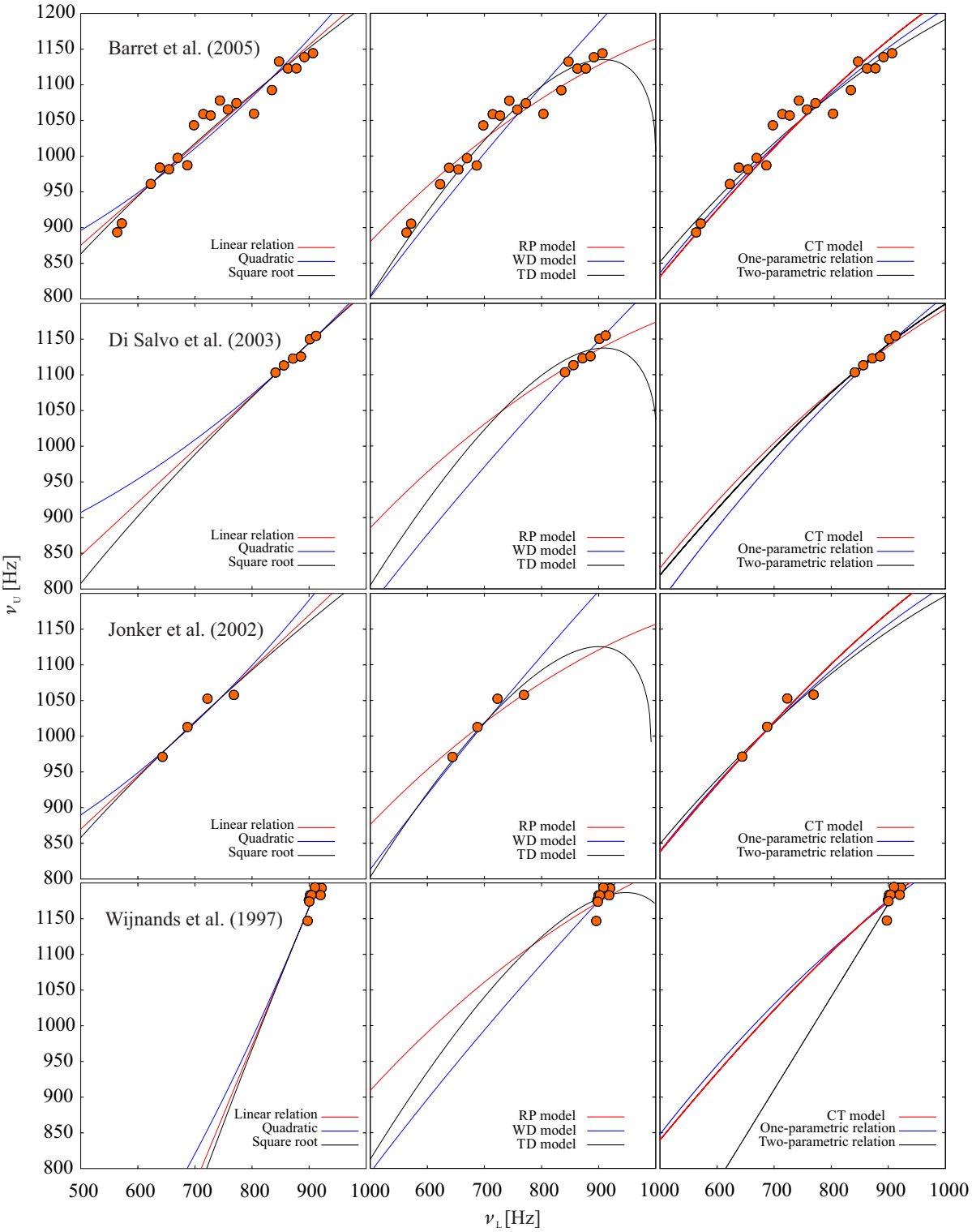

Figure 3.8. The same as in 3.4 but for 4U 1636-53 - the second part.

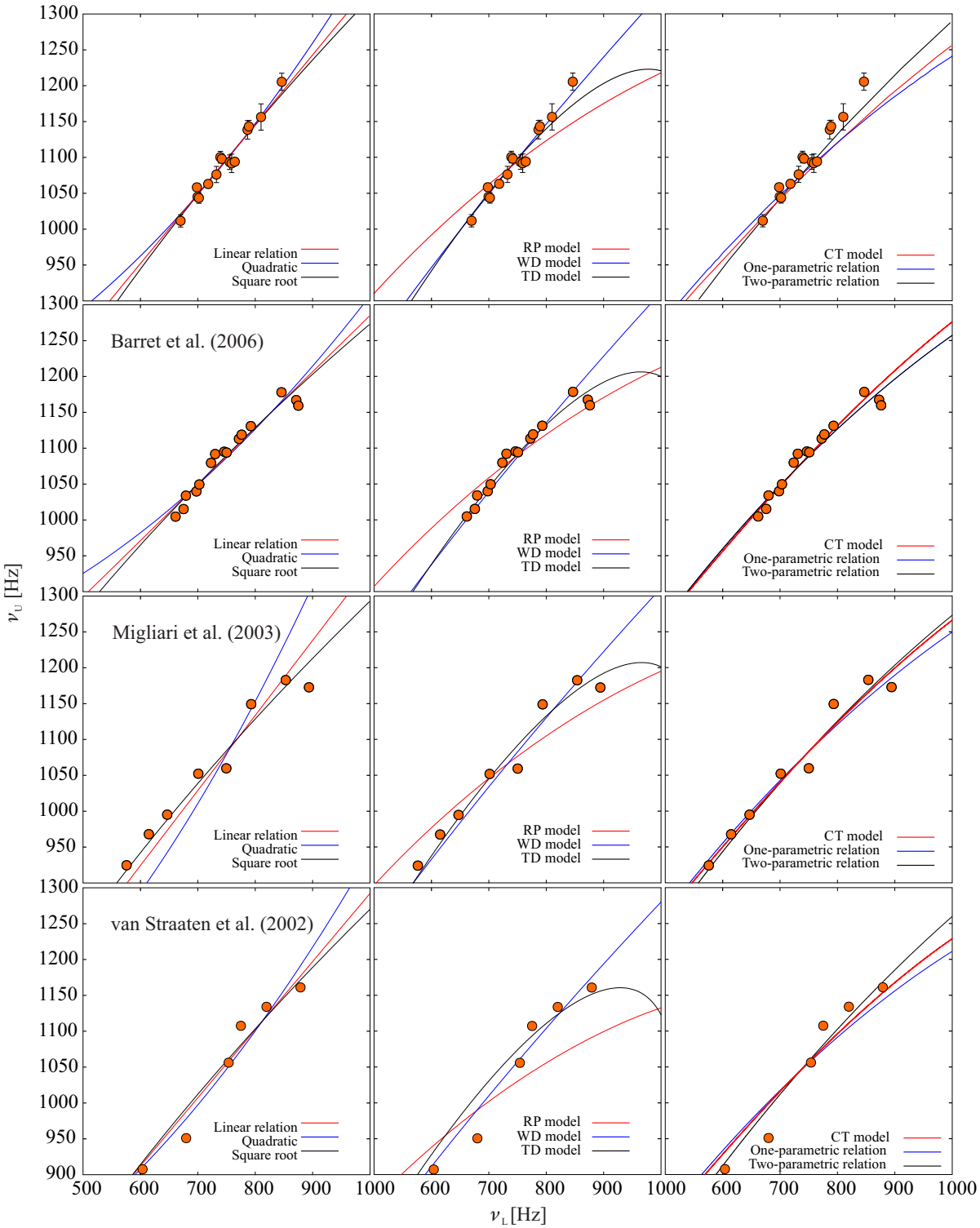

Figure 3.9. The same as in 3.4 but for 4U 1728-34 - the first part.

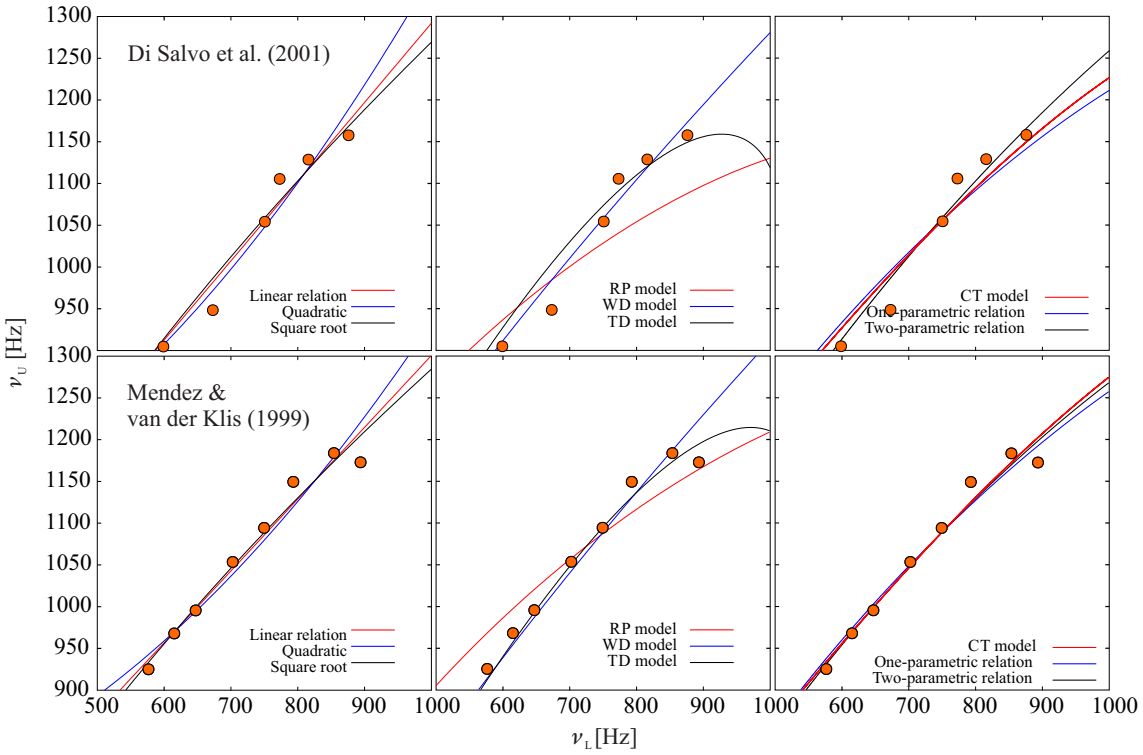

Figure 3.10. The same as in 3.4 but for 4U 1728-34 - the second part.

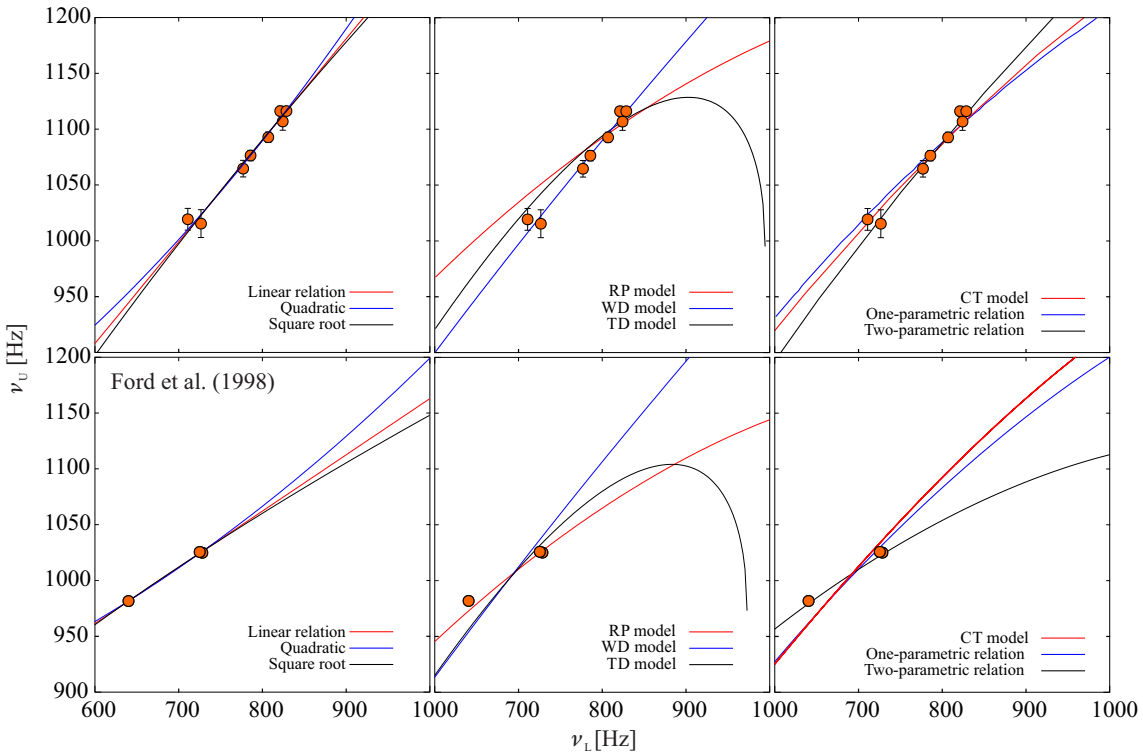

Figure 3.11. The same as in 3.4 but for 4U 1735-44.

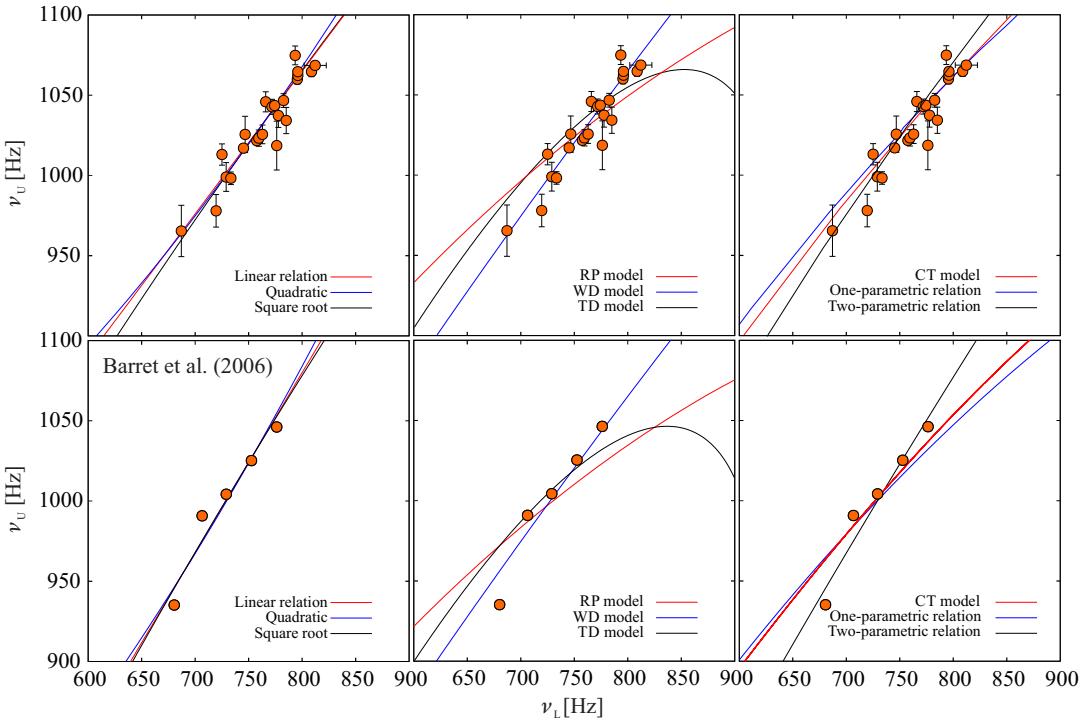

Figure 3.12. The same as in 3.4 but for 4U 1820-30.

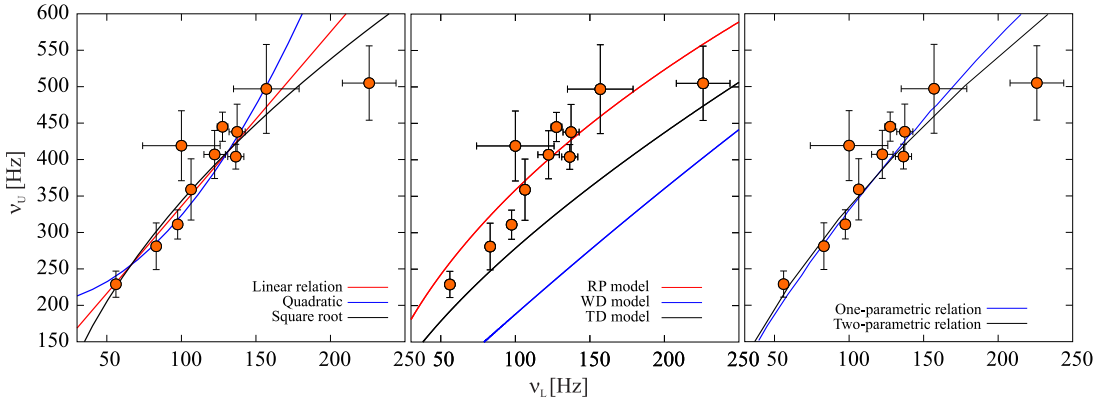

Figure 3.13. The same as in 3.4 but for Cir X-1.

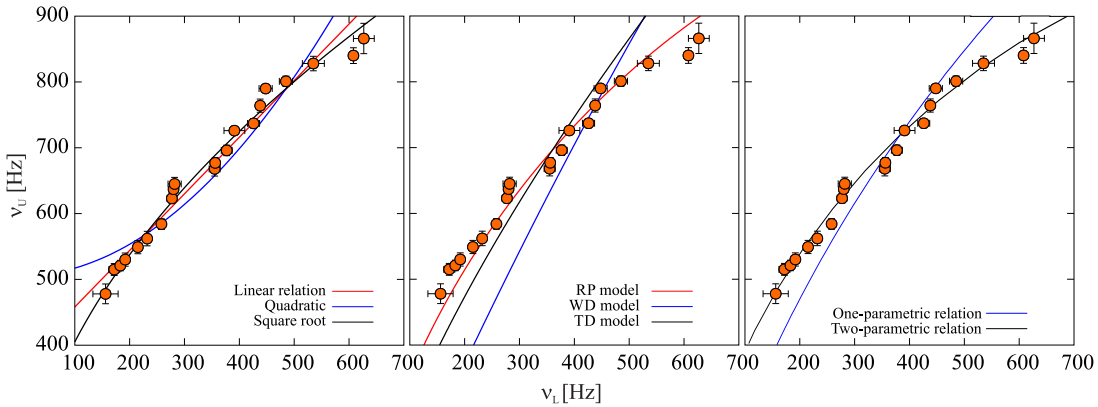

Figure 3.14. The same as in 3.4 but for GX 5-1.

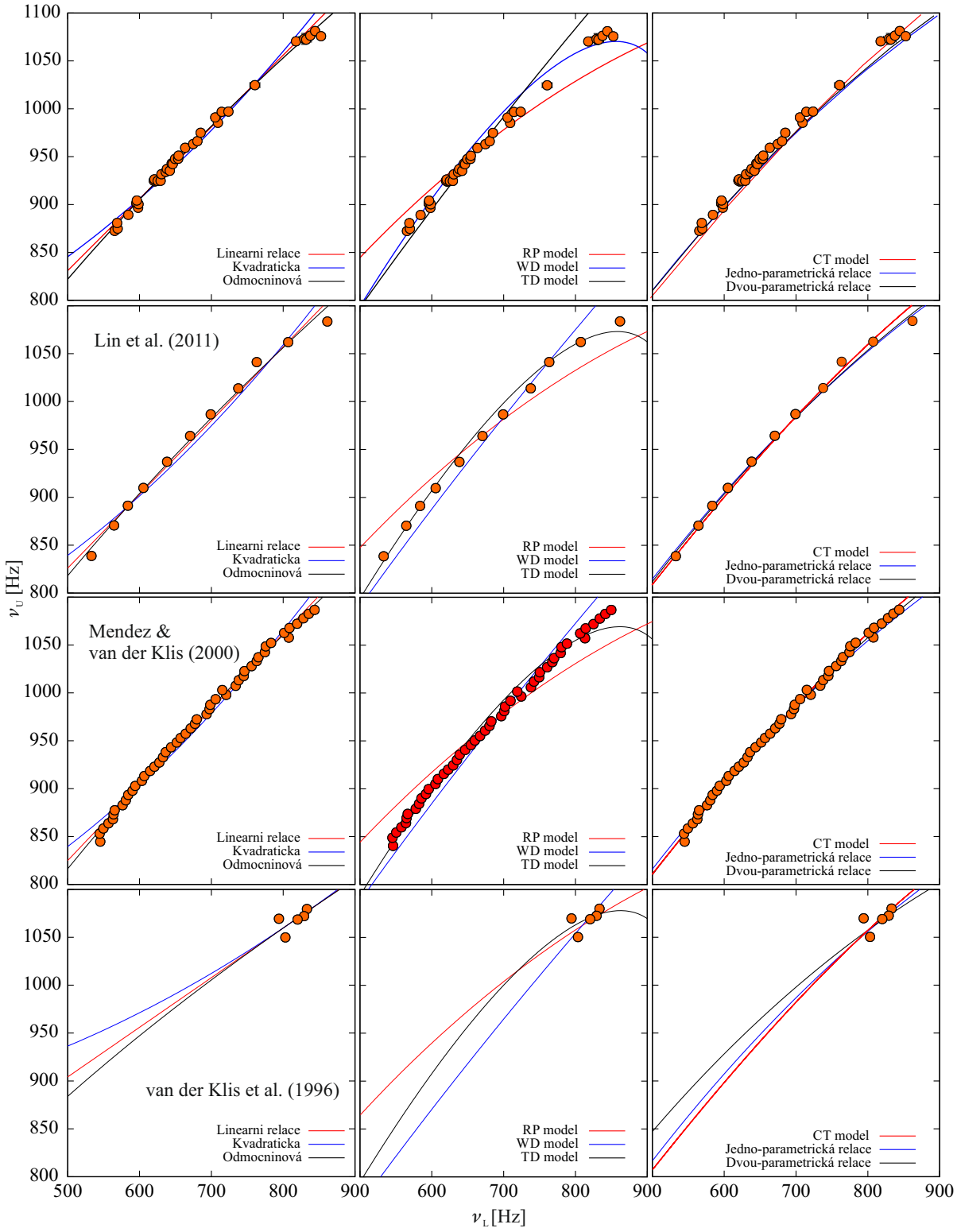

Figure 3.15. The same as in 3.4 but for SCO X-1.

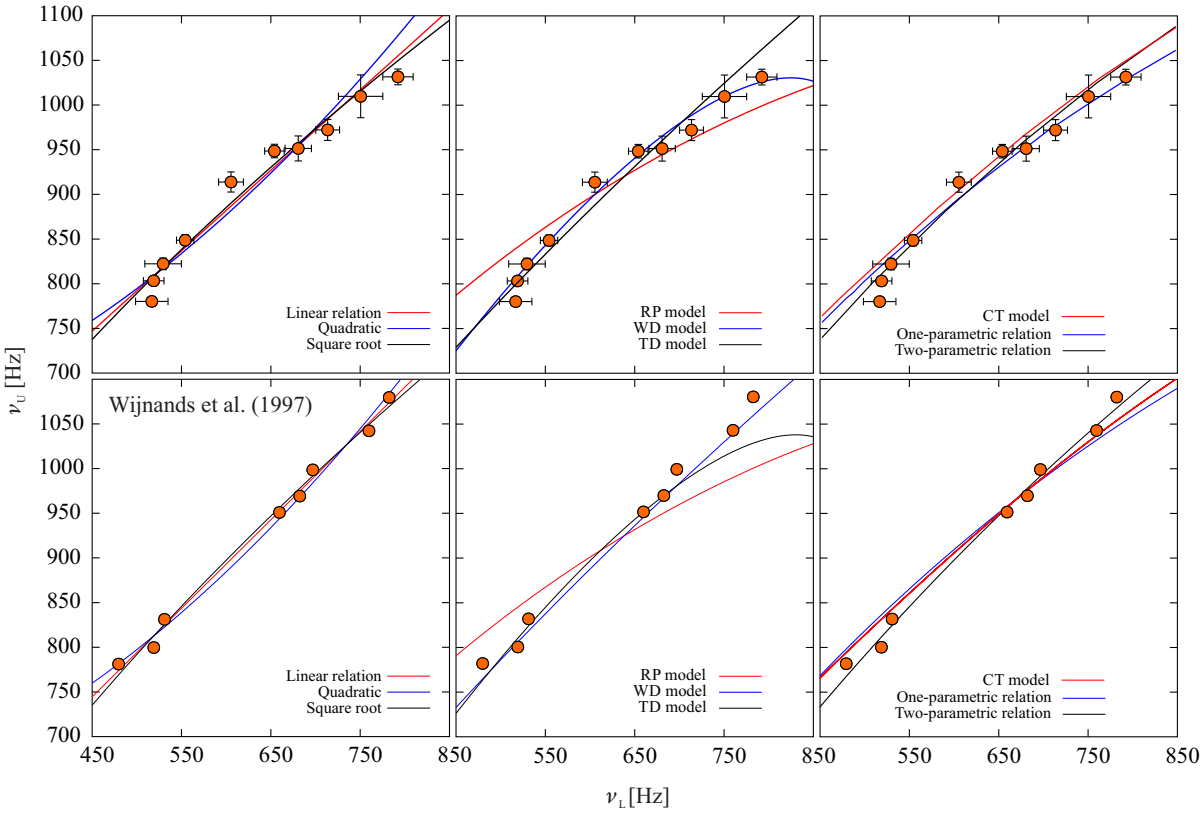

Figure 3.16. The same as in 3.4 but for GX 17-2.

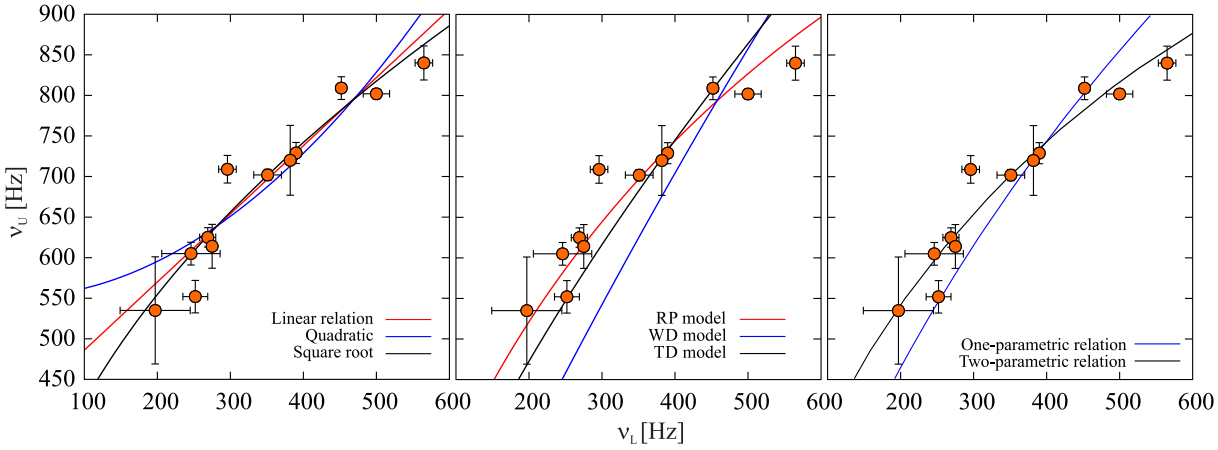

Figure 3.17. The same as in 3.4 GX 340+0.

3.1. Models adopted from the literature

In this subsection, I will assume the Schwarzschild geometry. One can see in papers [4, 7] that, in general, the transition to Kerr or Hartle-Thorne geometry does not imply any improvement of the fit.

In Table 3.1, I present the best-fit parameters of the selected models from the previous chapter applied to the data obtained by various authors. I used the Module kmpfit from the Kapteyn Package [105]. In papers [4–8, 13, 15, 48, 49], we used data sets with errors. This information, however, is not always present in all the papers from which the data were taken. For that reason, we do not use errors here.

For the sake of interest, Figures 3.18 - 3.33 show histograms of ε (see Equation 3.1) for all sources and models. The horizontal and vertical axes show the value of ε and the frequencies, respectively. Figures 3.24 - 3.35 illustrate the dependency of ε on ν_L.

Table 3.1. Best fit parameters for models given in Chapter 2 and different QPO sources. The meaning of the A, B, M parameters is given in Chapter 2. The p parameter is Pearson's correlation coefficient (the correlation between ε and ν_L). If $p < 0.3$, the value is highlighted in red colour. Lines named after given source are results based on data used in our papers [4–8, 13, 15, 48, 49] (their referencies can be found in Table 1.2). The rest of lines are named according to the authors who were reported the data.

	Linear model B, A, χ^2, p	Quadratic model B, A, χ^2, p	Square-root model B, A$x10^{-4}$, χ^2, p	*RP* model M, χ^2, p	*TD* model M, χ^2, p	*WD* model M, χ^2, p
4U 0614+52	$262^{\pm46}$, $1.08^{\pm0.07}$, 65 0.260	$625^{\pm2}$, $8^{\pm0.5}$, 70 0.275	$-469^{\pm91}$, $56^{\pm4}$, 64 0.271	$1.92^{\pm0.02}$, 427 , 0.926	$2.22^{\pm0.02}$, 108 0.580	$2.26^{\pm0.02}$, 71 0.423
[a]	$337^{\pm30}$, $0.98^{\pm0.05}$, 114 0.000	$646^{\pm12}$, $7.6^{\pm0.3}$, 70 0.000	$-293^{\pm72}$, $50^{\pm3}$, 154 0.001	$1.93^{\pm0.01}$, 244, 0.875	$2.12^{\pm0.04}$, 222, -0.184	$2.18^{\pm0.03}$, 130 0.095
[b]	$307^{\pm24}$, $1.02^{\pm0.04}$, 361 , 0.000	$525^{\pm27}$, $10.3^{\pm0.7}$, 1131 , 0.031	$-211^{\pm59}$, $46^{\pm2}$, 492, -0.049	$1.9^{\pm0.01}$, 952, 0.650	$2.15^{\pm0.04}$, 740, -0.387	$2.21^{\pm0.04}$, 426, -0.236
[c]	$302^{\pm23}$, $1.03^{\pm0.03}$, 77 -0.008	$651^{\pm11}$, $7.4^{\pm0.3}$, 73 -0.008	$-405^{\pm49}$, $54^{\pm2}$, 85 0.001	$1.93^{\pm0.01}$, 339, 0.943	$2.15^{\pm0.02}$, 163, 0.513	$2.22^{\pm0.02}$, 86, 0.299
4U 1608-52	$476^{\pm33}$, $0.73^{\pm0.05}$, 190 -0.200	$734^{\pm2}$, $5.0^{\pm0.4}$, 283 -0.175	$-46^{\pm60}$, $40^{\pm2}$, 299 -0.115	$1.94^{\pm0.01}$, 266 0.839	$2.26^{\pm0.02}$, 305 0.291	$2.45^{\pm0.04}$, 422 -0.615
[d]	$377^{\pm72}$, $0.89^{\pm0.11}$, 311 -0.000	$660^{\pm39}$, $6.9^{\pm0.9}$, 348 -0.000	$-194^{\pm140}$, $45^{\pm5}$, 37 0.000	$1.95^{\pm0.03}$, 519 0.715	$2.3^{\pm0.04}$, 251 -0.185	$2.33^{\pm0.06}$, 290 -0.299
[e]	$341^{\pm37}$, $0.93^{\pm0.06}$59 -0.000	$638^{\pm29}$, $7.2^{\pm0.7}$144 0.001	$-261^{\pm58}$, $47^{\pm2}$161 -0.001	$1.99^{\pm0.07}$847 0.990	$2.31^{\pm0.02}$43 0.822	$2.41^{\pm0.03}$38 -0.643
4U 1636-53	$504^{\pm15}$, $0.72^{\pm0.02}$110 -0.036	$1132^{\pm12}$, $11.4^{\pm2}$95 -0.049	$-30^{\pm30}$, $39.3^{\pm1.1}$102 -0.084	$1.88^{\pm0.01}$362 0.841	$2.16^{\pm0.01}$160 -0.204	$2.37^{\pm0.05}$537 -0.705
[f]	$309^{\pm70}$, $1.00^{\pm0.11}$298 -0.000	$622^{\pm37}$, $7.9^{\pm0.4}$325 0.005	$-322^{\pm139}$, $50^{\pm6}$295 0.000	$1.97^{\pm0.05}$822 0.842	$2.24^{\pm0.05}$282 0.034	$2.29^{\pm0.06}$254 -0.042
[g]	$362^{\pm30}$, $0.87^{\pm0.04}$326 0.000	$669^{\pm23}$, $6.0^{\pm0.4}$638 0.014	$-267^{\pm49}$, $47^{\pm2}$218 -0.005	$1.84^{\pm0.01}$1867 0.951	$2.20^{\pm0.02}$746 0.680	$2.55^{\pm0.04}$250 -0.242
[h]	$300^{\pm61}$, $1.00^{\pm0.09}$, 195 0.000	$643^{\pm28}$, $7.2^{\pm0.6}$, 167 0.002	$-397^{\pm135}$, $53^{\pm5}$, 233 0.002	$1.92^{\pm0.01}$549 0.931	$2.18^{\pm0.07}$565 0.584	$2.34^{\pm0.06}$179 0.250
[i]	$524^{\pm33}$, $0.70^{\pm0.04}$, 271 -0.000	$776^{\pm20}$, $4.8^{\pm0.4}$, 381 0.020	$19^{\pm60}$, $38^{\pm2}$, 229 -0.229	$1.83^{\pm0.01}$, 289 0.606	$2.20^{\pm0.01}$, 194 -0.295	$2.33^{\pm0.05}$, 571 -0.755
[j]	$475^{\pm72}$, $0.74^{\pm0.08}$, 16 0.001	$801^{\pm35}$, $4.2^{\pm0.5}$, 15 -0.003	$-1.78^{\pm146}$, $44^{\pm5}$, 16 0.002	$1.81^{\pm0.01}$, 63 0.879	$2.20^{\pm0.01}$, 206 0.877	$2.58^{\pm0.02}$, 17 -0.667
[k]	$494^{\pm120}$, $0.75^{\pm0.17}$, 154 -0.000	$755^{\pm65}$, $5.4^{\pm1.3}$, 174 0.003	$-29^{\pm232}$, $40^{\pm9}$, 144 -0.002	$1.84^{\pm0.02}$, 126 0.543	$2.22^{\pm0.03}$, 102 -0.396	$2.24^{\pm0.06}$, 166 -0.646
[l]	$-575^{\pm715}$, $1.93^{\pm0.79}$, 51 -0.000	$292^{\pm365}$, $10.8^{\pm4}$, 51 -0.004	$-2309^{\pm1475}$, $116^{\pm47}$, 51 0.003	$1.72^{\pm0.01}$, 129 0.708	$2.10^{\pm0.01}$, 157 0.520	$2.41^{\pm0.02}$, 75 -0.625
4U 1728-34	$304^{\pm43}$, $1.06^{\pm0.06}$, 47 0.362	$702^{\pm20}$, $7.0^{\pm0.4}$, 45 0.312	$-496^{\pm90}$, $58^{\pm3}$, 50 0.411	$1.72^{\pm0.02}$, 358 0.930	$2.02^{\pm0.02}$, 97 0.493	$2.05^{\pm0.01}$, 54 0.266
[m]	$500^{\pm41}$, $0.78^{\pm0.05}$, 123 0.000	$796^{\pm24}$, $5.2^{\pm0.4}$, 157 0.005	$-95^{\pm77}$, $43^{\pm3}$, 108 -0.003	$1.73^{\pm0.01}$, 209 0.766	$2.07^{\pm0.01}$, 68 -0.076	$2.11^{\pm0.03}$, 182 -0.747
[n]	$296^{\pm48}$, $1.05^{\pm0.07}$, 556 -0.000	$545^{\pm52}$, $9.5^{\pm1.1}$, 1814 -0.018	$-264^{\pm63}$, $49^{\pm2}$, 258 0.008	$1.77^{\pm0.04}$, 1343 0.926	$2.07^{\pm0.03}$, 253 -0.454	$2.13^{\pm0.05}$, 292 -0.175
[o]	$342^{\pm47}$, $0.95^{\pm0.07}$, 273 -0.000	$660^{\pm23}$, $6.9^{\pm0.5}$, 240 -0.008	$-309^{\pm101}$, $50^{\pm4}$, 314 -0.003	$1.90^{\pm0.01}$, 1202 0.907	$2.15^{\pm0.04}$, 432 0.258	$2.29^{\pm0.05}$, 259 -0.155
[p]	$343^{\pm44}$, $0.95^{\pm0.06}$, 240 -0.000	$660^{\pm22}$, $6.9^{\pm0.4}$, 221 -0.008	$-303^{\pm93}$, $50^{\pm4}$, 274 -0.003	$1.91^{\pm0.01}$, 1166 0.917	$2.15^{\pm0.04}$, 365 0.302	$2.29^{\pm0.05}$, 227 -0.261
[q]	$441^{\pm49}$, $0.86^{\pm0.07}$, 231 -0.000	$744^{\pm31}$, $6.0^{\pm0.6}$, 337 -0.003	$-175^{\pm88}$, $46^{\pm3}$, 190 -0.000	$1.74^{\pm0.03}$, 611 0.884	$2.05^{\pm0.02}$, 117 -0.281	$2.10^{\pm0.05}$, 270 -0.283
4U 1735-44	$371^{\pm44}$, $0.90^{\pm0.06}$, 25 -0.432	$717^{\pm21}$, $5.8^{\pm0.3}$, 23 -0.346	$-322^{\pm91}$, $50^{\pm3}$, 26 -0.476	$1.83^{\pm0.02}$, 211 0.656	$2.22^{\pm0.02}$, 116 0.314	$2.38^{\pm0.01}$, 22 0.972
[r]	$659^{\pm16}$, $0.50^{\pm0.02}$, 2 0.001	$830^{\pm8}$, $3.7^{\pm0.2}$, 2 0.002	$315^{\pm31}$, $26^{\pm1}$, 2 0.001	$1.88^{\pm0.01}$, 23 -0.979	$2.26^{\pm0.06}$, 197 -0.998	$1.66^{\pm0.09}$, 280 -1.000
4U 1820-30	$334^{\pm53}$, $0.91^{\pm0.07}$, 55 -0.024	$678^{\pm27}$, $6.0^{\pm0.5}$, 55 0.629	-356 ± 106, $50^{\pm0.4}$, 56 -0.043	$1.93^{\pm0.01}$, 162 0.807	$2.35^{\pm0.01}$, 151 0.756	$2.57^{\pm0.02}$, 53 -0.454
[s]	$182^{\pm117}$, $1.12^{\pm0.16}$, 63 0.000	$586^{\pm6}$, $7.8^{\pm1.2}$, 74 0.001	$-374^{\pm224}$, $51^{\pm8}$, 59 -0.000	$1.93^{\pm0.33}$, 403 0.944	$2.36^{\pm0.04}$, 256 0.851	$2.55^{\pm0.04}$, 77 0.472
4U 1915-05	$265^{\pm16}$, $1.13^{\pm0.03}$, 50 -0.396	$457^{\pm31}$, $13^{\pm1.0}$, 561 -0.364	$-183^{\pm26}$, $46^{\pm1}$, 34 0.269	$1.85^{\pm0.05}$, 655 0.969	$2.00^{\pm0.16}$, 832 -0.996	$2.00^{\pm0.16}$, 832 -0.963
SCO X-1	$368^{\pm7}$, $0.73^{\pm0.01}$, 70 -0.304	$722^{\pm5}$, $5.2^{\pm0.1}$, 43 -0.399	$-44^{\pm10}$, $39^{\pm1}$, 10 -0.224	$2.0^{\pm0.01}$, 170 0.983	$2.47^{\pm0.02}$, 170, 49 0.165	$1.82^{\pm0.01}$, 173 -0.714
[t]	$441^{\pm21}$, $0.77^{\pm0.03}$, 65 -0.000	$698^{\pm16}$, $5.6^{\pm0.3}$, 149 0.012	$-81^{\pm32}$, $40^{\pm1}$, 37 -0.007	$1.97^{\pm0.02}$, 314 0.979	$2.32^{\pm0.01}$, 40 0.030	$2.48^{\pm0.01}$, 219 -0.879
[u]	$430^{\pm5}$, $0.79^{\pm0.01}$, 15 0.487	$695^{\pm5}$, $5.8^{\pm0.1}$, 46 0.587	$-105^{\pm8}$, $41^{\pm1}$, 8 0.312	$1.96^{\pm0.01}$, 257 0.984	$2.33^{\pm0.01}$, 46 -0.648	$2.46^{\pm0.02}$, 115 -0.435
[v]	$646^{\pm253}$, $0.52^{\pm0.31}$, 81 -0.338	$858^{\pm126}$, $3.2^{\pm1.9}$, 81 0.001	$221^{\pm507}$, $30^{\pm18}$, 81 -0.000	$1.90^{\pm0.01}$, 61 0.069	$2.31^{\pm0.01}$, 70 0.400	$2.63^{\pm0.04}$, 76 -0.868
Cir X-1	$126^{\pm51}$, $2.15^{\pm0.40}$, 454 -0.179	$204^{\pm38}$, $122.8^{\pm28.3}$, 549 -0.254	$-85^{\pm82}$, $43^{\pm7}$, 367 -0.102	$2.06^{\pm0.13}$, 345 0.325	—	$1.29^{\pm0.12}$, 357 0.007
GX5-1	$378^{\pm13}$, $0.84^{\pm0.04}$, 287 -0.143	$503^{\pm14}$, $12^{\pm1}$, 920 -0.020	$100^{\pm18}$, $31^{\pm1}$, 143 -0.122	$2.16^{\pm0.03}$, 259 -0.763	$1.62^{\pm0.50}$, 4133 -0.969	$2.04^{\pm0.12}$, 1538 -0.951
GX 17+2	$355^{\pm37}$, $0.88^{\pm0.06}$, 176 -0.140	$625^{\pm24}$, $6.9^{\pm0.6}$, 281 -0.262	$-194^{\pm65}$, $44^{\pm3}$, 135 -0.110	$2.07^{\pm0.04}$, 645 0.932	$2.43^{\pm0.02}$, 82 0.281	$2.56^{\pm0.05}$, 169 -0.232
[w]	$300^{\pm20}$, $0.99^{\pm0.03}$, 43 0.000	$600^{\pm12}$, $7.9^{\pm0.3}$, 59 -0.001	$-313^{\pm44}$, $49^{\pm2}$, 54 -0.002	$2.04^{\pm0.01}$, 781 0.973	$2.30^{\pm0.02}$, 130 0.216	$2.40^{\pm0.02}$, 42 0.069
GX340+0	$378^{\pm32}$, $0.89^{\pm0.09}$, 598 0.172	$522^{\pm24}$, $13^{\pm2}$, 1049 0.941	$72^{\pm55}$, $33^{\pm3}$, 444 0.081	$2.08^{\pm0.05}$, 419 -0.351	$0.68^{\pm0.65}$, 3169 -0.889	$1.85^{\pm0.13}$, 1211 -0.764
Average $\lvert p \rvert$	0.100	0.136	0.084	0.808	0.469	0.492

[a] - Ford et al. (1997), [b] - van Straaten et al. (2000), [c] - Boutelier et al. (2009), [d] - du Buisson et al. (2019), [e] - van Straaten et al. (2003), [f] - van Doesburgh & van der Klis (2017), [g] - Lin et al. (2011), [h] - Altamirano et al. (2008), [i] - Barret et al. (2005), [j] - Di Salvo et al. (2003), [k] - Jonker et al. (2002), [l] - Wijnands et al. (1997), [m] - Barret et al. (2006), [n] - Migliari et al. (2003), [o] - van Straaten et al. (2002), [p] - Di Salvo et al. (2001) , [q] Mendez & van der Klis (1999), [r] - Ford et al. (1998), [s] - Barret et al. (2006), [t] - Lin et al. (2011), [u] - Mendez van der Klis (2000), [v] - van der Klis et al. (1996), [w] - Wijnands et al. (1997)

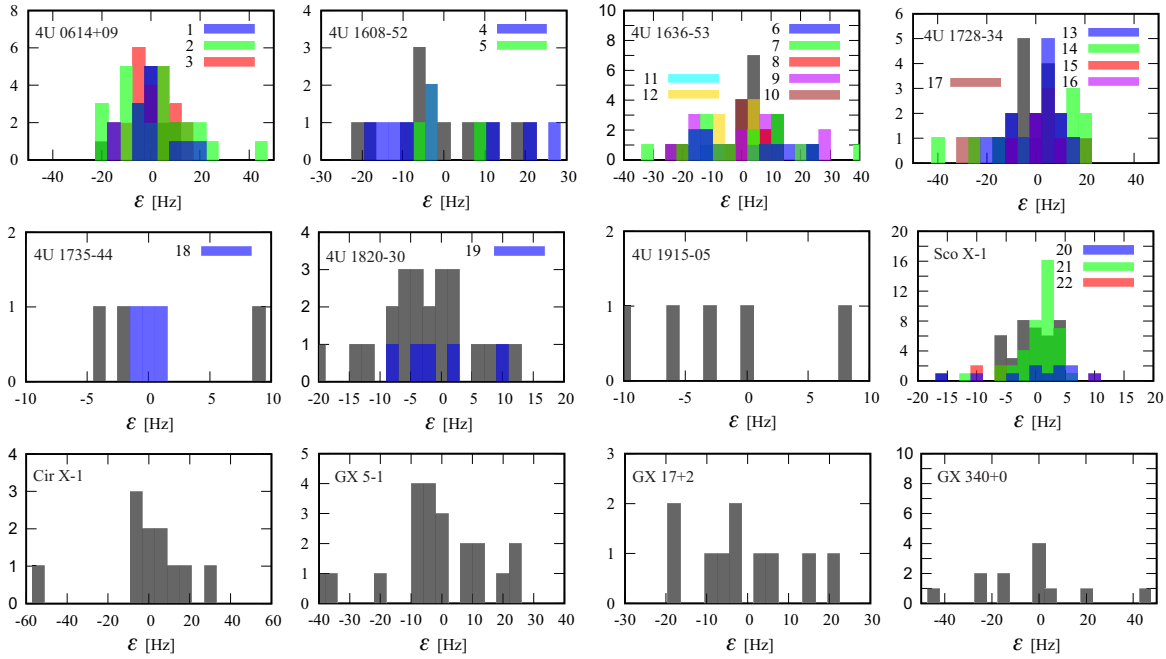

Figure 3.18. Histograms of ε for linear relation and different sources. References: 1-[43], 2-[44], 3 - [45], 4 - [22], 5-[23], 6 [24] , 7-[25] , 8-[26], 9-[19], 10-[27], 11-[28], 12-[29], 13-[38], 14-[39], 15-[40], 16-[41], 17-[42], 18-[30], 19-[38], 20-[25], 21-[35], 22-[36], 23-[33]. The black column corresponds to data which we originally used in papers [4–8, 13, 48, 49] and their referencies can be found in Table 1.2.

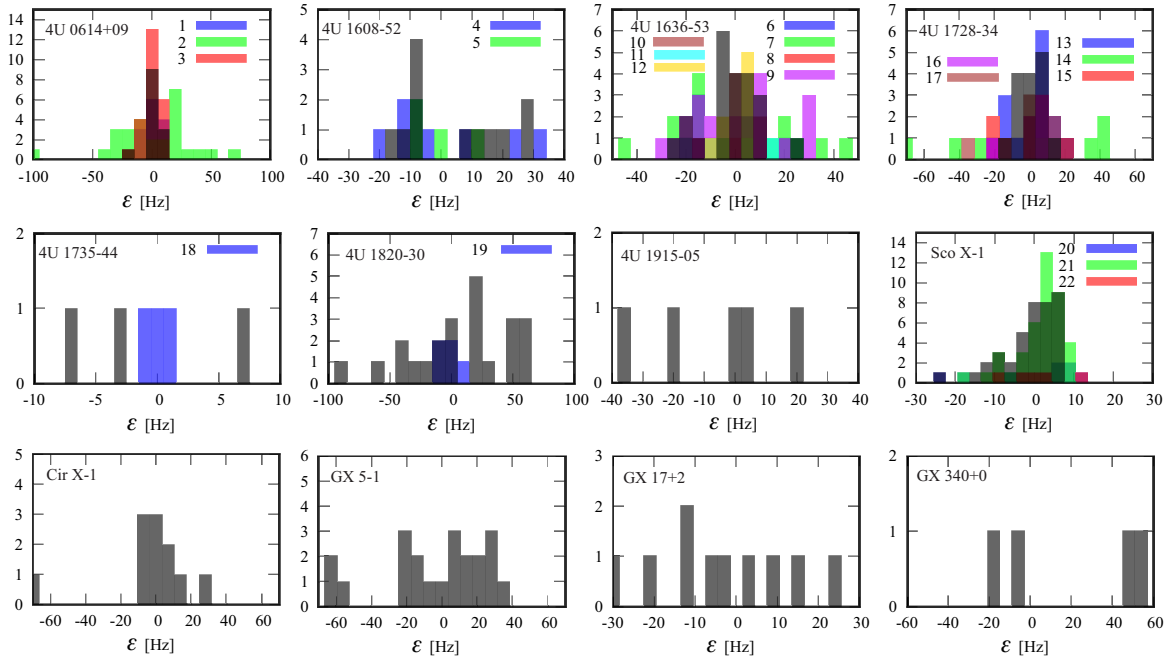

Figure 3.19. The same as 3.18 but for the quadratic relation.

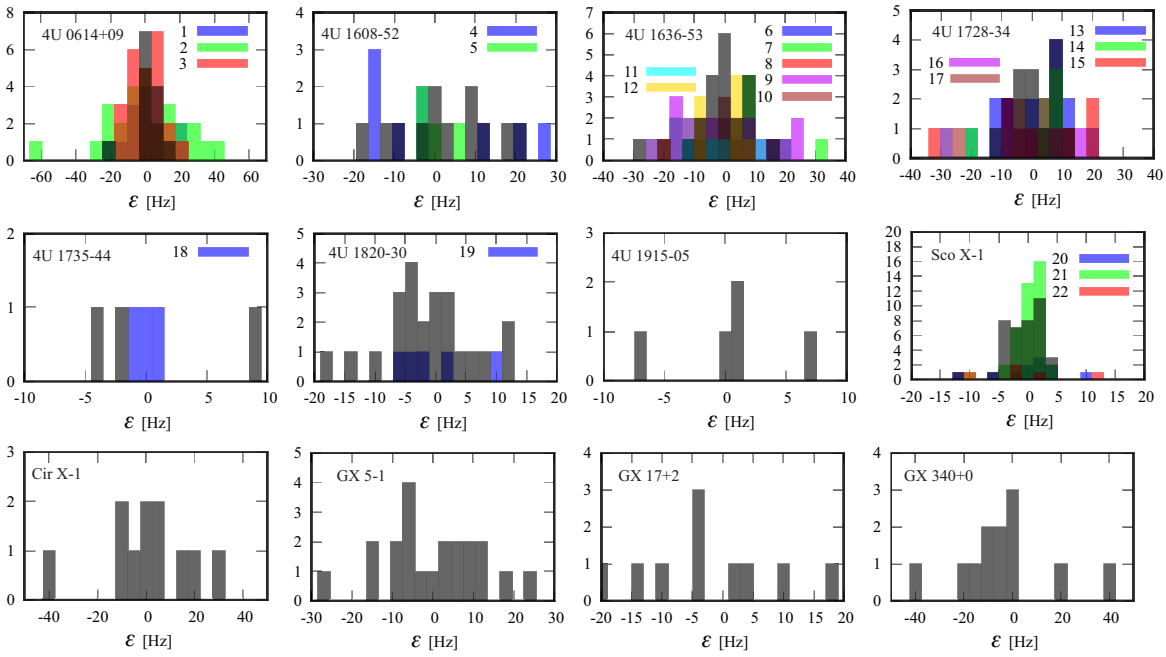

Figure 3.20. The same as 3.18 but for the square-root relation.

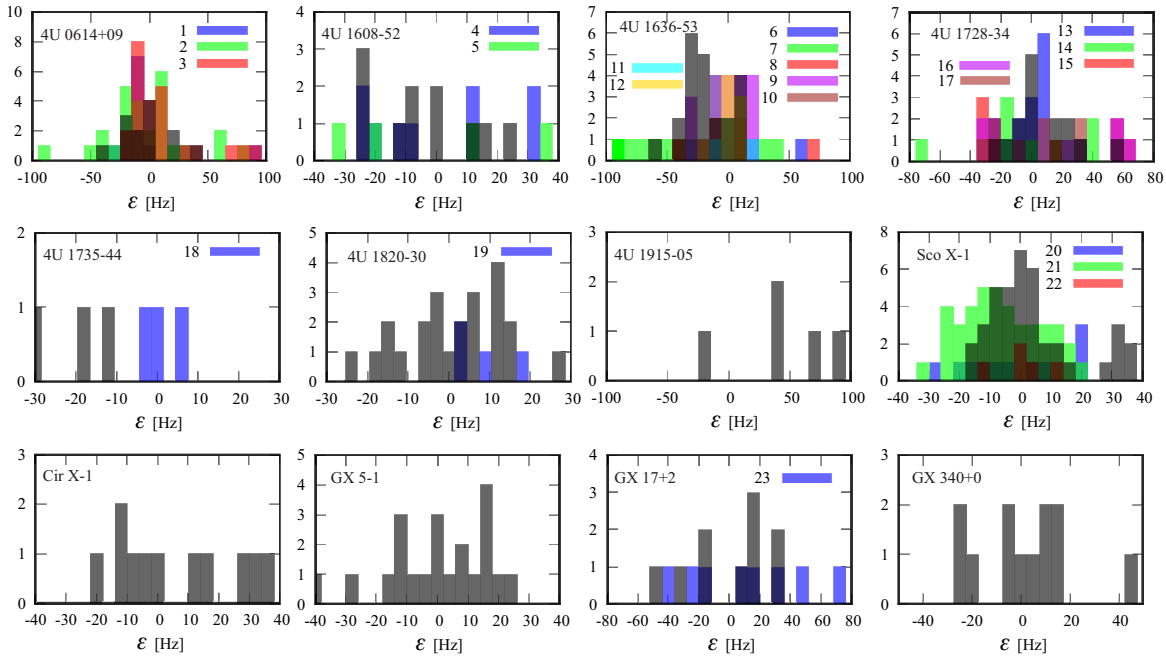

Figure 3.21. The same as 3.18 but for the RP model.

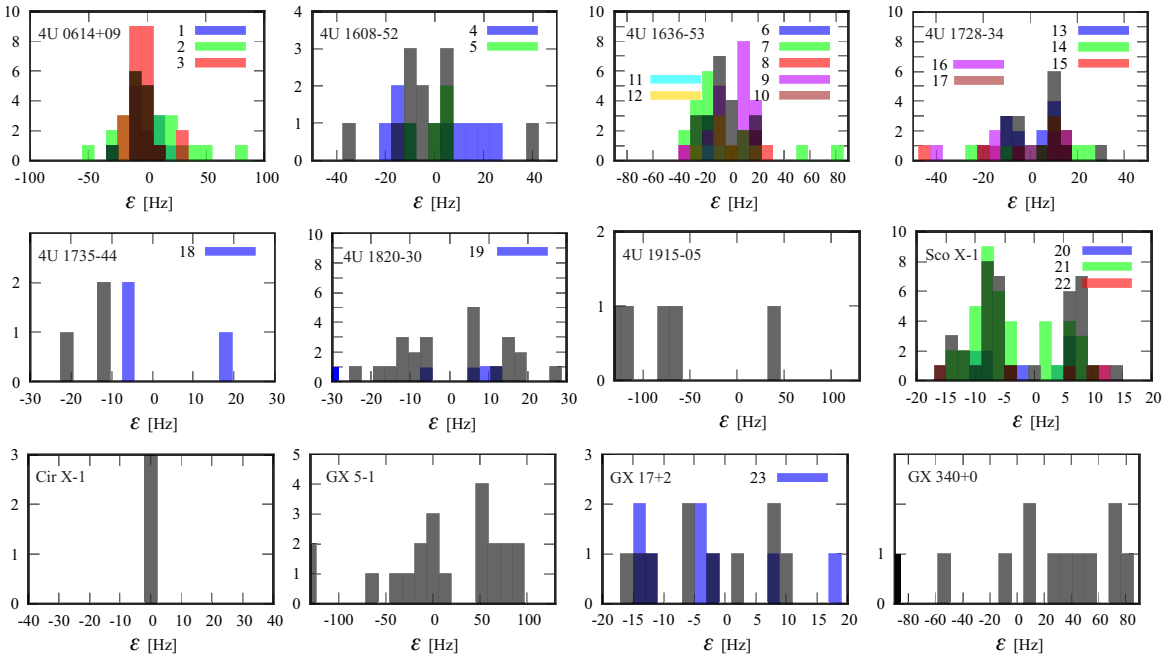

Figure 3.22. The same as 3.18 but for the TD model.

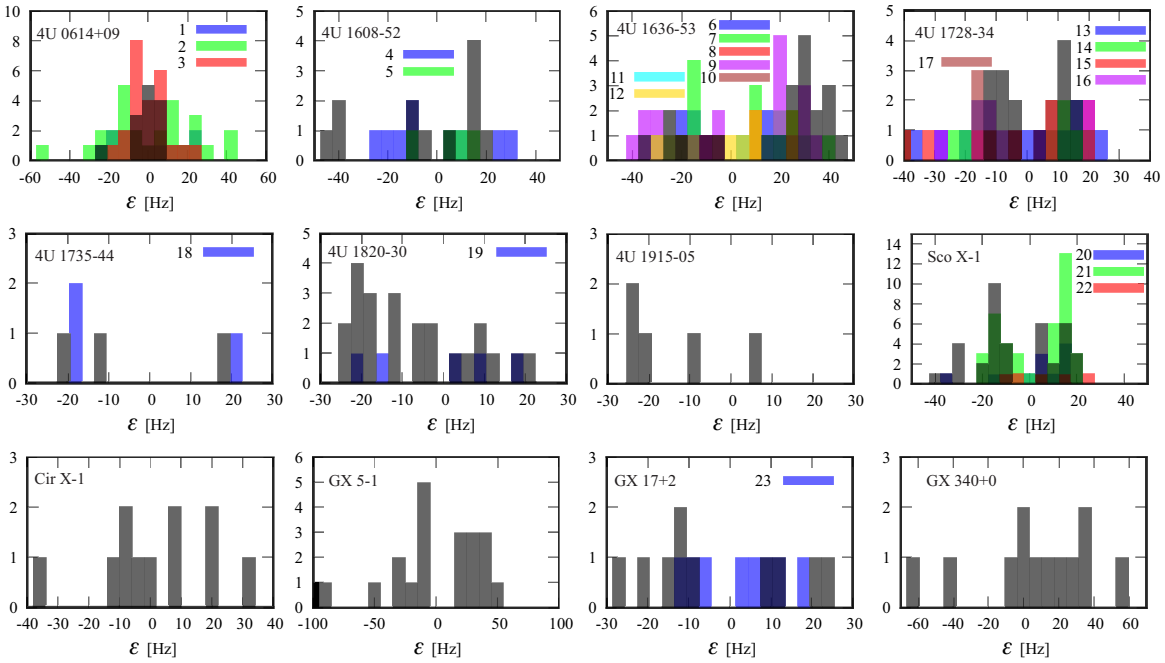

Figure 3.23. The same as 3.18 but for the WD model.

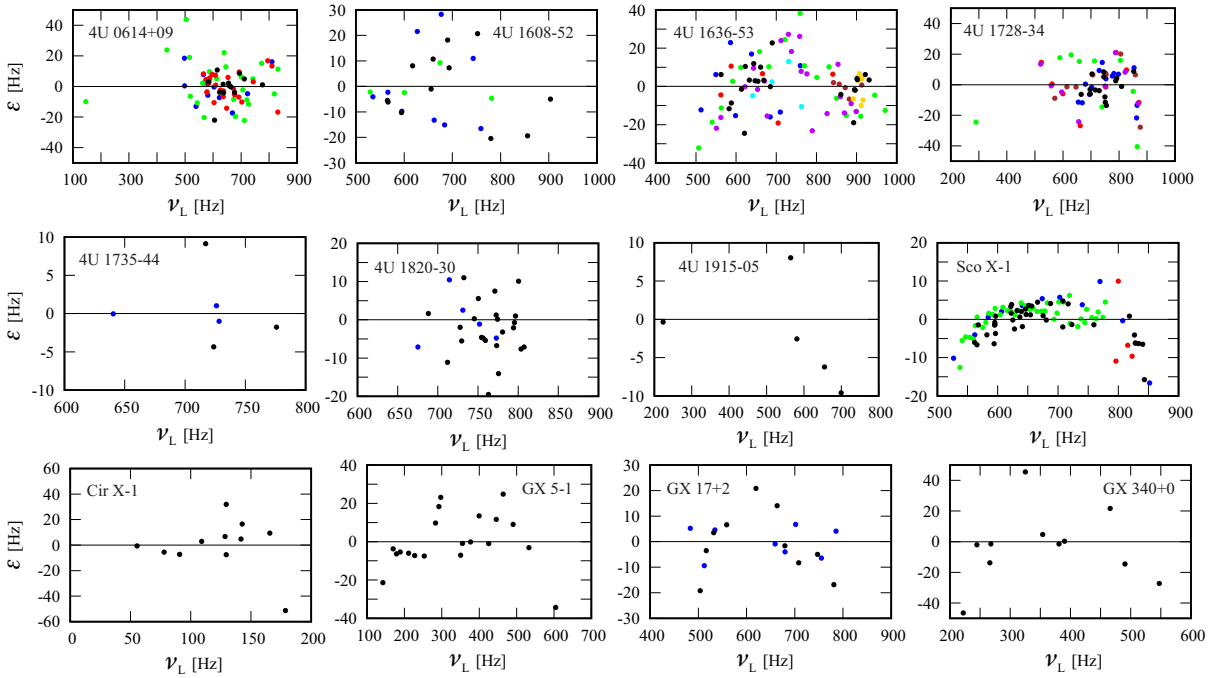

Figure 3.24. Dependency of ε on ν_L for the linear relation and different sources.

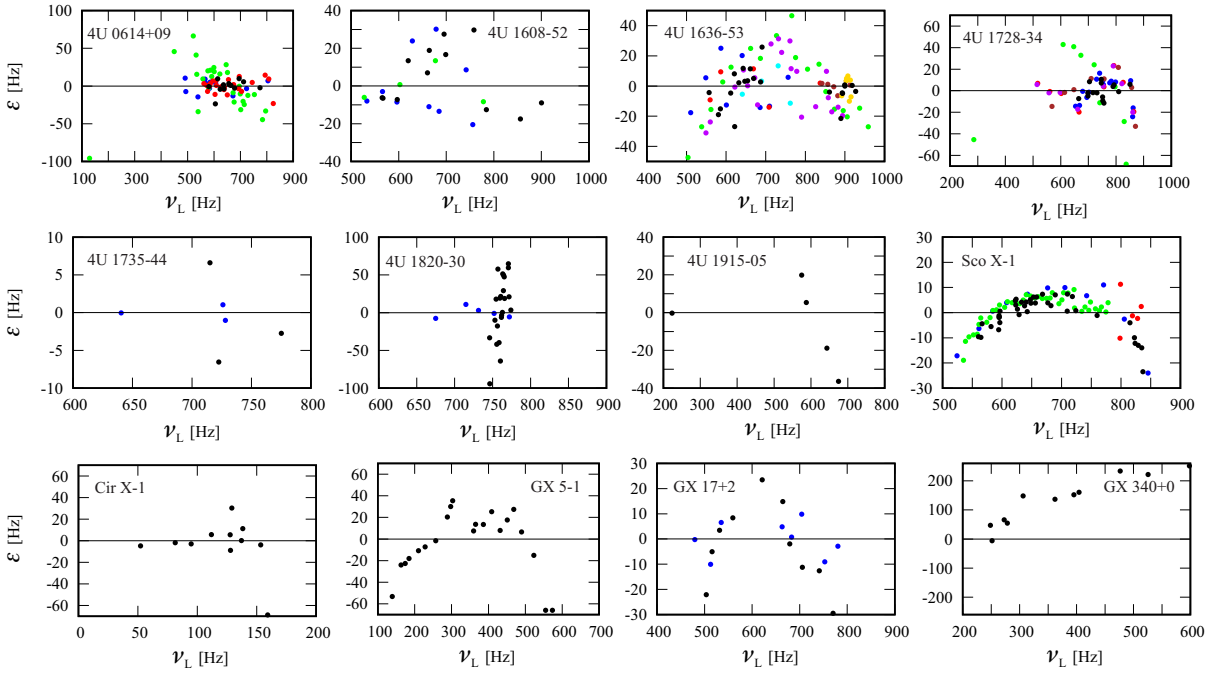

Figure 3.25. The same as 3.24 but for the quadratic relation.

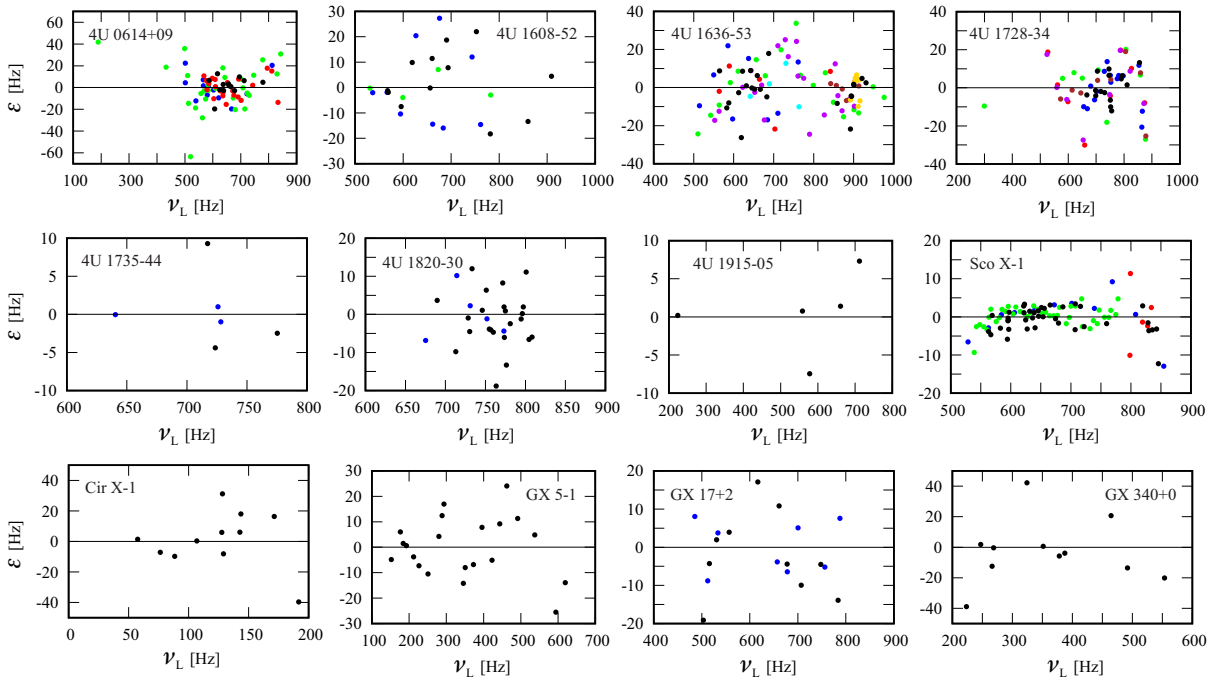

Figure 3.26. The same as 3.24 but for the square-root relation.

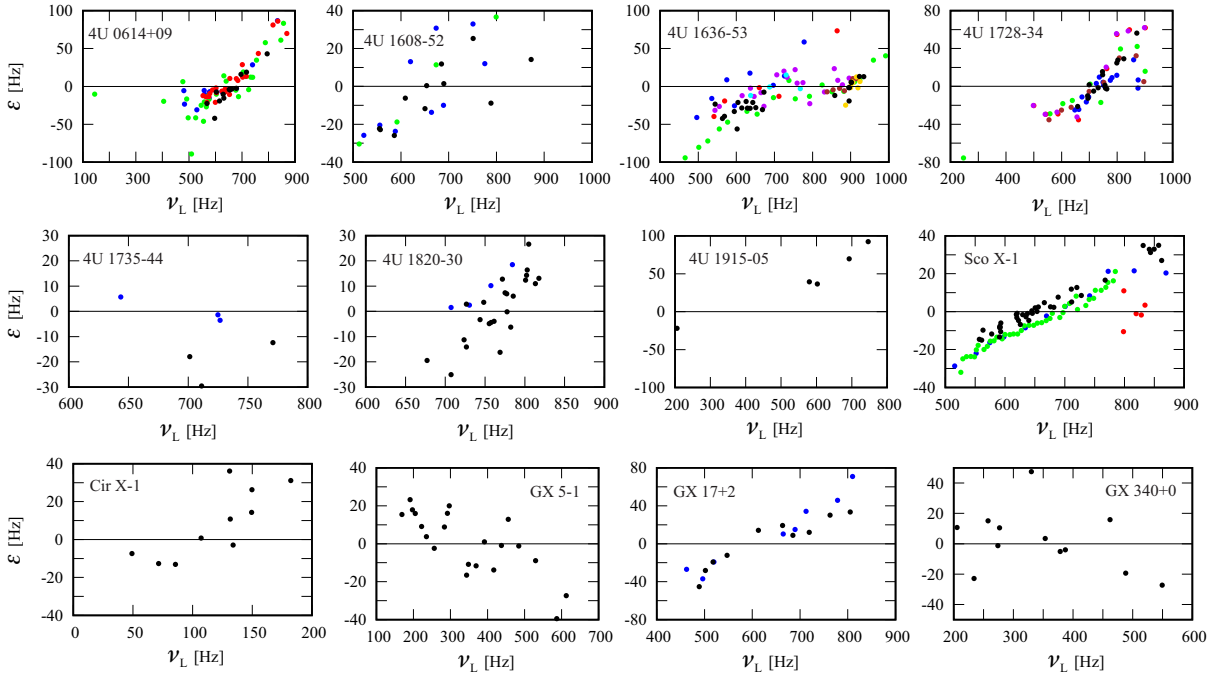

Figure 3.27. The same as 3.24 but for the RP model.

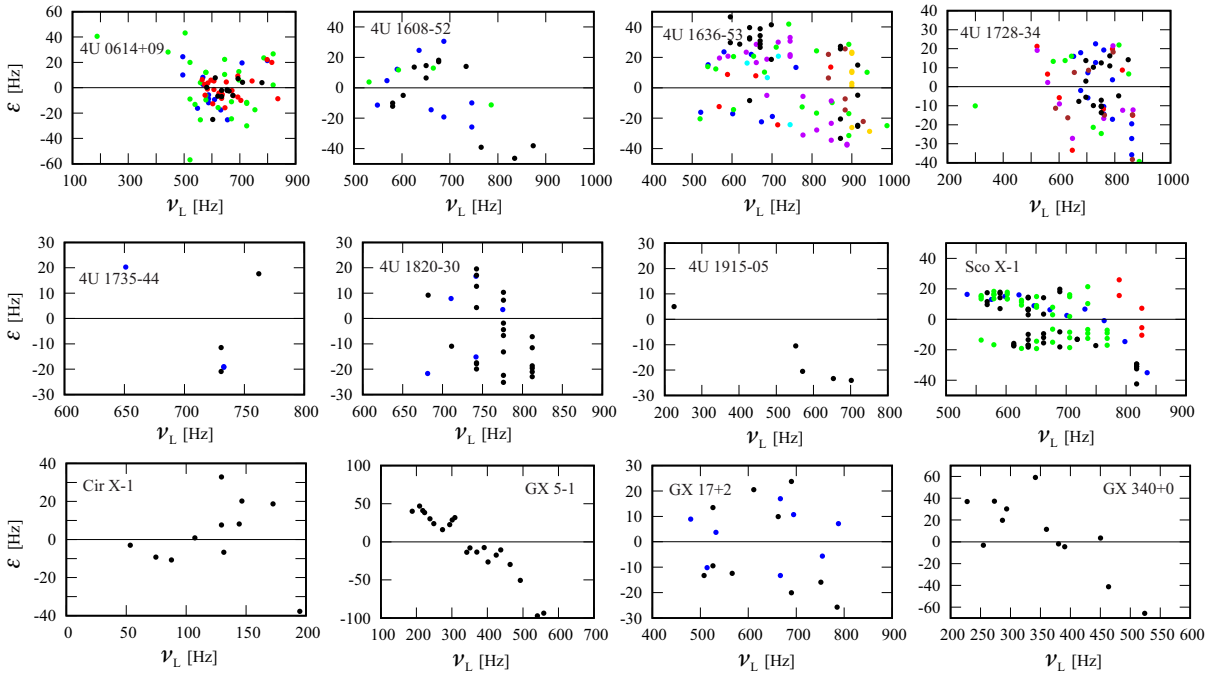

Figure 3.28. The same as 3.24 but for the WD model.

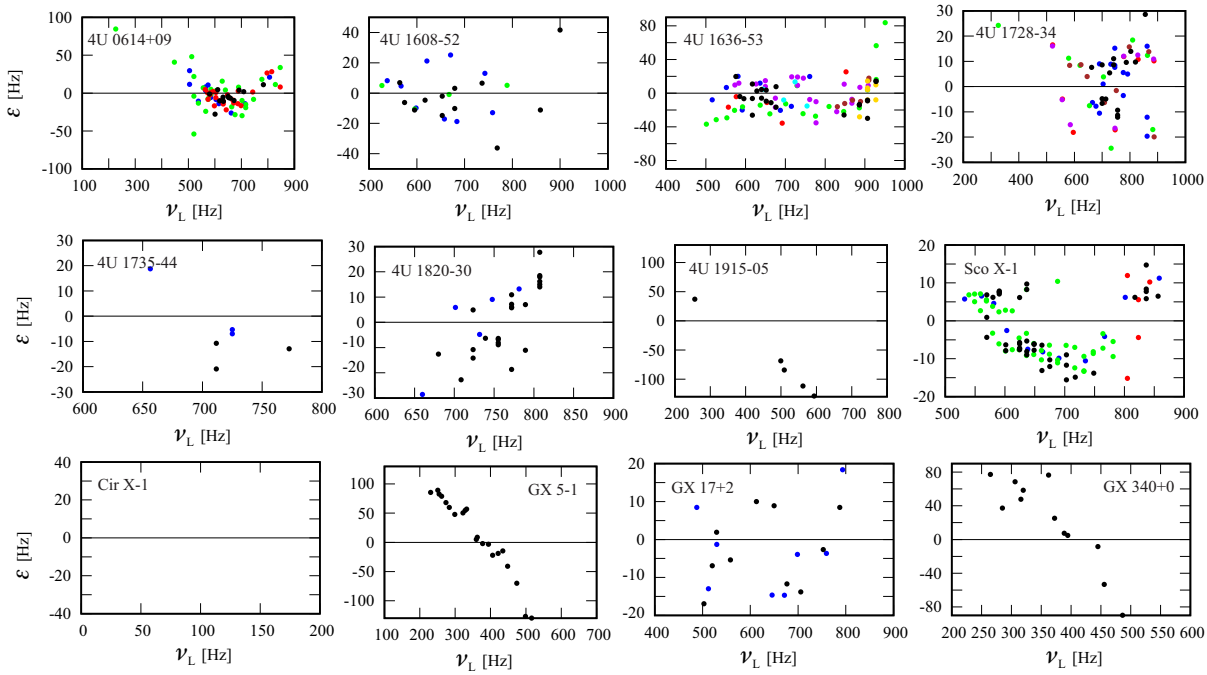

Figure 3.29. The same as 3.24 but for the TD model.

3.2. Our models

Here, I will focus on three models that were proposed by us in our publications. These are the Cusp torus model (see Section 2.4), and the one-parameter and two-parametric relations (see Section 2.5). In the left panel of Figure 3.30, one can see comparison between the one-parameter relation and the CT model in the Schwarzschild geometry. The one-parameter relation is a perfect approximation of the CT model. Therefore, we will no longer work with the CT model, but only with this approximation[1]. In the first two columns of Table 3.2, the best-fit parameters are obtained by fitting the observed data by the one-parameter and two-parametric relations.

So far, we have only worked with the one-parameter relation (CT model) in the Schwarzschild geometry. During the writing of this dissertation, we managed to generalise the relation for Kerr and Hartle-Thorne geometry (see article [15]). In the right panels of Figure 3.30, one can see a comparison between the CT model in the HT geometry and the new one-parameter relation

$$\nu_{\mathrm{L}} = \nu_{\mathrm{U}} \left[1 - (0.8 - 0.2j)\sqrt{1 + 8j\mathscr{V}_0 - 6\mathscr{V}_0^{2/3} - (\frac{1}{3}(8j^2 - 17q))\mathscr{V}_0^{4/3}} \right], \tag{3.2}$$

where $\mathscr{V}_0 \equiv \frac{\nu_{\mathrm{U}}/\nu_0}{6^{3/2} - j\nu_{\mathrm{U}}/\nu_0}$, $\nu_0 = 2198\frac{\mathrm{M}_\odot}{M}$.

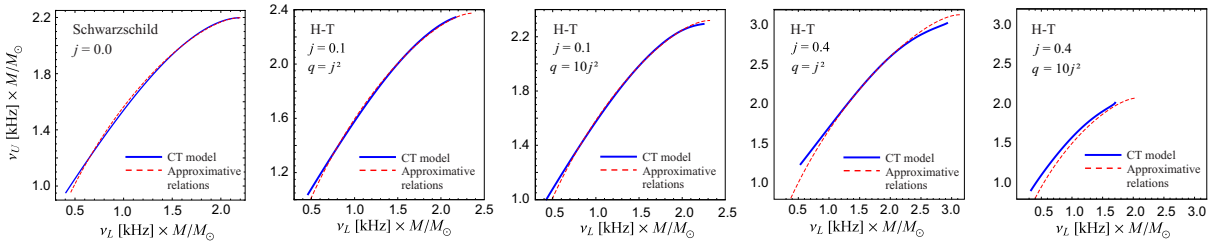

Figure 3.30. Comparison between the CT model (numerical calculations) and the one-parameter relation. Left: the Schwarzschild geometry. Right: the Hartle-Thorne geometry.

For most sources, this relation may be used as a very good approximation of the CT model. As usual (see [7]), the transition to HT geometry does not imply a significant improvement in the quality of the fit. Instead of the specific combination of mass M, quadrupole moment q, and spin j corresponding to the best fit, we obtain the dependence of one quantity on the others. You can see such dependence in Figure 3.30 for 4U 1636-53 and 4U 1728-34. For all the sources investigated in this thesis, the results are similar in the sense that all curves of the "best" mass as a function of q for all j intersect in approximately one place for a quadrupole moment around

[1] Here, it is worth mentioning that, in the case of the CT model, there is a lower limit on the value of frequencies, while there is no such thing for the one-parameter relation (see [8]).

Table 3.2. Similar to 3.1 but for for one-parameter and two-parametric relations.

	one-par. rel. M,p	two-par. rel. M,B,p	one-par. HT *Mass*		one-par. rel. M,p	two-par. rel. M,B,p	one-par. HT *Mass*
4U 0614+52	$1.72^{\pm0.02}$ 0.807	$1.29^{\pm0.14}$,$0.58^{\pm0.05}$ 0.229	1.78	4U 1735-44	$1.71^{\pm0.01}$ 0.145	$1.50^{\pm0.08}$,$0.63^{\pm0.05}$ -0.497	1.75
[a]	$0.70^{\pm0.02}$ 0.597	$1.47^{\pm0.1}$,$0.68^{\pm0.4}$ −0.066	1.75	[r]	$1.71^{\pm0.03}$ -0.996	$1.95^{\pm0.01}$,$1.16^{\pm0.04}$ 0.017	1.78
[b]	$1.7^{\pm0.02}$, 0.183	$1.56^{\pm0.08}$,$1.7^{\pm0.4}$, −0.168	1.75	4U 1820-30	$1.81^{\pm0.01}$ 0.605	$1.55^{\pm0.11}$,$0.59^{\pm0.06}$ −0.044	1.9
[c]	$1.69^{\pm0.02}$, 0.820	$1.35^{\pm0.07}$,$0.61^{\pm0.03}$, −0.024	1.75	[s]	$1.81^{\pm0.03}$ 0.884	$1.53^{\pm0.44}$,$0.58^{\pm0.11}$ 0.031	1.9
4U 1608-52	$1.79^{\pm0.02}$ 0.098	$1.78^{\pm0.04}$,$0.80^{\pm0.04}$ 0.018	1.84	4U 1915-05	$1.61^{\pm0.02}$ -0.414	$1.62^{\pm0.05}$,$0.80^{\pm0.03}$ 0.285	1.66
[d]	$1.77^{\pm0.03}$, 0.263	$1.68^{\pm0.14}$,$0.74^{\pm0.09}$ 0.019	1.84	SCO X-1	$1.82^{\pm0.01}$ 0.034	$1.82^{\pm0.01}$,$0.80^{\pm0.01}$ −0.104	1.87
[e]	$1.78^{\pm0.03}$ 0.933	$1.63^{\pm0.06}$,$0.68^{\pm0.03}$ 0.028	1.87	[t]	$1.82^{\pm0.01}$ 0.316	$1.80^{\pm0.02}$,$0.79^{\pm0.02}$ 0.062	1.87
4U 1636-53	$1.71^{\pm0.01}$ −0.155	$1.71^{\pm0.02}$,$0.81^{\pm0.02}$ −0.155	1.78	[u]	$1.80^{\pm0.01}$ 0.626	$1.78^{\pm0.01}$,$0.77^{\pm0.01}$ 0.027	1.87
[f]	$1.75^{\pm0.04}$ 0.554	$1.51^{\pm0.19}$,$0.66^{\pm0.08}$ −0.002	1.81	[v]	$1.80^{\pm0.01}$ −0.155	$1.87^{\pm0.18}$,$0.92^{\pm0.42}$ −0.015	1.87
[g]	$1.77^{\pm0.02}$ 0.827	$1.63^{\pm0.04}$,$0.65^{\pm0.03}$ 0.071	1.81	Cir X-1	$0.80^{\pm0.15}$ -0.330	$1.82^{\pm0.6}$,$0.96^{\pm0.10}$ −0.100	0.74
[h]	$1.74^{\pm0.05}$ 0.815	$1.40^{\pm0.18}$,$0.60^{\pm0.07}$ −0.049	1.81	GX5-1	$1.75^{\pm0.08}$ -0.951	$2.31^{\pm0.03}$,$1.11^{\pm0.02}$ −0.002	1.81
[i]	$1.7^{\pm0.01}$ -0.315	$1.75^{\pm0.03}$,$0.86^{\pm0.04}$ 0.028	1.75	GX 17+2	$1.89^{\pm0.02}$ 0.601	$1.78^{\pm0.07}$,$0.72^{\pm0.04}$ 0.011	1.96
[j]	$1.73^{\pm0.01}$ 0.663	$1.62^{\pm0.08}$,$0.65^{\pm0.08}$ −0.012	1.81	[w]	$1.79^{\pm0.03}$ 0.881	$1.56^{\pm0.06}$,$0.65^{\pm0.03}$ −0.042	1.87
[k]	$1.69^{\pm0.02}$ −0.178	$1.74^{\pm0.15}$,$0.85^{\pm0.16}$ 0.028	1.75	GX 340+0	$1.61^{\pm0.10}$ -0.771	$2.21^{\pm0.10}$,$1.08^{\pm0.06}$ 0.101	1.66
[l]	$1.64^{\pm0.01}$ 0.672	$0^{\pm0.02}$,$0.23^{\pm0.37}$ 0.336	1.72				
4U 1728-34	$1.55^{\pm0.01}$ 0.820	$1.19^{\pm0.10}$,$0.58^{\pm0.04}$ 0.414	1.63				
[m]	$1.58^{\pm0.01}$ 0.036	$1.58^{\pm0.05}$,$0.80^{\pm0.05}$ 0.037	1.63				
[n]	$1.60^{\pm0.02}$ 0.590	$1.50^{\pm0.06}$0.72$^{\pm0.04}$ 0.081	1.66				
[o]	$1.69^{\pm0.04}$ 0.662	$1.49^{\pm0.11}$,$0.65^{\pm0.06}$ −0.038	1.72				
[p]	$1.69^{\pm0.04}$ 0.676	$1.50^{\pm0.10}$,$0.66^{\pm0.06}$ −0.034	1.72				
[q]	$1.58^{\pm0.02}$ 0.321	$1.54^{\pm0.06}$,$0.76^{\pm0.05}$ 0.047	1.66				
				Average $\|p\|$	0.534	0.092	

[a] - Ford et al. (1997), [b] - van Straaten et al. (2000), [c] - Boutelier et al. (2009), [d] - du Buisson et al. (2019), [e] - van Straaten et al. (2003), [f] - van Doesburgh & van der Klis (2017), [g] - Lin et al. (2011), [h] - Altamirano et al. (2008), [i] - Barret et al. (2005), [j] - Di Salvo et al. (2003), [k] - Jonker et al. (2002), [l] - Wijnands et al. (1997), [m] - Barret et al. (2006), [n] - Migliari et al. (2003), [o] - van Straaten et al. (2002), [p] - Di Salvo et al. (2001) , [q] Mendez & van der Klis (1999), [r] - Ford et al. (1998), [s] - Barret et al. (2006), [t] - Lin et al. (2011), [u] - Mendez van der Klis (2000), [v] - van der Klis et al. (1996), [w] - Wijnands et al. (1997)

3-4 j^2 (see Figure 3.31). In the third column of Table 3.2, we therefore state the value of this mass (the mass for which the curves intersect)[2].

In Figures 3.32 and 3.33, there are histograms of ε (Equation 3.1). Figures 3.34 and 3.35 show the dependency of ε on ν_L.

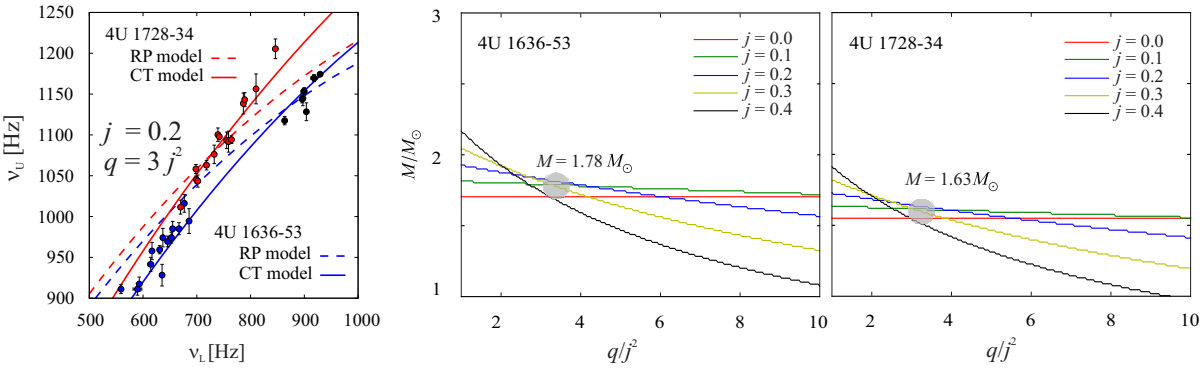

Figure 3.31. Best fits of the data of the 4U 1636-53 and 4U 1728-34 atoll sources found for the RP and CT models and a particular choice of the NS spin and oblateness. For the other choices within the range of parameters, $j \in [0, 0.4]$ and $q/j^2 \in [1, 10]$, the resulting fits are similar. The other atoll sources reveal a fully analogic behaviour.

[2] To obtain this mass, we fit the resulting plane of the best combinations of mass and spins for a given q by the relation: $\nu_L = a * j * q + b * j + mass$, where a, b are constants.

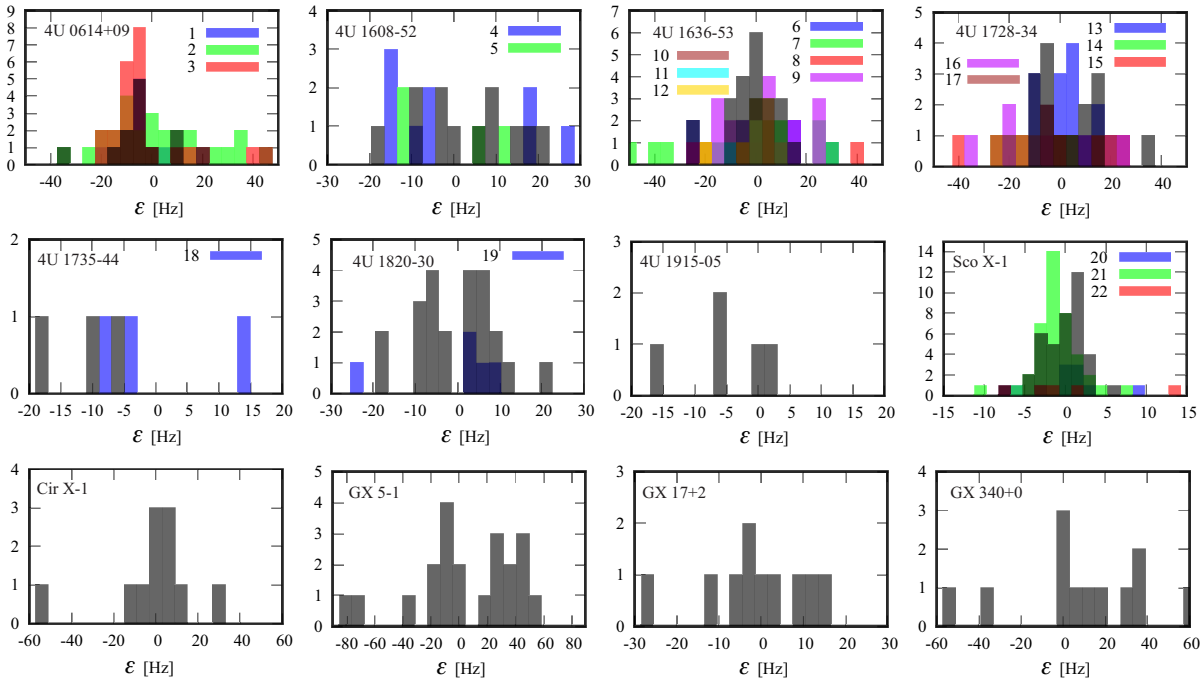

Figure 3.32. The same as in 3.18 but for the one-parameter relation 1.2

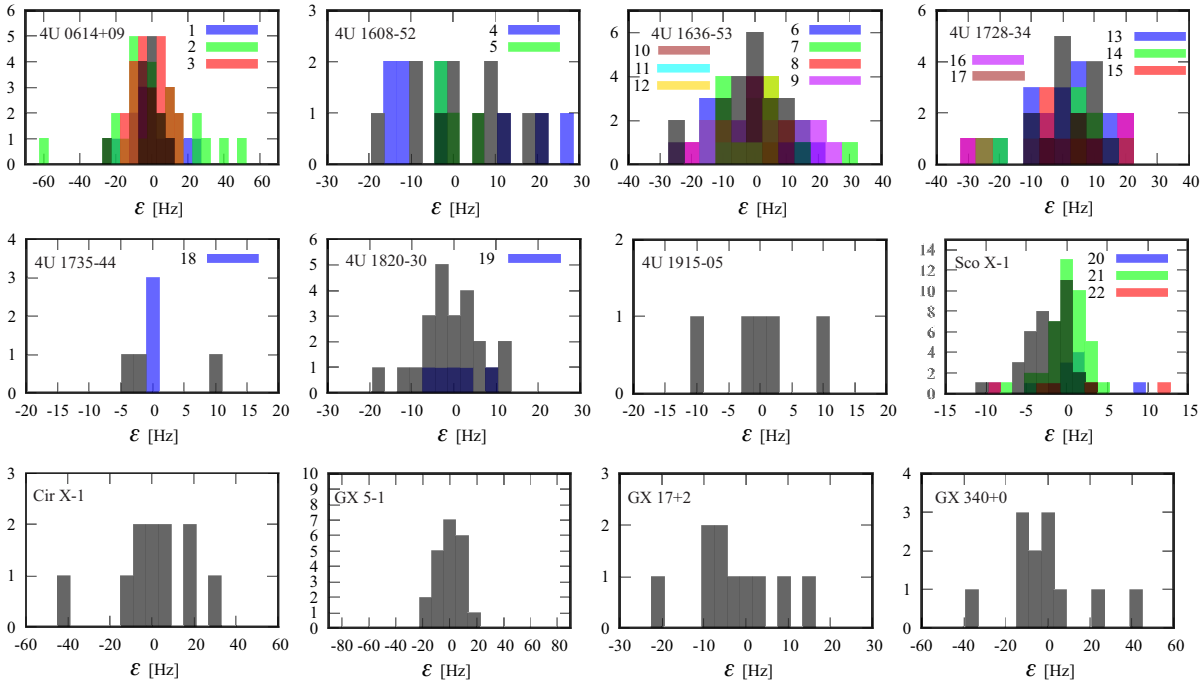

Figure 3.33. The same as 3.18 but for the two-parametric relation.

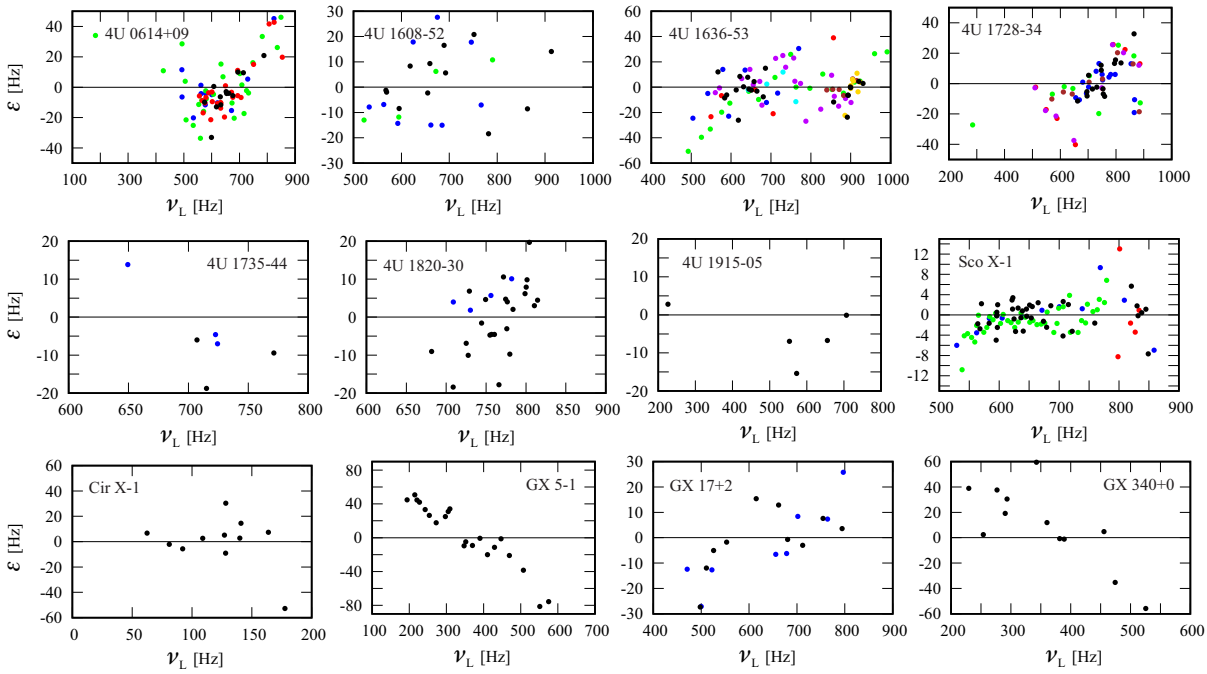

Figure 3.34. The same as 3.24 but for the one-parameter relation.

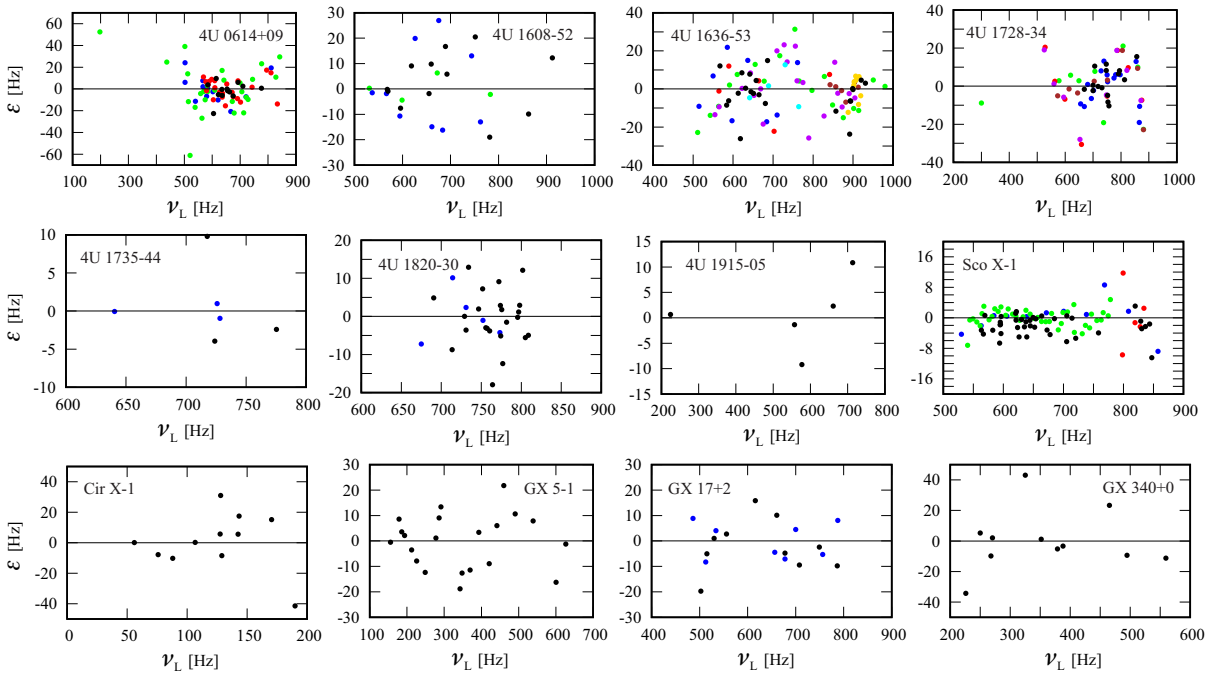

Figure 3.35. The same as 3.24 but for the two-pamametric relation.

3.3. Do parameters change between data from different authors?

It can be seen from Tables 3.1 and 3.2 that, in general, models with two parameters (the square-root, two-parametric, linear, and quadratic models) give a value of the correlation parameter smaller than 0.3. In comparison, models based on one parameter (the TD, WD, one-parameter, and RP models) give higher values.

Let us investigate whether the parameters change when we switch between data from different authors. From Figures 3.4 - 3.17, we can see that data points we used in our works [4–7, 9, 15**?**] in general cover interval in ν_L large enough to get a precise information. In other words, other authors (than those whose data we used in our papers) did not report data that would cover a larger range in ν_L, which could fundamentally change the values of the predicted parameters. Therefore, even though the predictions are slightly different, we can continue to use the same data.

Figure 3.36 displays the dependency of the A parameter on the B parameter for the linear, quadratic and the square-root relation. Although the values of the parameters change among different authors, typically (with minor exceptions), the A parameter is dependent on the B parameter. The bottom panels of the figure display masses obtained from the RP, TD, and WD models implied by different authors and sources.

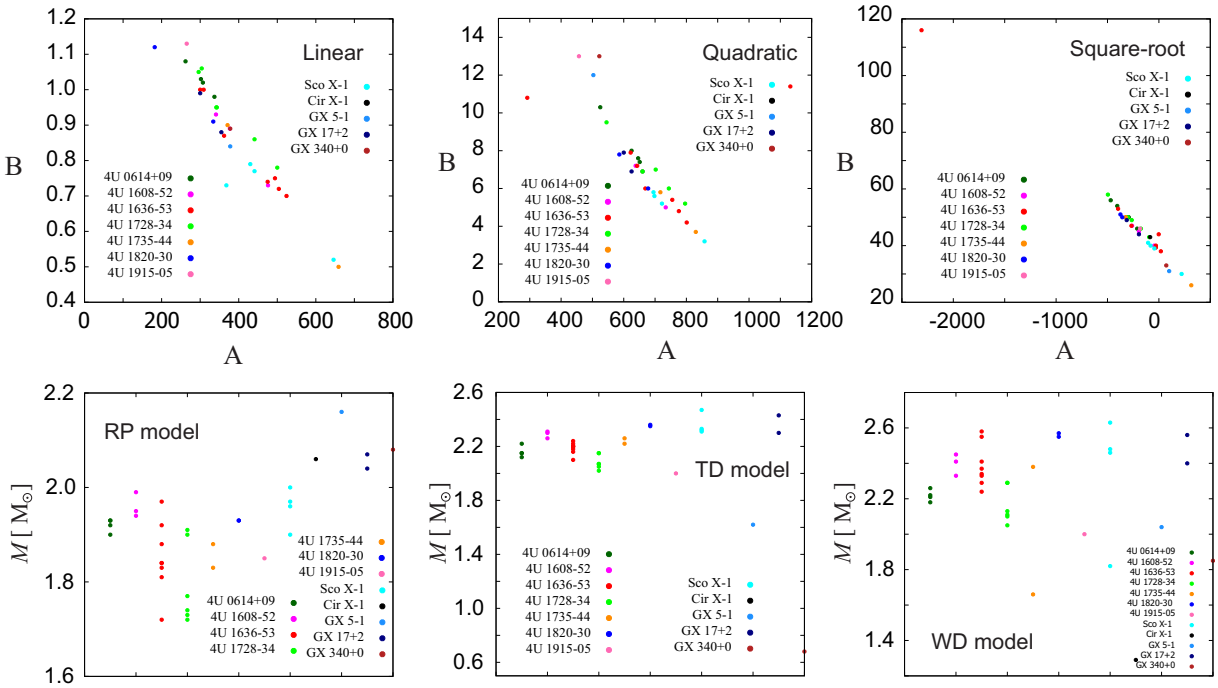

Figure 3.36. Values of parameters. Top line: Values of best-fitting parameters for data of individual authors and different adopted models with two parameters. The color-coding is the same as in Figures 3.18 - 3.33. Bottom line: Values of masses given by fitting QPO data from different authors, sources, and models.

Figure 3.37 shows similiar dependencies as 3.36 but this time for our models (one-parameter and two-parametric relations).

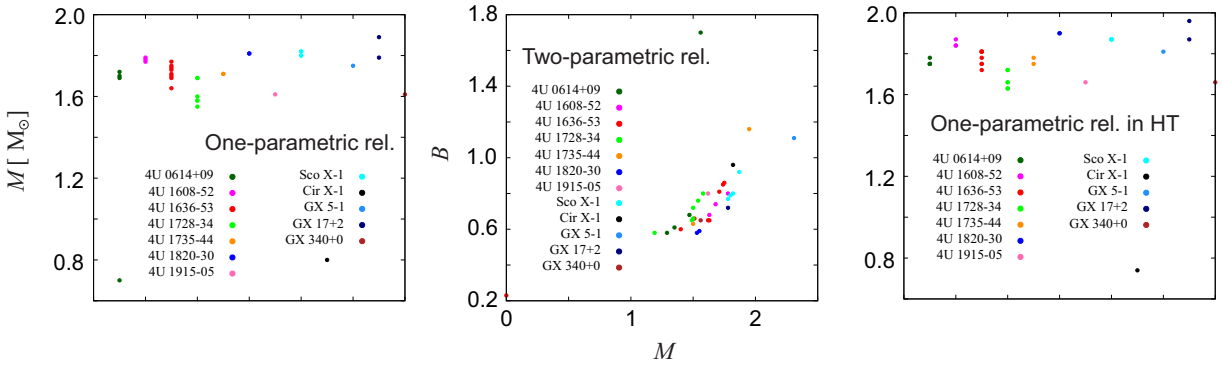

Figure 3.37. The same as on 3.36 but for our models.

Chapter 4

Oscillating torus

In the paper *Twin peak high-frequency quasi-periodic oscillations as a spectral imprint of dual oscillation modes of accretion tori* [49], we deal with the possibility that an oscillating torus is responsible for the QPOs. We explore the influence of the inclination of the observer and the spin of the compact object on the resulting power spectrum and the K_α iron lines profiles of a torus oscillating in radial and vertical directions. The article is a continuation of the work of other authors, namely [63, 90, 93, 94, 106–110].

At this point, I will focus on our results. The already published work will thus be supplemented by new results obtained for the purpose of this thesis. This will show the directions of our future work.

4.1. Torus configuration

The article considered an axially symmetric torus made by a perfect polytropic fluid with constant specific angular momentum. The material orbits the black hole in a purely azimuthal direction, and the radial extent of the torus is very small compared to its central radius. An illustration of the equilibrium state of such a torus can be seen in Figure 4.1.

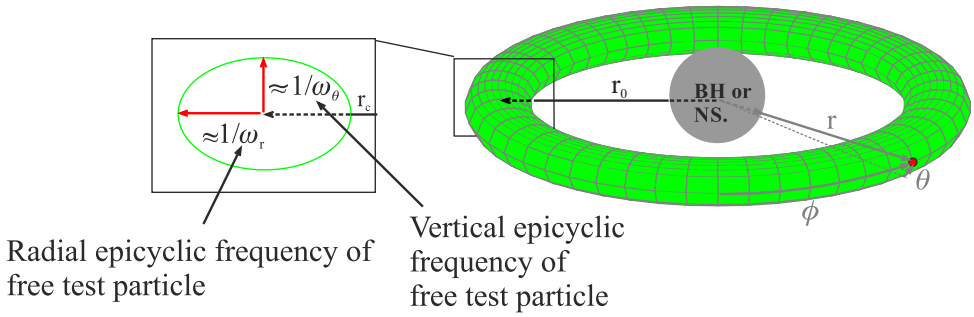

Figure 4.1. Equilibrium configuration. The cross-section of the torus is almost elliptical. Semi-major and semi-minor axes are roughly inversely proportional to the test particle's radial and vertical epicyclic frequencies.

The surface of such a torus is given by the relation (see, for example [49, 93, 94])

$$\frac{p_0}{\rho_0}\left(1-\overline{\omega}_{r0}^2(\bar{x})^2-\overline{\omega}_{\theta 0}^2(\bar{y})^2\right)=0, \tag{4.1}$$

where p_0 and ρ_0 are the pressure and density defined at the torus center. The $\bar{x},\bar{y}$ coordinates are connected to the Boyer-Lindquist coordinates by

$$\bar{x}^2 = \frac{1}{\beta}|g_{rr0}|\frac{(r-r_0)^2}{r_0^2}, \tag{4.2}$$

$$\bar{y}^2 = \frac{1}{\beta}|g_{\theta\theta 0}|\frac{\left(\frac{\pi}{2}-\theta\right)^2}{r_0^2}. \tag{4.3}$$

Furthermore, r_0 is the central radial position of the equilibrium torus and g_{rr0}, $g_{\theta\theta 0}$ are the metric tensor components in the Kerr geometry defined at the torus centre. The β parameter describes the torus thickness, $\overline{\omega}_r,\overline{\omega}_\theta$ are the radial and vertical epicyclic frequencies given in the units of the orbital frequency Ω_0 of a free test particle.

The torus oscillates in the radial and vertical directions. The surface of the oscillating torus is given by the equation (for more information see [49, 93, 94]):

$$1-\overline{\omega}_{r0}^2(\bar{x}+\delta x)^2-\overline{\omega}_{\theta 0}^2(\bar{y}+\delta y)^2=0, \tag{4.4}$$

where δx and δy are given by:

$$\delta x = -\frac{A_r\cos(m_r\varphi-(\overline{\omega}_r+m_r)\Omega_0 t)}{2\overline{\omega}_r^2}, \tag{4.5}$$

$$\delta y = -\frac{A_\theta\cos(m_\theta\varphi-(\overline{\omega}_\theta+m_\theta)\Omega_0 t)}{2\overline{\omega}_\theta^2}. \tag{4.6}$$

The free A_r, A_θ parameters are the oscillation amplitudes. The m_r, m_θ integers are the azimuthal numbers.

In the paper, we consider two configurations of oscillations:

- *The first configuration* with zero azimuthal numbers ($m_r=0,\ m_\theta=0$). This configuration corresponds to the ER model from Chapter 2.

- *The second configuration* with non-zero azimuthal numbers ($m_r=-1,\ m_\theta=-2$). This is the so-called RP2 model from Chapter 2.

The centre of the torus r_0 is chosen such that the radial and the vertical oscillation frequencies are in 2 to 3 ratio. The β parameter providing information about the torus thickness is chosen in such a way that the torus radial extension (measured by an observer at infinity) is $r_0/10$. The amplitudes of the oscillations are chosen such that $A_{r,\theta}=\overline{\omega}_{r,\theta}$.

In Figure 4.1 you can see how the individual oscillations look like.

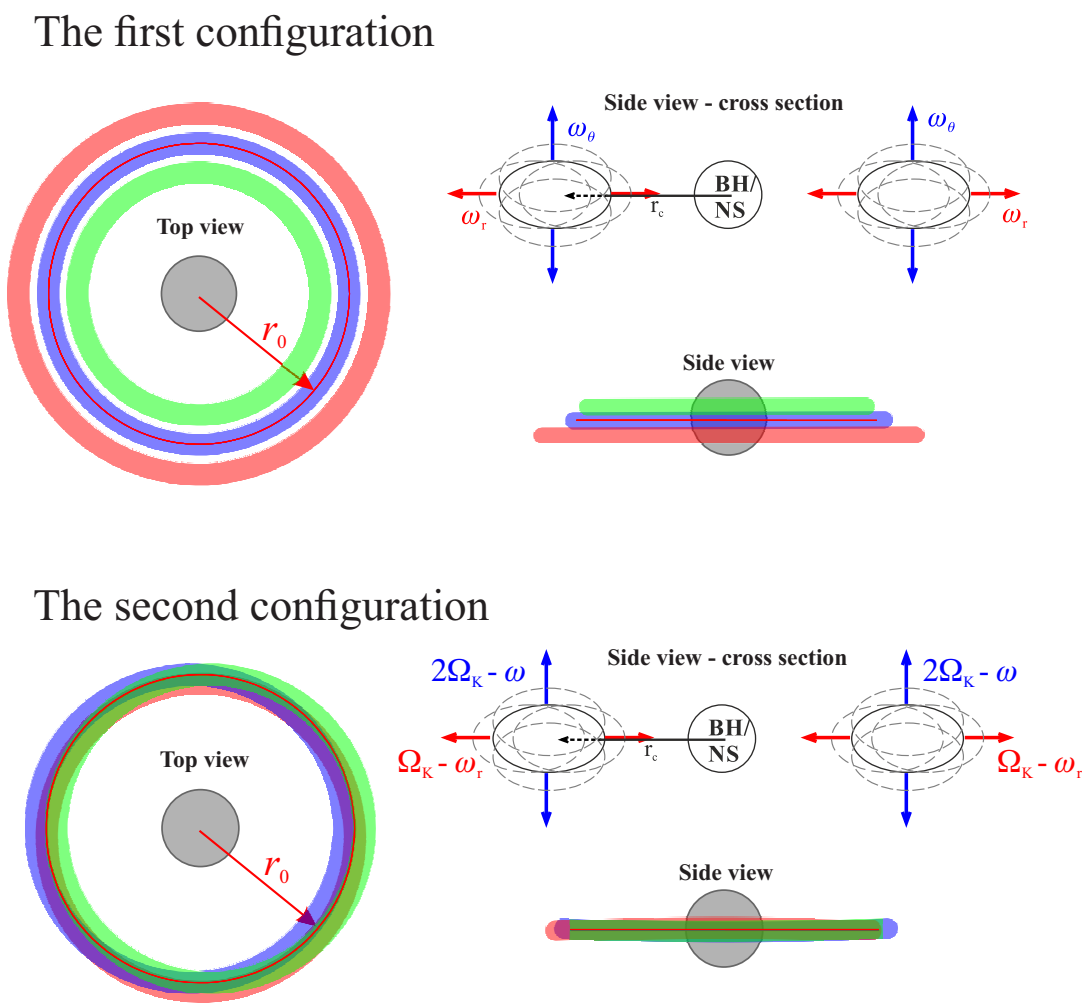

Figure 4.2. Illustration of two configurations that we consider here. The top line corresponds to the first (axially symmetric) oscillation configuration, and the bottom line shows the second (non-axially symmetric) configuration.

4.2. Oscillating tori as seen by a distant observer

I worked on an article under the supervision of Dr. Pavel Bakala (see Figure 4.3). In the article, we worked with a modified version of the LSDplus code ([49, 111]), one of Pavel's most important creations. Today, unfortunately, he is no longer among us, and at this point, I would like to express my gratitude for everything we have achieved together and I have learned from him. Without him, this dissertation might not have been completed.

In the paper, we implemented the above described torus into the relativistic ray-tracing LSDplus code ([49, 111]. Figure 4.4 illustrates where a given part of the torus is displayed on

the observer's screen. The resulting oscillating tori as viewed by a distant observer can be seen in Figures 4.5 and 4.6.

Figure 4.3. A tribute to Pavel Bakala.

4.2.1. Power spectra and Iron K_α line profiles

We applied the fast Fourier transformation on the resulting light curves, and obtained the power spectra.

In Figure 4.7, there are power spectra for different observer inclination angles, both configurations, and three different values of the black hole spin.

The first configuration leads to power spectra with the pair of dominant peaks corresponding to frequencies of the radial and vertical oscillation modes, except for the case of very high or very low observer inclinations, where higher harmonics are prominent.

The same is true also for the second configuration in the case of zero and a half spin. In the case of high spin and the second configuration, there are dominant peaks in the power spectrum corresponding to frequency of just the radial oscillation modes and their harmonics for all inclinations. This is so because the torus is located in the ergosphere.

Furthermore, we assume that every point of the torus surface radiates with Lorentzian profile with central energy $E = 6400$ eV. Along the photon path, a Lorentzian profile with a centre at 6400 eV is shifted due to the relativistic effects (like the Doppler shift or the gravitational redshift, see Figure 4.8). Each pixel of the observer's screen corresponds to a different spectral line profile. These profiles are summed across all pixels.

Similar behaviour can be seen in the resulting K_α line profiles as in the case of the power spectrum (see Figure 4.9).

Until now, we have dealt with already published results. Let us now look at something new. In Figure 4.10, we can see profiles of the K_α lines constructed as above. This time, however, a sphere is rotating at a certain angular velocity in the middle of the Keplerian disk. If we did not consider the accretion disk, we would get similar results as here [112]. The space-time is described by the Schwarzschild geometry, in which a spherically symmetric but generally rotating star is inserted. So far, the configuration is too simple to discuss these results further.

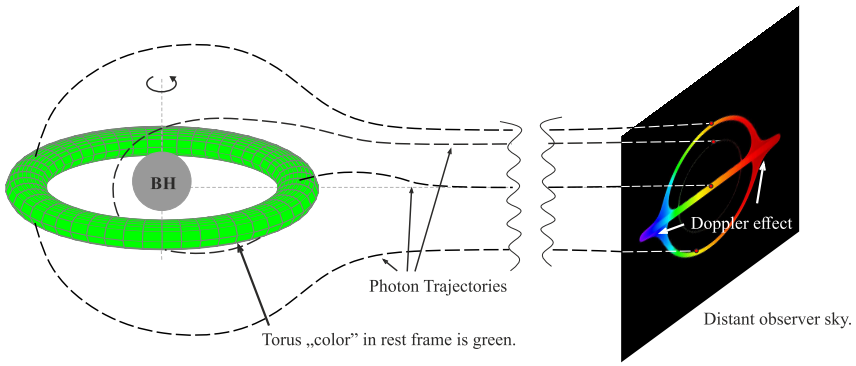

Figure 4.4. Illustration showing where each point is displayed on the observer's screen. The curves do not correspond to real photon trajectories.

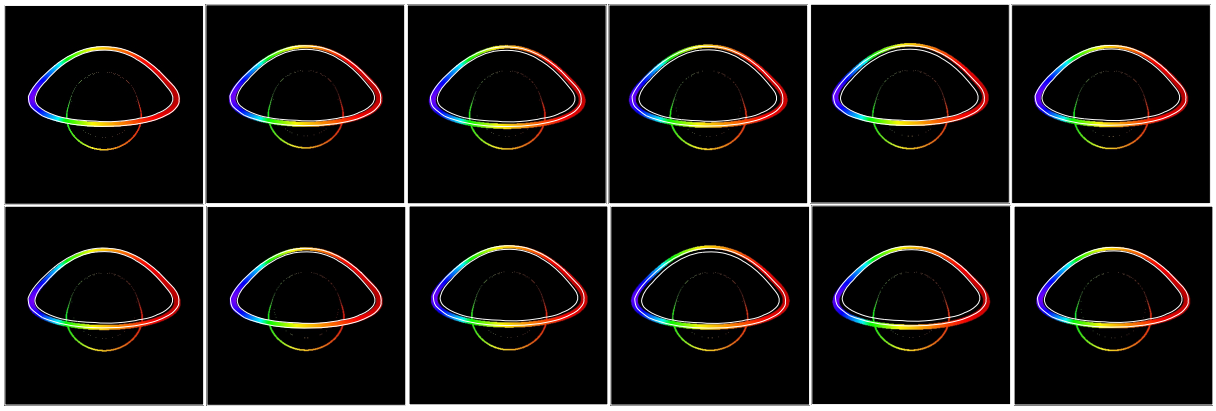

Figure 4.5. Illustration of a torus oscillating in the first configuration as would be seen by a distant observer. Each image was taken at a different time so that all twelve cover the entire period. The white lines indicate the position of the torus at the initial time.

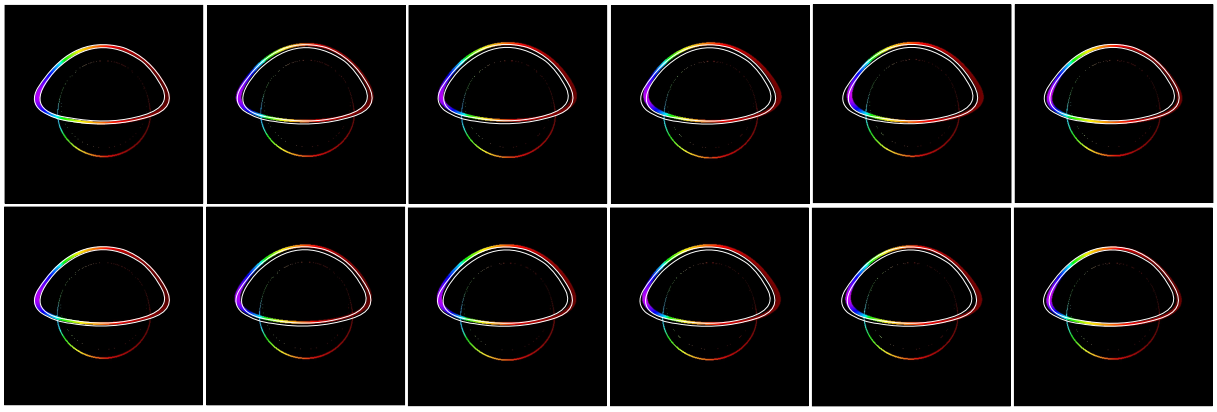

Figure 4.6. The same as in 4.5 but for the second configuration.

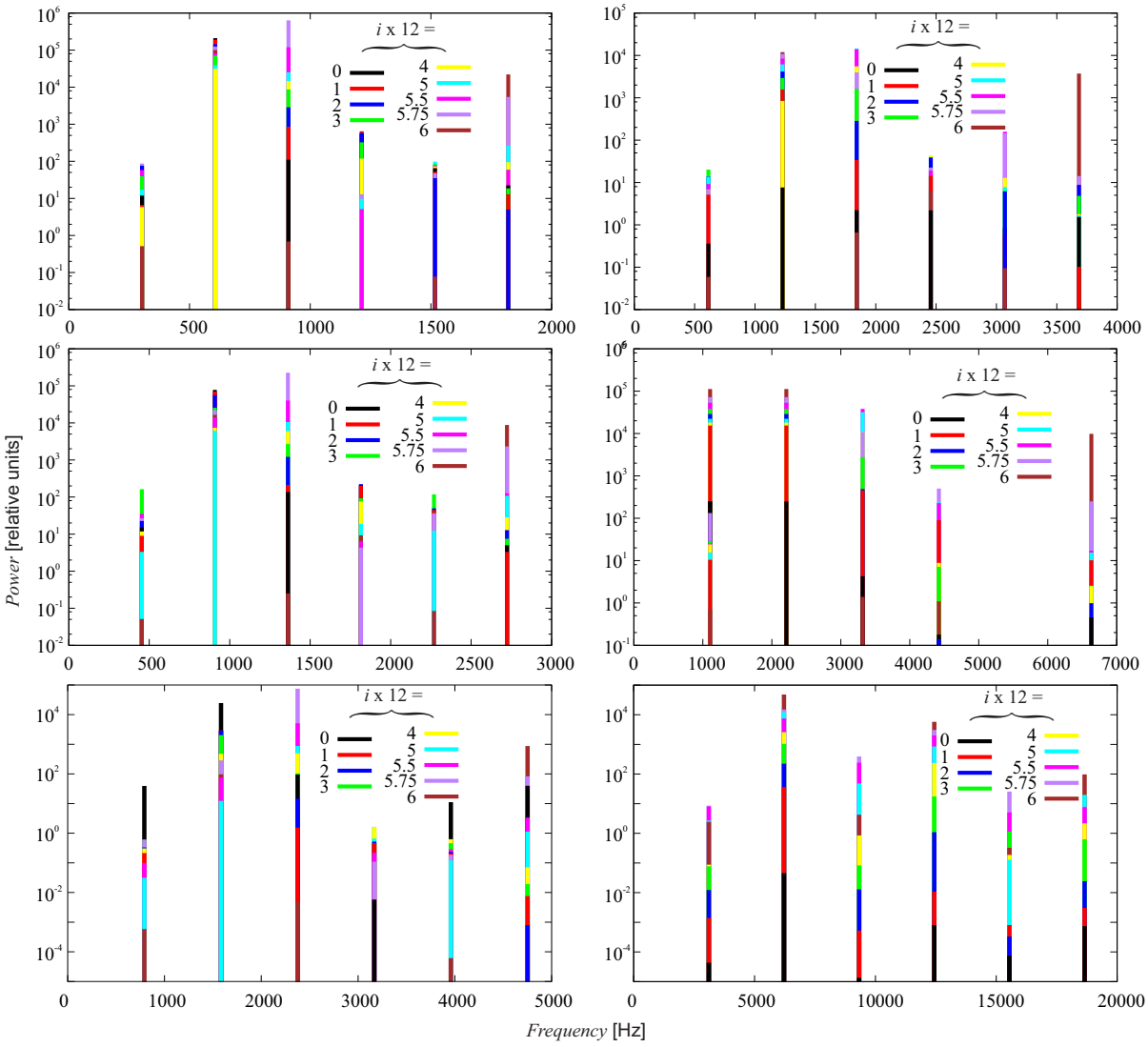

Figure 4.7. Power density spectrum of an oscillating torus. The left column corresponds to the first configuration. The right one is for the second configuration. The individual lines correspond to different spin values of the black hole. The colours mark different inclinations (i).

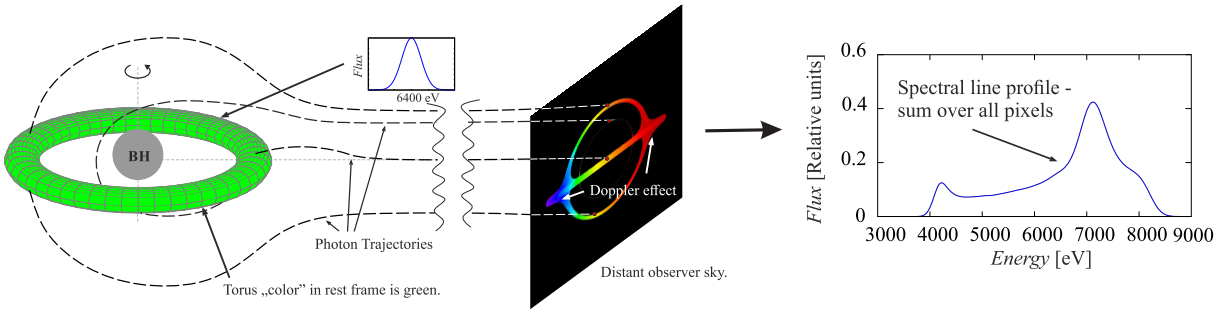

Figure 4.8. Illustration of obtaining the profile of a K_α line measured by a distant observer. In a torus local system, the K_α line has a Lorentz profile with a center value of 6400 eV.

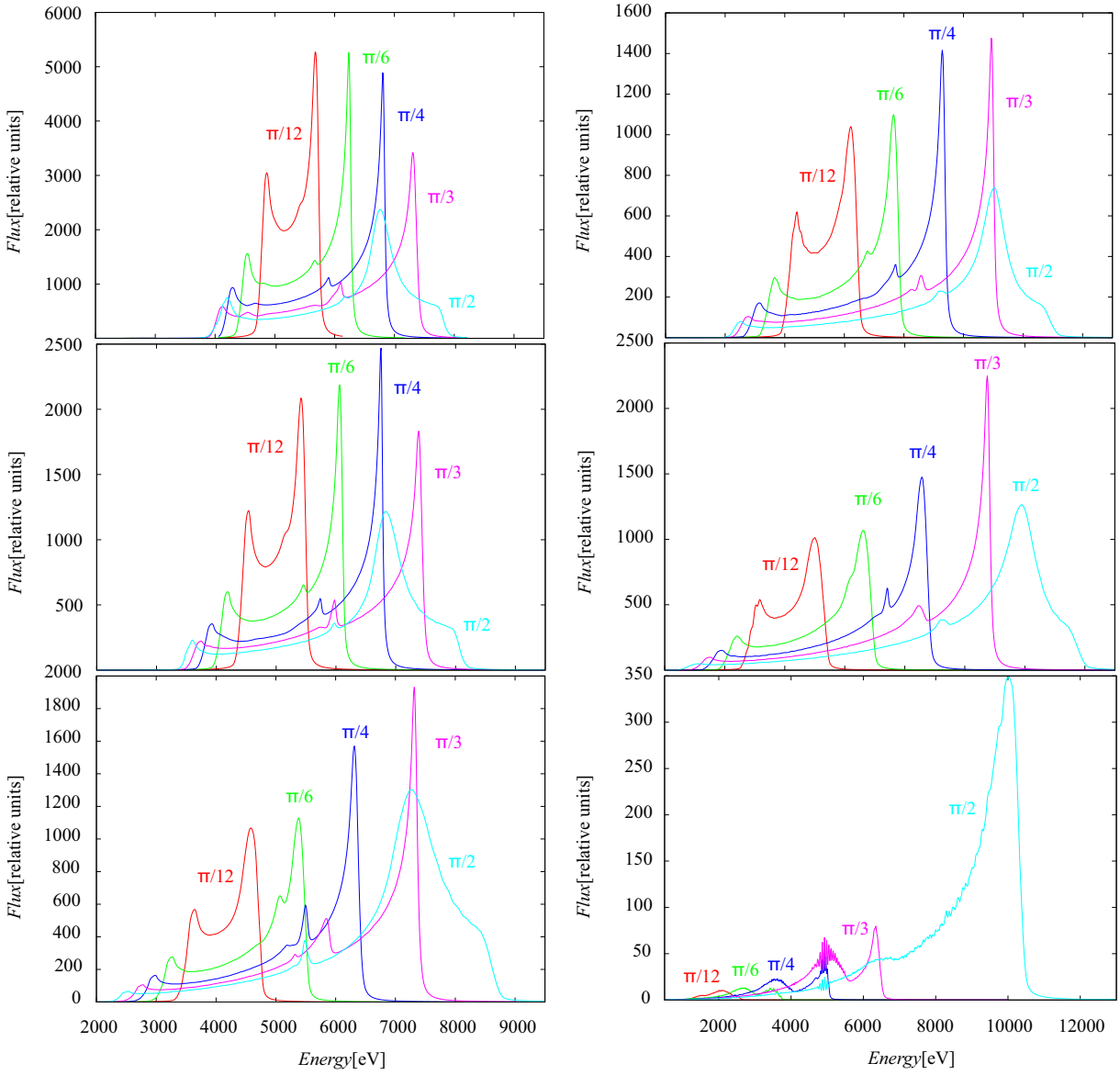

Figure 4.9. The K_α line profiles as seen by a distant observer. The left and right columns correspond to the first and cesond configuration, respectively. The individual lines then correspond to different spin values.

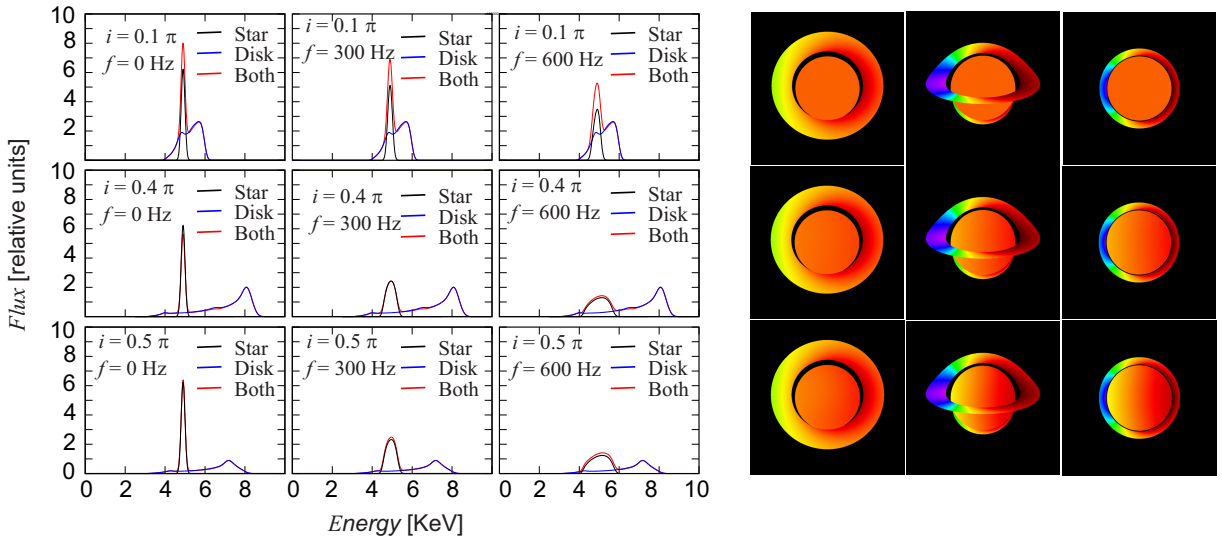

Figure 4.10. The K_α line profiles of a sphere around which is an accretion Kepler disk. Left block: line profiles for various inclinations of the observer (i) and NS rotation frequency (f). Right block: Sphere with the disks from Left block as seen by a distant observer.

Chapter 5

Summary and future prospects

During my study, I have collaborated on seventeen papers. Sixteen of them have already been published ([4–9, 48, 113–120]) and one of them has been sent to the Astrophysical Journal ([15]).

5.1. QPO data and their fits

From the above set of papers, I have selected eight whose results are briefly commented on within this work. All of them are in some way related to the phenomenon of QPOs. Instead of simply repeating what has been done in those individual papers, I have decided to do the work I had been thinking about for a long time. Most of these publications deal with fitting of the QPO data. We have always worked with a limited number of sources, models, and data. There was a danger that if we took data obtained by other authors, we could obtain different results. I decided to consider all the QPO data available in the literature and use the same procedure as was used in our articles. I present my conclusions in Chapter 3 where I demonstrate that the results reached by using data reported by various other authors are very similar to those obtained by us in the past.

Another outcome of Chapter 3 is the collection of a large amount of the HF QPO data itself (in fact, as much as was possible to collect at the time) that can be utilized in the future. I soon intend to complete and publish a short paper providing all this data along with their references.

5.2. Interpretation of the variability

Furthermore, I attempted in this thesis to create a comparison between fits predicted by the here considered models in a way different than usual. I conclude in Chapter 3 that the models can be sorted according to the quality of the fits in the following way (from best to worst): the square-root model, two-parameter relation, linear model, quadratic model, TD model, WD model, one-parameter relation, and the RP model.

As follows from the findings of the submitted paper [15], the two-parametric relation can be related to predictions of the CT model, whereas deviations of the $\mathscr{B}$ parameter from the value of $\mathscr{B} = 0.8$ can correspond to deviations of a real accretion flow from the simplified case of a

flow with constant angular momentum distribution. In the H-T spacetime, even for $\mathscr{B} = 0.8$, the CT model clearly provides better fits than the RP model while also implying realistic values of the NS mass.

These findings strongly support the validity of the CT model. In this model, the lower QPO frequency corresponds to the radial oscillation of the inner torus. The corrotation frequency associated to the upper QPO can be related to instabilities of the flow that can grow for some time but presumably does not survive due to the various stabilization effects [121–124]. Characteristic timescales of these processes are more than five orders of magnitude lower than the typical integration time required to well identify the two peaks in the PDS from the Proportional Counter Array on the board of the Rossi X-ray Timing Explorer ([125]). Both the considered modes can form Lorentzian profiles in the resulting PDS [126]. From the very nature of these modes it however follows that the radial mode has a much higher potential to produce narrow peaks in PDS. This well corresponds with the documented high coherence of the lower QPO [20, 38]. Taking into account all of the above, I suggest the CT model could represent a very promising concept.

5.3. Correlated spectral and timing behaviour

In Chapter 4, I discuss the results of article [49]. The article analyzes the timing properties of flux emitted from a fluid torus oscillating in the radial and vertical directions. The assumed oscillatory configurations correspond to models listed in Chapter 2. I include a sketch of a new preliminary result in Figure 4.10 showing a very simplified example of an iron line profile in the spectra of radiation emitted from the configuration of a Keplerian disk and a rotating star. With a little more effort, this incremental result itself could in the future help improve our investigations of the NS X-ray spectra. The main reason I include it here is nevertheless related to my desire of illustrating the potential of our codes for future investigations regarding oscillations of disk structures in the innermost accretion regions and the implied correlated spectral and timing behaviour of X-ray emissions from the vicinity of compacts objects.

References

[1] GIACCONI, R.; GURSKY, H.; PAOLINI, F. R. & ROSSI, B. B.: Evidence for x Rays From Sources Outside the Solar System. *Physical Review Letters*, **9**, pp. 439–443, December 1962.

[2] VAN DER KLIS, M.; JANSEN, F.; VAN PARADIJS, J.; LEWIN, W. H. G.; VAN DEN HEUVEL, E. P. J.; TRUMPER, J. E. & SZATJNO, M.: Intensity-dependent quasi-periodic oscillations in the X-ray flux of GX5 - 1. *Nature*, **316**, pp. 225–230, July 1985.

[3] MCCLINTOCK, J. E. & REMILLARD, R. A.: *Black hole binaries*, pp. 157–213, April 2006.

[4] TÖRÖK, G.; BAKALA, P.; ŠRÁMKOVÁ, E.; STUCHLÍK, Z.; URBANEC, M. & GOLUCHOVÁ, K.: Mass-Angular-momentum Relations Implied by Models of Twin Peak Quasi-periodic Oscillations. *The Astrophysical Journal*, **760**, 138, December 2012, 1408.4220.

[5] STUCHLIK, Z.; KOTRLOVA, A.; TOROK, G. & GOLUCHOVA, K.: Test of the Resonant Switch Model by Fitting the Data of Twin-Peak HF QPOs in the Atoll Source 4U 1636-53. *Acta Astronomica*, **64**, pp. 45–64, March 2014.

[6] STUCHLÌK, Z.; URBANEC, M.; KOTRLOVÀ, A.; TÖRÖK, G. & GOLUCHOVÀ, K.: Equations of State in the Hartle-Thorne Model of Neutron Stars Selecting Acceptable Variants of the Resonant Switch Model of Twin HF QPOs in the Atoll Source 4U 1636-53. *Acta Astronomica*, **65**, pp. 169–195, June 2015, 1507.00373.

[7] TÖRÖK, G.; GOLUCHOVÁ, K.; URBANEC, M.; ŠRÁMKOVÁ, E.; ADÁMEK, K.; URBANCOVÁ, G.; PECHÁČEK, T.; BAKALA, P.; STUCHLÍK, Z.; HORÁK, J. & JURYŠEK, J.: Constraining Models of Twin-Peak Quasi-periodic Oscillations with Realistic Neutron Star Equations of State. *The Astrophysical Journal*, **833**, 273, December 2016, 1611.06087.

[8] TÖRÖK, G.; GOLUCHOVÁ, K.; HORÁK, J.; ŠRÁMKOVÁ, E.; URBANEC, M.; PECHÁČEK, T. & BAKALA, P.: Twin peak quasi-periodic oscillations as signature of oscillating cusp torus. *Monthly Notices of the Royal Astronomical Society: Letters*, **457**, pp. L19–L23, March 2016, 1512.03841.

[9] TÖRÖK, G.; GOLUCHOVÁ, K.; ŠRÁMKOVÁ, E.; HORÁK, J.; BAKALA, P. & URBANEC, M.: On one-parametric formula relating the frequencies of twin-peak quasi-periodic oscillations. *Monthly Notices of the Royal Astronomical Society*, **473**, pp. L136–L140, January 2018, 1710.10901.

[10] TÖRÖK, G.; URBANEC, M.; GOLUCHOVÁ, K.; BAKALA, P.; ŠRÁMKOVÁ, E. & STUCHLÍK, Z.: Restrictions to neutron star models based on twin-peak quasi-periodic oscillations. J. VAN LEEUWEN, editor, *Neutron Stars and Pulsars: Challenges and Opportunities after 80 years*, volume 291 of *IAU Symposium*, pp. 524–526, March 2013.

[11] TÖRÖK, G.; BAKALA, P.; ŠRÁMKOVÁ, E.; STUCHLÍK, Z.; URBANEC, M. & GOLUCHOVÁ, K.: Restrictions to Neutron Star Properties Based on Twin-Peak Quasi-Periodic Oscillations. C. M. ZHANG; T. BELLONI; M. MÉNDEZ & S. N. ZHANG, editors, *Feeding Compact Objects: Accretion on All Scales*, volume 290 of *IAU Symposium*, pp. 319–320, February 2013, 1212.6670.

[12] TÖRÖK, G.; GOLUCHOVÁ, K.; URBANEC, M.; ŠRÁMKOVÁ, E.; ADÁMEK, K.; URBANCOVÁ, G.; PECHÁČEK, T.; BAKALA, P.; STUCHLÍK, Z.; HORÁK, J. & JURYŠEK, J.: Confronting models of twin peak quasi-periodic oscillations: Mass and spin estimates fixed by neutron star equation of state. *Proceedings of RAGtime 14-16: Workshops on black holes and neutron stars*, pp. 269–282, December 2014.

[13] TÖRÖK, G.; GOLUCHOVÁ, K.; ŠRÁMKOVÁ, E.; HORÁK, J.; BAKALA, P. & URBANEC, M.: A one-parametric formula relating the frequencies of twin-peak quasi-periodic oscillations. *Proceedings of RAGtime 17-19: Workshops on black holes and neutron stars, 17-19/23-26 Oct., 1-5 Nov. 2015/2016/2017, Opava, Czech Republic, Z. Stuchlík, G. Török and V. Karas editors, Silesian University in Opava, 2017, ISBN 978-80-7510-257-7, ISSN 2336-5676, p. 177-193*, pp. 177–193, December 2017.

[14] TÖRÖK, G.; GOLUCHOVÁ, K. & ŠRÁMKOVÁ: Rapid x-ray variability and properties of compact-stars, 2018.

[15] TÖRÖK, G.; KOTRLOVÁ, A.; MATUSZKOVÁ, M.; KLIMOVIČOVÁ, K.; LANČOVÁ, D.; URBANCOVÁ, G. & ŠRÁMKOVÁ, E.: Simple analytic formula relating the mass and spin of accreting compact objects to their rapid x-ray variability, submitted to APJ.

[16] VAN DER KLIS, M.: Millisecond Oscillations in X-ray Binaries. *Annual Review of Astronomy and Astrophysics*, **38**, pp. 717–760, 2000, astro-ph/0001167.

[17] BELLONI, T.; PSALTIS, D. & VAN DER KLIS, M.: A Unified Description of the Timing Features of Accreting X-Ray Binaries. *The Astrophysical Journal*, **572**, pp. 392–406, June 2002, astro-ph/0202213.

[18] VAN DER KLIS, M.: *Rapid X-ray Variability*, pp. 39–112, April 2006.

[19] BARRET, D.; OLIVE, J.-F. & MILLER, M. C.: An abrupt drop in the coherence of the lower kHz quasi-periodic oscillations in 4U 1636-536. *Monthly Notices of the Royal Astronomical Society*, **361**, pp. 855–860, August 2005, astro-ph/0505402.

[20] BARRET, D.; OLIVE, J.-F. & MILLER, M. C.: Drop of coherence of the lower kilo-Hz QPO in neutron stars: Is there a link with the innermost stable circular orbit? *Astronomische Nachrichten*, **326**, pp. 808–811, November 2005, astro-ph/0510094.

[21] BARRET, D.; OLIVE, J.-F. & MILLER, M. C.: The coherence of kilohertz quasi-periodic oscillations in the X-rays from accreting neutron stars. *Monthly Notices of the Royal Astronomical Society*, **370**, pp. 1140–1146, August 2006, astro-ph/0605486.

[22] DU BUISSON, L.; MOTTA, S. & FENDER, R.: Mass and spin measurements for the neutron star 4U1608-52 through the relativistic precession model. *Monthly Notices of the Royal Astronomical Society*, **486**(4), pp. 4485–4497, July 2019, 1905.00366.

[23] VAN STRAATEN, S.; VAN DER KLIS, M. & MÉNDEZ, M.: The Atoll Source States of 4U 1608-52. *The Astrophysical Journal*, **596**(2), pp. 1155–1176, October 2003, astro-ph/0307041.

[24] VAN DOESBURGH, M. & VAN DER KLIS, M.: Testing the relativistic precession model using low-frequency and kHz quasi-periodic oscillations in neutron star low-mass X-ray binaries with known spin. *Monthly Notices of the Royal Astronomical Society*, **465**(3), pp. 3581–3606, March 2017, 1611.05860.

[25] LIN, Y.-F.; BOUTELIER, M.; BARRET, D. & ZHANG, S.-N.: Studying Frequency Relationships of Kilohertz Quasi-periodic Oscillations for 4U 1636-53 and Sco X-1: Observations Confront

Theories. *The Astrophysical Journal*, **726**, 74, January 2011, 1010.6198.

[26] ALTAMIRANO, D.; VAN DER KLIS, M.; MÉNDEZ, M.; JONKER, P. G.; KLEIN-WOLT, M. & LEWIN, W. H. G.: X-Ray Time Variability Across the Atoll Source States of 4U 1636-53. *The Astrophysical Journal*, **685**(1), pp. 436–450, September 2008, 0806.0962.

[27] DI SALVO, T.; MÉNDEZ, M. & VAN DER KLIS, M.: On the correlated spectral and timing properties of 4U 1636-53: An atoll source at high accretion rates. *Astronomy & Astrophysics*, **406**, pp. 177–192, July 2003, astro-ph/0304090.

[28] JONKER, P. G.; MÉNDEZ, M. & VAN DER KLIS, M.: Kilohertz quasi-periodic oscillations difference frequency exceeds inferred spin frequency in 4U 1636-53. *Monthly Notices of the Royal Astronomical Society*, **336**(1), pp. L1–L5, October 2002, astro-ph/0204113.

[29] WIJNANDS, R. A. D.; VAN DER KLIS, M.; VAN PARADIJS, J.; LEWIN, W. H. G.; LAMB, F. K.; VAUGHAN, B. & KUULKERS, E.: Discovery in 4U 1636-53 of Two Simultaneous Quasi-periodic Oscillations near 900 HZ and 1176 HZ. *The Astrophysical Journal Letters*, **479**(2), pp. L141–L144, April 1997.

[30] FORD, E. C.; VAN DER KLIS, M.; VAN PARADIJS, J.; MÉNDEZ, M.; WIJNANDS, R. & KAARET, P.: Discovery of a Second Kilohertz QPO in the X-Ray Binary 4U 1735-44. *The Astrophysical Journal Letters*, **508**(2), pp. L155–L158, December 1998, astro-ph/9809407.

[31] BOIRIN, L.; BARRET, D.; OLIVE, J. F.; BLOSER, P. F. & GRINDLAY, J. E.: Low and high frequency quasi-periodic oscillations in 4U1915-05. *Astronomy & Astrophysics*, **361**, pp. 121–138, September 2000, astro-ph/0007071.

[32] HOMAN, J.; VAN DER KLIS, M.; JONKER, P. G.; WIJNANDS, R.; KUULKERS, E.; MÉNDEZ, M. & LEWIN, W. H. G.: RXTE Observations of the Neutron Star Low-Mass X-Ray Binary GX 17+2: Correlated X-Ray Spectral and Timing Behavior. *The Astrophysical Journal*, **568**, pp. 878–900, April 2002, astro-ph/0104323.

[33] WIJNANDS, R.; HOMAN, J.; VAN DER KLIS, M.; MÉNDEZ, M.; KUULKERS, E.; VAN PARADIJS, J.; LEWIN, W. H. G.; LAMB, F. K.; PSALTIS, D. & VAUGHAN, B.: Discovery of Kilohertz Quasi-Periodic Oscillations in GX 17+2. *The Astrophysical Journal Letters*, **490**(2), pp. L157–L160, December 1997, astro-ph/9710013.

[34] VAN DER KLIS, M.; WIJNANDS, R. A. D.; HORNE, K. & CHEN, W.: Kilohertz Quasi-Periodic Oscillation Peak Separation Is Not Constant in Scorpius X-1. *The Astrophysical Journal*, **481**, pp. L97–L100, June 1997, astro-ph/9703025.

[35] MÉNDEZ, M. & VAN DER KLIS, M.: The harmonic and sideband structure of the kilohertz quasi-periodic oscillations in Sco X-1. *Monthly Notices of the Royal Astronomical Society*, **318**(3), pp. 938–942, November 2000, astro-ph/0006243.

[36] VAN DER KLIS, M.; SWANK, J. H.; ZHANG, W.; JAHODA, K.; MORGAN, E. H.; LEWIN, W. H. G.; VAUGHAN, B. & VAN PARADIJS, J.: Discovery of Submillisecond Quasi-periodic Oscillations in the X-Ray Flux of Scorpius X-1. *The Astrophysical Journal Letters*, **469**, p. L1, September 1996, astro-ph/9607047.

[37] BOUTLOUKOS, S.; VAN DER KLIS, M.; ALTAMIRANO, D.; KLEIN-WOLT, M.; WIJNANDS, R.; JONKER, P. G. & FENDER, R. P.: Discovery of Twin kHz QPOs in the Peculiar X-Ray Binary Circinus X-1. *The Astrophysical Journal*, **653**, pp. 1435–1444, December 2006, astro-ph/0608089.

[38] BARRET, D.; OLIVE, J.-F. & MILLER, M. C.: The coherence of kilohertz quasi-periodic oscillations

in the X-rays from accreting neutron stars. *Monthly Notices of the Royal Astronomical Society*, **370**(3), pp. 1140–1146, August 2006, astro-ph/0605486.

[39] MIGLIARI, S.; VAN DER KLIS, M. & FENDER, R. P.: Evidence of a decrease of kHz quasi-periodic oscillation peak separation towards low frequencies in 4U 1728-34 (GX 354-0). *Monthly Notices of the Royal Astronomical Society*, **345**(3), pp. L35–L39, November 2003, astro-ph/0309288.

[40] VAN STRAATEN, S.; VAN DER KLIS, M.; DI SALVO, T. & BELLONI, T.: A Multi-Lorentzian Timing Study of the Atoll Sources 4U 0614+09 and 4U 1728-34. *The Astrophysical Journal*, **568**(2), pp. 912–930, April 2002, astro-ph/0107562.

[41] DI SALVO, T.; MÉNDEZ, M.; VAN DER KLIS, M.; FORD, E. & ROBBA, N. R.: Study of the Temporal Behavior of 4U 1728-34 as a Function of Its Position in the Color-Color Diagram. *The Astrophysical Journal*, **546**(2), pp. 1107–1120, January 2001, astro-ph/0008361.

[42] MÉNDEZ, M. & VAN DER KLIS, M.: Precise Measurements of the Kilohertz Quasi-periodic Oscillations in 4U 1728-34. *The Astrophysical Journal Letters*, **517**(1), pp. L51–L54, May 1999, astro-ph/9903303.

[43] FORD, E.; KAARET, P.; TAVANI, M.; BARRET, D.; BLOSER, P.; GRINDLAY, J.; HARMON, B. A.; PACIESAS, W. S. & ZHANG, S. N.: Evidence from Quasi-Periodic Oscillations for a Millisecond Pulsar in the Low-Mass X-Ray Binary 4U 0614+091. *The Astrophysical Journal Letters*, **475**(2), pp. L123–L126, February 1997, astro-ph/9610110.

[44] VAN STRAATEN, S.; FORD, E. C.; VAN DER KLIS, M.; MÉNDEZ, M. & KAARET, P.: Relations between Timing Features and Colors in the X-Ray Binary 4U 0614+09. *The Astrophysical Journal*, **540**(2), pp. 1049–1061, September 2000, astro-ph/0001480.

[45] BOUTELIER, M.; BARRET, D. & MILLER, M. C.: kHz quasi-periodic oscillations in the low-mass X-ray binary 4U 0614+09. *Monthly Notices of the Royal Astronomical Society*, **399**(4), pp. 1901–1906, November 2009, 0907.3223.

[46] JONKER, P. G.; VAN DER KLIS, M.; WIJNANDS, R.; HOMAN, J.; VAN PARADIJS, J.; MÉNDEZ, M.; FORD, E. C.; KUULKERS, E. & LAMB, F. K.: The Power Spectral Properties of the Z Source GX 340+0. *The Astrophysical Journal*, **537**, pp. 374–386, July 2000, astro-ph/0002022.

[47] JONKER, P. G.; VAN DER KLIS, M.; HOMAN, J.; MÉNDEZ, M.; LEWIN, W. H. G.; WIJNANDS, R. & ZHANG, W.: Low- and high-frequency variability as a function of spectral properties in the bright X-ray binary GX 5-1. *Monthly Notices of the Royal Astronomical Society*, **333**, pp. 665–678, July 2002, astro-ph/0202420.

[48] BAKALA, P.; TÖRÖK, G.; KARAS, V.; DOVČIAK, M.; WILDNER, M.; WZIENTEK, D.; ŠRÁMKOVÁ, E.; ABRAMOWICZ, M.; GOLUCHOVÁ, K.; MAZUR, G. P. & VINCENT, F. H.: Power density spectra of modes of orbital motion in strongly curved space-time: obtaining the observable signal. *Monthly Notices of the Royal Astronomical Society*, **439**, pp. 1933–1939, April 2014, 1401.4468.

[49] BAKALA, P.; GOLUCHOVÁ, K.; TÖRÖK, G.; ŠRÁMKOVÁ, E.; ABRAMOWICZ, M. A.; VINCENT, F. H. & MAZUR, G. P.: Twin peak high-frequency quasi-periodic oscillations as a spectral imprint of dual oscillation modes of accretion tori. *Astronomy & Astrophysics*, **581**, A35, September 2015, 1505.06673.

[50] GOLUCHOVÁ, K.; BAKALA, P.; TÖRÖK, G.; ŠRÁMKOVÁ, E.; STUCHLÍK, Z.; VINCENT, F. H. & ABRAMOWICZ, M. A.: Simulations of flux variability of oscillating accretion fluid tori around kerr black holes. *WDS'14 Proceedings of Contributed Papers, Physics*, 2014.

[51] GOLUCHOVÁ, K. & STUCHLÍK, Z.: Embedding diagrams of Bardeen geometry. *Proceedings of RAGtime 14-16: Workshops on black holes and neutron stars*, pp. 99–106, December 2014.

[52] GOLUCHOVÁ, K.; TÖRÖK, G.; URBANEC, M.; URBANCOVÁ, G. & ŠRÁMKOVÁ, E.: Innermost stable circular orbits around compact stars: Terms that are quadratic in spin. *Proceedings of RAGtime 17-19: Workshops on black holes and neutron stars,*, pp. 23–32, December 2017.

[53] ALPAR, M. A. & SHAHAM, J.: Is GX5 - 1 a millisecond pulsar? *Nature*, **316**, pp. 239–241, July 1985.

[54] LAMB, F. K.; SHIBAZAKI, N.; ALPAR, M. A. & SHAHAM, J.: Quasi-periodic oscillations in bright galactic-bulge X-ray sources. *Nature*, **317**, pp. 681–687, October 1985.

[55] MILLER, M. C.; LAMB, F. K. & PSALTIS, D.: Sonic-Point Model of Kilohertz Quasi-periodic Brightness Oscillations in Low-Mass X-Ray Binaries. *The Astrophysical Journal*, **508**, pp. 791–830, December 1998, astro-ph/9609157.

[56] PSALTIS, D.; WIJNANDS, R.; HOMAN, J.; JONKER, P. G.; VAN DER KLIS, M.; MILLER, M. C.; LAMB, F. K.; KUULKERS, E.; VAN PARADIJS, J. & LEWIN, W. H. G.: On the Magnetospheric Beat-Frequency and Lense-Thirring Interpretations of the Horizontal-Branch Oscillation in the Z Sources. *The Astrophysical Journal*, **520**, pp. 763–775, August 1999, astro-ph/9903105.

[57] STELLA, L. & VIETRI, M.: Quasi-Periodic Oscillations from Low-Mass X-ray Binaries and Strong Field Gravity. R. GIACCONI; S. SERIO & L. STELLA, editors, *X-ray Astronomy 2000*, volume 234 of *Astronomical Society of the Pacific Conference Series*, p. 213, 2001.

[58] WAGONER, R. V.; SILBERGLEIT, A. S. & ORTEGA-RODRÍGUEZ, M.: "Stable" Quasi-periodic Oscillations and Black Hole Properties from Diskoseismology. *The Astrophysical Journal*, **559**, pp. L25–L28, September 2001, astro-ph/0107168.

[59] KLUZNIAK, W. & ABRAMOWICZ, M. A.: The physics of kHz QPOs—strong gravity's coupled anharmonic oscillators. *ArXiv Astrophysics e-prints astro-ph/0105057*, May 2001, astro-ph/0105057.

[60] KATO, S.: Basic Properties of Thin-Disk Oscillations ¡SUP¿1¡/SUP¿. *Publications of the Astronomical Society of Japan*, **53**, pp. 1–24, February 2001.

[61] TITARCHUK, L. & WOOD, K.: On the Low and High Frequency Correlation in Quasi-periodic Oscillations among White Dwarf, Neutron Star, and Black Hole Binaries. *The Astrophysical Journal*, **577**, pp. L23–L26, September 2002, astro-ph/0208212.

[62] ABRAMOWICZ, M. A.; KARAS, V.; KLUZNIAK, W.; LEE, W. H. & REBUSCO, P.: Non-Linear Resonance in Nearly Geodesic Motion in Low-Mass X-Ray Binaries. *Publications of the Astronomical Society of Japan*, **55**, pp. 467–466, April 2003, astro-ph/0302183.

[63] REZZOLLA, L.; YOSHIDA, S. & ZANOTTI, O.: Oscillations of vertically integrated relativistic tori - I. Axisymmetric modes in a Schwarzschild space-time. *Monthly Notices of the Royal Astronomical Society*, **344**, pp. 978–992, September 2003, astro-ph/0307488.

[64] KLUŹNIAK, W.; ABRAMOWICZ, M. A.; KATO, S.; LEE, W. H. & STERGIOULAS, N.: Nonlinear Resonance in the Accretion Disk of a Millisecond Pulsar. *The Astrophysical Journal*, **603**, pp. L89–L92, March 2004, astro-ph/0308035.

[65] ZHANG, C.: The MHD Alfven wave oscillation model of kHz Quasi Periodic Oscillations of Accreting X-ray binaries. *Astronomy & Astrophysics*, **423**, pp. 401–404, August 2004, astro-ph/

0402028.

[66] PÉTRI, J.: An explanation for the kHz-QPO twin peaks separation in slow and fast rotators. *Astronomy & Astrophysics*, **439**, pp. L27–L30, August 2005, astro-ph/0507167.

[67] BURSA, M.: High-frequency QPOs in GRO J1655-40: Constraints on resonance models by spectral fits. S. HLEDÍK & Z. STUCHLÍK, editors, *RAGtime 6/7: Workshops on black holes and neutron stars*, pp. 39–45, December 2005.

[68] ČADEŽ, A.; CALVANI, M. & KOSTIĆ, U.: On the tidal evolution of the orbits of low-mass satellites around black holes. *Astronomy & Astrophysics*, **487**, pp. 527–532, August 2008, 0809.1783.

[69] MUKHOPADHYAY, B.: Higher-Order Nonlinearity in Accretion Disks: Quasi-Periodic Oscillations of Black Hole and Neutron Star Sources and Their Spin. *The Astrophysical Journal*, **694**, pp. 387–395, March 2009, 0811.2033.

[70] STUCHLÍK, Z.; KOTRLOVÁ, A. & TÖRÖK, G.: Multi-resonance orbital model of high-frequency quasi-periodic oscillations: possible high-precision determination of black hole and neutron star spin. *Astronomy & Astrophysics*, **552**, A10, April 2013, 1305.3552.

[71] ABRAMOWICZ, M. A. & KLUŹNIAK, W.: Epicyclic Frequencies Derived From The Effective Potential: Simple And Practical Formulae. *Astrophysics and Space Science*, **300**, pp. 127–136, November 2005, astro-ph/0411709.

[72] ALIEV, A. N.: Epicyclic Frequencies and Resonant Phenomena Near Black Holes: The Current Status. *ArXiv Astrophysics e-prints, astro-ph/0612730*, December 2006, astro-ph/0612730.

[73] HARTLE, J. B. & THORNE, K. S.: Slowly Rotating Relativistic Stars. II. Models for Neutron Stars and Supermassive Stars. *Astrophysical Journal*, **153**, p. 807, September 1968.

[74] ABRAMOWICZ, M. A.; ALMERGREN, G. J. E.; KLUZNIAK, W. & THAMPAN, A. V.: The Hartle-Thorne circular geodesics. *ArXiv General Relativity and Quantum Cosmology e-prints gr-qc/0312070*, December 2003, gr-qc/0312070.

[75] URBANCOVÁ, G.; URBANEC, M.; TÖRÖK, G.; STUCHLÍK, Z.; BLASCHKE, M. & MILLER, J. C.: Epicyclic Oscillations in the Hartle-Thorne External Geometry. *The Astrophysical Journal*, **877**(2), 66, June 2019, 1905.00730.

[76] STELLA, L. & VIETRI, M.: KHz Quasi Periodic Oscillations in Low Mass X-ray Binaries as Probes of General Relativity in the Strong Field Regime. J. PAUL; T. MONTMERLE & E. AUBOURG, editors, *19th Texas Symposium on Relativistic Astrophysics and Cosmology*, December 1998.

[77] STELLA, L. & VIETRI, M.: Lense-Thirring Precession and Quasi-periodic Oscillations in Low-Mass X-Ray Binaries. *The Astrophysical Journal Letters*, **492**, pp. L59–L62, January 1998, astro-ph/9709085.

[78] STELLA, L. & VIETRI, M.: kHz Quasiperiodic Oscillations in Low-Mass X-Ray Binaries as Probes of General Relativity in the Strong-Field Regime. *Physical Review Letters*, **82**, pp. 17–20, January 1999, astro-ph/9812124.

[79] STELLA, L. & VIETRI, M.: Strong Field Gravity and Quasi-Periodic Oscillations from Low-Mass X-Ray Binaries. V. G. GURZADYAN; R. T. JANTZEN & R. RUFFINI, editors, *The Ninth Marcel Grossmann Meeting*, pp. 426–437, December 2002.

[80] MORSINK, S. M. & STELLA, L.: Relativistic Precession around Rotating Neutron Stars: Effects Due to Frame Dragging and Stellar Oblateness. *The Astrophysical Journal*, **513**, pp. 827–844,

March 1999, astro-ph/9808227.

[81] KOSTIĆ, U.; ČADEŽ, A.; CALVANI, M. & GOMBOC, A.: Tidal effects on small bodies by massive black holes. *Astronomy & Astrophysics*, **496**, pp. 307–315, March 2009, 0901.3447.

[82] GERMANÀ, C.; KOSTIĆ, U.; ČADEŽ, A. & CALVANI, M.: Tidal Disruption of Small Satellites Orbiting Black Holes. J. RODRIGUEZ & P. FERRANDO, editors, *American Institute of Physics Conference Series*, volume 1126 of *American Institute of Physics Conference Series*, pp. 367–369, May 2009, 0902.2134.

[83] ABRAMOWICZ, M. A.; BULIK, T.; BURSA, M. & KLUŹNIAK, W.: Evidence for a 2:3 resonance in Sco X-1 kHz QPOs. *Astronomy & Astrophysics*, **404**, pp. L21–L24, June 2003, astro-ph/0206490.

[84] ABRAMOWICZ, M. A.; KARAS, V.; KLUZNIAK, W.; LEE, W. H. & REBUSCO, P.: Non-Linear Resonance in Nearly Geodesic Motion in Low-Mass X-Ray Binaries. *Publications of the Astronomical Society of Japan*, **55**, pp. 467–466, April 2003, astro-ph/0302183.

[85] KATO, S.: Basic Properties of Thin-Disk Oscillations [1]. *Publications of the Astronomical Society of Japan*, **53**, pp. 1–24, February 2001.

[86] KATO, S.: Frequency Correlations of QPOs Based on a Disk Oscillation Model in Warped Disks. *Publications of the Astronomical Society of Japan*, **59**, pp. 451–455, April 2007, astro-ph/0701085.

[87] KATO, S.: Resonant Excitation of Disk Oscillations in Deformed Disks II: A Model of High-Frequency QPOs. *Publications of the Astronomical Society of Japan*, **60**, pp. 111–123, February 2008, 0709.2467.

[88] TÖRÖK, G.; STUCHLÍK, Z. & BAKALA, P.: A remark about possible unity of the neutron star and black hole high frequency QPOs. *Central European Journal of Physics*, **5**, pp. 457–462, December 2007.

[89] TÖRÖK, G.; BAKALA, P.; ŠRÁMKOVÁ, E.; STUCHLÍK, Z. & URBANEC, M.: On Mass Constraints Implied by the Relativistic Precession Model of Twin-peak Quasi-periodic Oscillations in Circinus X-1. *The Astrophysical Journal*, **714**, pp. 748–757, May 2010, 1008.0088.

[90] STRAUB, O. & ŠRÁMKOVÁ, E.: Epicyclic oscillations of non-slender fluid tori around Kerr black holes. *Classical and Quantum Gravity*, **26**(5), 055011, March 2009, 0901.1635.

[91] FRAGILE, P. C.; STRAUB, O. & BLAES, O.: High-frequency and type-C QPOs from oscillating, precessing hot, thick flow. *Monthly Notices of the Royal Astronomical Society*, **461**, pp. 1356–1362, September 2016, 1602.08082.

[92] ABRAMOWICZ, M.; JAROSZYNSKI, M. & SIKORA, M.: Relativistic, accreting disks. *Astronomy & Astrophysics*, **63**, pp. 221–224, February 1978.

[93] ABRAMOWICZ, M. A.; BLAES, O. M.; HORÁK, J.; KLUZNIAK, W. & REBUSCO, P.: Epicyclic oscillations of fluid bodies: II. Strong gravity. *Classical and Quantum Gravity*, **23**, pp. 1689–1696, March 2006, astro-ph/0511375.

[94] BLAES, O. M.; ARRAS, P. & FRAGILE, P. C.: Oscillation modes of relativistic slender tori. *Monthly Notices of the Royal Astronomical Society*, **369**, pp. 1235–1252, July 2006, astro-ph/0601379.

[95] ABRAMOWICZ, M. A.; BARRET, D.; BURSA, M.; HORÁK, J.; KLUŹNIAK, W.; REBUSCO, P. & TÖRÖK, G.: The correlations and anticorrelations in QPO data. *Astronomische Nachrichten*, **326**, pp. 864–866, November 2005, astro-ph/0510462.

[96] ABRAMOWICZ, M. A.; BARRET, D.; BURSA, M.; HORÁK, J.; KLUŹNIAK, W.; REBUSCO, P. & TÖRÖK, G.: A note on the slope-shift anticorrelation in the neutron star kHz QPOs data. S. HLEDÍK & Z. STUCHLÍK, editors, *RAGtime 6/7: Workshops on black holes and neutron stars*, pp. 1–9, December 2005.

[97] STUCHLIK, Z.; TOROK, G. & BAKALA, P.: On a multi-resonant origin of high frequency quasiperiodic oscillations in the neutron-star X-ray binary 4U 1636-53. *arXiv e-prints*, April 2007, 0704.2318.

[98] J. SANDERS, M. G. O. B. O. I., H. BRUNNER & ESASS TEAM (MPE) / E. CHURAZOV: The first all-sky x-ray map to be released in 30 years reveals new wonders of the hot and energetic universe, 2020, URL https://skyandtelescope.org/astronomy-news/first-all-sky-map-erosita/?fbclid=IwAR3JLje8GC9AuIte8fKXfbJ9RvgKIvHaAylG8kpvXXbe9Xvq9aAl4DfAoeQ.

[99] SMALE, A. P.; ZHANG, W. & WHITE, N. E.: Discovery of Kilohertz Quasi-periodic Oscillations from 4U 1820-303 with Rossi X-Ray Timing Explorer. *The Astrophysical Journal Letters*, **483**(2), pp. L119–L122, July 1997.

[100] BOIRIN, L.; BARRET, D.; OLIVE, J. F.; BLOSER, P. F. & GRINDLAY, J. E.: Low and high frequency quasi-periodic oscillations in 4U1915-05. *Astronomy & Astrophysics*, **361**, pp. 121–138, September 2000, astro-ph/0007071.

[101] WIJNANDS, R.; MÉNDEZ, M.; VAN DER KLIS, M.; PSALTIS, D.; KUULKERS, E. & LAMB, F. K.: Discovery of Kilohertz Quasi-periodic Oscillations in the Z Source GX 5-1. *The Astrophysical Journal Letters*, **504**(1), pp. L35–L38, September 1998, astro-ph/9806050.

[102] JONKER, P. G.; WIJNANDS, R.; VAN DER KLIS, M.; PSALTIS, D.; KUULKERS, E. & LAMB, F. K.: Discovery of Kilohertz Quasi-periodic Oscillations in the Z Source GX 340+0. *The Astrophysical Journal Letters*, **499**(2), pp. L191–L194, June 1998, astro-ph/9804070.

[103] ABRAMOWICZ, M. A.; BARRET, D.; BURSA, M.; HORÁK, J.; KLUŹNIAK, W.; REBUSCO, P. & TÖRÖK, G.: The correlations and anticorrelations in QPO data. *Astronomische Nachrichten*, **326**, pp. 864–866, November 2005, astro-ph/0510462.

[104] ZWILLINGER, D. & KOKOSKA, S.: *CRC Standard Probability and Statistics Tables and Formulae*. Chapman & Hall: New York, 2000.

[105] TERLOUW, J. P. & VOGELAAR, M. G. R.: Kapteyn Package: Tools for developing astronomical applications, November 2016, 1611.010.

[106] SCHNITTMAN, J. D. & REZZOLLA, L.: Quasi-periodic Oscillations in the X-Ray Light Curves from Relativistic Tori. *The Astrophysical Journal Letters*, **637**(2), pp. L113–L116, February 2006, astro-ph/0506702.

[107] ŠRÁMKOVÁ, E.: Epicyclic oscillation modes of a Newtonian, non-slender torus. *Astronomische Nachrichten*, **326**(9), pp. 835–837, November 2005.

[108] BURSA, M.; ABRAMOWICZ, M. A.; KARAS, V. & KLUŹNIAK, W.: The Upper Kilohertz Quasi-periodic Oscillation: A Gravitationally Lensed Vertical Oscillation. *The Astrophysical Journal Letters*, **617**(1), pp. L45–L48, December 2004, astro-ph/0406586.

[109] MAZUR, G. P.; VINCENT, F. H.; JOHANSSON, M.; ŠRAMKOVÁ, E.; TÖRÖK, G.; BAKALA, P. & ABRAMOWICZ, M. A.: Towards modeling quasi-periodic oscillations of microquasars with oscillating slender tori. *Astronomy & Astrophysics*, **554**, A57, June 2013, 1303.3834.

[110] VINCENT, F. H.; PAUMARD, T.; GOURGOULHON, E. & PERRIN, G.: GYOTO: a new general relativistic ray-tracing code. *Classical and Quantum Gravity*, **28**(22), 225011, November 2011, 1109.4769.

[111] BAKALA, P.; ČERMÁK, P.; HLEDÍK, S.; STUCHLÍK, Z. & TRUPAROVÁ, K.: Extreme gravitational lensing in vicinity of Schwarzschild-de Sitter black holes. *Central European Journal of Physics*, **5**(4), pp. 599–610, December 2007, 0709.4274.

[112] ÖZEL, F. & PSALTIS, D.: Spectral Lines from Rotating Neutron Stars. *The Astrophysical Journal Letters*, **582**(1), pp. L31–L34, January 2003, astro-ph/0209225.

[113] ŠRÁMKOVÁ, E.; TÖRÖK, G.; KOTRLOVÁ, A.; BAKALA, P.; ABRAMOWICZ, M. A.; STUCHLÍK, Z.; GOLUCHOVÁ, K. & KLUŹNIAK, W.: Black hole spin inferred from 3:2 epicyclic resonance model of high-frequency quasi-periodic oscillations. *Astronomy & Astrophysics*, **578**, A90, June 2015, 1505.02712.

[114] GOLUCHOVÁ, K.; KULCZYCKI, K.; VIEIRA, R. S. S.; STUCHLÍK, Z.; KLUŹNIAK, W. & ABRAMOWICZ, M.: Hořava's quantum gravity illustrated by embedding diagrams of the Kehagias-Sfetsos spacetimes. *General Relativity and Gravitation*, **47**, 132, November 2015, 1511.01345.

[115] KOTRLOVÁ, A.; ŠRÁMKOVÁ, E.; TÖRÖK, G.; STUCHLÍK, Z. & GOLUCHOVÁ, K.: Super-spinning compact objects and models of high-frequency quasi-periodic oscillations observed in Galactic microquasars. II. Forced resonances. *Astronomy & Astrophysics*, **607**, A69, November 2017, 1708.04300.

[116] KOTRLOVÁ, A.; ŠRÁMKOVÁ, E.; TÖRÖK, G.; GOLUCHOVÁ, K.; HORÁK, J. & STRAUB, O.: Non-geodesic corrections to mass-spin estimates for Galactic microquasars implied by quasiperiodic oscillation models. *Astronomische Nachrichten*, **340**(112), pp. 112–115, January 2019.

[117] GOLUCHOVÁ, K.; TÖRÖK, G.; ŠRÁMKOVÁ, E.; ABRAMOWICZ, M. A.; STUCHLÍK, Z. & HORÁK, J.: Mass of the active galactic nucleus black hole XMMUJ134736.6+173403. *Astronomy & Astrophysics*, **622**, L8, February 2019, 1901.05419.

[118] TÖRÖK, G.; GOLUCHOVÁ, K.; ŠRÁMKOVÁ, E.; URBANEC, M. & STRAUB, O.: Time-scale of twin-peak quasi-periodic oscillations and mass of accreting neutron stars. *Monthly Notices of the Royal Astronomical Society*, **488**(3), pp. 3896–3903, September 2019, 1907.05174.

[119] BAKALA, P.; DE FALCO, V.; BATTISTA, E.; GOLUCHOVÁ, K.; LANČOVÁ, D.; FALANGA, M. & STELLA, L.: Three-dimensional general relativistic Poynting-Robertson effect. II. Radiation field from a rigidly rotating spherical source. *Physical Review D*, **100**(10), 104053, November 2019, 1911.00540.

[120] KOTRLOVÁ, A.; ŠRÁMKOVÁ, E.; TÖRÖK, G.; GOLUCHOVÁ, K.; HORÁK, J.; STRAUB, O.; LANČOVÁ, D.; STUCHLÍK, Z. & ABRAMOWICZ, M. A.: Models of high-frequency quasi-periodic oscillations and black hole spin estimates in Galactic microquasars. *Astronomy & Astrophysics*, **643**, A31, November 2020, 2008.12963.

[121] HAWLEY, J. F. & BALBUS, S. A.: The Dynamical Structure of Nonradiative Black Hole Accretion Flows. *The Astrophysical Journal*, **573**(2), pp. 738–748, July 2002, astro-ph/0203309.

[122] DE VILLIERS, J.-P. & HAWLEY, J. F.: A Numerical Method for General Relativistic Magnetohydrodynamics. *The Astrophysical Journal*, **589**(1), pp. 458–480, May 2003, astro-ph/0210518.

[123] TAGGER, M. & VARNIÈRE, P.: Accretion-Ejection Instability, MHD Rossby Wave Instability, Diskoseismology, and the High-Frequency QPOs of Microquasars. *The Astrophysical Journal*,

652(2), pp. 1457–1465, December 2006, astro-ph/0608123.

[124] BLAES, O. M.; ŠRÁMKOVÁ, E.; ABRAMOWICZ, M. A.; KLUŹNIAK, W. & TORKELSSON, U.: Epicyclic Oscillations of Fluid Bodies: Newtonian Nonslender Torus. *The Astrophysical Journal*, **665**(1), pp. 642–653, August 2007, 0706.4483.

[125] JAHODA, K.; SWANK, J. H.; GILES, A. B.; STARK, M. J.; STROHMAYER, T.; ZHANG, W. & MORGAN, E. H.: In-orbit performance and calibration of the Rossi X-ray Timing Explorer (RXTE) Proportional Counter Array (PCA). O. H. SIEGMUND & M. A. GUMMIN, editors, *EUV, X-Ray, and Gamma-Ray Instrumentation for Astronomy VII*, volume 2808 of *Society of Photo-Optical Instrumentation Engineers (SPIE) Conference Series*, pp. 59–70, October 1996.

[126] PECHÁČEK, T.; KARAS, V. & CZERNY, B.: Hot-spot model for accretion disc variability as random process. *Astronomy & Astrophysics*, **487**(3), pp. 815–830, September 2008, 0807.0224.

Part II

Individual papers

Collection of the papers

On the following pages, one can find copies of papers commented on in the text of this thesis. Here is a list of them:

- TÖRÖK, G.; BAKALA, P.; ŠRÁMKOVÁ, E.; STUCHLÍK, Z.; URBANEC, M. & GOLUCHOVÁ, K.: Mass-Angular-momentum Relations Implied by Models of Twin Peak Quasi-periodic Oscillations. *The Astrophysical Journal*, **760**, 138, 2012, 1408.4220.

- BAKALA, P.; GOLUCHOVÁ, K.; TÖRÖK, G.; ŠRÁMKOVÁ, E.; ABRAMOWICZ, M. A.; VINCENT, F. H. & MAZUR, G. P.: Twin peak high-frequency quasi-periodic oscillations as a spectral imprint of dual oscillation modes of accretion tori. *Astronomy & Astrophysics*, **581**, A35, 2015, 1505.06673.

- STUCHLÍK, Z.; URBANEC, M.; KOTRLOVÁ, A.; TÖRÖK, G. & GOLUCHOVÁ, K.: Equations of State in the Hartle-Thorne Model of Neutron Stars Selecting Acceptable Variants of the Resonant Switch Model of Twin HF QPOs in the Atoll Source 4U 1636-53. *Acta Astronomica*, **65**, 169–195, 2015, 1507.00373.

- TÖRÖK, G.; GOLUCHOVÁ, K.; URBANEC, M.; ŠRÁMKOVÁ, E.; ADÁMEK, K.; URBANCOVÁ, G.; PECHÁČEK, T.; BAKALA, P.; STUCHLÍK, Z.; HORÁK, J. & JURYŠEK, J.: Constraining Models of Twin-Peak Quasi-periodic Oscillations with Realistic Neutron Star Equations of State. *The Astrophysical Journal*, **833**, 273, 2016, 1611.06087.

- TÖRÖK, G.; GOLUCHOVÁ, K.; HORÁK, J.; ŠRÁMKOVÁ, E.; URBANEC, M.; PECHÁČEK, T. & BAKALA, P.: Twin peak quasi-periodic oscillations as signature of oscillating cusp torus. *Monthly Notices of the Royal Astronomical Society: Letters*, **457**, L19–L23, 2016, 1512.03841.

- TÖRÖK, G.; GOLUCHOVÁ, K.; ŠRÁMKOVÁ, E.; HORÁK, J.; BAKALA, P. & URBANEC, M.: On one-parametric formula relating the frequencies of twin-peak quasi-periodic oscillations. *Monthly Notices of the Royal Astronomical Society*, **473**, L136–L140, 2018, 1710.10901.

- GOLUCHOVÁ, K.; TÖRÖK, G.; ŠRÁMKOVÁ, E.; ABRAMOWICZ, M. A.; STUCHLÍK, Z.; HORÁK, J.: Mass of the active galactic nucleus black hole XMMUJ134736.6+173403. *Astronomy & Astrophysics*, **622**, id.L8, 2019.

- Török, G.; Goluchová, K.; Šrámková, E.; Urbanec, M.; Straub, O.: Timescale of twin-peak quasi-periodic oscillations and mass of accreting neutron stars. Accepted for publication in MNRAS.

- GABRIEL TÖRÖK, ANDREA KOTRLOVÁ, MONIKA MATUSZKOVÁ, KATEŘINA KLIMOVIČOVÁ, DEBORA LANČOVÁ, GABRIELA URBANCOVÁ, EVA ŠRÁMKOVÁ Simple analytic formula relating the mass and spin of accreting compact objects to their rapid X-ray variability. *Submitted to The Astrophysical Journal*.

Paper I

6.1. Mass-angular momentum relations implied by models of twin peak Quasi-periodic oscillations

Török Gabriel Bakala Pavel, Šrámková Eva, Stuchlík Zdeněk, Urbanec Martin & Goluchová, Kateřina

The Astrophysical Journal, 2012,
Volume 760, Issue 2, article id. 138

The Astrophysical Journal, 760:138 (15pp), 2012 December 1 doi:10.1088/0004-637X/760/2/138

MASS–ANGULAR-MOMENTUM RELATIONS IMPLIED BY MODELS OF TWIN PEAK QUASI-PERIODIC OSCILLATIONS

Gabriel Török, Pavel Bakala, Eva Šrámková, Zdeněk Stuchlík, Martin Urbanec, and Kateřina Goluchová
Institute of Physics, Faculty of Philosophy and Science, Silesian University in Opava, Bezručovo nám. 13, CZ-746 01 Opava, Czech Republic;
pavel.bakala@fpf.slu.cz, martin.urbanec@fpf.slu.cz, zdenek.stuchlik@fpf.slu.cz, terek@volny.cz, sram_eva@centrum.cz, www.physics.cz
Received 2010 November 30; accepted 2012 September 26; published 2012 November 16

ABSTRACT

Twin peak quasi-periodic oscillations (QPOs) appear in the X-ray power-density spectra of several accreting low-mass neutron star (NS) binaries. Observations of the peculiar Z-source Circinus X-1 display unusually low QPO frequencies. Using these observations, we have previously considered the relativistic precession (RP) twin peak QPO model to estimate the mass of the central NS in Circinus X-1. We have shown that such an estimate results in a specific mass–angular-momentum ($M-j$) relation rather than a single preferred combination of M and j. Here we confront our previous results with another binary, the atoll source 4U 1636−53 that displays the twin peak QPOs at very high frequencies, and extend the consideration to various twin peak QPO models. In analogy to the RP model, we find that these imply their own specific $M-j$ relations. We explore these relations for both sources and note differences in the χ^2 behavior that represent a dichotomy between high- and low-frequency sources. Based on the RP model, we demonstrate that this dichotomy is related to a strong variability of the model predictive power across the frequency plane. This variability naturally comes from the radial dependence of characteristic frequencies of orbital motion. As a consequence, the restrictions on the models resulting from observations of low-frequency sources are weaker than those in the case of high-frequency sources. Finally we also discuss the need for a correction to the RP model and consider the removing of $M-j$ degeneracies, based on the twin peak QPO-independent angular momentum estimates.

Key words: stars: neutron – X-rays: binaries

1. INTRODUCTION

Several low-mass neutron star binaries (NS LMXBs) exhibit in the high-frequency part of their X-ray power-density spectra (PDS) two distinct peaks, so-called twin peak quasi-periodic oscillations (QPOs). The two peaks are referred to as the upper and lower QPO. Centroid frequencies of these QPOs, ν_L and ν_U, vary over time, but follow frequency correlations specific to individual sources. However, these specific correlations are qualitatively similar (see Psaltis et al. 1999; Stella et al. 1999; Abramowicz et al. 2005a, 2005b, and references therein). In some cases, the frequency ranges spanned by a single source are as large as a few hundreds of Hz. At present, there is no consensus on the QPO origin. Numerous models have been proposed, mostly assuming that the two twin QPOs carry important information about the inner accreting region dominated by the effects of strong Einstein's gravity. In principle, several of these models imply restrictions to neutron star (NS) parameters (a systematic treatment of these restrictions through the fitting of twin peak QPO correlations was pioneered by Psaltis et al. 1998). A brief introduction to QPOs and their models can be found in van der Klis (2006).

In our previous work, Török et al. (2010), hereafter Paper I, we focused on restrictions of a particular "relativistic precession" (RP) QPO model and a peculiar bright Z-source Circinus X-1. The RP model introduced by Stella & Vietri (1999) and Stella et al. (1999) identifies the lower and upper kHz QPOs with the periastron precession ν_P and Keplerian ν_K frequency of a perturbed circular geodesic motion at the given radii r,

$$\nu_L(r) = \nu_P(r) = \nu_K(r) - \nu_r(r), \quad \nu_U(r) = \nu_K(r), \qquad (1)$$

where ν_r is the radial epicyclic frequency of the Keplerian motion. In Paper I we noticed that the RP model well matches the data points of Circinus X-1 for any dimensionless NS angular momentum, $j \equiv cJ/GM^2$, when the assumed NS mass reads $M \sim 2.2\, M_\odot[1+0.55(j+j^2)]$. We have shown that the existence of such a mass–angular-momentum ($M-j$) relation is generic for the model.

Circinus X-1 that we discussed in Paper I is a relatively well-known source, since it displays twin QPOs at unusually low frequencies, $\nu_L \in$ (50 Hz, 250 Hz) and $\nu_U \in$ (200 Hz, 500 Hz) (see Boutloukos et al. 2006, who discovered its QPOs). Here we consider another binary, a faint atoll source 4U 1636−53 that, on the contrary, displays twin peak QPOs at very high frequencies, $\nu_L \in$ (550 Hz, 1000 Hz) and $\nu_U \in$ (800 Hz, 1250 Hz) (Barret et al. 2005b, 2005c). As illustrated in Figure 1(a), also assuming this source we can confront the two representatives of high- and low-frequency twin peak QPO sources (in general, twin peak QPOs are more often detected at rather low frequencies in Z-sources and high frequencies in atoll sources, but there are some counterexamples, e.g., Z-source Sco X-1; see van der Klis 2006). Apart from the RP model, we extend our consideration to several other twin peak QPO models. The text is organized as follows.

In Section 2, we briefly recall some points from Paper I that are of generic importance for the present work. In Section 3, we briefly recall the data used and their origin along with the set of QPO models that are considered within the paper. In Section 4, we fit the data points with the frequency relations predicted by individual models and show that, in analogy to the RP model, each of them implies its specific mass–angular-momentum relation. In Section 5, we discuss the issue of the models' predictive power variability across the frequency plane. We also briefly investigate the requirement of a correction to the RP model and suggest that it can be relevant to both high- and low-frequency sources. In Section 6, we discuss our results and present some concluding remarks.

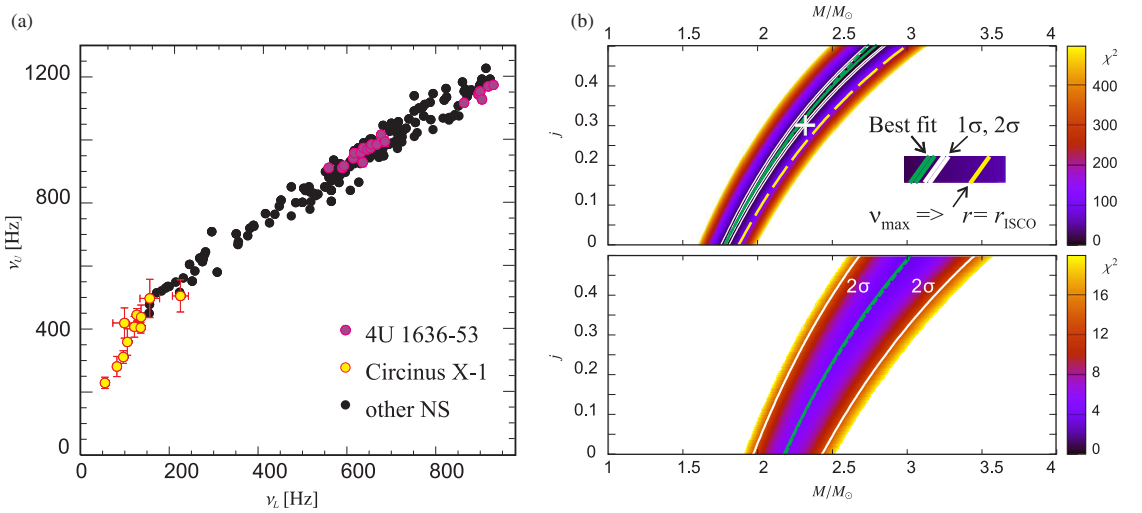

Figure 1. (a) Twin peak QPO frequencies in the atoll source 4U 1636−53 (22 data points in purple), Z-source Circinus X-1 (11 data points in red/yellow), and several other atoll and Z-sources (data points in black). (b) The χ^2 dependence on M and j for the RP model. The top panel corresponds to 4U 1636−53 while the bottom panel corresponds to Circinus X-1. For 4U 1636−53 $\xi = 4$ is assumed. The dashed green line indicates the best χ^2 for a fixed M. The continuous green line denotes its quadratic approximation. The white lines indicate corresponding 1σ and 2σ confidence levels. The white cross-marker denotes the mass and angular momentum reported for 4U 1636−53 and the RP model by Lin et al. (2011; see Section 6). The dashed yellow line in the top panel indicates a simplified estimate on the upper limits on M and j assuming that the highest observed upper QPO frequency in 4U 1636−53 is associated with the ISCO. This estimate is not included for Circinus X-1 because the observed frequencies clearly point to radii far away from ISCO which can be seen from Figure 6.

2. MASS–ANGULAR-MOMENTUM RELATION FROM RP MODEL

As found in Paper I, the data points of Circinus X-1 are well matched by the RP model when the combinations of the source mass and angular momentum are in the form of $M \sim 2.2\, M_\odot[1+0.55(j+j^2)]$. The existence of such an $(M-j)$ relation is generic to the model. Let us briefly recall the major points and implications of our previous results.

We found that due to the properties of the RP model and the NS spacetime the quality of fit for a given source should not differ much from the following general relation:

$$M \sim M_0[1 + k(j + j^2)]. \tag{2}$$

In this relation, M_0 is the mass that provides the best fit assuming a non-rotating star ($j = 0$). The coefficient k, implied by the model, would read $k = 0.7$ if the measured data points were sampled uniformly along the large range of frequencies

$$\nu_L \in (\nu \ll \nu_{\rm ISCO},\ \nu_{\rm ISCO}), \tag{3}$$

where $\nu_{\rm ISCO}$ denotes the Keplerian orbital frequency at the innermost stable circular orbit $r_{\rm ms}$ (hereafter ISCO). The available data points are, however, unequally sampled and often cluster, either simply due to incomplete sampling and weakness of the two QPOs outside the limited frequency range, or due to the intrinsic source clustering (Abramowicz et al. 2003a; Belloni et al. 2005, 2007b; Török et al. 2008a, 2008b, 2008c; Barret & Boutelier 2008; Boutelier et al. 2010).

2.1. Importance of Frequency Ratio for the RP Model Predictions in Different Sources

In the detailed analysis presented in Appendix A.2 of Paper I, we elaborated the influence of unequal sampling of the frequency correlation $\nu_U(\nu_L)$. It is important that frequencies predicted from the RP model scale as $1/M$ for a fixed j, and in this sense the expected frequency ratio, $R \equiv \nu_U/\nu_L$, is mass independent. Moreover, in the RP model, it is

$$R = \nu_K/(\nu_K - \nu_r). \tag{4}$$

The frequency ν_r vanishes when the radial coordinate approaches ISCO, $r \to r_{\rm ms}$, and therefore $R \to 1$. On the other hand, when $r \to \infty$ the spacetime becomes flat, reaching the Newtonian limit where $\nu_r \to \nu_K$ and R diverges. The QPOs that are expected to arise close to ISCO therefore always reveal a low R, while those expected to arise in a large radial distance from the NS reveal a high R. For any NS parameters, the top part (relatively high frequencies) of a given frequency correlation $\nu_U(\nu_L)$ predicted by the RP model then reveals a frequency ratio close to $R = 1$. The bottom part (relatively low frequencies) of the frequency correlation reveals a high frequency ratio $R \gtrsim 3$.[1]

Based on the above-mentioned theoretical prediction of the RP model, in Paper I we found that the value of k in mass–angular-momentum relation (2) must tend to $k \sim 0.75$ when the range of the ratio of the lower and upper QPO frequencies in the sample falls to low values close to $R = 1$. On the other hand, it is $k \sim 0.5$ when the range of R has a high value ($R \sim 5$). This consequence of unequal sampling does not depend on the absolute values of the QPO frequencies.

As noticed first by Stella & Vietri (1999) and Stella et al. (1999) and later discussed in several works (e.g., Belloni et al. 2007a), the frequencies of the twin peak QPOs observed in most of the NS sources are roughly matched by the frequency correlation implied by the RP model for the

[1] In Paper I we have shown that more than 60% of the length of the expected curve $\nu_U(\nu_L)$ corresponds to $R < 3$ (see Figure 9 of Paper I).

NS mass $M \sim 2\ M_{\odot}$. Assuming this mass, the low frequency ratio $R \lesssim 1.5$ roughly corresponds to high QPO frequencies, $\nu_L \sim 0.6$–1 kHz, while $R \sim (2$–$5)$ corresponds to low QPO frequencies, $\nu_L \sim 50$–500 Hz. This roughly matches the phenomenological division between "low-" and "high"-frequency twin peak QPO sources based on the distribution of typical frequencies of QPOs observed in individual continuous observations. Thus, in practice, the expected value of $k = 0.7$ changes due to unequal sampling only very slightly to $k \sim 0.7$–0.75 for available data on high-frequency twin peak QPO sources. For the available data on low-frequency twin peak QPO sources, the effect of unequal sampling is more important, changing k to ∼0.5–0.65, which also corresponds to the case of Circinus X-1 elaborated in Paper I. Detailed quantification of restrictions on k can be found in Table 1 of Paper I.

Next we justify our result by comparing the case of Circinus X-1 to the case of the high-frequency source 4U 1636−53, for which we expect $k \sim 0.7$–0.75. Then we explore whether several other QPO models imply their own $M - j$ relations or not.

3. DATA AND MODELS

Figure 1(a) shows several twin peak QPO data points coming from the works of Barret et al. (2005b, 2005c), Boirin et al. (2000), Di Salvo et al. (2003), Homan et al. (2002), Jonker et al. (2002a, 2002b), Méndez & van der Klis (2000), Méndez et al. (2001), van Straaten et al. (2000, 2002), Zhang et al. (1998), and Boutloukos et al. (2006). For the analysis presented in this paper we use the twin peak QPO data of 4U 163−53 (from Barret et al. 2005b, 2005c) and Circinus X-1 (from Boutloukos et al. 2006). These data points are denoted in the figure by the color-coded symbols. Each of them corresponds to an individual continuous segment of the source observation. One can see that our choice of the two representative NSs allows us to demonstrate the confrontation between the low- and high-frequency sources, as mentioned in the previous section. Details of the observations, data analysis techniques, and properties of the twin peak QPOs in the two sources discussed can be found in Barret et al. (2005b, 2005c, 2006), Boutloukos et al. (2006), Méndez (2006), and van der Klis (2006).

Each of the many QPO models proposed (e.g., Alpar & Shaham 1985; Lamb et al. 1985; Miller at al. 1998; Psaltis et al. 1999; Wagoner 1999; Wagoner et al. 2001; Abramowicz & Kluźniak 2001; Titarchuk & Kent 2002; Rezzolla et al. 2003; Pétri 2005; Zhang 2005; Kato 2007; Stuchlík et al. 2008; Mukhopadhyay 2009) still faces several difficulties and, at present, none of them is favored. In such a situation, we expect that the estimations of mass and angular momentum based on the individual models could be helpful for the further development or falsification of an appropriate model. In the next section we therefore consider several of these models in addition to the RP model investigated in Paper I, and examine what mass–angular-momentum relations they imply. Since we do not attempt to describe the individual models and resolve all their specific issues in detail, in what follows we just give a short summary of the models examined and highlight some of their distinctions along with the related references.[2]

3.1. Individual Models

The RP model has been proposed in a series of papers by Stella & Vietri (1998a, 1998b, 1999, 2002) and Morsink & Stella (1999) and explains the kHz QPOs as a direct manifestation of modes of relativistic epicyclic motion of blobs at various radii r in the inner parts of the accretion disk. Within the model, the twin peak QPO frequency correlation arises due to periastron precession of the relativistic orbits. Because of the existence of another so-called Lense–Thirring RP the model also predicts another frequency correlation extending to higher timescales. The kHz QPO frequencies are indeed correlated with the low-frequency QPO features observed far below 100 Hz, which were first noticed and discussed in the works of Psaltis et al. (1999), Stella & Vietri (1999), and Stella et al. (1999). Here we restrict our attention mostly to kHz features but the low-frequency QPO interpretation within the RP model is briefly considered in Section 6 and Appendix B.1.

Recently, Čadež et al. (2008), Kostić et al. (2009), and Germana et al. (2009) have introduced a similar concept in which the QPOs were generated by a "tidal disruption" (TD) of large accreting inhomogeneities. It is assumed—and is supported by some hydrodynamic simulations—that blobs orbiting the central compact object are stretched by tidal forces forming "ring-section" features that are responsible for the observed modulation. The model has been proposed for black hole (BH) sources (both supermassive and stellar mass) but, in principle, it should work for compact NS sources as well. In some cases at least, the PDS produced within the model seem to well reproduce those observed.

It is often argued that QPOs arise due to "disk oscillations" (in contrast to the above models considering "hot-spot motion") and that some resonances can be involved. The disk-oscillation concept has a good potential for explaining the high QPO coherence times observed in some NS systems (see Barret et al. 2005a, who first recognized the importance of the high QPO quality factor measured in 4U 1636−53, $Q \sim 200$). The resonance hypothesis is supported by the appearance of the 3:2 frequency ratio observed in BH sources (Abramowicz & Kluźniak 2001; McClintock & Remillard 2006; Török et al. 2005). There is also a less straightforward evidence for the importance of the same 3:2 ratio in the case of NS sources which was first noticed in terms of the frequency ratio $R \equiv \nu_U/\nu_L$ clustering (see Abramowicz et al. 2003a; Belloni et al. 2005, 2007b; Török et al. 2008a, 2008b, 2008c; Boutelier et al. 2010, for details and related discussion). As found recently, in the six atoll NS systems including 4U 1636−53, the difference between the rms amplitudes of the upper and lower QPOs changes its sign for resonant frequency ratios $R = 3{:}2$ (Török 2009). This interesting effect still requires some further investigation, since the rms amplitudes of kHz QPOs are energy dependent and this must be taken into account. Nevertheless, we note that it was suggested by Horák et al. (2009) that the "energy switch" effect could be naturally explained in terms of the theory of the nonlinear resonance.

Two examples of the often quoted resonant disk-oscillation models are the epicyclic resonance (ER) model (Kluźniak & Abramowicz 2001; Abramowicz et al. 2003b, 2003c; Kluźniak et al. 2004) assuming axisymmetric modes and the "warped disk" (WD) oscillation model suggested by Kato (2001, 2007, 2008) that assumes non-axisymmetric modes. We consider these and also another two QPO resonance models dealing with different combinations of non-axisymmetric disk-oscillation modes. The latter two models are of particular interest because they involve oscillation modes whose frequencies almost coincide with the frequencies predicted by the RP model when the NS rotates slowly. We denote them as the RP1 (Bursa 2005) and RP2

[2] Some more details on these models and a discussion of their relevance to black-hole QPOs can be found in Török et al. (2011).

Table 1
The Main Definition Relations for the Models Considered and the Mass–Angular-momentum Relations Found for 4U 1636−53 and Circinus X-1

Model	Atoll Source 4U 1636−53		Z-source Circinus X-1	
	χ^2/dof ∼	$(M_0/M_\odot) \times f(j)$	χ^2/dof ∼	$(M_0/M_\odot) \times f(j)$
RP $\nu_L = \nu_K - \nu_r$, $\nu_U = \nu_K$	16	$1.78[\pm0.03] \times [1 + 0.7(j + j^2)]$	1.3	$2.2[\pm0.3] \times [1 + 0.5(j + j^2)]$
TD $\nu_L = \nu_K$, $\nu_U = \nu_K + \nu_r$	7	$2.15[\pm0.02] \times [1 + 0.7(j + j^2)]$	30	X
WD $\nu_L = 2(\nu_K - \nu_r)$, $\nu_U = 2\nu_K - \nu_r$	21	$2.49[\pm0.1] \times [1 + 0.7(j + j^2)]$	1.1	1.3[a]
RP1 $\nu_L = \nu_K - \nu_r$, $\nu_U = \nu_\theta$	16	$1.78[\pm0.03] \times [1 + 0.5(j + j^2)]$	1.3	$2.2[\pm0.3] \times [1 + 0.4(j + j^2)]$
RP2 $\nu_L = \nu_K - \nu_r$, $\nu_U = 2\nu_K - \nu_\theta$	16	$1.78[\pm0.03] \times [1 + 1.0(j + j^2)]$	1.3	$2.2[\pm0.3] \times [1 + 0.7(j + j^2)]$
ER $\nu_L = \nu_r + \Delta\nu_L$[b], $\nu_U = \nu_\theta + \Delta\nu_U$	3	$0.95[\pm0.1] \times [1 + 0.8j - 2j^2]$	1.5	$3.5[\pm0.3] \times [1 + 1.9(j + j^2)]$[c]

Notes. Symbols ν_K, ν_r, and ν_θ denote the orbital Keplerian, radial epicyclic, and vertical epicyclic frequencies (see Appendix A.1 for the explicit terms in the Kerr spacetimes). For both sources, except for the ER model, the errors in the estimated mass corresponds to the 2σ confidence level. For the ER model, the errors are given by the scatter in the estimated resonant eigenfrequencies (see Urbanec et al. 2010b).
[a] The mass–angular-momentum relation that we found reads $M = 1.3[+0.3, -0.2]\ M_\odot \times [1 + 0.4(j + j^2)]$. Due to the low M_0, the angular momentum dependence cannot be taken seriously (see Section 6 for a comment on this).
[b] See Section 4.4 for details.
[c] The possibility that the observed frequencies are the resonant combinational frequencies is taken into account.

(Török et al. 2007, 2010) models and assume that the resonant corrections to the eigenfrequencies are negligible.

3.1.1. Frequency Relations

The relations that define the upper and lower QPO frequencies in terms of the orbital frequencies are given for each of the above models in the first column of Table 1. We include these terms for the case of the Kerr spacetimes in Appendix A.1. The applicability of an approach assuming the Kerr spacetimes for high-mass NSs was elaborated in Paper I. The relevance and limitations of the same approach within the work and results presented here are discussed more in Section 6 and Appendix A.3.

For the RP model, one can easily solve the definition relations to arrive at the explicit formula which relates the upper and lower QPO frequencies. A similar simple evaluation of an explicit relation between the two observed QPO frequencies is also possible for the TD model. For the RP and TD models, we give the explicit formulas in Equations (A3) and (A4). For the WD, RP1, and RP2 models the definition relations lead to high-order polynomial equations that relate the lower and upper QPO frequencies. In these cases, in Appendix A.1 we give only the implicit form of the $\nu_U(\nu_L)$ function which has to be treated numerically.

For the version of the ER model assumed here, we expect the $\nu_U(\nu_L)$ function in the form of a linear relation. This approach follows the work of Abramowicz et al. (2005a, 2005b) and related details are briefly recalled in Section 4.4.

4. DATA MATCHING

In this section we fit the data points of 4U 1636−53 and Circinus X-1 with frequency relations predicted from each of the individual models (i.e., by functions (A3) and (A4) for the RP and TD model, respectively, by a straight line for the ER model, and by the numerically given solutions of Equations (A5)–(A7) for the other models).[3] As in Paper I, we restrict the range of mass and angular momentum considered to $[M \in (1, 4)\ M_\odot] \times [j \in (0, 0.5)]$. For all the models except the ER model (Section 4.4), we first find the best fit in the Schwarzschild spacetime ($j = 0$) for a single free parameter M using the least-squares fitting procedure (e.g., Press et al. 2007). Then we also inspect the two-dimensional χ^2 behavior for the free M and j.

Within the numerical approach adopted the model frequency curve is parameterized along its full length through a parameter p which ranges from p_∞ to $p_{\rm ISCO}$. The exact definition of χ^2 that we use here is then given as

$$\chi^2 \equiv \sum_{n=1}^{m} \Delta_n^2, \quad \text{with } \Delta_n = \text{Min}\left(\frac{l_{n,p}}{\sigma_{n,p}}\right)_{p_\infty}^{p_{\rm ISCO}}, \qquad (5)$$

where $l_{n,p}$ is the length of a line between the nth measured data point $[\nu_L(n), \nu_U(n)]$ and a point $[\nu_L(p), \nu_U(p)]$ belonging to the model frequency curve. The quantity $\sigma_{n,p}$ equals the length of the part of this line located within the error ellipse around the data point.

4.1. Results for the RP, RP1, and RP2 Models

Considering $j = 0$ for fitting the data of 4U 1636−53 with the RP model, we find a narrow χ^2 minimum for $M_0 \sim 1.8\ M_\odot$

[3] At this point we should also note that our choice of models represents a subset of those recently discussed by Lin et al. (2011) for the two sources 4U 1636−53 and Sco X-1. An overlap with their work is discussed in Section 6.

but its value is rather high, $\chi^2 \doteq 350/21$ dof. We also find that there is no sufficient improvement along the whole given range of mass even up to the upper limit of j. Thus, assuming that the model is valid, we can only speculate that there is an unknown systematic uncertainty. Then it follows from Equation (5) that the χ^2 of the best fit for $j = 0$ drops to an acceptable value $\chi^2 = 1$ dof when the uncertainties in the measured QPO frequencies are multiplied (underestimated) by factor $\xi \equiv \sqrt{\chi^2/\mathrm{dof}} \doteq 4$. Under this consideration we find the NS mass from the best-fit reading $M_0 = 1.78\ M_\odot$. We express the corresponding scatter in the estimated mass as $\delta M = [\pm 0.03]\ M_\odot$, assuming the 2σ confidence level which we henceforth use as the reference one.

On the other hand, the best match to the data of Circinus X-1 for the RP model and $j = 0$ already reveals an acceptable value of $\chi^2 \doteq 12.9/10$ dof, and in summary we can write the quantities M_0 inferred from the RP model for both sources as

$$M_0 = 1.78[\pm 0.03]\ M_\odot \quad \text{in 4U 1636–53} \quad (\chi^2 = 1\ \text{dof} \Leftrightarrow \xi \doteq 4) \tag{6}$$

and

$$M_0 = 2.19[\pm 0.3]\ M_\odot \quad \text{in Circinus X-1} \quad (\chi^2 = 12.9/10\ \text{dof}). \tag{7}$$

As found in Paper I and briefly recalled here in Section 2, for the RP model and a given source the χ^2 should not differ much along the $M-j$ relation $M \sim M_0[1 + k(j + j^2)]$ where $k \sim 0.7$–0.75 for high-frequency sources and $k \sim 0.5$–0.6 for low-frequency sources. The results of the two-dimensional fitting of the parameters M and j agree well with this finding. The χ^2 behavior for 4U 1636−53 is depicted and compared to the case of Circinus X-1 in the form of color-coded maps in Figure 1(b). Clearly, the best fits are reached when M and j are related through the specific relations denoted by the dashed green lines. We approximate these relations in the form $M = M_0 \times [1 + k(j + j^2)]$ arriving at the following terms:

$$M = 1.78[\pm 0.03]\ M_\odot \times [1 + 0.73(j + j^2)] \quad \text{in 4U 1636–53} \tag{8}$$

and

$$M = 2.19[\pm 0.3]\ M_\odot \times [1 + 0.52(j + j^2)] \quad \text{in Circinus X-1.} \tag{9}$$

4.1.1. Results for the RP1 Model

The frequencies predicted by the RP and RP1 models are very similar for slowly rotating NSs. The two models commonly define the lower observable QPO frequency as

$$\nu_L = \nu_\kappa - \nu_\mathrm{r}. \tag{10}$$

The upper observable QPO frequencies differ, reading

$$\nu_U^{\mathrm{RP}} = \nu_\kappa\,, \quad \nu_U^{\mathrm{RP1}} = \nu_\theta. \tag{11}$$

In the Schwarzschild limit $j = 0$, $\nu_\theta = \nu_\kappa$ and ν_U is common to both RP and RP1. Consequently,

$$M_0^{\mathrm{RP1}} = M_0^{\mathrm{RP}}, \tag{12}$$

where M_0^{RP} is given in Equations (6) and (7) for 4U 1636−53 and Circinus X-1, respectively. For 4U 1636−53, the quality of the fits does not differ much between $j = 0$ and $j \neq 0$ and the same conclusions on the possible unknown systematic uncertainty as in the case of the RP model are valid.

One can expect that fits to the data based on the RP1 model for $j \neq 0$ should exhibit $M-j$ degeneracy qualitatively similar to the case of the RP model. We do not repeat for the RP1 model the full analysis of $M-j$ degeneracy presented in Paper I for the RP model. Instead, we just inspect the behavior of χ^2 for free M and j to check whether such degeneracy is present and evaluate it. The χ^2 behavior resulting for free M and j is depicted in the form of color-coded maps in Figure 2(a). The two χ^2 maps displayed clearly reveal $M-j$ degeneracy qualitatively similar to that of the RP model. Related $M-j$ relations (best χ^2 for a fixed M) are denoted by dashed green lines in Figure 2(a). We approximate these relations in the form $M = M_0 \times [1+k(j+j^2)]$ arriving at the following terms:

$$M = 1.78[\pm 0.03]\ M_\odot \times [1 + 0.48(j + j^2)] \quad \text{in 4U 1636–53} \tag{13}$$

and

$$M = 2.19[\pm 0.3]\ M_\odot \times [1 + 0.39(j + j^2)] \quad \text{in Circinus X-1.} \tag{14}$$

4.1.2. Results for the RP2 Model

As in the previous case, the frequencies predicted by the RP2 model are very similar to those of the RP model for a slowly rotating NS. The lower observable QPO frequency is commonly defined by Equation (10). The upper observable QPO frequency differs from the RP model and reads

$$\nu_U^{\mathrm{RP2}} = 2\nu_\kappa - \nu_\theta. \tag{15}$$

However, in the Schwarzschild limit $j = 0$ $\nu_\theta = \nu_\kappa$ and the expression for the upper observable QPO frequency $\nu_U = \nu_\kappa$ is common for all the three models RP, RP1, and RP2. For $j = 0$, therefore, the frequency relations implied by these models merge (although the expected mechanisms generating the QPOs are different). Thus we can write

$$M_0^{\mathrm{RP2}} = M_0^{\mathrm{RP1}} = M_0^{\mathrm{RP}}, \tag{16}$$

where M_0^{RP} is given in Equation (6) for 4U 1636−53 and Equation (7) for Circinus X-1. For 4U 1636−53, the quality of the fits is again not much different between $j = 0$ and $j \neq 0$ and the same conclusions are valid on the possible unknown systematic uncertainty as in the case of the RP1 and RP2 models.

The χ^2 behavior resulting from fitting the data points for free M and j is depicted in the form of color-coded maps in Figure 2(b). These χ^2 maps again clearly reveal $M-j$ degeneracy qualitatively similar to that in the case of the RP and RP1 models. The best χ^2 for a fixed M ($M-j$ relation) is in each case denoted by the dashed green line. The corresponding approximate relations in the form $M = M_0 \times [1 + k(j + j^2)]$ read

$$M = 1.78[\pm 0.03]\ M_\odot \times [1 + 0.98(j + j^2)] \quad \text{in 4U 1636–53} \tag{17}$$

and

$$M = 2.19[\pm 0.3]\ M_\odot \times [1 + 0.65(j + j^2)] \quad \text{in Circinus X-1.} \tag{18}$$

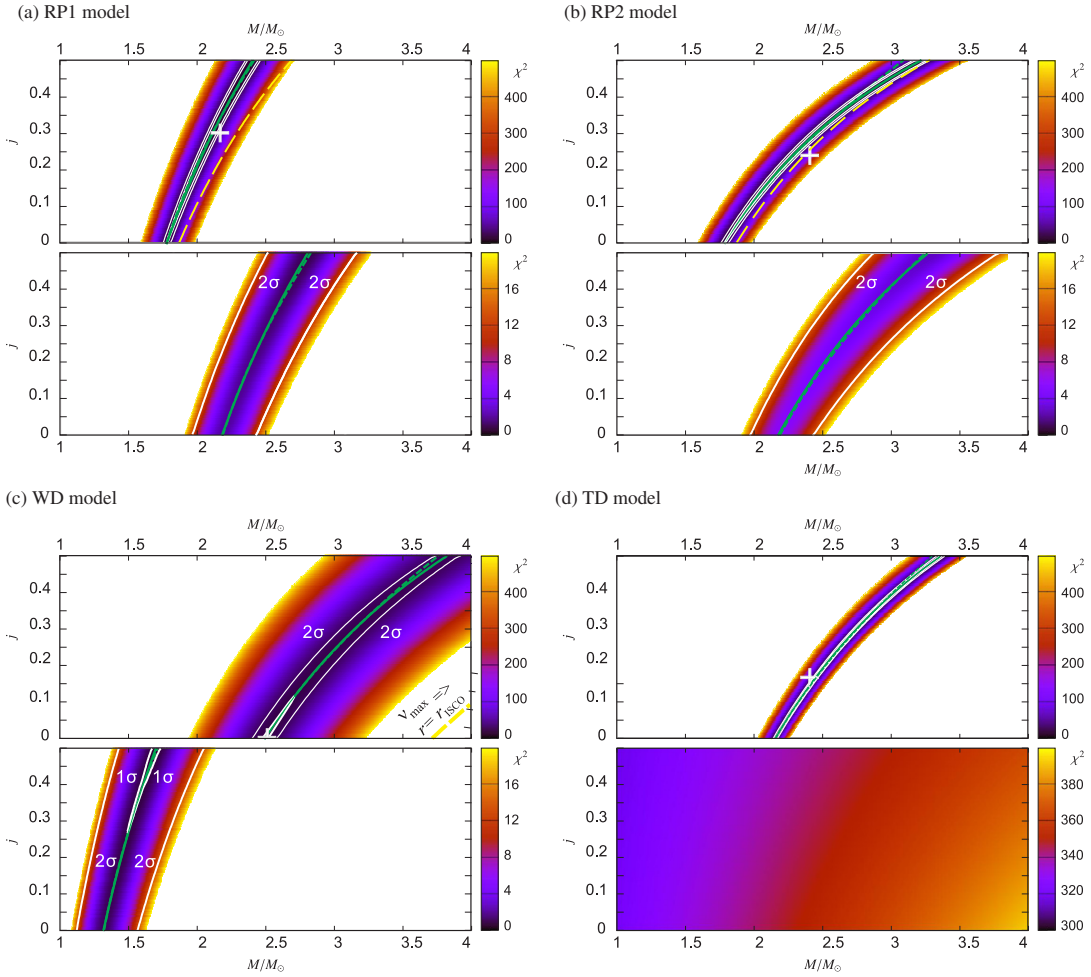

Figure 2. Same as Figure 1(b), but for the other models. In 4U 1636−53 $\xi = 4$ is assumed for the RP1 and RP2 models, $\xi = 4.6$ for the WD model, and $\xi = 2.5$ for the TD model. For the TD model the ISCO estimate on the upper limits on M and j from the highest observed QPO frequency in 4U 1636−53 is not included since the model does not associate this frequency to the ISCO but to the radius where the term $\nu_K(r) + \nu_r(r)$ reaches its maximum.

4.2. Results for the WD Model

Considering $j = 0$ for fitting the data of 4U 1636−53 we find a narrow χ^2 minimum for $M_0 \sim 2.5\ M_\odot$ but its absolute value is somewhat higher than in the case of the RP model, $\chi^2 \doteq 450/21$ dof. Moreover, there is also no sufficient improvement along the whole given range of mass even up to the upper limit of j. Thus, we can again only speculate that there is an unknown systematic uncertainty. The χ^2 of the best fit for $j = 0$ drops to an acceptable value $\chi^2 = 1$ dof for $\xi \doteq 4.6$. The related mass corresponding to the best fit then reads $M_0 = 2.49[\pm 0.1]\ M_\odot$.

In analogy to the RP model, the best match to the data of Circinus X-1 for $j = 0$ reveals an acceptable value of $\chi^2 \doteq 10.6/10$ dof. In summary, we can write the quantities M_0 for both sources as

$$M_0 = 2.49[\pm 0.1]\ M_\odot \quad \text{in 4U 1636–53} \quad (\chi^2 = 1 \text{ dof} \Leftrightarrow \xi = 4.6) \tag{19}$$

and

$$M_0 = 1.31[+0.3, -0.2]\ M_\odot \quad \text{in Circinus X-1} \quad (\chi^2 = 10.6/10 \text{ dof}). \tag{20}$$

The χ^2 behavior resulting from fitting the data points for free M and j that again exhibits the $M - j$ degeneracy is depicted in Figure 2(c). The exact $M - j$ relations in this figure are denoted by the dashed green lines. Their approximations in the form $M = M_0 \times [1 + k(j + j^2)]$ are, as in the previous cases, marked by the continuous green lines and read

$$M = 2.49[\pm 0.1]\ M_\odot \times [1 + 0.68(j + j^2)] \quad \text{in 4U 1636–53} \tag{21}$$

and

$$M = 1.31[+0.3, -0.2]\ M_\odot \times [1 + 0.4(j + j^2)] \quad \text{in Circinus X-1.} \tag{22}$$

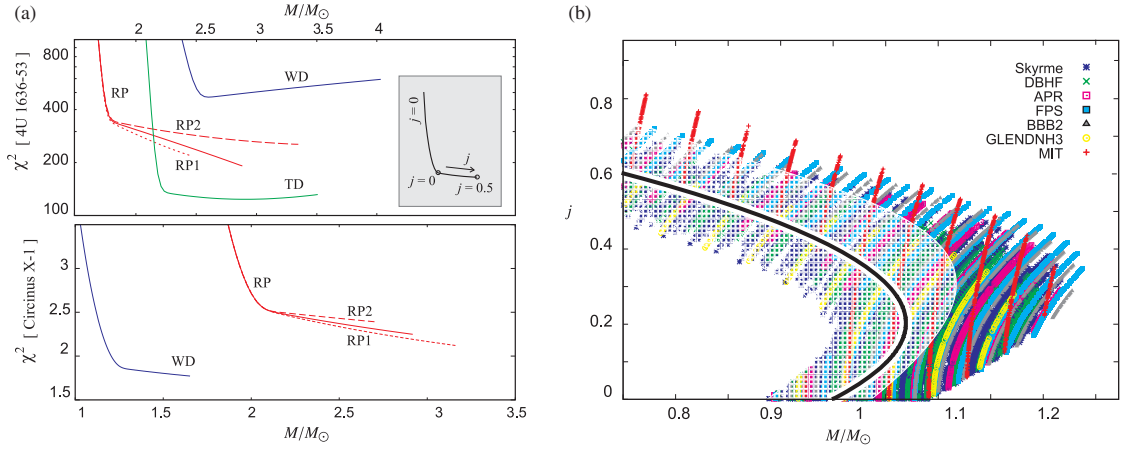

Figure 3. (a) Profiles of the lowest χ^2 for a given M plotted for various models. As in the previous figures, the case of 4U 1636−53 is shown in the top panel and Circinus X-1 in the bottom panel. The schematic drawing in the inset indicates the relation between the χ^2 behavior and j common to all the plotted curves. (b) The mass–angular-momentum combinations allowed by the ER model. The color symbols indicate different equations of state (after Urbanec et al. 2010a, 2010b, see these papers for details). The lightened subset of these symbols is compatible with the 4U 1636−53 data. The black line denotes its quadratic approximation (Equation (25)).

4.3. Results for the TD Model

Considering $j = 0$ for fitting the data of 4U 1636−53 we find a narrow χ^2 minimum for $M_0 \sim 2.15\ M_\odot$ while its value $\chi^2 \doteq 137/21$ dof is again unacceptable, although it is approximately 2× lower than in the case of the RP model. Moreover, there is also no sufficient improvement along the whole given range of mass, even up to the upper limit of j. Thus, again we can only speculate that there is an unknown systematic uncertainty. The χ^2 of the best fit for $j = 0$ drops to the acceptable value $\chi^2 = 1$ dof for $\xi \doteq 2.5$. The related mass corresponding to the best fit then reads:

$$M_0 = 2.15[\pm 0.02]\ M_\odot \quad (\chi^2 = 1 \text{ dof} \Leftrightarrow \xi = 2.5). \qquad (23)$$

For the Circinus X-1 data we find no clear χ^2 minimum. It is roughly $\chi^2 \sim 300/10$ dof along the interval of mass considered and χ^2 is only slowly decreasing with M decreasing (or j increasing).

Color-coded maps of χ^2 resulting for free M and j are shown in Figure 2(d). In the case of 4U 1636−53 there is clearly an $M-j$ degeneracy. The $M-j$ relation is well approximated in the form $M = M_0 \times [1 + k(j + j^2)]$ as

$$M = 2.15[\pm 0.02]\ M_\odot \times [1 + 0.71(j + j^2)]. \qquad (24)$$

On the other hand, the χ^2 distribution for Circinus X-1 is rather flat, exhibiting roughly $\chi^2 \sim 300/10$ dof, whereas it slightly decreases for decreasing M and increasing j.

For the case of 4U 1636−53 the detailed profile of χ^2 along the relation (24) is shown and compared to the RP, RP1, RP2, and WD models in Figure 3(a). In the same figure we also show an analogous comparison for Circinus X-1. The absence of an $M-j$ relation and the behavior of χ^2 for the TD model in the case of Circinus X-1 is then discussed in Section 6.

4.4. Results for the ER Model

Adopting the assumption that the observed frequencies are nearly equal to the resonant eigenfrequencies, $\nu_U = \nu_\theta(r)$ and $\nu_L = \nu_r(r)$, the ER model does not fit the NS data (e.g., Belloni et al. 2005; Urbanec et al. 2010b; Lin et al. 2011). A somewhat more complicated case in which this assumption is not fulfilled has been recently elaborated by Urbanec et al. (2010b), who assumed data for 12 NS sources, including 4U 1636−53. They investigated the suggestion made by Abramowicz et al. (2005a, 2005b) that the resonant eigenfrequencies in 12 NS sources roughly read $\nu_L^0 = 600$ Hz versus $\nu_U^0 = 900$ Hz and the observed correlations follow from the resonant corrections to the eigenfrequencies, $\nu_L = \nu_L^0 + \Delta\nu_L$ versus $\nu_U = \nu_U^0 + \Delta\nu_U$. In this concept the resonance occurs at the fixed radius $r_{3:2}$ and the data of the individual sources are expected as a linear correlation. Intersection of this correlation with the $\nu_U/\nu_L = 3/2$ relation gives the resonant eigenfrequencies since it is expected that $\Delta\nu_L = \Delta\nu_U = 0$ when $R = 3/2$. More details and references to the model can be found in Urbanec et al. (2010b).

For the sake of the comparison with the RP and other models examined here, we plot Figure 3(b) based on the results of Urbanec et al. (2010b). The figure displays combinations of mass and angular momentum required by the model. The color-coded symbols indicate solutions for different equations of state (EoS). We denote the subset of these solutions compatible with the data of 4U 1636−53 by lighter symbols. The determination of this subset comes from the fit of 4U 1636−53 data by a straight line ($\chi^2 = 37/20$/dof). It is clear from the figure that, as in the previous cases, for the ER model there is a preferred mass–angular-momentum relation. In contrast to the other models examined, it tends to a positive correlation between M and j only for low values of the angular momentum, $j \lesssim 0.2$, while for higher j the required mass decreases with increasing j. This trend is connected to the high influence of the NS quadrupole momentum and large deviation from the Kerr geometry that arise for the low-mass NS configurations (see Urbanec et al. 2010b for details). We find that the mass–angular-momentum relation implied by the ER model for 4U 1636−53 can be approximated by a quadratic term roughly as (black curve in Figure 3(b))

$$M = 0.95\ M_\odot \times [1 + 0.8j - 2j^2] \pm 10\%. \qquad (25)$$

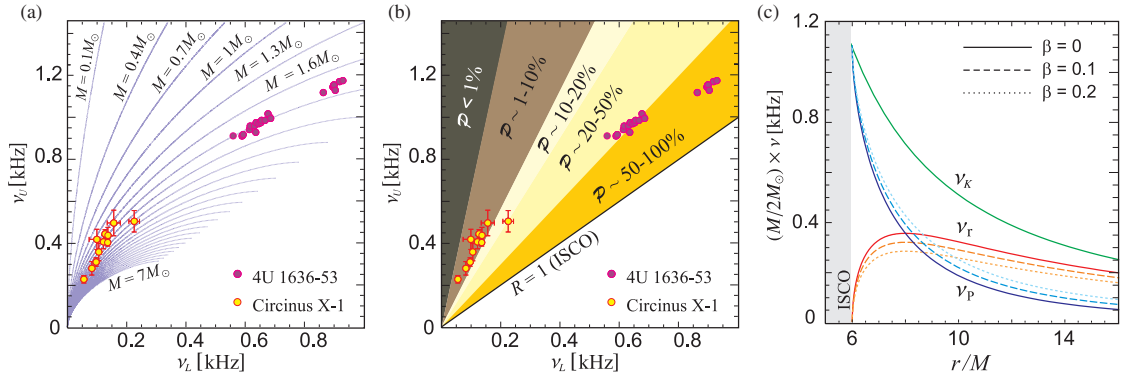

Figure 4. (a) Frequency relations predicted by the (geodesic) RP model for $j = 0$ vs. data for 4U 1636−53 and Circinus X-1. (b) Quantity P illustrating the variability of the predictive power of the RP model across the frequency plane. (c) Profiles of the orbital, radial epicyclic, and periastron frequencies of the perturbed circular motion. Solid curves correspond to the geodesic case ($\beta = 0$). The dashed and dotted curves correspond to the case of non-geodesic radial oscillations ($\beta > 0$).

For Circinus X-1, the observed frequency ratio is far away from $R = 3/2$ and the ER model assumed above cannot fit the Circinus X-1 data without additional assumptions. The high frequency ratio can be reproduced only if the resonant combination frequencies are taken into account (e.g., Török et al. 2006). In such a case, the lower observed QPO frequency would correspond to a difference between the resonant eigenfrequencies having values about (300 Hz, 200 Hz), i.e., approximately 3× less than the typical twin peak QPO frequencies observed in 4U 1636−53. The related non-rotating mass would then be approximately 3× higher than that corresponding to 4U 1636−53, i.e., $M_0 \sim 3\ M_\odot$. The related fit of the Circinus X-1 data by a straight line has $\chi^2 = 16/10$ dof. Taking into account the change in eigenfrequencies due to the NS angular momentum and assuming the Kerr spacetime with $j < 0.5$, we can express the formula for the mass of Circinus X-1 implied by the ER model approximately as

$$M = 3\ M_\odot \times [1 + 1.9(j + j^2)] \pm 10\%. \qquad (26)$$

While for 4U 1636−53 the mass decreases with increasing j (Equation (25)), for Circinus X-1 the trend is opposite. This behavior is associated with the choice of the spacetime geometry. The low mass $M_0 \sim 1\ M_\odot$ inferred from the model for 4U 1636−53 implies high deviations from the Kerr geometry due to the NS oblateness (Urbanec et al. 2010a, 2010b). In such situations orbital frequencies can decrease with increasing j. For Circinus X-1, the high mass $M_0 = 3\ M_\odot$ justifies the applicability of the Kerr geometry chosen. For this geometry, the orbital frequencies must increase with increasing j (provided that $j < 1$). This issue is well illustrated by the behavior of ISCO frequencies in the right panel of Figure 3 in Paper I.

5. CHI-SQUARED DICHOTOMY AND CORRECTIONS TO THE RP OR OTHER MODELS

It has been noticed by Stella & Vietri (1999) and later by a number of other authors that data for sources with QPOs sampled mostly on low frequencies are better fitted by the RP model than data for sources with QPOs sampled mostly on high frequencies. Inspecting the χ-squared maps (Figures 1 and 2) and Table 1, we can see that the comparison between Circinus X-1 (good χ^2) and 4U 1636−53 (bad χ^2) well demonstrates such a "dichotomy". The χ^2 maps and profiles for the RP model are qualitatively similar for both 4U 1636−53 and Circinus X-1. Both sources also exhibit a decrease of χ^2 with increasing j (see Figure 3(a)). The χ^2 values reached for 4U 1636−53 are, however, much worse than those in the case of Circinus X-1 (≈10 versus 1 dof), and their spread with M is much narrower. Moreover, we find that a similar dichotomy also arises for all the other models considered assuming that the observed twin peak QPO frequency correlation arises directly from a correlation between characteristic frequencies of the orbital motion. Below we briefly discuss the relation between this dichotomy, the predictive power of the model, and possible non-geodesic corrections. We restrict our attention mostly to the RP model but argue that there is a straightforward generalization to the other models.

5.1. Data versus Predictive Power of the RP Model

Figure 4(a) shows the frequency relations predicted by the RP model for a non-rotating NS and several values of mass M. These curves run from the common point $[\nu_L, \nu_U] = [0\,\mathrm{Hz}, 0\,\mathrm{Hz}]$ corresponding to infinite r. They terminate at specific points $[\nu_{\mathrm{ISCO}}, \nu_{\mathrm{ISCO}}]$ corresponding to $r = r_{\mathrm{ms}} = r_{\mathrm{ISCO}}$. This behavior follows from the fact that for low excitation radii close to ISCO, a certain change in M leads to a modification of the orbital frequency that is much higher than those for radii far away from ISCO. In other words, the predictive power of the RP model is much weaker for radii far away from ISCO than for radii close to ISCO.

As recalled in Section 1, in the RP model the radius r is proportional to R (e.g., Török et al. 2008c). Because of this, the predictive power of the RP model is strongly decreasing with increasing R. In Appendix A.2 we discuss this in terms of the quantity $\mathcal{P} \propto R^{-3}$ determining the squared distance ds^2 measured in the frequency plane between data points related to different masses. This quantity has a direct impact on the spread of χ^2. For a certain variation of the mass, $\delta \equiv \Delta M/M$, it is

$$ds^2 \propto \frac{\delta^2}{(1+\delta)^2}\mathcal{P}. \qquad (27)$$

Detailed formulas are given in Equations (A11) and (A12). Figure 4(b) shows the behavior of $\mathcal{P}$ in the frequency plane.

Taking into account the data points included in Figures 4(a) and (b) and the behavior of $\mathcal{P}$ we can deduce that the difference

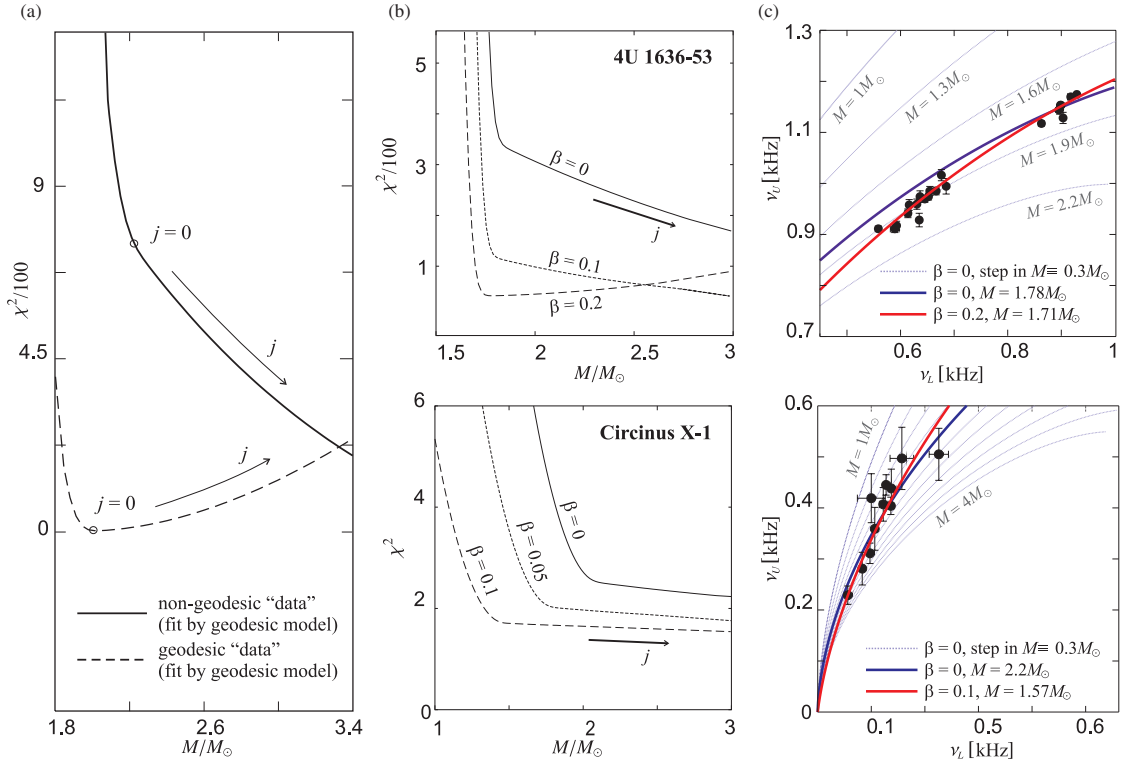

Figure 5. (a) Profile of the best χ^2 for a fixed M calculated when the simulated data are matched by the geodesic RP model. The continuous line is plotted for $M = 2\ M_\odot$, $j = 0$, and $\beta = 0.1$. The dashed line is plotted for $\beta = 0$. The arrows indicate increasing j. (b) Profiles of the best χ^2 for a fixed M in the case when Equation (29) is assumed for fitting the real data. The arrows in each panel indicate increasing j. The vertical arrow denotes the improvement $\Delta\chi^2$. (c) Comparison of the geodesic ($\beta = 0$, thick blue line) and non-geodesic ($\beta > 0$, red line) fits is included in the "zoom" from Figure 4(a). The top panel is plotted for 4U 1636−53 while the bottom panel is plotted for Circinus X-1. Both panels have the same scaling of the axes.

in the spread of χ^2 in 4U 1636−53 and Circinus X-1, as well as the very different values of the χ^2 minima in these sources, can be related to both the size of the error bars (affected by a low significance of kHz QPOs on low frequencies) and the location of data points. In Circinus X-1, the data points lie in the region of relatively low frequencies related to high R. For these, the predictive power of the model is low, since the curves $\nu_U(\nu_L)$ expected for various parameters M and j converge. On the other hand, in 4U 1636−53, the data points lie in the region of relatively high frequencies related to low R. These correspond to the strong gravity zone where different correlations are much more distinguished and the predictive power of the model is high. A similar consideration is also valid for several other models that predict frequency curves converging at low R. Clearly, from Figures 1 and 2 we can see that the uncertainties of the inferred mass expressed at 2σ confidence levels in 4U 1636−53 are ∼20× smaller compared to Circinus X-1 for each of the RP, RP1, RP2, and WD models.

5.2. Toy Non-geodesic Modification of the RP Model

Based on the above findings, we can speculate that the same systematic deviation from the particular model considered may be involved in both sources. We justify this speculation using an arbitrary example of a toy non-geodesic version of the RP model. We attempt to use a modification that would mimic the behavior of real data. In the vicinity of the inner edge of an accretion disk it is natural to expect a modification of the radial epicyclic frequency rather than a modification of the Keplerian frequency. The orbital motion in this region is highly sensitive to radial perturbations and even very small deviations from the geodesic idealization can strongly affect the radial oscillations (see in this context Stuchlík et al. 2011). In our example we therefore assume that the frequency of the hot-spot radial oscillations is somewhat lowered due to pressure or magnetic field effects (e.g., Straub & Šrámková 2009; Bakala et al. 2010, 2012). For simplicity, we postulate that the effective frequency of the radial oscillations is

$$\tilde{\nu}_\mathrm{r} = \nu_\mathrm{r}(1-\beta), \tag{28}$$

where β is a small constant. The related lower QPO frequency actually observed is then given by

$$\tilde{\nu}_L = \nu_L + \beta\,(\nu_U - \nu_L)\,, \tag{29}$$

where $\nu_L(\nu_U)$ is the frequency relation of the geodesic RP model given in Equation (A3). Assuming Equation (29), $\beta = 0.1$, $j = 0$, and $M = 2\ M_\odot$ we produce 20 data points uniformly distributed along the frequency correlation. We then fit the simulated data by the geodesic model. Figure 5(a) shows the

resulting χ^2 profile calculated in the same way as those in Figure 3(a). Clearly, χ^2 decreases with growing j similarly to the results obtained for real data points in both sources discussed. For comparison, we also present the fit of data simulated for $\beta = 0$, where, in contrast, χ^2 increases with growing j. Having this boost we use Equation (29) for the fitting of the real data points. The resulting "best χ^2" improves for both sources, although in the case of Circinus X-1 the improvement is only marginal. More specifically, for 4U 1636−53 the best χ^2 improves up to $\beta \sim 0.2$ with $\Delta\chi^2 \sim 300$, while for Circinus X-1 it improves up to $\beta \sim 0.1$ with $\Delta\chi^2 \sim 2$. The representative χ^2 profiles are illustrated in Figure 5(b), which also shows the related impact on mass restrictions. The strong improvement in 4U 1636−53 data corresponds to only a marginal effect on the mass restriction ($\Delta M \lesssim 0.1\ M_\odot$). On the other hand, the small improvement of χ^2 in Circinus X-1 causes a large modification of the mass restriction ($\Delta M \sim 0.6\ M_\odot$). The related fits to the data are shown in Figure 5(c).

The toy model (29) naturally does not represent an elaborate attempt to describe the QPO mechanisms, but it demonstrates well that, in spite of the good quality of fit, in both 4U 1636−53 and Circinus X-1 sources, the same physical correction to the RP model could be involved. A similar consideration should also be valid for several other models discussed. In this context, we note that sophisticated implementations of non-geodesic corrections have been developed in the past within the framework of various models of accretion flow dynamics and QPOs (see, e.g., Wagoner et al. 1999, 2001; Kato 2001; Alpar & Psaltis 2008, and references therein). We also note that some corrections to the orbital frequencies can arise directly due to corrections to the Kerr or Hartle–Thorne (HT) spacetimes that we assume here (see, e.g., Kotrlová et al. 2008; Psaltis et al. 2008; Stuchlík & Kotrlová 2009; Johannsen & Psaltis 2011).

6. DISCUSSION AND CONCLUSIONS

Except the TD model applied to Circinus X-1 data, all applications of the models examined to the 4U 163−53 and Circinus X-1 data result in the preferred mass–angular-momentum relations. These are summarized in Table 1.

Comparing the χ^2 map of the TD model and Circinus X-1 (Figure 2(d)) to the other χ^2 maps we can see that it is very different with its flat χ^2 behavior. Moreover, the TD model is the only model of those considered here giving very bad χ^2 for Circinus X-1 ($\chi^2 \sim 300/10$ dof versus $\chi^2 \sim 10/10$ dof for the other models). This can be well understood in terms of the frequency ratio R implied by the model. The TD model states

$$\nu_L = \nu_K\,, \quad \nu_U = \nu_K + \nu_r, \tag{30}$$

where $\nu_r \leqslant \nu_K$. In more detail, ν_r vanishes at $r = r_{\rm ISCO}$ and, in a flat spacetime limit ($r = \infty$), $\nu_r = \nu_K$. Consequently, the TD model allows only $R \in (1, 2)$. The Circinus X-1 data, however, reveal values between $R \sim 2.5$ and $R \sim 4.5$ which is clearly higher than the Newtonian limit, $R = 2$. This disfavors the TD model.

6.1. Quality of Fits and Inferred Masses: Models with $\nu(r)$

Table 1 provides a summary of results of fits to the data for both sources by individual models. The comparison between fits by individual models is illustrated in Figure 6 which also indicates the inferred QPO excitation radii. Within the RP, RP1, RP2, and WD models, the quality of fits is rather comparable (bad for 4U 1636 and good for Circinus X-1). The mass–angular-momentum relations are similar for the RP, RP1, and RP2 models while for the WD model they differ (see Table 1). In more detail, the RP, RP1, and RP2 models require relatively similar masses for both sources, namely $M_0 \sim 1.8\ M_\odot$ for 4U 1636−53 versus $2.2\ M_\odot$ for Circinus X-1. On the other hand, the required masses differ quite a lot when the WD model is assumed. We then have $M_0 \sim 2.5\ M_\odot$ for 4U 1636−53 versus $1.3\ M_\odot$ for Circinus X-1. We note that the QPO excitation radii inferred for each model in 4U 1636−53 lie within the innermost part of the accretion disk. This is depicted in detail in Figure 6(b) assuming a non-rotating star. We can see that the radii span the interval $r \in (6M - 8M)$ for the RP model, $r \in (7M - 8M)$ for the WD model, and the largest interval $r \in (6M - 9M)$ for the TD model. On the contrary, the radii inferred in Circinus X-1 are above $r = 10M$, belonging to the interval $r \in (10M - 16M)$ for the RP model and $r \in (15M - 25M)$ for the WD model.

The above models have, along with few others, recently been considered for 4U 1636−53 by Lin et al. (2011). They reported mass and angular momentum corresponding to χ^2 minima for each of the models. The data points they investigated especially for this purpose come from a sophisticated, careful application of a so-called shift–add procedure over a whole set of the available *RXTE* observations (see their paper for details and references). The data we use here for 4U 1636−53 come from the previously well-investigated individual continuous observations of the source (see Barret et al. 2005b, 2005c; Török 2009). While the two sets of the applied data come from different methods, the values of mass and angular momentum reported by Lin et al. (2011) agree with the mass–angular-momentum relations that we find here (see Figures 1(b) and 2). One should note that, in contrast to $M - j$ relations, the single $M - j$ combination corresponding to the χ^2 minimum of a given model is not very informative as the (bad) χ^2 is comparable along a large range of mass. Moreover, in each case examined here the χ^2 minima correspond only to the end of the angular momentum interval considered since the quality of fit is a monotonic function of j. Thus, we can conclude that the differences between the M_0 coefficients in Table 1 provide the main information about the differences between predictions of the individual QPO models.

In relation to the quality of fits by the RP, RP1, RP2, and WD models, we can also note that these models need some correction, as has also been noted by Lin et al. (2011). As demonstrated in Section 5, differences in the χ^2 behavior between low- and high-frequency sources can be related to the variability of the model's predictive power across the frequency plane. This variability naturally comes from the radial dependence of the characteristic frequencies of orbital motion. As a consequence, the restrictions to the models resulting from the observations of low-frequency sources are weaker than those in the case of high-frequency sources. A small required correction is then likely to be common to both classes of sources, which has been demonstrated using the non-geodesic modification of the RP model based on Equation (29).

6.1.1. Applicability of Results Based on the Spacetime Description Adopted

Both the poor quality of fits to the data by geodesic models and the mass–angular-momentum relations associated with these models have been obtained assuming the Kerr spacetimes. This approximate description of the exterior of rotating NSs neglects the NS oblateness. As argued in Paper I, the uncertainty in

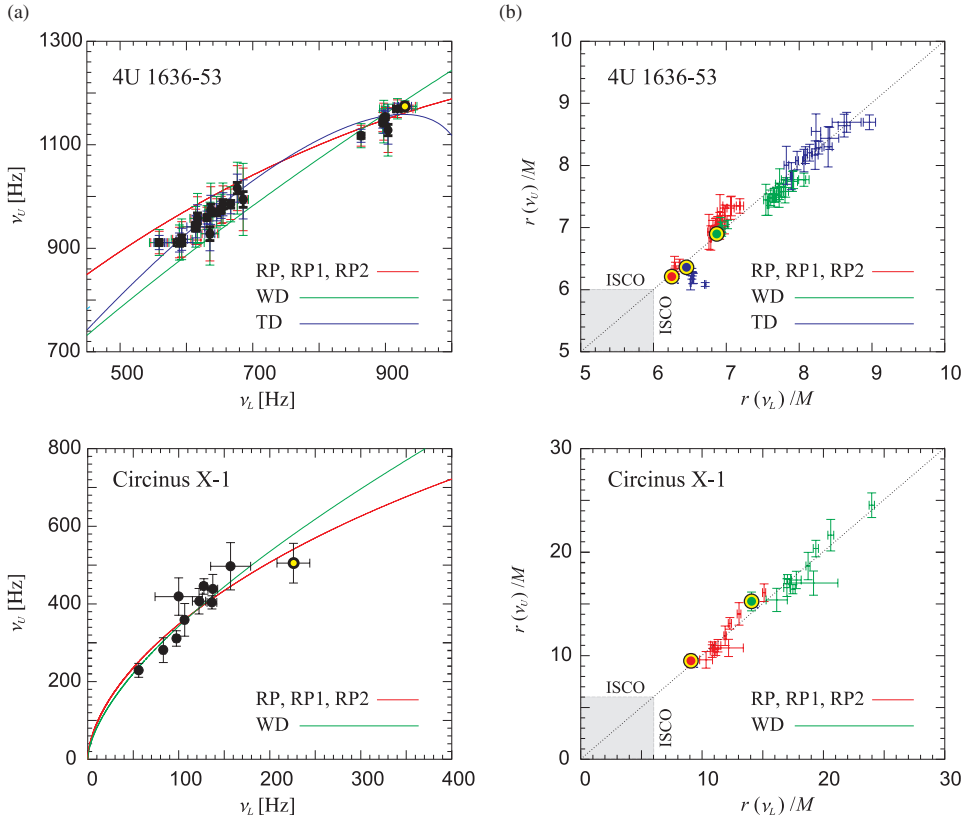

Figure 6. Best fits to the data by individual models for $j = 0$. (a) Frequency relations. Error bars corresponding to $\xi = 4$ for RP models, $\xi = 4.6$ for WD model, and $\xi = 2.5$ for TD model are color-coded. The pair of the highest twin peak QPO frequencies observed in the source is marked by a yellow circle. (b) The QPO excitation radii inferred from the data and each of the fits are shown in panel (a). The color-coded circles correspond to the highest observed twin peak QPO frequencies. The TD model is included for 4U 1636−53 only because it does not match the data for Circinus X-1 (see Section 6 for a discussion).

NS oblateness causes only small inaccuracies in the modeling of kHz QPOs for compact high-mass NSs. In the case of the WD model applied to the Circinus X-1 data, a consequent application of a more sophisticated approach is still needed. The Kerr approximation suggested in Paper I is clearly not valid here due to low $M_0 \sim 1.3\ M_\odot$. Such a low mass can imply high deviations from the Kerr geometry due to the strong influence of the NS oblateness. In principle, the related mass–angular-momentum relation can be very different in this case from that qualitatively implied, e.g., by the RP model, and corrections to the quadrupole moment should be included in analogy to the ER model and 4U 1636−53. For the other applications of the WD, RP, RP1, and RP2 models reported here we can trust the $M - j$ trends following from the Kerr approximation since the inferred masses M_0 are rather high.

We justify the applicability of our results in Appendix A.3. In general, the differences between geodesic frequencies associated with Kerr spacetimes and those given for realistic NSs due to their oblateness are roughly of the same order as the corrections required to obtain a good match between the predicted and observed QPO frequencies (e.g., Morsink & Stella 1999). We illustrate however, that these differences cannot improve the fits sufficiently for NSs with $j \lesssim 0.3$ and $M \gtrsim 1.4\ M_\odot$. We show that in HT spacetimes describing the exterior of oblate NSs there is a degeneracy not only between the NS mass and angular momentum but also between these quantities and the NS quadrupole moment q. Within such "generalized degeneracy" the frequency curves predicted by QPO models scale with the quantities M, j, and q but the related qualitative change in their shape is only small. Thus, our results obtained for the Kerr spacetimes have a more general relevance except for the case of high values of j (see Appendix A.3 for details).

6.1.2. Prospects of Eliminating the $M - j$ Degeneracy

The $M - j$ degeneracies implied by individual kHz QPO models can in principle be eliminated using angular momentum estimates independent of the kHz QPOs. In Appendix B we subsequently focus on the RP model and discuss such possible elimination. Based on the X-ray burst observations of Strohmayer & Markwardt (2002) we assume that the rotational frequency (spin) of the NS in 4U 1636−53 is around 290 Hz or 580 Hz. Applying a few concrete NS EoS we show that the modified RP model well matches these spins for $j \sim 0.1$ or $j \sim 0.2$. We also show that a further consideration of low-frequency QPOs and the Lense–Thirring precession mechanism within the model can be finally crucial for fixing the value of j and challenging for application of the concrete EoS (see illustration in Figure 7). We note that this issue as well as modeling of kHz QPO correlations for rapidly rotating NSs require an additional detailed treatment.

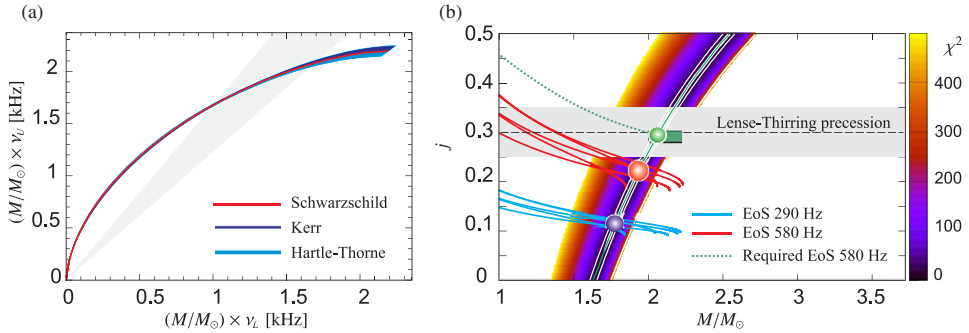

Figure 7. (a) The ambiguities of the parameters of the RP model frequency relations illustrated for the range $j \in (0, 0.3)$ and $\tilde{q} \in (1, 8)$. The red curve indicates the relation plotted for the mass M_0 in the Schwarzschild spacetime. The dark blue set of curves marked as "Kerr" represents the degeneracy in the Kerr spacetimes given by Equation (A14). The light blue set marked as "Hartle–Thorne" includes curves resulting from the generalized degeneracy in HT spacetimes given by Equation (A15). The shadow cone denotes the range of frequency ratio R corresponding to the data for 4U 1636−53. (b) Removing the $M-j$ degeneracy in the case of 4U 1636−53 and the RP model. The χ^2 map displayed is calculated for $\beta \neq 0$ while the best fits correspond to $\beta = 0.15$–0.20. The blue spot roughly indicates the combination of mass and spin restricted when the spin frequency 290 Hz and several concrete equations of state are assumed. The red spot indicates the same but for the spin frequency 580 Hz. The shaded region around the dashed horizontal line indicates the angular momentum $j = 0.3 \pm 0.05$ which can be roughly expected when the Lense–Thirring precession is assumed. The green box corresponds to a detailed consideration of a few points in the 3D frequency space (see Appendix B for details).

6.2. Resonance between $m = 0$ Axisymmetric Disk-oscillation Modes

Last but not least, we can draw conclusions about the version of the ER model examined assuming the fixed radius $r = r_{3:2}$. It well fits the data for both the sources discussed here with a χ^2/dof of the order of unity. The good fits, however, arise only because the present model predicts a linear correlation which has slope and intercept given by unspecified (free) parameters. One should also note that for Circinus X-1 the model requires additional consideration of the resonant combinational frequencies. Moreover, application of the ER model leads to a questionably low mass for 4U 1636−53, $M \leqslant 1\ M_\odot$, while for Circinus X-1 the implied mass is on the contrary questionably high, $M \geqslant 3\ M_\odot$. All these along with the results of Urbanec et al. (2010b) suggest that if a resonance is involved in the process of generating the NS QPOs, modes other than those corresponding to the radial and vertical axisymmetric oscillations should be considered.

We thank Marek Abramowicz, Wlodek Kluźniak, Milan Šenkýř, and Yong-Feng Lin for discussions. We also thank the anonymous referee for his/her comments and suggestions that helped greatly to improve the paper. This work has been supported by the Czech grants MSM 4781305903, LC 06014, GAČR 202/09/0772, and GAČR 209/12/P740. The authors further acknowledge the project CZ.1.07/2.3.00/20.0071 "Synergy" supporting the international collaboration of IF Opava and also the internal student grants of the Silesian University in Opava, SGS/1/2010 and SGS/2/2010.

APPENDIX A

APPROXIMATIONS, FORMULAS, AND EXPECTATIONS

A.1. Relations for the Upper and Lower QPO Frequencies in the RP, TD, WD, RP1, and RP2 Models

Formulas for the Keplerian, radial, and vertical epicyclic frequency were first derived by Aliev & Galtsov (1981). In a commonly used form (e.g., Török & Stuchlík 2005) they read

$$\Omega_\kappa = \frac{\mathcal{F}}{j + x^{3/2}}, \quad \nu_\mathrm{r} = \Gamma\Omega_\kappa, \quad \nu_\theta = \Delta\Omega_\kappa, \tag{A1}$$

where

$$\Gamma = \sqrt{\frac{-3j^2 + 8j\sqrt{x} + (-6+x)\,x}{x^2}},$$
$$\Delta = \sqrt{1 + \frac{j(3j - 4\sqrt{x})}{x^2}}, \tag{A2}$$

$x \equiv r/M$, and the "relativistic factor" $\mathcal{F}$ reads $\mathcal{F} \equiv c^3/(2\pi GM)$.

Relations defining the upper and lower QPO frequencies in terms of the orbital frequencies are given for each of the models considered in the first column of Table 1. For the RP model, one can easily solve these relations to arrive at an explicit formula which relates the upper and lower QPO frequencies in units of Hertz as (Paper I)

$$\nu_L = \nu_U\left\{1 - \left[1 + \frac{8j\nu_U}{\mathcal{F} - j\nu_U} - 6\left(\frac{\nu_U}{\mathcal{F} - j\nu_U}\right)^{2/3} - 3j^2\left(\frac{\nu_U}{\mathcal{F} - j\nu_U}\right)^{4/3}\right]^{1/2}\right\}. \tag{A3}$$

A similar simple evaluation of the explicit relation between the two observed QPO frequencies is also possible for the TD model, where we find

$$\nu_U = \nu_L\left\{1 + \left[1 + \frac{8j\nu_L}{\mathcal{F} - j\nu_L} - 6\left(\frac{\nu_L}{\mathcal{F} - j\nu_L}\right)^{2/3} - 3j^2\left(\frac{\nu_L}{\mathcal{F} - j\nu_L}\right)^{4/3}\right]^{1/2}\right\}. \tag{A4}$$

An apparent "asymmetry" between relations (A3) and (A4) arises from an analogical asymmetry in the model definition

of the observable frequencies (see Table 1). We note that in both models, one of the two observable frequencies simply equals the Keplerian orbital frequency, which makes the evaluation of the explicit formula very straightforward.

For the WD, RP1, and RP2 models, the definition relations lead to high-order polynomial equations that relate the lower and upper QPO. In these cases we can give only a parametric form relating ν_U and ν_L. The upper and lower QPO frequencies for the WD model can then be expressed as

$$\nu_U = 2\,(1-\Gamma)\,\Omega_K\,, \quad \nu_L = (2-\Gamma)\,\Omega_K. \tag{A5}$$

For the RP1 model they can be written as

$$\nu_U = \Omega_K \Delta\,, \quad \nu_L = (1-\Gamma)\,\Omega_K, \tag{A6}$$

and for the RP2 model as

$$\nu_U = (2-\Delta)\,\Omega_K\,, \quad \nu_L = (1-\Gamma)\,\Omega_K. \tag{A7}$$

A.2. Predictive Power of the RP Model

Let us assume a non-rotating star. The radial epicyclic frequency vanishes at ISCO, $x = 6$, where the orbital frequency takes the value of

$$\nu_K = \nu_{\rm ISCO} = \frac{c^3}{12\sqrt{6}\,GM\pi} \tag{A8}$$

and within the RP model it is

$$\nu_U = \nu_L = \nu_{\rm ISCO}. \tag{A9}$$

When a certain variation of the mass, $\delta \equiv \Delta M/M$, is assumed, the point in the frequency plane given by Equation (A9) changes its position. The corresponding square of the distance ds^2 (important for the fitting of data) reads

$$ds^2_{\rm ISCO} = \nu_{\rm ISCO}\frac{\delta^2}{(1+\delta)^2}. \tag{A10}$$

For any other specific orbit inside the accretion disk (e.g., $x = 8$, where the radial epicyclic frequency takes its maximal value), the analogous change of the related data point position in the frequency plane is always smaller, $ds^2 < ds^2_{\rm ISCO}$.

It is useful to utilize the fact that each specific orbit can be related to a certain frequency ratio R higher than $R = 1$ corresponding to ISCO (e.g., for $x = 8$ it is $R = 2$). Using the relation between x and R (e.g., Török et al. 2008c), one can find that

$$ds^2 = ds^2_{\rm ISCO} \times \mathcal{P}, \tag{A11}$$

where

$$\mathcal{P} = \frac{(R^2+1)(2R-1)^3}{2R^8}. \tag{A12}$$

The quantity $\mathcal{P} = \mathcal{P}(R)$ reads $\mathcal{P} = 1$ for $R = 1$ and strongly decreases with increasing R. This naturally illustrates that the predictive power of the model is high only for orbits close to ISCO. For instance, for the maximum of the radial epicyclic frequency where $R = 2$, it is roughly $\mathcal{P} = 0.25$.

We note that in this subsection we neglected the influence of the NS spin for simplicity. Calculating P for a non-zero j is less straightforward and does not bring any new interesting information.

A.3. Generalized Degeneracy

As recalled in Section 2, the frequency curves predicted by the model (and other kHz QPO models) scale with the NS mass and angular momentum, but do not change their shape much when $j \lesssim 0.5$. This was explored in detail assuming the Kerr spacetimes. The exterior of a rotating NS is in general well described by the HT spacetimes which are determined by the NS mass M, angular momentum j, and a quadrupole moment q reflecting the NS oblateness. One can ask whether there can be a "generalized degeneracy" related to all these three quantities similar to those related just to M and j in the Kerr spacetimes. We briefly attempt to resolve this issue using formulas for epicyclic frequencies in HT spacetimes derived by Abramowicz et al. (2003a).

The orbital frequency at a marginally stable circular orbit increases with increasing angular momentum j while it decreases with increasing quadrupole moment q. Thus, following Appendix A.2 of Paper I, we can expect that the eventual generalized degeneracy can, to first order in q and second order in j, be expressed as

$$M \sim M_0(1 + k_1\, j + k_2\, j^2 - k_3\, q). \tag{A13}$$

In the limit of $\tilde{q} = 1$, where $\tilde{q} \equiv q/j^2$ is the so-called "Kerr parameter", relation (A13) has to merge with the mass spin relation derived for the Kerr spacetimes. This relation is represented by Equation (2) which, assuming whole frequency curves, reads

$$M \sim M_0[1 + 0.7(j + j^2)]. \tag{A14}$$

Therefore we choose $k_1 = 0.7$ and $k_2 = k_1 + k_3$. Then only k_3 remains as a "tunable" parameter.

We searched for a value of k_3 providing the eventual generalized degeneracy. For a particular choice of $k_3 = 0.32$,

$$M = M_0(1 + 0.7\,j + 1.02\,j^2 - 0.32q), \tag{A15}$$

we found results in full analogy to those that we had previously obtained for the Kerr spacetimes. This finding is illustrated in Figure 7(a). The figure is plotted for $j \in (0, 0.3)$ and $\tilde{q} \in (1, 8)$. Clearly, for any curve drawn for a particular combination of M, j, and q there is a nearly identical curve drawn for the Schwarzschild spacetime given by Equation (A15). Thus, consideration of NS oblateness cannot improve the poor quality of fits of models to the data within the limits of j and q assumed for the figure. These limits correspond to almost any NS modeled using the usual EoS for the mass $M > 1.4\ M_\odot$ and spin frequencies up to 600 Hz (Lattimer & Prakash 2001, 2007).

Considering the above facts, we can summarize the findings as follows: the results on $M-j$ relations obtained for the Kerr spacetimes have rather general validity and NS oblateness could only cause some correction to the slope of a particular $M-j$ relation. The only exceptions exceeding the framework of the work presented are represented by the cases of $j \gg 0.3$, $M < 1.4\ M_\odot$, or some unusual NS models that have to be treated in detail assuming concrete EoS.

APPENDIX B

REMOVING DEGENERACY IN THE CASE OF THE RP MODEL AND 4U 1636−53

For the atoll source 4U 1636−53 there is good evidence on the NS spin frequency based on X-ray burst measurements.

Depending on the (two- or one-) hot-spot model consideration, the spin frequency ν_s reads either $\nu_s \sim 290$ Hz or $\nu_s \sim 580$ Hz (Strohmayer & Markwardt 2002). Thus, one can, in principle, infer the angular momentum j and remove the $M-j$ degeneracies related to the individual twin peak QPO models.

In Figure 7 we illustrate the potential of such an approach requiring a complex usage of various versions of a detailed ultra-dense matter description. The figure is made for the non-geodesic version of the RP model based on Equation (29) with $\beta \neq 0$. It includes a χ^2 map resulting from the fitting of 4U 1636−53 data with the model together with the $M-j$ relations inferred from the equalities $\nu_s = 290$ Hz or $\nu_s = 580$ Hz. These $M-j$ relations that depend on ultra-dense matter properties were calculated using the approach of Hartle (1967), Hartle & Thorne (1968), Chandrasekhar & Miller (1974), Miller (1977), and Urbanec et al. (2010a). They assume the same set of several EoS as we used in Paper I, namely SLy 4 (Rikovska Stone et al. 2003), APR (Akmal et al. 1998), AU-WFF1, UU-WFF2, and WS-WFF3 (Wiringa et al. 1988; Stergioulas & Friedman 1995).

Comparing the χ^2 map to the $M-j$ relations based on our choice of EoS we can conclude that the parameters of the NS implied by the model must be either $j \sim 0.11$ and $M \sim 1.9\,M_\odot$, or $j \sim 0.22$ and $M \sim 2\,M_\odot$. In panel (b) of Figure 7 we can check that in both cases the quality of fit to twin peak QPO data is acceptable (the best fits were obtained for the value of $\beta \sim 0.17$).

B.1. Adding Low-frequency QPOs

The RP model associates the observed low-frequency QPOs to the Lense–Thirring precession that occurs at the same radii as the periastron precession crucial for the high-frequency part of the model. It is then expected that their frequencies ν_ℓ equal the Lense–Thirring precession frequency,

$$\nu_\ell = \nu_{\rm LT}. \tag{B1}$$

Naturally, the value of $\nu_{\rm LT}$ depends more strongly on the angular momentum j than on the concrete radius r, since it vanishes for $j \to 0$ at any radius. Thus, within the framework of the RP model, it represents a sensitive spin indicator (Stella & Vietri 1998a, 1998b; Morsink & Stella 1999). Although in this paper we focus on the high-frequency QPOs, it is interesting to mention this consideration, especially because of the relation to the above-mentioned implications of briefly X-ray burst measurements.

There are several published observational works on QPOs in atoll sources including data points in the three-dimensional (3D) frequency space $\mathcal{S} = \{\nu_\ell, \nu_L, \nu_U\}$. For instance, Jonker et al. (2005) reported clear measurements of low-frequency QPOs in 4U 1636−53 as well as their relation to the high-frequency part of the PDS. For the PDS related to the middle part of the frequency correlation,

$$[\nu_L, \nu_U] = [700\text{–}800\ \text{Hz}, 1000\text{–}1100\ \text{Hz}], \tag{B2}$$

the frequencies ν_ℓ were approximately around

$$\nu_\ell \doteq 42\ \text{Hz}. \tag{B3}$$

For the PDS related to the upper part of the frequency correlation,

$$[\nu_L, \nu_U] = [800\text{–}850\ \text{Hz}, 1100\text{–}1150\ \text{Hz}], \tag{B4}$$

the frequencies ν_ℓ were around

$$\nu_\ell \doteq 43.5\ \text{Hz}. \tag{B5}$$

Assuming these frequency intervals we can apply the equalities

$$\nu_U = \nu_K, \nu_L = \nu_{\rm RP} = \nu_K - \nu_{\rm r} \quad \text{and} \quad \nu_\ell = \nu_{\rm LT} = \nu_K - \nu_\theta. \tag{B6}$$

For the application we consider Equation (29) with $\beta = 0.17$ which provides acceptable fits to the twin peak QPOs. The spin j is then fixed just by the ratio between the observed frequencies (B6). Consequently we find that j must be about $j = 0.285-0.3$. Moreover, when using the measured frequency values, the relations (B6) determine both M and j just for a single point in the 3D frequency space $\mathcal{S}$. Using this fact and the values of Jonker et al. (2005) we find that $M = (2.0 - 2.2)\,M_\odot$ for $j = 0.285 - 0.3$.

The resulting values of M and j are marked in Figure 7 by the green box. Note, however, that the consideration needs to be further expanded for a larger set of data and some χ^2 mapping in the 3D frequency space $\mathcal{S}$ should be done. This can be somewhat complicated by the fact that low-frequency QPOs are, in general, broader than the kHz features. In addition, the quadrupole momentum influence on $\nu_{\rm LT}$ could be overestimated due to the Kerr geometry approximation considered here. Nevertheless, assuming all these uncertainties we can still expect from the above numbers that a further detailed consideration should confirm the value of j roughly inside the interval

$$j_{\rm LT} = 0.3 \pm 0.05. \tag{B7}$$

Figure 7 finally integrates both the implications of X-ray burst measurements and the Lense–Thirring precession model for low-frequency QPOs. We can see that an EoS relatively distant from those which we consider here could be needed in order to match both phenomena and fix the NS spin. This challenging issue clearly requires further future work joining data analysis in the field of 3D frequency space and modeling the detailed influence of the NS EoS.

REFERENCES

Abramowicz, M. A., Almergren, G. J. E., Kluźniak, W., & Thampan, A. V. 2003a, arXiv:gr-qc/0312070

Abramowicz, M. A., Barret, D., Bursa, M., et al. 2005a, Astron. Nachr., 326, 864

Abramowicz, M. A., Barret, D., Bursa, M., et al. 2005b, in Proc. RAGtime 6/7: Workshops on Black Holes and Neutron Stars, Opava, ed. S. Hledík & Z. Stuchlík (Opava, Czech Republic: Silesian Univ. in Opava), 1

Abramowicz, M. A., Bulik, T., Bursa, M., & Kluźniak, W. 2003b, A&A, 404, L21

Abramowicz, M. A., Karas, V., Kluźniak, W., Lee, W. H., & Rebusco, P. 2003c, PASJ, 55, 466

Abramowicz, M. A., & Kluźniak, W. 2001, A&A, 374, L19

Akmal, A., Pandharipande, V. R., & Ravenhall, D. G. 1998, Phys. Rev. C, 58, 1804

Aliev, A. N., & Galtsov, D. V. 1981, Gen. Rel. Grav., 13, 899

Alpar, M. A., & Psaltis, D. 2008, MNRAS, 391, 1472

Alpar, M. A., & Shaham, J. 1985, Nature, 316, 239

Bakala, P., Šrámková, E., Stuchlík, Z., & Török, G. 2010, Class. Quantum Grav., 27, 045001

Bakala, P., Urbanec, M., Šrámková, E., Stuchlík, Z., & Török, G. 2012, Class. Quantum Grav., 29, 065012

Barret, D., & Boutelier, M. 2008, New Astron. Rev., 51, 835

Barret, D., Kluźniak, W., Olive, J. F., Paltani, S., & Skinner, G. K. 2005a, MNRAS, 357, 1288

Barret, D., Olive, J. F., & Miller, M. C. 2005b, MNRAS, 361, 855

Barret, D., Olive, J. F., & Miller, M. C. 2005c, Astron. Notes, 326, 808

Barret, D., Olive, J. F., & Miller, M. C. 2006, MNRAS, 370, 1140

Belloni, T., Méndez, M., & Homan, J. 2005, A&A, 437, 209
Belloni, T., Méndez, M., & Homan, J. 2007a, MNRAS, 376, 1133
Belloni, T., Méndez, M., & Homan, J. 2007b, MNRAS, 379, 247
Boirin, L., Barret, D., Olive, J. F., Bloser, P. F., & Grindlay, J. E. 2000, A&A, 361, 121
Boutelier, M., Barret, D., Lin, Y., & Török, G. 2010, MNRAS, 401, 1290
Boutloukos, S., van der Klis, M., Altamirano, D., et al. 2006, ApJ, 653, 1435 (also Volume 664, Issue 1, pp 596–596)
Bursa, M. 2005, in Proc. RAGtime 6/7: Workshops on Black Holes and Neutron Stars, Opava, ed. S. Hledík & Z. Stuchlík (Opava, Czech Republic: Silesian Univ. in Opava), 39
Čadež, A., Calvani, M., & Kostić, U. 2008, A&A, 487, 527
Chandrasekhar, S., & Miller, J. C. 1974, MNRAS, 167, 63
Di Salvo, T., Méndez, M., & van der Klis, M. 2003, A&A, 406, 177
Germana, C., Kostič, U., Čadež, A., & Calvani, M. 2009, in AIP Conf. Proc. 1126, SIMBOL-X: Focusing on the Hard X-Ray Universe: Proc. 2nd International Simbol-X Symposium, ed. J. Rodriguez & P. Ferrando (Melville, NY: AIP), 367
Hartle, J. B. 1967, ApJ, 150, 1005
Hartle, J. B., & Thorne, K. S. 1968, ApJ, 153, 807
Homan, J., van der Klis, M., Jonker, P. G., et al. 2002, ApJ, 568, 878
Horák, J., Abramowicz, M. A., Kluźniak, W., et al. 2009, A&A, 499, 535
Johannsen, T., & Psaltis, D. 2011, ApJ, 726, 11
Jonker, P. G., Méndez, M., & van der Klis, M. 2002a, MNRAS, 336, L1
Jonker, P. G., Méndez, M., & van der Klis, M. 2005, MNRAS, 360, 921
Jonker, P. G., van der Klis, M., Homan, J., et al. 2002b, MNRAS, 333, 665
Kato, S. 2001, PASJ, 53, 1
Kato, S. 2007, PASJ, 59, 451
Kato, S. 2008, PASJ, 60, 111
Kluźniak, W., & Abramowicz, M. A. 2001, arXiv:astro-ph/0105057
Kluźniak, W., Abramowicz, M. A., Kato, S., Lee, W. H., & Stergioulas, N. 2004, ApJ, 603, L89
Kostić, U., Čadež, A., Calvani, M., & Gomboc, A. 2009, A&A, 496, 307
Kotrlová, A., Stuchlík, Z., & Török, G. 2008, Class. Quantum Grav., 25, 225016
Lamb, F. K., Shibazaki, N., Alpar, M. A., & Shaham, J. 1985, Nature, 317, 681
Lattimer, J. M., & Prakash, M. 2001, ApJ, 550, 426
Lattimer, J. M., & Prakash, M. 2007, Phys. Rep., 442, 109
Lin, Y. F., Boutelier, M., & Barret, D. 2011, ApJ, 726, 74
McClintock, J. E., & Remillard, R. A. 2006, in Compact Stellar X-Ray Sources, ed. W. Lewin & M. van der Klis (Cambridge: Cambridge Univ. Press), 157
Méndez, M. 2006, MNRAS, 371, 1925
Méndez, M., & van der Klis, M. 2000, MNRAS, 318, 938
Méndez, M., van der Klis, M., & Ford, E. C. 2001, ApJ, 561, 1016
Miller, J. C. 1977, MNRAS, 179, 483
Miller, M. C., Lamb, F. K., & Psaltis, D. 1998, ApJ, 508, 791
Morsink, S. M., & Stella, L. 1999, ApJ, 513, 827
Mukhopadhyay, B. 2009, ApJ, 694, 387
Pétri, J. 2005, A&A, 439, L27
Press, W. H., Teukolsky, S. A., Vetterling, W. T., & Flannery, B. P. 2007, Numerical Recipes: The Art of Scientific Computing (3rd ed.; Cambridge: Cambridge Univ. Press)
Psaltis, D., Belloni, T., & van der Klis, M. 1999, ApJ, 520, 262
Psaltis, D., Mendez, M., Wijnands, R., et al. 1998, ApJ, 501, L95
Psaltis, D., Perrodin, D., Dienes, K. R., & Mocioiu, I. 2008, Phys. Rev. Lett., 100, 091101
Psaltis, D., Wijnands, R., Homan, J., et al. 1999, ApJ, 520, 763
Rezzolla, L., Yoshida, S., & Zanotti, O. 2003, MNRAS, 344, 978
Rikovska Stone, J., Miller, J. C., Koncewicz, R., Stevenson, P. D., & Strayer, M. R. 2003, Phys. Rev. C, 68, 3
Stella, L., & Vietri, M. 1998a, in Abstracts of the 19th Texas Symposium on Relativistic Astrophysics and Cosmology, ed. J. Paul, T. Montmerle, & E. Aubourg (Saclay, France: CEA)
Stella, L., & Vietri, M. 1998b, ApJ, 492, L59
Stella, L., & Vietri, M. 1999, Phys. Rev. Lett., 82, 17
Stella, L., & Vietri, M. 2002, in The Ninth Marcel Grossmann Meeting, Proc. MGIXMM Meeting held at The University of Rome "La Sapienza," 2000 July 2–8, ed. V. G. Gurzadyan, R. T. Jantzen, & R. Ruffini (Singapore: World Scientific), Part A, 426
Stella, L., Vietri, M., & Morsink, S. M. 1999, ApJ, 524, L63
Stergioulas, N., & Friedman, J. L. 1995, ApJ, 444, 306
Straub, O., & Šrámková, E. 2009, Class. Quantum Grav., 26, 055011
Strohmayer, T. E., & Markwardt, C. B. 2002, ApJ, 577, 337
Stuchlík, Z., Konar, S., Miller, J. C., & Hledík, S. 2008, A&A, 489, 963
Stuchlík, Z., & Kotrlová, A. 2009, Gen. Rel. Grav., 41, 1305
Stuchlík, Z., Kotrlová, A., & Török, G. 2011, A&A, 525, A82
Titarchuk, L., & Kent, W. 2002, ApJ, 577, L23
Török, G. 2009, A&A, 497, 661
Török, G., Abramowicz, M. A., Bakala, P., et al. 2008a, Acta Astron., 58, 15
Török, G., Abramowicz, M. A., Bakala, P., et al. 2008b, Acta Astron., 58, 113
Török, G., Abramowicz, M. A., Kluźniak, W., & Stuchlík, Z. 2005, A&A, 436, 1
Török, G., Abramowicz, M. A., Kluźniak, W., Stuchlík, Z., & Šrámková, E. 2006, in Proc. VI Microquasar Workshop: Microquasars and Beyond, 2006 September 18–22, Como, Italy, 96.1
Török, G., Bakala, P., Šrámková, E., Stuchlík, Z., & Urbanec, M. 2010, ApJ, 714, 748
Török, G., Bakala, P., Stuchlík, Z., & Čech, P. 2008c, Acta Astron., 58, 1
Török, G., Kotrlová, A., Šrámková, E., & Stuchlík, Z. 2011, A&A, 531, A59
Török, G., & Stuchlík, Z. 2005, A&A, 437, 775
Török, G., Stuchlík, Z., & Bakala, P. 2007, Cent. Eur. J. Phys., 5, 457
Urbanec, M., Běták, E., & Stuchlík, Z. 2010a, Acta Astron., 60, 149
Urbanec, M., Török, G., Šrámková, E., et al. 2010b, A&A, 522, A72
van der Klis, M. 2006, in Compact Stellar X-Ray Sources, ed. W. H. G. Lewin & M. van der Klis (Cambridge: Cambridge Univ. Press), 39, (see also astro-ph/0410551)
van Straaten, S., Ford, E. C., van der Klis, M., Méndez, M., & Kaaret, P. 2000, ApJ, 540, 1049
van Straaten, S., van der Klis, di Salvo, T., & Belloni, T. 2002, ApJ, 568, 912
Wagoner, R. V. 1999, Phys. Rep., 311, 259
Wagoner, R. V., Silbergleit, A. S., Lehr, D. E., & Ortega, M. A. 1999, BAAS, 31, 708
Wagoner, R. V., Silbergleit, A. S., & Ortega-Rodríguez, M. 2001, ApJ, 559, L25
Wiringa, R. B., Fiks, V., & Fabrocini, A. 1988, Phys. Rev. C, 38, 1010
Zhang, C. M. 2005, Chin. J. Astron. Astrophys., 5, 21
Zhang, W., Smale, A. P., Strohmayer, T. E., & Swank, J. H. 1998, ApJ, 500, L171

Paper II

6.2. Test of the Resonant Switch Model by Fitting the Data of Twin-Peak HF QPOs in the Atoll Source 4U 1636-53

Stuchlík Zdeněk, Kotrlová Andrea, Török Gabriel & Goluchová Kateřina

Acta Astronomica, 2014,
Volume 64, no 1, p. 45-64

ACTA ASTRONOMICA
Vol. **64** (2014) pp. 45–64

Test of the Resonant Switch Model by Fitting the Data of Twin-Peak HF QPOs in the Atoll Source 4U 1636–53

Z. Stuchlík, A. Kotrlová, G. Török and K. Goluchová

Institute of Physics, Faculty of Philosophy and Science, Silesian University in Opava,
Bezručovo nám. 13, CZ-74601 Opava, Czech Republic
e-mail: andrea.kotrlova@fpf.slu.cz

Received May 28, 2013

ABSTRACT

Resonant Switch (RS) model has recently been proposed as an alternative to the standard models of twin-peak high-frequency quasi-periodic oscillations (HF QPOs) observed in low-mass X-ray binaries containing a neutron star. The model assumes switch of twin oscillations at a resonant point, where frequencies of the upper and lower oscillations ν_U and ν_L become commensurable and one pair of the oscillating modes (corresponding to a specific model of HF QPOs) changes to some other pair due to non-linear resonant phenomena. We test the RS model for the atoll source 4U 1636–53, where we assume two resonant points observed at frequency ratios $\nu_U : \nu_L = 3:2,\ 5:4$, by fitting the pairs of the oscillatory modes to the observed data in the regions related to the resonant points. Among acceptable variants of the RS model the most promising are those combining the relativistic precession (RP) and the total precession (TP) frequency relations or their modifications. The precision of the fits is shown to be strongly increased in comparison to fits realized by individual pairs along the whole data range. We demonstrate that the χ^2 test is significantly improved. Fitting of the HF QPO data in the source 4U 1636–53 by the RP1–RP variant of the RS model gives the best results and implies that the neutron star mass and dimensionless spin are $M \approx 2.2\ \mathrm{M}_\odot$ and $a \approx 0.27$.

Key words: *Accretion, accretion disks – Stars: neutron – X-rays: binaries*

1. Introduction

The Galactic low mass X-ray binaries (LMXBs) containing black holes or neutron (quark) stars demonstrate quasiperiodic oscillations (QPOs) of X-ray brightness at low-(Hz) and high-(kHz) frequencies (see, *e.g.*, Remillard and McClintock 2006, van der Klis 2006, 2000, Barret *et al.* 2005a). Since the high frequencies are close to the orbital frequency of the marginally stable circular orbit representing the inner edge of Keplerian disks orbiting neutron stars, the strong gravity effects are expected to be relevant in explaining the HF QPOs (Kluźniak 1998).

The HF QPOs in neutron star (NS) systems are often demonstrated as two simultaneously observed pairs of peaks (twin peaks) in the Fourier power spectra,

corresponding to oscillations at the upper and lower frequencies (ν_U, ν_L). The twin peaks at the upper and lower frequencies substantially change over time (in one observational sequence). Sometimes only one of the frequencies is observed and evolves and the other disappears, but it is not clear if this effect is related to detectability of the oscillations by recent observational technology (Belloni *et al.* 2007, Boutelier *et al.* 2010). Nevertheless, detection of twin-peak HF QPOs is strongly influenced by definition of the observational level of the HF QPOs and we can expect some improvements in detection of HF QPOs by planned high-precision X-ray satellite observatories, especially by the LOFT (Feroci *et al.* 2012).

Most of the twin HF QPOs in the so-called atoll sources (van der Klis 2006) have been detected at lower frequencies 600–800 Hz *vs.* upper frequencies 900–1200 Hz, demonstrating a clustering of the twin HF QPOs frequency ratio around $3:2$. This clustering (Abramowicz *et al.* 2003, 2005b, Belloni *et al.* 2007, Török *et al.* 2008abc, Boutelier *et al.* 2010) indicates some analogy to the black hole (BH) case where twin peaks with fixed pair of frequencies at the ratio $3:2$ are usually observed and can be explained by the internal non-linear resonance of oscillations with geodetical radial and vertical epicyclic frequencies (Török *et al.* 2005). It is probable that a $3:2$ resonance plays a significant role also in the atoll sources containing neutron stars. However, this case is much more complicated, as the frequency ratio, although concentrated around $3:2$, falls in a much wider range than in the BH systems (Belloni *et al.* 2005, Török *et al.* 2005, Abramowicz *et al.* 2005a, Török *et al.* 2008c, Török 2009, Boutelier *et al.* 2010, Wang *et al.* 2013, 2014). It remains controversial whether in the atoll NS sources the peak in distribution of the twin-peak frequency ratios ν_U/ν_L at $3:2$ is physical (Montero and Zanotti 2012).

In fact, a multi-peaked distribution in the frequency ratios has been observed (Belloni *et al.* 2005, Stuchlík *et al.* 2007, Török *et al.* 2008c), *i.e.*, more than one resonance could be realized if a resonant mechanism is involved in generating the neutron star HF QPOs. For some atoll NS sources the upper and lower HF QPO frequencies can be traced along the whole observed range, but the probability to detect both QPOs simultaneously increases when the frequency ratio is close to ratio of small natural numbers, namely $3:2$, $4:3$, $5:4$ – this has been observed in six atoll sources: 4U 1636–53, 4U 1608–52, 4U 0614+09, 4U 1728–34, 4U 1820–30, 4U 1735–44 (Török 2009, Boutelier *et al.* 2010). The analysis of root-mean-squared-amplitude evolution in the group of six atoll sources shows that the upper and lower HF QPO amplitudes equal each other and alter their dominance while passing rational frequency ratios corresponding to the datapoints clustering (Török 2009). Such an "energy switch effect" can be well explained in the framework of non-linear resonant orbital models as shown in Horák *et al.* (2009). Moreover, the analysis of the twin-peak HF QPO amplitudes in the atoll sources 4U 1636–53, 4U 1608–52, 4U 1820–30, and 4U 1735–44 indicates a cut-off at resonant radii corresponding to the frequency ratios $5:4$ and $4:3$ respectively, implying a possibility that the accretion disk inner edge is located at the innermost resonant

radius rather than at the innermost stable circular geodesic (ISCO, Stuchlík *et al.* 2011). The situation is slightly different for the Z-sources where the twin-peak frequency ratios alter strongly again but they are clustering close to $2:1$, and $3:1$ ratios as demonstrated in the Z-source Circinus X-1 (Boutloukos *et al.* 2006). Then the resonant radii are expected at slightly larger distance from the ISCO than in the atoll sources (Török *et al.* 2010).

The evolution of the lower and upper twin HF QPOs frequencies in the atoll and Z-sources suggests (a very rough) agreement of the data distribution with so-called hot spot models of HF QPOs, especially with the relativistic precession model prescribing the evolution of the upper frequency by $\nu_U = \nu_K$ and the lower frequency by $\nu_L = \nu_K - \nu_r$ (Stella and Vietri 1999, 1998). In all of the acceptable models the frequency difference $\nu_U - \nu_L$ has to decrease with increase of the lower and upper frequencies, in accord with trends given by the observational data (Belloni *et al.* 2007, Boutelier *et al.* 2010). This qualitative property of the observational data excludes the simple model of epicyclic oscillations with $\nu_U = \nu_\theta$ and $\nu_L = \nu_r$ (Urbanec *et al.* 2010b) that works quite well in the case of HF QPOs in LMXBs containing black holes (Török *et al.* 2005).

The ν_U/ν_L frequency relations, given by a variety of the relevant frequency-relation models, can be fitted to the observational data for the atoll and Z-sources containing neutron stars, *e.g.*, data determined for the atoll source 4U 1636–53 (Barret *et al.* 2005a, Török *et al.* 2008abc), or the Z-source Circinus X-1 (Boutloukos *et al.* 2006). The parameters of the neutron star spacetime can be then determined due to the fitting procedure. The rotating neutron stars are described quite well by the Hartle–Thorne geometry characterized by three parameters: mass M, internal angular momentum J, and quadrupole moment Q, or by dimensionless parameters $a = J/M^2$ (spin) and $q = QM/J^2$ (dimensionless quadrupole moment) (Hartle and Thorne 1968). In the special case where $q \approx 1$, the Hartle–Thorne geometry reduces to the well known and well studied Kerr geometry that is convenient for relativistic calculations in a strong gravitational field regime because of the simplicity of relevant formulae. It has recently been shown that near-maximum-mass neutron (quark) star Hartle–Thorne models constructed for any given equation of state imply $q \approx 1$, and the Kerr geometry is quite correctly applicable in such situations instead of the Hartle–Thorne geometry (Urbanec *et al.* 2013, Török *et al.* 2010). The Keplerian (orbital) frequency ν_K, the vertical epicyclic frequency ν_θ, and the radial epicyclic frequency ν_r take in the Kerr spacetime the form (*e.g.*, Aliev and Galtsov 1981, Perez *et al.* 1997, Kato *et al.* 1998, Stella and Vietri 1998, Török and Stuchlík 2005, Stuchlík and Schee 2012)

$$\nu_\theta^2 = \alpha_\theta \nu_K^2, \qquad \nu_r^2 = \alpha_r \nu_K^2, \tag{1}$$

$$\nu_K = \frac{1}{2\pi}\left(\frac{GM}{r_G^3}\right)^{1/2} \frac{1}{x^{3/2}+a} = \frac{1}{2\pi}\left(\frac{c^3}{GM}\right)\frac{1}{x^{3/2}+a}, \tag{2}$$

$$\alpha_\theta = 1 - \frac{4a}{x^{3/2}} + \frac{3a^2}{x^2}, \tag{3}$$

$$\alpha_r = 1 - \frac{6}{x} + \frac{8a}{x^{3/2}} - \frac{3a^2}{x^2} \tag{4}$$

where $x = r/(GM/c^2)$ is the dimensionless radius, expressed in terms of the gravitational radius.

Assuming the geodesic orbital and epicyclic frequencies determined for the Kerr geometry, the fitting procedure applied to the relativistic precession model of the frequency-relation evolution for the Z-source Circinus X-1 implies mass–spin relation $M(a) = M_0\left[1 + k(a + a^2)\right]$ with $M_0 \approx 2.2$ $M_\odot$ and $k \approx 0.5$ rather than concrete values of the neutron star parameters M and a (Török *et al.* 2010). The same mass–spin relations, but with different values of the Schwarzschild (no-rotation) mass $M_0 \approx 1.8$ $M_\odot$ and the constant $k \approx 0.75$, were obtained for the atoll source 4U 1636–53 (Török *et al.* 2012). Quality of the fitting procedure is very poor for the atoll source 4U 1636–53 (Török *et al.* 2012). Similar very bad fit of observational data was found by Lin *et al.* (2011) for the atoll source 4U 1636–53 and Z-source Sco X-1 also for some models of the HF QPOs having the frequency relations based on phenomena of non-geodesic origin (Miller *et al.* 1998, Osherovich and Titarchuk 1999, Zhang 2004, Zhang *et al.* 2006, Chakrabarti *et al.* 2008, Mukhopadhyay 2009, Shi and Li 2009, Shi 2011, Mukherjee and Bhattacharyya 2012).

The disagreement of the data distribution and their fitting by the frequency-relation models based on the assumption of the geodesic character of the oscillatory frequencies caused attempts to find a correction of a non-geodesic origin reflecting some important physical ingredients, *e.g.*, influence of the magnetic field of the neutron star onto slightly charged innermost parts of the disk (Bakala *et al.* 2012, 2010, Kovář *et al.* 2008), of thickness of non-slender oscillating tori (Rezzolla *et al.* 2003, Blaes *et al.* 2007, Straub and Šrámková 2009) or of its stringy origin (Stuchlík and Kološ 2012ab, Cremaschini and Stuchlík 2013, Kološ and Stuchlík 2013, Stuchlík and Kološ 2014). Another possible modifications are related to the models developed for braneworld compact objects (Kotrlová *et al.* 2008, Stuchlík and Kotrlová 2009, Schee and Stuchlík 2009, Aliev *et al.* 2013). Such modifications of the frequency-relation models could make the quality of the fitting procedure much better, as shown in Török *et al.* (2012) for a simple toy model with one additional free parameter.

On the other hand, it is important to consider another possibility to improve the data fitting that keeps the relevance of the frequencies governed by the geodesic orbital and epicyclic motion, namely the Resonant Switch (RS) model considering switch of the frequency relations at a resonant radius (Stuchlík *et al.* 2012, 2013). The RS model keeps the assumption of only two free parameters, namely the mass and the dimensionless spin of the central neutron star. The RS model has been applied in the case of the atoll source 4U 1636–53, giving for all considered fre-

quency relations relatively extended restrictions on the mass and spin parameters of the 4U 1636–53 neutron star (Stuchlík *et al.* 2012). Here we test the RS model for this atoll source by fitting the observational data by the combinations of the frequency relations that are predicted by the RS model as acceptable due to the neutron star structure theory, *i.e.*, having acceptable values of the mass and spin parameters of the neutron star at the atoll source 4U 1636–53 (Stuchlík *et al.* 2012). The RS model can be considered to be relevant, if substantial improvement of the fitting of the observational data occurs for some of the frequency-relation combinations. Moreover, we expect also substantial improvement of limits on the neutron star parameters M and a due to the fitting procedure.

2. Resonant Switch Model of HF QPOs Observed in 4U 1636–53 Atoll System

The RS model of twin-peak HF QPOs assumes switching of the twin oscillatory modes creating sequences of the lower and upper HF QPOs at a resonant point. The non-linear resonant phenomena can cause excitation of a new oscillatory mode (or two new oscillatory modes) and vanishing of one of the previously acting modes (or both the previous modes). Two resonant points at the disk radii $x_{\rm out}$ and $x_{\rm in}$ are assumed, with observed frequencies $\nu_U^{\rm out}$, $\nu_L^{\rm out}$ and $\nu_U^{\rm in}$, $\nu_L^{\rm in}$, being in commensurable ratios $p^{\rm out} = n^{\rm out} : m^{\rm out}$ and $p^{\rm in} = n^{\rm in} : m^{\rm in}$; observations require $\nu_U^{\rm in} > \nu_U^{\rm out}$ and $p^{\rm in} < p^{\rm out}$. In the region covering the resonant point at $x_{\rm out}$ the twin oscillatory modes with the upper (lower) frequency are determined by the function $\nu_U^{\rm out}(x;M,a)$ ($\nu_L^{\rm out}(x;M,a)$). Near the inner resonant point at $x_{\rm in}$ different oscillatory modes given by the frequency functions $\nu_U^{\rm in}(x;M,a)$ and $\nu_L^{\rm in}(x;M,a)$ occur. All the frequency functions are assumed to be combinations of the orbital and epicyclic frequencies of the geodesic motion in the Kerr backgrounds. Such an assumption is correct for very compact (and very massive) neutron stars or strange stars (Urbanec *et al.* 2013), but for neutron (strange) stars having small compactness the Kerr geometry cannot be correct and the Hartle–Thorne geometry must be used to describe the external spacetime (Gondek-Rosińska *et al.* 2014).

The frequency-relation functions ν_U/ν_L have to meet the observationally given resonant frequencies determined by the energy switch effect, *i.e.*, by the alteration of the *rms*-amplitude dominance of the oscillations on the lower and upper frequencies of the twin HF QPOs that occurs at the resonance points where the frequency ratio takes rational values (Török 2009). Independence of the frequency ratio on the mass parameter M implies that the conditions $\nu_U^{\rm out}(x,a) : \nu_L^{\rm out}(x,a) = p^{\rm out}$, $\nu_U^{\rm in}(x,a) : \nu_L^{\rm in}(x,a) = p^{\rm in}$ determine relations for the spin a in terms of the dimensionless radius x and the resonant frequency ratio p. They can be expressed in the form $a^{\rm out}(x,p^{\rm out})$ and $a^{\rm in}(x,p^{\rm in})$, or in an inverse form $x^{\rm out}(a,p^{\rm out})$ and $x^{\rm in}(a,p^{\rm in})$. At the resonant points, the conditions

$$\nu_U^{\rm out} = \nu_U^{\rm out}(x;M,a)\,, \qquad \nu_U^{\rm in} = \nu_U^{\rm in}(x;M,a) \tag{5}$$

are satisfied along the functions $M^{\rm out}_{p_{\rm out}}(a)$ and $M^{\rm in}_{p_{\rm in}}(a)$ obtained by using the functions $x^{\rm out}(a,p^{\rm out})$ and $x^{\rm in}(a,p^{\rm in})$. The parameters of the neutron (quark) star are then given by the condition

$$M^{\rm out}_{p_{\rm out}}(a) = M^{\rm in}_{p_{\rm in}}(a) \tag{6}$$

that determines M and a with precision given by the error occurring in determination of the resonant frequencies by the energy switch effect – for details see Stuchlík *et al.* (2012).

2.1. Frequency Relations Used in the RS Model

We consider here the frequency relations related to the so-called hot spot models of HF QPOs, or models of accretion disk oscillations. In both cases we assume that the oscillatory frequencies are governed by the geodetical orbital and epicyclic motion. We thus take into account the widely discussed (R)elativistic (P)recession (RP) model prescribing the evolution of the upper frequency by $\nu_U = \nu_K$ and the lower frequency by $\nu_L = \nu_K - \nu_r$ (Stella and Vietri 1999, 1998) and a similar (T)otal (P)recession (TP) model (Stuchlík *et al.* 2007), where the evolution of the upper frequency is given by $\nu_U = \nu_\theta$ and the lower frequency by $\nu_L = \nu_\theta - \nu_r$. We consider also their modifications where the upper frequency is modified by interchange (frequency relations RP1 – Bursa 2005, and TP1) or by adding the beat frequency (RPB, and TPB). We further consider also the (T)idal (D)isruption (TD) model (Čadež *et al.* 2008, Kostić *et al.* 2009), and the (W)arped (D)isc oscillations (WD) model (Kato 2004, 2008).

The frequency relations corresponding to these models are summarized in Table 1. For each of the frequency relations under consideration the frequency resonance functions and the resonance conditions determining the resonant radii $x_{n:m}(a)$ are given in Stuchlík *et al.* (2012) where all the details can be found.

T a b l e 1

Frequency relations corresponding to individual QPO models

Model	Relations	
RP	$\nu_L = \nu_K - \nu_r$	$\nu_U = \nu_K$
RP1	$\nu_L = \nu_K - \nu_r$	$\nu_U = \nu_\theta$
RPB	$\nu_L = \nu_K - \nu_r$	$\nu_U = \nu_K + \nu_r$
TP	$\nu_L = \nu_\theta - \nu_r$	$\nu_U = \nu_\theta$
TP1	$\nu_L = \nu_\theta - \nu_r$	$\nu_U = \nu_K$
TPB	$\nu_L = \nu_\theta - \nu_r$	$\nu_U = \nu_\theta + \nu_r$
TD	$\nu_L = \nu_K$	$\nu_U = \nu_K + \nu_r$
WD	$\nu_L = 2(\nu_K - \nu_r)$	$\nu_U = 2\nu_K - \nu_r$

2.2. Restrictions on the Mass and Spin due to Theory of Neutron Star Structure

Predictions of the RS model have to be confronted with theoretical limits on the mass and spin of neutron (quark) stars. The restriction on the neutron star mass reads

$$M < 2.8\ \mathrm{M}_{\odot} \tag{7}$$

(see, *e.g.*, Müther *et al.* 1987, Müller and Serot 1996, Akmal and Pandharipande 1997, Akmal *et al.* 1998, Postnikov *et al.* 2010, Urbanec *et al.* 2010a). The upper limit on the neutron star spin reads $a_{\mathrm{maxNS}} \approx 0.7$ as demonstrated in Lo and Lin (2011).

For the quark stars the maximal mass is expected to be somewhat smaller in comparison with the neutron stars because of softer equations of state assumed in modeling the quark stars, but masses around $M_{\mathrm{maxQ}} \approx 2\ \mathrm{M}_{\odot}$ are allowed (*e.g.*, Glendenning 2000, Lo and Lin 2011). However, a substantial difference occurs in the limit on maximal spin, since even slightly superspinning states of quark stars with $a_{\mathrm{maxQ}} \geq 1$, exceeding the black hole limit $a = 1$, have recently been reported by Lo and Lin (2011). Such a sharp difference between the limits on the maximal spin of neutron and quark stars can be explained by the strong nuclear force acting in binding the strange stars, while no such effect can occur in the case of neutron stars.

In the Hartle–Thorne model of rotating neutron stars the spin of the star is related to its rotational frequency (Hartle and Thorne 1968, Chandrasekhar and Miller 1974). The rotational frequency of the neutron star at the atoll source 4U 1636–53 has been observed at $f_{\mathrm{rot}} = 580$ Hz (or $f_{\mathrm{rot}} = 290$ Hz, if we observe doubled radiating structure, Strohmayer and Markwardt 2002). Such a rotational frequency is low in comparison with the mass-shedding frequency ($f_{\mathrm{mass-shedding}} \approx 1100$ Hz), and the Hartle–Thorne model can be applied quite well, predicting spins significantly lower than the maximally allowed spin. We have checked that the Hartle–Thorne model implies for a wide variety of realistic equations of state used in Urbanec *et al.* (2013) the spin in the range

$$0.1 < a < 0.4. \tag{8}$$

We assume that this restriction has to be relevant for acceptable combinations of frequency relations in their predictions related to the neutron star spin.

2.3. Predictions of the RS Model for the Source 4U 1636–53

The observational data from the atoll source 4U 1636–53 clearly demonstrate possible existence of two "resonant points" where the energy switch effect occurs. The RS model assumes that the switch of the frequency relations occurs at the outer resonant point. The results of Török (2009) give the resonant frequencies determined by the energy switch effect that are in accord with those given by crossing of observational data by the lines of constant frequency ratios $3:2$ and $5:4$ as given in the standard papers (Barret *et al.* 2005a, Belloni *et al.* 2007). However,

the precision of determination of the upper and lower frequencies at the outer and inner resonant points due to the energy switch effect is rather low.

In the framework of the RS model the mass and spin parameters, M and a, of the neutron (quark) star at the 4U 1636–53 source were determined for a large variety of the frequency relations ν_U/ν_L in Stuchlík *et al.* (2012). The ranges of the neutron star mass and spin of the 4U 1636–53 source allowed by the procedure of the RS model are summarized in Table 1 of Stuchlík *et al.* (2012) for all the frequency pairs constituted by the simple combinations of the geodetical orbital and epicyclic frequencies. We see that the range of the mass and spin parameters of the neutron star determined by the RS model due to the energy switch effect at the resonant points is very large. The mass and spin estimates presented in Table 1

T a b l e 2

Intervals of mass and spin of the neutron star in the atoll source 4U 1636–53 implied by the procedure of the RS model

Combination of models	spin a	mass M [$M_\odot$]
RP(3 : 2) – TP1(5 : 4)	0.27–0.74	2.28–4.20
RP(3 : 2) – TPB(5 : 4)	0.18–0.65	2.24–3.45
RP1(3 : 2) – RP(5 : 4)	0.14–0.42	1.98–2.49
RP1(3 : 2) – TP(5 : 4)	0.25–0.67	2.11–2.94
RP1(3 : 2) – TP1(5 : 4)	0.10–0.34	1.94–2.36
TP(3 : 2) – RP(5 : 4)	0.29–0.70	2.25–3.57
TP(3 : 2) – TP1(5 : 4)	0.17–0.52	2.07–2.93
TP1(3 : 2) – RPB(5 : 4)	0.18–0.67	2.30–4.11
TP1(3 : 2) – TPB(5 : 4)	0.08–0.38	2.10–2.70
WD(3 : 2) – TD(5 : 4)	0.00–0.69	2.14–4.22
TD(3 : 2) – TD(5 : 4)	0.00–0.69	2.14–4.22

Note that the model WD(3 : 2) gives identical solution as TD(3 : 2).

of Stuchlík *et al.* (2012) are compared to the restrictions implied by the theoretical models of neutron stars and the observed rotational frequency of the neutron star at 4U 1636–53. Some combinations of the frequency relations applied at the resonant points are clearly disfavored, predicting mass and spin ranges that are completely out of the ranges given by the theoretical restrictions (for example the combination of the RP and TD relations). Some combinations cover the theoretically allowed region partially (*e.g.*, for combination of the RP and TP frequency relations) or completely (*e.g.*, for combination of the RP1 and TP1 frequency relations). The combinations of the frequency relations that are at least at partial agreement with the theoretical limits are given in Table 2 of the present paper and are further tested by fitting the observational data to the related frequency relations in the regions of observational data separated by the outer resonant point.

3. Fitting the Twin-Peak HF QPO Data by the Switched Twin Frequency Relations

According to the RS model, the fitting procedure is separated into two segments determined by the resonant points that has been deduced for the atoll source 4U 1636–53 by the energy switch effect (Török 2009). These two segments of observational data are separated by the outer resonant point corresponding to the frequency ratio $3:2$. Therefore, for the data with frequency ratio larger than $3:2$, corresponding to radii larger than the outer resonant radius, the first frequency relation of the combination under consideration is used for the fitting procedure, while for the data with frequency ratio smaller than $3:2$, at radii between the outer and inner resonant radius, the second frequency relation of the combination is used in the fitting procedure.

For analysis presented in this paper we use the HF QPO data in the 4U 1636–53 source taken from Barret *et al.* (2005ab). In the fitting procedure we apply those switched twin frequency relations predicted by the RS model that are acceptable due to the neutron (quark) star structure theory as found in Stuchlík *et al.* (2012). All the twin frequency relations considered in our testing are presented in Table 2 where the ranges of values of the mass M and spin a of the neutron star predicted by the RS model are explicitly given. In fitting the observational data we use the standard least-squares (χ^2) method (*e.g.*, Press *et al.* 2007). There is

$$\chi^2 \equiv \sum_{n=1}^{m} \Delta_n^2, \qquad \Delta_n = \mathrm{Min}\left(\frac{l_{n,p}}{\sigma_{n,p}}\right)_{p_\infty}^{p_{\mathrm{ISCO}}} \tag{9}$$

where $l_{n,p}$ is the length of a line between the nth measured data point $[\nu_L(n), \nu_U(n)]$ and a point $[\nu_L(p), \nu_U(p)]$ belonging to the relevant frequency curve of the model. The quantity $\sigma_{n,p}$ equals the length of the part of this line located within the error ellipse around the data point. The χ^2 test was applied solely to the RP, TP and TD frequency relations along the whole range of the observational data, however, the results were quite unsatisfactory, giving $\chi^2/\mathrm{dof} \approx 16$ as demonstrated in Török *et al.* (2012).

We use the pairs of the frequency relations of the RS model in the regions of observational data related to the corresponding resonant points. We look first for the quality of the fits χ^2 in the $M-a$ plane. For each value of M from the interval allowed by the RS model we find related spin a implying minimal value of χ^2 for given M – we find a function giving "local" best fits $M_{\mathrm{lbf}}(a)$. Then we look for the "global" best fit M_{bf} represented by the minimal value of χ^2 along the function $M_{\mathrm{lbf}}(a)$. We then find the neutron star mass as the mass corresponding to $\chi^2_{\mathrm{min}}(M_{\mathrm{lbf}}(a))$. The error of the neutron star mass is given by $\Delta\chi^2 = 2$ around the $\chi^2_{\mathrm{min}}(M_{\mathrm{lbf}}(a))$. Using the function $M_{\mathrm{lbf}}(a)$, we determine the neutron star spin a and the related error.

The results of the fitting procedure are presented in Fig. 1 for the combinations of the frequency relations RP1–RP, RP1–TP1, and RP1–TP, in Fig. 2 for the com-

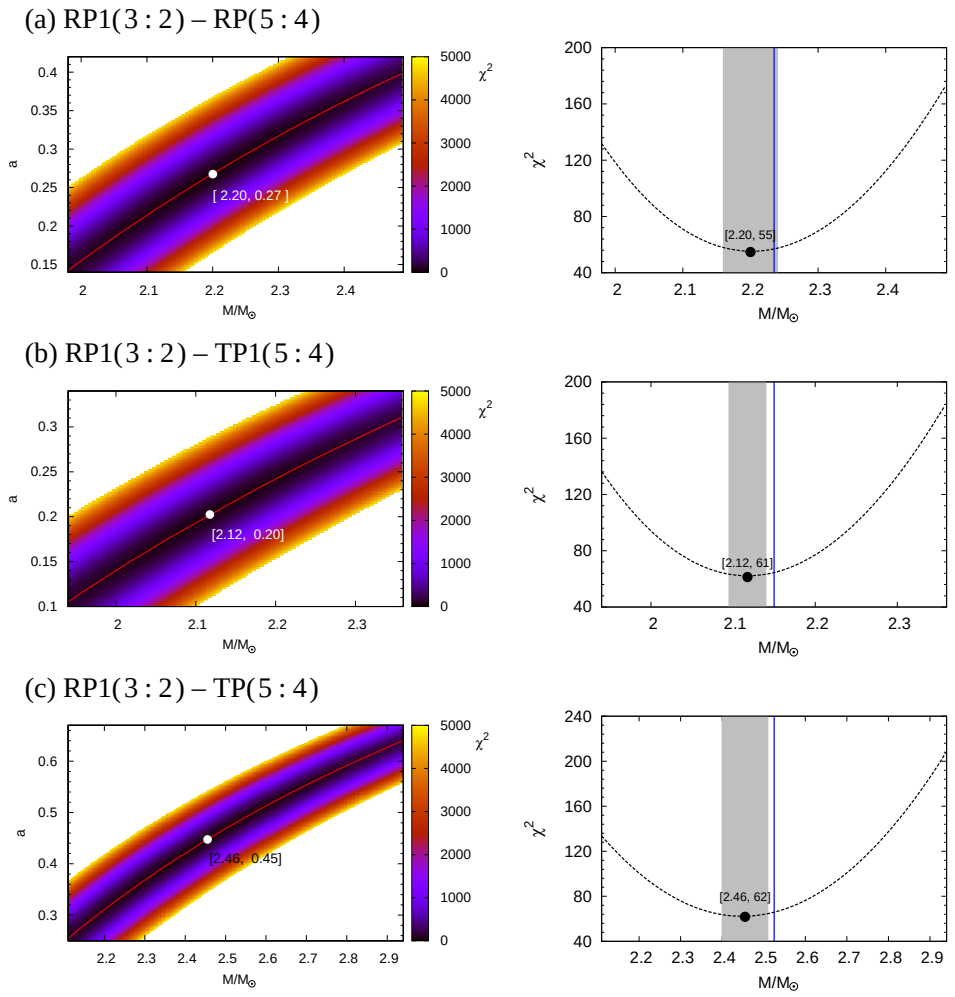

Fig. 1. Results of the fitting the data of twin-peak HF QPOs in the atoll source 4U 1636–53 by the procedure of the RS model for the combinations of the RP1–RP *(a)*, RP1–TP1 *(b)*, and RP1–TP *(c)* frequency relations. *Left panel*: The χ^2 dependence on M and a. The red line indicates the best χ^2 for a fixed M (*i.e.*, the function giving "local" best fits $M_{\rm lbf}(a)$). *Right panel*: Profile of the lowest χ^2 as a function of the parameter M, constructed for the parameter a corresponding to the best fit obtained for the given combination of frequency relations. Thick blue vertical lines give mean value of M as determined by the RS model from the frequency ratio governed by the energy switch effect. The gray region corresponds to the precision of the fit ($\chi^2 \leq \chi^2_{\rm min} \pm 2$).

binations of the frequency relations TP–RP, TP–TP1, and RP–TP1, in Fig. 3 for the combination of the frequency relations WD–TD and TD–TD, and in Fig. 4 for the combinations of the frequency relations RP–TPB, TP1–RPB, TP1–TPB.

The best fits and the corresponding mass and spin parameters of the neutron (quark) star located in the 4U 1636–53 source are presented in Table 3, along with related errors in determining mass and spin of the neutron star. The best fit $\chi^2 = 55$ occurs for two frequency pairs. One of them (TP–RP) is excluded because of too

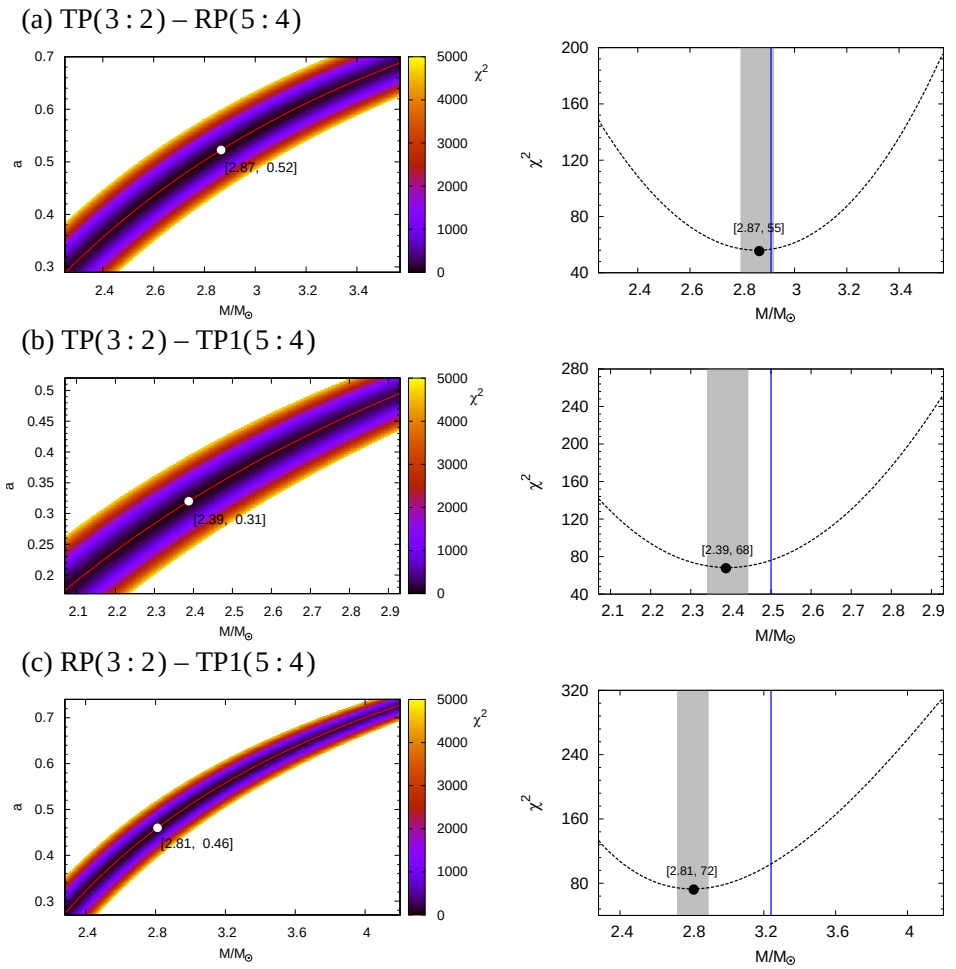

Fig. 2. Results of the fitting the data of twin-peak HF QPOs in the atoll source 4U 1636–53 by the procedure of the RS model for the combinations of the TP–RP *(a)*, TP–TP1 *(b)*, and RP–TP1 *(c)* frequency relations. *Left panel*: The χ^2 dependence on M and a. The red line indicates the best χ^2 for a fixed M (the function $M_{\rm lbf}(a)$). *Right panel*: Profile of the lowest χ^2 as a function of the parameter M, constructed for the parameter a corresponding to the best fit obtained for the given combination of frequency relations. Thick blue vertical lines give mean value of M as determined by the RS model from the frequency ratio governed by the energy switch effect. The gray region corresponds to the precision of the fit ($\chi^2 \leq \chi^2_{\rm min} \pm 2$).

high mass and spin predicted ($M \approx 2.87$ M$_\odot$, $a \approx 0.52$). The other one (RP1–RP) predicts the parameters ($M \approx 2.20$ M$_\odot$, $a \approx 0.27$) that are quite acceptable by the neutron star theory and can be considered as the best prediction of the RS model. The second best fit with $\chi^2 = 61$ occurs for the frequency pair RP1–TP1 and predicts neutron star parameters that are again acceptable by the theory ($M \approx 2.12$ M$_\odot$, $a \approx 0.20$). For the best fits we present in Fig. 5 the pairs of relevant frequency relations RP1–RP and RP1–TP1 related to the observational data of the

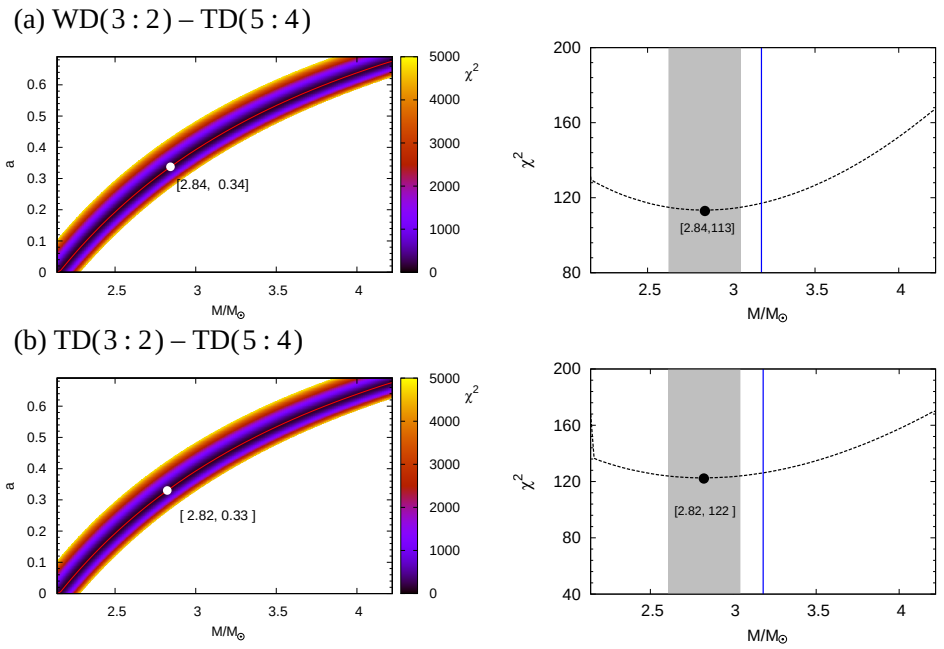

Fig. 3. Results of the fitting the data of twin-peak HF QPOs in the atoll source 4U 1636–53 by the procedure of the RS model for the combinations of the WD–TD *(a)* and TD–TD *(b)* frequency relations. *Left panel*: The χ^2 dependence on M and a. The red line indicates the best χ^2 for a fixed M (the function $M_{\rm lbf}(a)$). *Right panel*: Profile of the lowest χ^2 as a function of the parameter M, constructed for the parameter a corresponding to the best fit obtained for the given combination of frequency relations. Thick blue vertical line gives mean value of M as determined by the RS model from the frequency ratio governed by the energy switch effect. The gray region corresponds to the precision of the fit ($\chi^2 \leq \chi^2_{\rm min} \pm 2$).

twin HF QPOs in the source 4U 1636–53 as given in Török *et al.* (2012). We can see that the distribution of the observational data probably excluded obtaining of better $\chi^2_{\rm min}$ in comparison to those obtained by using the RS model.

We can also state using Figs. 1–4 that for the best fits of mass parameter M the value of $M_{\rm bf}$ is close to the mean value of the mass estimate given by the RS model with frequency ratios determined by the energy switch effect as represented by the solid vertical lines in Figs. 1–4. Notice that the best fit values of $M_{\rm bf}$ are always shifted to the left of the mean value given by the energy switch effect, with exception of the fits constructed for the frequency relation containing in the upper frequency the beat frequency corresponding to the radial epicyclic frequency. We expect that the shift is caused by the fact that the inner resonant point corresponds to the innermost radius of the Keplerian disk, as suggested in Stuchlík *et al.* (2011). Therefore, the data at the inner resonant point are more restricted than those at the outer resonant point.

Our results have to be compared to the detailed theoretical models of neutron stars based on a large variety of equations of state in the framework of the Hartle–Thorne approach describing slowly rotating neutron stars that is quite rele-

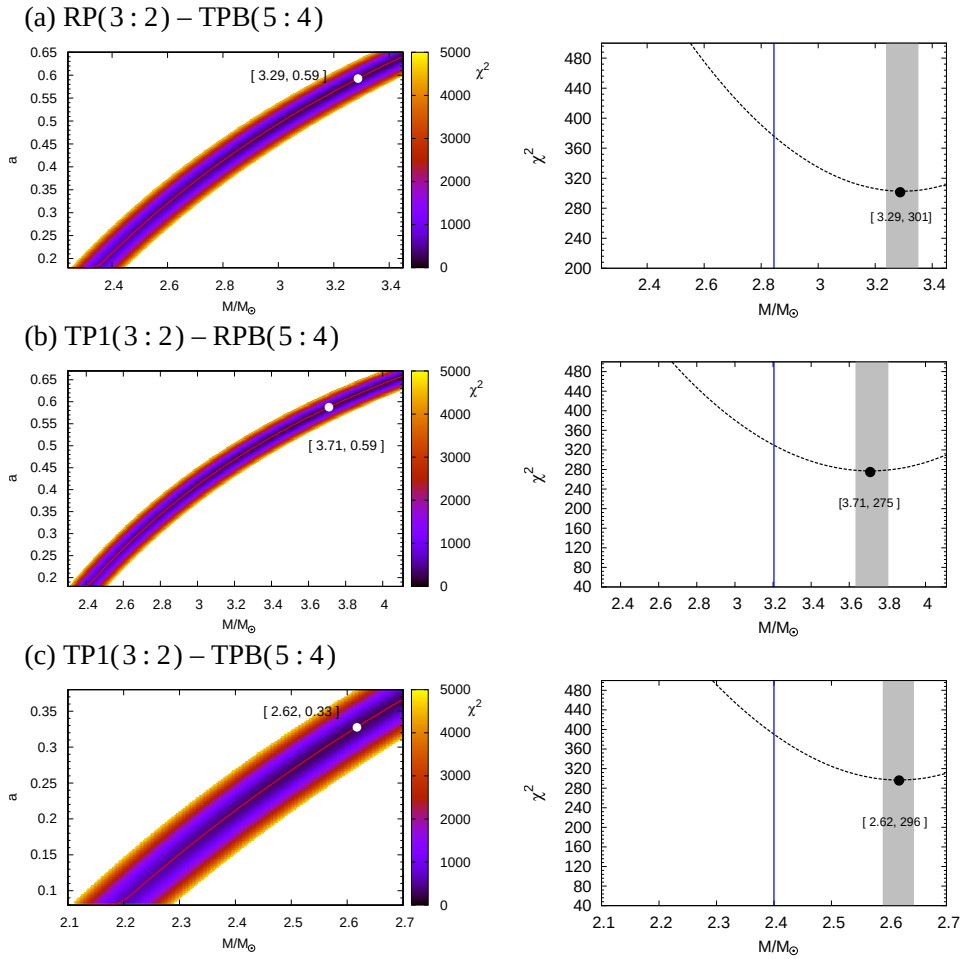

Fig. 4. Results of the fitting the data of twin-peak HF QPOs in the atoll source 4U 1636–53 by the procedure of the RS model for the combinations of the RP–TPB *(a)*, TP1–RPB *(b)*, and TP1–TPB *(c)* frequency relations. *Left panel*: The χ^2 dependence on M and a. The red line indicates the best χ^2 for a fixed M (the function $M_{\rm lbf}(a)$). *Right panel*: Profile of the lowest χ^2 as a function of the parameter M, constructed for the parameter a corresponding to the best fit obtained for the given combination of frequency relations. Thick blue vertical lines give mean value of M as determined by the RS model from the frequency ratio governed by the energy switch effect. The gray region corresponds to the precision of the fit ($\chi^2 \leq \chi^2_{\rm min} \pm 2$).

vant for the 4U 1636–53 neutron star with observationally given rotation frequency of 580 Hz (or 290 Hz, Urbanec *et al.* 2013, Boshkayev *et al.* 2013, Chandrasekhar and Miller 1974, Hartle and Thorne 1968). We can expect that our results could imply, then, relevant restrictions on the applicability of the equations of state in this particular source.

We have to check in our study, if the RS model implies significant improvement in fitting the observational data from the point of view of the probabilistic theory. For these purposes, the so called F-test is the most convenient tool.

Table 3

The best fits and the corresponding spin and mass parameters of the neutron star located in the 4U 1636–53 atoll source, along with related errors in determining spin and mass of the neutron star due to the fitting procedure

Combination of models	$\chi^2_{\rm min}$	a	Δa	M [M$_\odot$]	ΔM [M$_\odot$]
RP1(3 : 2) – RP(5 : 4)	55	0.27	0.02	2.20	0.04
TP(3 : 2) – RP(5 : 4)	55	0.52	0.02	2.87	0.06
RP1(3 : 2) – TP1(5 : 4)	61	0.20	0.01	2.12	0.03
RP1(3 : 2) – TP(5 : 4)	62	0.45	0.03	2.46	0.06
TP(3 : 2) – TP1(5 : 4)	68	0.31	0.02	2.39	0.05
RP(3 : 2) – TP1(5 : 4)	72	0.46	0.03	2.81	0.09
WD(3 : 2) – TD(5 : 4)	113	0.34	0.08	2.84	0.21
TD(3 : 2) – TD(5 : 4)	122	0.33	0.08	2.82	0.22
TP1(3 : 2) – RPB(5 : 4)	275	0.59	0.02	3.71	0.09
TP1(3 : 2) – TPB(5 : 4)	296	0.33	0.02	2.62	0.03
RP(3 : 2) – TPB(5 : 4)	301	0.59	0.02	3.29	0.06

Shaded rows are the fits that are in agreement with the theoretical restrictions on the neutron star parameters.

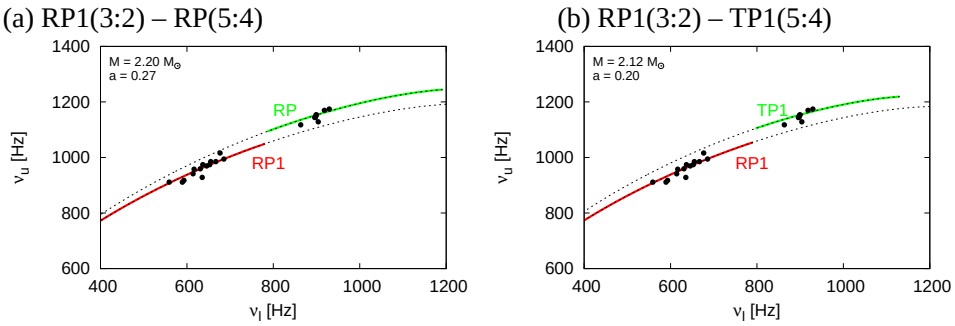

Fig. 5. The pairs of relevant frequency relations RP1–RP *(a)* and RP1–TP1 *(b)* for the best fits related to the observational data of the twin HF QPOs in the atoll source 4U 1636–53.

4. *F*-Test of the Resonant Switch Model

The significance statistics test of the RS model can be given by the F-test which compares fits realized by nested models, where one of the models is a subset of the other model (*e.g.*, Bevington and Robinson 2003). We shall use the F-test assuming that the RS model contains one free parameter in addition to the two free parameters occurring in the standard RP model. The additional parameter is related to the position of the switch in the oscillatory modes. The F-test is applied to the best version of the RS model in fitting the observational data (RP1–RP model), and the related individual RP model.

According to the F-test theory, we have to introduce quantity F-ratio that is the ratio of the relative increase of the parameter χ^2 reflecting the precision of the fitting of the observational data and the relative increase of the degrees of freedom in the models

$$F = \frac{\left(\chi_1^2 - \chi_2^2\right)/\chi_2^2}{(N_1 - N_2)/N_2} \tag{10}$$

where χ_2^2 corresponds to the model with smaller number of the degrees of freedom, while χ_1^2 corresponds to the model with larger number of degrees of freedom. N_1 (N_2) denotes the number of degrees of freedom for the model with the higher (lower) number of free parameters. Then the F-ratio implies the F-distribution having two degrees of freedom defined by the relations

$$p_1 = N_1 - N_2, \tag{11}$$

$$p_2 = N_2. \tag{12}$$

The relevance of the model with higher number of the free parameters is given by the so called p-value that is determined by integration of the standard probability density function of the F-distribution (*e.g.*, Brandt 1999).

In the situation considered here, where the model with higher number of degrees of freedom is the RP model, and the model with lower number of degrees of freedom is the RP1–RP model, we obtain

$$\chi_1^2 = \chi_{\mathrm{RP}}^2 = 347, \tag{13}$$

$$\chi_2^2 = \chi_{\mathrm{RP1-RP}}^2 = 55. \tag{14}$$

For the RP1–RP model, the χ^2 has been determined in the previous section of the present paper, for the RP model we use the result obtained in Török *et al.* (2012). The numbers of the degrees of freedom are given by

$$N_1 = N_{\mathrm{RP}} = 20, \tag{15}$$

$$N_2 = N_{\mathrm{RP1-RP}} = 19. \tag{16}$$

The F-ratio then takes the value

$$F = \frac{(347 - 55)/55}{(20 - 19)/19} = 100.873, \tag{17}$$

and the integration of the related probability distribution function implies the corresponding p-value of the F-test to be

$$p\mathrm{-value} \approx 5 \times 10^{-9}. \tag{18}$$

The p-value gives the probability that additional parameter improves the fit by chance. We can thus conclude that the RP1–RP variant of the RS model that is most precise in fitting the observational data is really statistically significantly better in the fitting in comparison with the RP model.

5. Discussion

We have tested all the combinations of the frequency pairs of the RS model predicting the range of the 4U 1636–53 neutron star mass and spin in (at least partial) accord with neutron star structure theory by fitting the frequency relation pairs to the observational data of the twin HF QPOs. We have considered only the frequency relations containing geodetical orbital and epicyclic frequencies or some combinations of these frequencies governed by the Kerr geometry. Nevertheless, it should be noted that the cause of the switch of the pairs of the oscillatory modes is not necessarily tied to the resonant phenomena related to the oscillations governed by the frequencies of the geodetical motion. The switch can be related, *e.g.*, to the influence of the magnetic field of the neutron star on slightly magnetized disk and after the switch, the Alfvén wave model can be relevant (Zhang 2004, Zhang *et al.* 2006, 2007, Shi 2011). However, we would like to study the resonant phenomena first, leaving other causes to future studies.

Generally, the TP–RP combination of the RS model, and its modifications, enable acceptable explanation of the observational data for 4U 1636–53 source (Stuchlík *et al.* 2012). This expectation has been explicitly tested in the present paper by fitting procedure realized for the observed twin HF QPO sequences related to the resonant points. Of course, we plan to test the RS model also in the case of some other atoll (4U 1608–52) or Z (Circinus X-1) sources containing a neutron (quark) star with observational data indicating possible existence of two resonant radii, and estimate allowed values of the spin and mass of the neutron (quark) stars.

In the case of the 4U 1636–53 source we have found very interesting results. The fitting procedure turns to be by almost one order more precise in comparison to those based on the individual frequency relations that were used in pairs in the RS model. For example, the fitting by the RP model gives the maximal precision along the mass–spin relation $M(a) = M_0[1 + 0.75(a + a^2)]$ rather poor (Török *et al.* 2012),

$$\chi^2_{\rm RP} \approx 347, \qquad \chi^2_{\rm RP}/{\rm dof} \approx 16, \tag{19}$$

and the other frequency relations give comparable poor precision. Similar results with rather poor precision were obtained also for models with frequency relations of non-geodesic origin (Lin *et al.* 2011). On the other hand, the best fit obtained for the RS model with frequency relation pairs RP1–RP (and TP–RP excluded by the theoretical models of neutron star structure) gives

$$\chi^2_{\rm RP1-RP} \approx 55, \qquad \chi^2_{\rm RP1-RP}/{\rm dof} \approx 2.6, \tag{20}$$

while the second best fit obtained for the frequency relation RP1–TP1 gives

$$\chi^2_{\rm RP1-TP1} \approx 61, \qquad \chi^2_{\rm RP1-TP1}/{\rm dof} \approx 2.9. \tag{21}$$

These fits are quite acceptable when related to the character of the observational data. The best fits of the acceptable frequency relations of the RS model predict also

acceptable values of the neutron star mass and spin: $M \approx 2.20\ \mathrm{M}_\odot$ and $a \approx 0.27$ for the best fit, or $M \approx 2.12\ \mathrm{M}_\odot$ and $a \approx 0.20$ for the second best fit. The best fits of the other acceptable frequency relation pairs predict much higher mass and spin that cannot be in accord with the detailed models of the neutron star structure for the observational restrictions of the rotational frequency of the neutron star in the 4U 1636–53 source. The mass predicted by the RS model is in accord with previous estimate given by Kluźniak (1998), but it is significantly higher than the estimate giving the upper limit of $M \approx 1.65\ \mathrm{M}_\odot$, presented in Fujimoto and Taam (1986).

Moreover, the F-test clearly demonstrates that the RP1–RP version of the RS model improves significantly the quality of the data fits, giving the characteristic p-value $\sim 5 \times 10^{-9}$.

In the special situations related to accreting neutron stars with near-maximum masses the Kerr metric can be well applied in calculating the orbital and epicyclic geodetical frequencies, as has been done in the present paper, where the results of the mass and spin interval findings are in agreement with the assumption of near-maximum masses of the neutron stars. Therefore, we are approved to use in our study the frequency formula related to the Kerr metric. In general situations, when the neutron star mass is not close to its maximum value allowed by the equation of state, the Hartle–Thorne geometry describing rotating neutron stars has to be considered and the orbital and epicyclic frequencies reflecting influence of mass, spin and quadrupole moment of the neutron star have to be used. The role of the quadrupole moment is relevant only very close to the inner edge of the accretion disk (Török *et al.* 2010).

6. Conclusions

The RS model has been tested for the atoll source 4U 1636–53 demonstrating possible two resonant radii in the observed data. For relevant pairs of the oscillatory frequency relations the range of allowed values of the mass and dimensionless spin of the neutron star are determined giving in some cases acceptable pairs of frequency relations, while some other pairs are excluded because of predicting unacceptable values of the spin and/or mass of the neutron star at 4U 1636–53 (Stuchlík *et al.* 2012).

We have shown that for some of the frequency-relation combinations of the RS model of the twin HF QPOs observed in the neutron-star system 4U 1636–53, the fits of the observational data are improved significantly in comparison to those obtained for the individual frequency relations used in the fitting procedure. In the case of the best variant of the RS model, the ratio of the χ^2 test takes the value

$$\frac{\chi^2_{\mathrm{RP}}}{\chi^2_{\mathrm{RP1-RP}}} = \frac{347}{55} = 6.67 \qquad (22)$$

indicating a substantial improvement of the data fitting by the RS model. The restrictions on the mass and spin of the neutron star are significantly shrunk due to the fitting procedure in comparison with the restrictions given by the RS model using only the frequency data restricted to the resonant radius and governed by the energy switch effect only. Moreover, the best agreement of the mass and spin of the neutron star predicted by the fitting procedures with the theoretical limits occurs for the frequency-relation combinations giving the best fits to the observational data.

We can conclude that the RS model can be considered as a plausible explanation of the twin HF QPOs observed in the source 4U 1636–53. We can expect that it could be successfully applied to some other LMXBs containing neutron stars and indicating two resonant points in the observed data.

Nevertheless, the results of the RS model have to be related to the limits on the 4U 1636–53 neutron star parameters indicated by other possible observational phenomena. In fact, a preliminary result of simultaneous treatment of the twin-peak HF QPOs and profiled (X-ray) spectral lines indicates the neutron star mass to be $M \approx 2.4\ \mathrm{M}_\odot$ (Sanna *et al.* 2012) that gives an important restriction on the results of the RS model and restricts substantially the variety of allowed combinations of frequency relations used in the RS model. However, we clearly need more detailed study of the profiled spectral lines.

Acknowledgements. We would like to express our gratitude to the Czech GAČR excellence grant No. 14-37086G, and the internal grants of the Silesian University in Opava SGS/11/2013 and SGS/23/2013. The authors further acknowledge the project Supporting Integration with the International Theoretical and Observational Research Network in Relativistic Astrophysics of Compact Objects, CZ.1.07/2.3.00/20.0071, supported by Operational Programme *Education for Competitiveness* funded by Structural Funds of the European Union and the state budget of the Czech Republic.

REFERENCES

Abramowicz, M.A., Bulik, T., Bursa, M., and Kluźniak, W. 2003, *A&A*, **404**, L21.
Abramowicz, M.A., Barret, D., Bursa, M., Horák, J., Kluźniak, W., Rebusco, P., and Török, G. 2005a, in: "Proceedings of RAGtime 6/7: Workshops on black holes and neutron stars", Opava, 16–18/18–20 September 2004/2005, Ed. S. Hledík and Z. Stuchlík, Opava: Silesian University in Opava, 1.
Abramowicz, M.A., Barret, D., Bursa, M., Horák, J., Kluźniak, W., Rebusco, P., and Török, G. 2005b, *Astron. Nachr.*, **326**, 864.
Akmal, A. and Pandharipande, V.R. 1997, *Phys. Rev. C*, **56**, 2261.
Akmal, A., Pandharipande, V.R., and Ravenhall, D.G. 1998, *Phys. Rev. C*, **58**, 1804.
Aliev, A.N., and Galtsov, D.V. 1981, *General Relativity and Gravitation*, **13**, 899.
Aliev, A.N., Esmer, G.D., and Talazan, P. 2013, *Classical Quantum Gravity*, **30**, 045010.
Bakala, P., Šrámková, E., Stuchlík, Z., and Török, G. 2010, *Classical Quantum Gravity*, **27**, 045001.
Bakala, P., Urbanec, M., Šrámková, E., Stuchlík, Z., and Török, G. 2012, *Classical Quantum Gravity*, **29**, 065012.

Barret, D., Olive, J.-F., and Miller, M.C. 2005a, *MNRAS*, **361**, 855.
Barret, D., Olive, J.-F., and Miller, M.C. 2005b, *Astron. Nachr.*, **326**, 808.
Belloni, T., Méndez, M., and Homan, J. 2005, *A&A*, **437**, 209.
Belloni, T., Homan, J., Motta, S., Ratti, E., and Méndez, M. 2007, *MNRAS*, **379**, 247.
Bevington, P.R., and Robinson, D.K. 2003, "Data reduction and error analysis for the physical sciences", 3rd edn., New York: McGraw-Hill Higher Education.
Blaes, O.M., Šrámková, E., Abramowicz, M.A., Kluźniak, W., and Torkelsson, U. 2007, *ApJ*, **665**, 642.
Boshkayev, K., Rueda, J.A., Ruffini, R., and Siutsou, I. 2013, *ApJ*, **762**, 117.
Boutelier, M., Barret, D., Lin, Y., and Török, G. 2010, *MNRAS*, **401**, 1290.
Boutloukos, S., van der Klis, M., Altamirano, D., Klein-Wolt, M., Wijnands, R., Jonker, P.G., and Fender, R.P. 2006, *ApJ*, **653**, 1435.
Brandt, S. 1999, "Data Analysis: Statistical and computational methods for scientists and engineers", 3rd edn., New York: Springer-Verlag.
Bursa, M. 2005, in: "Proceedings of RAGtime 6/7: Workshops on black holes and neutron stars", Opava, 16–18/18–20 September 2004/2005, Ed. S. Hledík and Z. Stuchlík, Opava: Silesian University in Opava, 39.
Čadež, A., Calvani, M., and Kostić, U. 2008, *A&A*, **487**, 527.
Chakrabarti, S.K., *et al.* 2008, in: "Proceedings of The Eleventh Marcel Grossmann Meeting on Recent Developments in Theoretical and Experimental General Relativity, Gravitation and Relativistic Field Theories", Berlin, Germany, 23–29 July 2006, Ed. H. Kleinert and R.T. Jantzen, Singapore: World Scientific, 569.
Chandrasekhar, S., and Miller, J.C. 1974, *MNRAS*, **167**, 63.
Cremaschini, C., and Stuchlík, Z. 2013, *Phys. Rev. E*, **87**, 043113.
Feroci, M., *et al.* 2012, *Experimental Astronomy*, **34**, 415.
Fujimoto, M.Y., and Taam, R.E. 1986, *ApJ*, **305**, 246.
Glendenning, N.K. 2000, "Compact Stars: Nuclear Physics, Particle Physics, and General Relativity", New York: Springer-Verlag.
Gondek-Rosińska, D., Kluźniak, W., Stergioulas, N., and Wiśniewicz, M. 2014, arXiv:1403.1129.
Hartle, J.B., and Thorne, K. 1968, *ApJ*, **153**, 807.
Horák, J., Abramowicz, M.A., Kluźniak, W., Rebusco, P., and Török, G. 2009, *A&A*, **499**, 535.
Kato, S. 2004, *PASJ*, **56**, 905.
Kato, S. 2008, *PASJ*, **60**, 111.
Kato, S., Fukue, J., and Mineshige, S. 1998, in: "Black-hole accretion disks", Ed. S. Kato, J. Fukue, and S. Mineshige, Kyoto, Japan: Kyoto University Press.
Kluźniak, W. 1998, *ApJ*, **509**, L37.
Kološ, M., and Stuchlík, Z. 2013, *Phys. Rev. D*, **88**, 065004.
Kostić, U., Čadež, A., Calvani, M., and Gomboc, A. 2009, *A&A*, **496**, 307.
Kotrlová, A., Stuchlík, Z., and Török, G. 2008, *Classical Quantum Gravity*, **25**, 225016.
Kovář, J., Stuchlík, Z., and Karas, V. 2008, *Classical Quantum Gravity*, **25**, 095011.
Lin, Y.-F., Boutelier, M., Barret, D., and Zhang, S.-N. 2011, *ApJ*, **726**, 74.
Lo, K.-W., and Lin, L.-M. 2011, *ApJ*, **728**, 12.
Miller, M.C., Lamb, F.K., and Psaltis, D. 1998, *ApJ*, **508**, 791.
Montero, P.J., and Zanotti, O. 2012, *MNRAS*, **419**, 1507.
Mukherjee, A., and Bhattacharyya, S. 2012, *ApJ*, **756**, 55.
Mukhopadhyay, B. 2009, *ApJ*, **694**, 387.
Müller, H., and Serot, B.D. 1996, *Nuclear Physics A*, **606**, 508.
Müther, H., Prakash, M., and Ainsworth, T.L. 1987, *Physics Letters B*, **199**, 469.
Osherovich, V., and Titarchuk, L. 1999, *ApJ*, **522**, L113.
Perez, C.A., Silbergleit, A.S., Wagoner, R.V., and Lehr, D.E. 1997, *ApJ*, **476**, 589.
Postnikov, S., Prakash, M., and Lattimer, J.M. 2010, *Phys. Rev. D*, **82**, 024016.

Press, W.H., Teukolsky, S.A., Vetterling, W.T., and Flannery, B.P. 2007, "Numerical Recipes: The Art of Scientific Computing", Cambridge: Cambridge University Press, 1256.
Remillard, R.A., and McClintock, J.E. 2006, *Ann. Rev. Astron. Astrophys.*, **44**, 49.
Rezzolla, L., Yoshida, S., and Zanotti, O. 2003, *MNRAS*, **344**, 978.
Sanna, A., Méndez, M., Belloni, T., and Altamirano, D. 2012, poster presentation at IAU General Assembly XXVIII, 20–31 August 2012, Beijing, China.
Schee, J., and Stuchlík, Z. 2009, *International Journal of Modern Physics D*, **18**, 983.
Shi, C. 2011, *Research in Astronomy and Astrophysics*, **11**, 1327.
Shi, C., and Li, X.-D. 2009, *MNRAS*, **392**, 264.
Stella, L., and Vietri, M. 1998, *ApJ*, **492**, L59.
Stella, L., and Vietri, M. 1999, *Phys. Rev. Lett.*, **82**, 17.
Straub, O., and Šrámková, E. 2009, *Classical Quantum Gravity*, **26**, 055011.
Strohmayer, T.E., and Markwardt, C.B. 2002, *ApJ*, **577**, 337.
Stuchlík, Z., Török, G., and Bakala, P. 2007, arXiv:0704.2318.
Stuchlík, Z., and Kotrlová, A. 2009, *General Relativity and Gravitation*, **41**, 1305.
Stuchlík, Z., Kotrlová, A., and Török, G. 2011, *A&A*, **525**, A82.
Stuchlík, Z., Kotrlová, A., and Török, G. 2012, *Acta Astron.*, **62**, 389.
Stuchlík, Z., and Schee, J. 2012, *Classical Quantum Gravity*, **29**, 065002.
Stuchlík, Z., and Kološ, M. 2012a, *Phys. Rev. D*, **85**, 065022.
Stuchlík, Z., and Kološ, M. 2012b, *Journal of Cosmology and Astroparticle Physics*, **10**, 008.
Stuchlík, Z., Kotrlová, A., and Török, G. 2013, *A&A*, **552**, A10.
Stuchlík, Z., and Kološ, M. 2014, *Phys. Rev. D*, **89**, 065007.
Török, G. 2009, *A&A*, **497**, 661.
Török, G., and Stuchlík, Z. 2005, *A&A*, **437**, 775.
Török, G., Abramowicz, M.A., Kluźniak, W., and Stuchlík, Z. 2005, *A&A*, **436**, 1.
Török, G., Abramowicz, M.A., Bakala, P., Bursa, M., Horák, J., Kluźniak, W., Rebusco, P., and Stuchlik, Z. 2008a, *Acta Astron.*, **58**, 15.
Török, G., Bakala, P., Stuchlík, Z., and Čech, P. 2008b, *Acta Astron.*, **58**, 1.
Török, G., Abramowicz, M.A., Bakala, P., Bursa, M., Horák, J., Rebusco, P., and Stuchlik, Z. 2008c, *Acta Astron.*, **58**, 113.
Török, G., Bakala, P., Šrámková, E., Stuchlík, Z., and Urbanec, M. 2010, *ApJ*, **714**, 748.
Török, G., Bakala, P., Šrámková, E., Stuchlík, Z., Urbanec, M., and Goluchová, K. 2012, *ApJ*, **760**, 138.
Urbanec, M., Bělták, E., and Stuchlík, Z. 2010a, *Acta Astron.*, **60**, 149.
Urbanec, M., Török, G., Šrámková, E., Čech, P., Stuchlík, Z., and Bakala, P. 2010b, *A&A*, **522**, A72.
Urbanec, M., Miller, J.C., and Stuchlík, Z. 2013, *MNRAS*, **433**, 1903.
van der Klis, M. 2000, *Ann. Rev. Astron. Astrophys.*, **38**, 717.
van der Klis, M. 2006, in: "Compact Stellar X-Ray Sources", Ed. W.H.G. Lewin and M. van der Klis, Cambridge University Press), 39.
Wang, D.H., Chen, L., Zhang, C.M., Lei, Y.J., and Qu, J.L. 2013, *MNRAS*, **435**, 3494.
Wang, D.H., Chen, L., Zhang, C.M., Lei, Y.J., and Qu, J.L. 2014, *Astron. Nachr.*, **335**, 168.
Zhang, C. 2004, *A&A*, **423**, 401.
Zhang, C., Yin, H.X., Kojima, Y., Chang, H. K., Xu, R.X., Li, X.D., Zhang, B., and Kiziltan, B. 2007, *MNRAS*, **374**, 232.
Zhang, C.M., Yin, H.X., Zhao, Y.H., Zhang, F., and Song, L.M. 2006, *MNRAS*, **366**, 1373.

Paper III

6.3. Twin peak high-frequency quasi-periodic oscillations as a spectral imprint of dual oscillation modes of accretion tori

Bakala Pavel, Goluchová Kateřina, Török Gabriel, Šrámková Eva, Abramowicz Marek A., Vincent Frederic H. & Mazur, Grzegorz P.

Astronomy & Astrophysics, 2015,
Volume 581, id.A35, 12 pp.

A&A 581, A35 (2015)
DOI: 10.1051/0004-6361/201525867

Astronomy & Astrophysics

Twin peak high-frequency quasi-periodic oscillations as a spectral imprint of dual oscillation modes of accretion tori

P. Bakala[1], K. Goluchová[1], G. Török[1], E. Šrámková[1], M. A. Abramowicz[1,2,4], F. H. Vincent[2], and G. P. Mazur[2,3]

[1] Institute of Physics, Faculty of Philosophy and Science, Silesian University in Opava, Bezručovo nám. 13, 746 01 Opava, Czech Republic
e-mail: pavel.bakala@fpf.slu.cz
[2] Nicolaus Copernicus Astronomical Center, ul. Bartycka 18, 00-716 Warszawa, Poland
[3] Institute of Physics, Polish Academy of Sciences, aleja Lotnikow 32/46, 02-668 Warszawa, Poland
[4] Physics Department, Gothenburg University, 412-96 Göteborg, Sweden

Received 11 February 2015 / Accepted 24 May 2015

ABSTRACT

Context. High-frequency (millisecond) quasi-periodic oscillations (HF QPOs) are observed in the X-ray power-density spectra of several microquasars and low-mass X-ray binaries. Two distinct QPO peaks, so-called twin peak QPOs, are often detected simultaneously exhibiting their frequency ratio close or equal to 3:2. A widely discussed class of proposed QPOs models is based on oscillations of accretion toroidal structures orbiting in the close vicinity of black holes or neutron stars.
Aims. Following the analytic theory and previous studies of observable spectral signatures, we aim to model the twin peak QPOs as a spectral imprint of specific dual oscillation regime defined by a combination of the lowest radial and vertical oscillation mode of slender tori. We consider the model of an optically thick slender accretion torus with constant specific angular momentum. We examined power spectra and fluorescent Kα iron line profiles for two different simulation setups with the mode frequency relations corresponding to the epicyclic resonance HF QPOs model and modified relativistic precession QPOs model.
Methods. We used relativistic ray-tracing implemented in the parallel simulation code LSDplus. In the background of the Kerr spacetime geometry, we analyzed the influence of the distant observer inclination and the spin of the central compact object. Relativistic optical projection of the oscillating slender torus is illustrated by images in false colours related to the frequency shift.
Results. We show that performed simulations yield power spectra with the pair of dominant peaks that correspond to the frequencies of radial and vertical oscillation modes and with the peak frequency ratio equal to the proper value 3:2 on a wide range of inclinations and spin values. We also discuss exceptional cases of a very low and very high inclination, as well as unstable high spin relativistic precession-like configurations that predict a constant frequency ratio equal to 1:2. We demonstrate a significant dependency of broadened Kα iron line profiles on the inclination of the distant observer.
Conclusions. This study presents a further step towards the proper model of oscillating accretion tori producing HF QPOs. More realistic future simulations should be based on incorporating the resonant coupling of oscillation modes, the influence of torus opacity, and the pressure effects on the mode frequencies and the torus shape.

Key words. accretion, accretion disks – black hole physics – relativistic processes

1. Introduction

High-frequency quasi-periodic oscillations (HF QPOs) have been observed in several microquasars and low-mass X-ray binaries (LMXBs). Their frequencies are roughly comparable to frequencies of the orbital motion of test particles in the vicinity of the central compact object. The black hole HF QPOs occur at frequencies that are characteristic of a particular source and that seem to be constant in time. Strictly speaking, the current observational data only enables HF QPOs to be distinguished for fairly specific spectral states (Belloni et al. 2012). However, provided that HF QPOs with lower amplitudes and different frequencies exist in the remaining time, their detection goes beyond our present technological capabilities.

Two kinds of sharp HF QPO peaks can be distinguished, so-called lower and upper HF QPOs (see van der Klis 2004; Remillard & McClintock 2006, for a review). If both HF QPO peaks are observed simultaneously (twin-peak HF QPOs), the ratio of frequencies of upper and lower HF QPO peaks is often close to 3:2, indicating the possible presence of unspecified resonant phenomena (Abramowicz & Kluźniak 2001; Török et al. 2005)[1]. At present, there is no consensus about the QPO nature. However, the inverse mass scaling of the QPOs frequencies (Abramowicz & Kluźniak 2001) provides a strong argument for interpreting the observed QPO peaks by the frequencies of perturbed orbital motion in the strong gravitational field or oscillation of some accretion structures. Such interpreting naturally promises an attractive possibility of measuring the mass and spin of the black hole (e.g. Abramowicz & Kluźniak 2001; Abramowicz & Fragile 2013; Ingram & Motta 2014; Motta et al. 2014; Török 2005; Török et al. 2012). Many QPO models have

[1] In the case of LMXBs, there are indications that the ratio of twin peak HF QPOs frequencies is not only clustered around 3:2, but 4:3 and 5:4 ratios are also observed (see e.g. Török et al. 2007, 2008a,b,c).

A&A 581, A35 (2015)

been proposed (Alpar & Shaham 1985; Lamb et al. 1985; Miller et al. 1998; Psaltis et al. 1999; Stella & Vietri 1999; Abramowicz & Kluźniak 2001, 2004; Kato 2001, 2007; Titarchuk & Wood 2002; Rezzolla et al. 2003; Schnittman & Bertschinger 2004; Pétri 2005; Zhang 2005; Tagger & Varnière 2006; Stuchlík et al. 2008; Mukhopadhyay 2009; Čadež et al. 2008; Kostić et al. 2009; Germanà et al. 2009; Germanà 2013; Lai et al. 2013; Pecháček et al. 2008, 2013); however, each model still faces several difficulties. Moreover, the capabilities of the present X-ray observatories (e.g. Rossi X-ray Timing Explorer – RTXE) are insufficient for adequately analysing the harmonic content of the power spectra of observed lightcurves, which can be crucial for distinguishing between particular QPO models (Bakala et al. 2014; Karas et al. 2014). Hopefully, the proposed future instruments represented by the Large Observatory for X-ray Timing (LOFT) project (Feroci et al. 2014), for instance, which is targeted to explore strong gravity environment, will advance QPOs observational possibilities.

A specific class of QPO models assumes oscillations excited in accretion tori. The first QPO model involving numerically modelled thick accretion tori was developed by Rezzolla et al. (2003), and related lightcurves and power spectra were analysed by Schnittman & Rezzolla (2006). Lightcurves and power spectra of radially and vertically oscillating slender torus with a circular cross-section were investigated in the background of the Schwarzschild geometry by Bursa et al. (2004). Numerical simulations of epicyclic modes of tori oscillations were compared to the analytical results by Šrámková (2005). Later on, several studies devoted to more realistic analytic treatment of oscillating slender tori appeared (e.g. Abramowicz et al. 2006; Blaes et al. 2006). These studies were extended to the case of non-slender tori by Šrámková et al. (2007) and Straub & Šrámková (2009).

In this paper, we examine the timing properties of the numerically simulated flux emitted from a slender, polytropic, perfect fluid, non-self-gravitating accretion torus with constant specific angular momentum, which oscillates simultaneously in radial and vertical directions[2]. The article is a follow-up of the studies of Mazur et al. (2013) and Vincent et al. (2014), who investigated the observable signatures of simple time-periodic slender torus deformations, as well as the slender torus motion described by the set of oscillation modes derived by Blaes et al. (2006). Using their results, we took the next step towards a fully realistic model of HF QPO based on oscillations of accretion tori. To model detected twin-peak HF QPOs pairs, we defined a new dual oscillation mode as a linear combination of the two lowest slender torus oscillation modes: radial and vertical ones. We assumed that the observed twin peaks HF QPOs can be identified with the pairs of the most prominent peaks in the modelled power spectra. We examined two different setups of the dual oscillation regime corresponding to the twin peaks HF QPOs frequency relation of epicyclic resonance HF QPOs model (Abramowicz & Kluźniak 2001) and slightly modified analogous relations of relativistic precession QPOs model (Stella & Vietri 1999; Török et al. 2012). Those two competing QPOs models are probably the most discussed ones at present (Feroci et al. 2014).

Our simulations were performed in the background of the Kerr geometry that corresponds to the case of microquasars with the black hole binary component. It was shown that the spacetime around slowly rotating high-mass neutron stars can be approximated fairly well by the Kerr metric (Török et al. 2010, 2012; Urbanec et al. 2013). Therefore, such a finding sets conditions and constraints for the applicability of our results for the case of LMXBs with neutron star.

The commonly accepted model of X-ray energy spectrum of microquasars and LMXBs assumes that the illumination of the cold accretion disk or torus by the primary component of X-ray spectrum, interpreted as the inverse Compton scattering of thermal photons in a hot corona, produces spectral lines by fluorescence. The strongest observed line is the Kα iron line located at 6.4 keV in the rest frame. Observed broad profiles of the spectral lines are substantially influenced by the spacetime metric, the geometry of the emitting region and the distant observer inclination (Fabian et al. 1989; Čadež & Calvani 2005; Bambi 2013). To develop an additional tool for distinguishing various configurations of radiating slender torus, we computed related Kα iron line profiles.

The article consits of the following parts. Section 2 is devoted to the theory that describes the slender torus model and its dual oscillation regime. Section 3 provides more details of the investigated particular setup of the model of slender torus. Section 4 describes our numerical implementation of relativistic ray-tracing and the following construction of lightcurves, power spectra, and iron Kα line profiles. Section 5 is devoted to the methodology of simulations performance and results analysis. Section 6 shows the obtained results, and Sect. 7 gives conclusions and future research perspectives.

2. Slender torus

2.1. Equilibrium torus configuration

We consider an axisymmetric, non self-gravitating, perfect fluid, constant specific angular momentum, circularly orbiting accretion torus in the background of the Kerr geometry. Using the $(-+++)$ signature and geometrical units ($c = G = M = 1$), the line element of the Kerr spacetime in Boyer-Lindquist coordinates parameterized by specific angular momentum (spin) a reads

$$\begin{aligned} \mathrm{d}s^2 &= -\left(1-\frac{2r}{\Sigma}\right)\mathrm{d}t^2 - \frac{4ra}{\Sigma}\sin^2\theta\,\mathrm{d}t\,\mathrm{d}\varphi + \frac{\Sigma}{\Delta}\mathrm{d}r^2 \\ &\quad + \Sigma\,\mathrm{d}\theta^2 + \left(r^2 + a^2 + \frac{2ra^2\sin^2\theta}{\Sigma}\right)\sin^2\theta\,\mathrm{d}\varphi^2, \end{aligned} \tag{1}$$

where $\Sigma \equiv r^2 + a^2\cos^2\theta$ and $\Delta \equiv r^2 - 2r + a^2$. Moreover, we assume that the radial extent of the torus cross-section is smaller than its central radius. The perfect fluid that forms the torus is described by the polytropic equation of state (with a polytropic constant K and polytropic index n). In this case, the energy density e is a function of pressure p and mass density ρ. The pressure is a function of mass density alone. The torus surface is given by the zero pressure, while the pressure gradient is equal to zero in the torus centre. Using the conservation law, one can get (see Abramowicz et al. 2006; Blaes et al. 2006)

$$\frac{p}{\rho} = \frac{p_0}{\rho_0} f(r,\theta), \tag{2}$$

where the surface function f is constant at isobaric and isodensity surfaces. Naturally, the surface function vanishes at the torus surface. Here and below, values of the quantities denoted with a subscript $_0$ are taken in the centre of the torus in the equilibrium state.

[2] The slender torus geometry considered here accords well with the truncated disk model (see e.g. Done et al. 2007). Also, the power spectral fits of Ingram & Done (2012a) predict that the hot inner flow (corona) has a small scale height in the relevant spectral state.

Following Abramowicz et al. (2006), we use the new radial and vertical coordinates

$$\bar{x} = (\sqrt{g_{rr}})_0 \left(\frac{r - r_0}{\beta r_0}\right), \quad \bar{y} = (\sqrt{g_{\theta\theta}})_0 \left(\frac{\pi/2 - \theta}{\beta r_0}\right) \tag{3}$$

with zero in the torus centre. Parameter β determines the torus thickness and is given by formula

$$\beta^2 = \frac{2nc_{s0}^2}{r_0^2 (u_0^t)^2 \Omega_0^2}, \tag{4}$$

where u_0^t denotes the four-velocity of the fluid and square of the sound speed $c_{s0}^2 \ll 1$ can be expressed in the form

$$c_{s0}^2 = \left(\frac{\partial p}{\partial \rho}\right)_0 = \frac{n+1}{n}\frac{p_0}{\rho_0}. \tag{5}$$

Keplerian angular velocity Ω_{K0} in the Kerr spacetime reads as

$$\Omega_{K0} = 1/(r_0^{3/2} + a). \tag{6}$$

In the case of slender torus, the parameter β must fulfil the condition

$$\beta \ll 1. \tag{7}$$

In such a coordinate frame, the surface function $f(r, \theta)$ can be rewritten as

$$f(\bar{x}, \bar{y}) = 1 - \bar{\omega}_r^2 \bar{x}^2 - \bar{\omega}_\theta^2 \bar{y}^2, \tag{8}$$

where

$$\bar{\omega}_r = \sqrt{1 - \frac{6}{r_0} + \frac{8a}{r_0^{3/2}} - \frac{3a^2}{r_0^2}}, \tag{9}$$

$$\bar{\omega}_\theta = \sqrt{1 - \frac{4a}{r_0^{3/2}} + \frac{3a^2}{r_0^2}}, \tag{10}$$

are radial and vertical epicyclic frequencies of free test particles in the centre of the torus scaled to Ω_{K0} (see e.g. Aliev & Galtsov 1981; Abramowicz & Kluźniak 2005; Aliev 2008). We can easily see that the slender torus cross-section (given by $f(\bar{x}, \bar{y}) = 0$) has elliptical shape in the $\bar{x}$-$\bar{y}$ plane.

2.2. Oscillating slender torus

We assume small pressure perturbation in the form

$$\delta p \propto \mathrm{e}^{\mathrm{i}(m\varphi - \Omega t)}, \tag{11}$$

where m is azimuthal wave number ($m \in \mathbf{N}$), and Ω is oscillation angular frequency. It is useful to introduce a new variable – eigenfunction W_i, which is the function of perturbation in pressure in the form

$$W_i = -\frac{\delta p}{u_0^t \rho \sigma_i}, \tag{12}$$

where related eigenfrequency σ_i reads

$$\sigma_i = \Omega_i - m_i \Omega_{K0}. \tag{13}$$

The perturbative surface equation $\tilde{f}(r, \theta)$ and torus four-velocity can be expressed in the form (Vincent et al. 2014)

$$\tilde{f}(r, \theta) = f(r, \theta) - \frac{1}{n+1}\frac{\rho_0}{p_0} u_0^t \mathrm{Re}\{W_i\}\, \sigma_i, \tag{14}$$

$$u^\mu = u_0^\mu + \mathrm{Re}\left\{\frac{\mathrm{i}\rho_0}{p_0 + e_0}\left(\frac{\partial W_i}{\partial x^\mu}\right)\right\}. \tag{15}$$

A discrete set of eigefunctions W_i and related eigenfrequencies σ_i describing different oscillation modes was found by Blaes et al. (2006) solving Papaloizou-Pringle equation for slender torus case corresponding to the condition $\beta \to 0$ (Abramowicz et al. 2006; Papaloizou & Pringle 1984). Here we use only the two simplest solutions: radial oscillation mode and vertical oscillation mode. In the case of radial oscillation mode, the eigenfunction and related eigenfrequency are given as

$$W_r = a_r \bar{x} \mathrm{e}^{\mathrm{i}(m_r\varphi - \Omega_r t)}, \qquad \sigma_r = \bar{\omega}_r \Omega_{K0}, \tag{16}$$

where a_r is a free parameter related to the amplitude of oscillations. Then the surface Eq. (14) takes the form

$$1 - \bar{\omega}_r^2 \bar{x}^2 - \bar{\omega}_\theta^2 \bar{y}^2 - A_r \bar{x} \cos(m_r\varphi - \Omega_r t) = 0, \tag{17}$$

where amplitude A_r is given by the formula

$$A_r = \frac{1}{n+1}\frac{\rho_0}{p_0} u_0^t \sigma_r a_r, \tag{18}$$

and the mode oscillation angular frequency reads as

$$\Omega_r = \sigma_r + \Omega_{K0} m_r. \tag{19}$$

To rewrite the surface Eq. (17) to the form

$$1 - \bar{\omega}_r^2 (\bar{x} + \delta\bar{x})^2 - \bar{\omega}_\theta^2 \bar{y}^2 = 0, \tag{20}$$

the term

$$\left(\frac{A_r}{2\bar{\omega}_r} \cos(m_r\varphi - \Omega_r t)\right)^2 \tag{21}$$

must be added. Then the displacement $\delta\bar{x}$ can be expressed by the formula

$$\delta\bar{x} = \frac{A_r}{2\bar{\omega}_r^2} \cos(m_r\varphi - \Omega_r t). \tag{22}$$

In this approximation, the added term should be small enough, which corresponds to the condition for radial amplitudes

$$\frac{A_r^2}{4\bar{\omega}_r^2} \ll 1. \tag{23}$$

The radial component of the surface four-velocity is simply given by a derivative of the displacement $\delta\bar{x}$ with respect to proper time τ as

$$u^r_{sur} = \frac{\mathrm{d}r}{\mathrm{d}\tau} = \frac{\mathrm{d}\bar{x}}{\mathrm{d}\tau}\frac{\beta r_0}{(\sqrt{g_{rr}})_0} = \frac{\mathrm{d}(-\delta\bar{x})}{\mathrm{d}\tau}\frac{\beta r_0}{(\sqrt{g_{rr}})_0}, \tag{24}$$

and it takes the covariant form

$$u_r^{\mathrm{sur}} = -\beta r_0 (\sqrt{g_{rr}})_0 \frac{A_r}{2\bar{\omega}_r} \Omega_{K0} u_0^t \sin(m_r\varphi - \Omega_r t). \tag{25}$$

Analogously, in the case of the vertical oscillation mode, the eigenfunction and related eigenfrequency are given as

$$W_\theta = a_\theta \bar{y} \mathrm{e}^{\mathrm{i}(m_\theta\varphi - \Omega_\theta t)}, \qquad \sigma_\theta = \bar{\omega}_\theta \Omega_{K0}. \tag{26}$$

A&A 581, A35 (2015)

Using the condition for vertical amplitudes $\frac{A_\theta^2}{4\bar{\omega}_\theta^2} \ll 1$, the surface equation, displacement $\delta\bar{y}$ and surface four-velocity component $u_\theta^{\rm sur}$ for the vertical mode can be expressed as

$$1 - \bar{\omega}_{\rm r}^2\bar{x}^2 - \bar{\omega}_\theta^2(\bar{y}+\delta\bar{y})^2 = 0, \tag{27}$$

$$\delta\bar{y} = \frac{A_\theta}{2\bar{\omega}_\theta^2}\cos(m_\theta\varphi - \Omega_\theta t), \tag{28}$$

$$u_\theta^{\rm sur} = \beta r_0(\sqrt{g_{\theta\theta}})_0\frac{A_\theta}{2\bar{\omega}_\theta}\Omega_{\rm K0}u_0^t\sin(m_\theta\varphi - \Omega_\theta t), \tag{29}$$

where amplitude A_θ given by formula

$$A_\theta = \frac{1}{n+1}\frac{\rho_0}{p_0}u_0^t\sigma_\theta a_\theta, \tag{30}$$

and mode oscillation angular frequency reads

$$\Omega_\theta = \sigma_\theta + \Omega_{\rm K0}m_\theta. \tag{31}$$

2.3. Dual oscillation mode

In such an approximation, radial and vertical oscillations are independent, and we can easily combine them into a new surface equation

$$1 - \bar{\omega}_r^2(\bar{x}+\delta\bar{x})^2 - \bar{\omega}_\theta^2(\bar{y}+\delta\bar{y})^2 = 0. \tag{32}$$

The equation above defines the dual oscillation mode with four parameters: amplitudes A_r, A_θ and azimuthal wave numbers m_r, m_θ.

3. Investigated model of oscillating slender torus

3.1. Location, thickness, and frequencies identification

Radial and vertical angular frequencies $\Omega_{\rm r}, \Omega_\theta$ of the dual oscillation mode are given as a linear combination of eigenfrequencies $\sigma_{\rm r}, \sigma_\theta$, and Keplerian angular velocity $\Omega_{\rm K0}$. Therefore the location of the torus centre in equilibrium r_0, value of the spin of the central Kerr black hole and wave number pair $m_{\rm r}$, m_θ fully determine the ratio of oscillation angular frequencies $\Omega_\theta/\Omega_{\rm r}$. Considering the properties of epicyclic and orbital frequencies in the Kerr spacetime (Török & Stuchlík 2005), our model identifies the lower and upper kHz QPOs frequencies with $\nu_{\rm l} = |\Omega_{\rm r}/2\pi|$ and $\nu_{\rm u} = |\Omega_\theta/2\pi|$, respectively. As the aim of the article is to model twin peak HF QPOs with peaks frequency ratio close to 3:2, we choose r_0 in such a way that the ratio $\Omega_\theta/\Omega_{\rm r}$ is just equal to 3:2 for a given wave number pair[3]. In each of these positions of the torus centre, we set the radial extent of the torus cross-section to $r_0/10$. Corresponding values of the parameter β are in accordance with a slender torus condition (7). Arbitrary amplitudes of oscillations are fixed by setting $A_{r,\theta} = \bar{\omega}_{r,\theta}$.

3.2. Optical properties of the torus

The torus described above is assumed to be optically thick. Moreover, we use two other very simple assumptions. The torus surface emits radiation isotropically in its comoving local frame and the local flux integrated over the surface area of a thin vertical slice of the torus is conserved. Such a surface area is proportional to $r_{\rm c}(t_{\rm em},\phi)\times C(t_{\rm em},\phi)$, where $C(t_{\rm em},\phi)$ is the torus cross-section circumference, $t_{\rm em}$ the time of emission, and $r_{\rm c}(t_{\rm em},\phi)$ the radial coordinate of the centre of the torus cross-section. In the case of the approximation we used, the investigated dual oscillation mode describes pure radial and vertical displacements, and the torus cross-section circumference remains constant. Therefore, using normalization to 1 for the equilibrium state, the local emitted intensity simply reads as

$$I_{\rm em}(t_{\rm em},\phi) = r_0/r_{\rm c}(t_{\rm em},\phi). \tag{33}$$

3.3. Epicyclic resonance axisymmetric setup

The first investigated torus setup combines pure epicyclic axisymmetric vertical and radial oscillation, where radial and vertical oscillation frequencies are identical with radial $\nu_r = \bar{\omega}_r\Omega_{\rm K0}/2\pi$ and vertical $\nu_\theta = \bar{\omega}_\theta\Omega_{\rm K0}/2\pi$ epicyclic frequencies, respectively. This setup corresponds to the often quoted epicyclic resonance (ER) HF QPOs model (Abramowicz & Kluźniak 2001) based on the presence of non-linear resonant phenomena between epicyclic disc oscillation modes (Kluźniak & Abramowicz 2001; Abramowicz et al. 2003a,b; Horák 2008). The dual oscillation mode with such behaviour is related to wave number pair $m_{\rm r} = 0$, $m_\theta = 0$. Therefore the frequency relation determining the radial coordinate of the torus centre r_0 reads as

$$\left.\frac{\nu_{\rm u}}{\nu_{\rm l}}\right|_{m_r=0}^{m_\theta=0} = \frac{\nu_\theta}{\nu_r} = \frac{3}{2}. \tag{34}$$

3.4. Relativistic precession-like non-axisymmetric setup

The dual oscillation mode related to wave number pair $m_{\rm r} = -1$, $m_\theta = -2$ yields the frequency relation in the form

$$\left.\frac{\nu_{\rm u}}{\nu_{\rm l}}\right|_{m_r=-1}^{m_\theta=-2} = \frac{2\nu_{\rm K}-\nu_\theta}{\nu_{\rm K}-\nu_r} = \frac{3}{2}, \tag{35}$$

where $\nu_{\rm K} = \Omega_{\rm K0}/2\pi$ is the Keplerian orbital frequency at r_0. As the denominator matches the periastron precession frequency, in the Schwarzschild case the relation corresponds exactly to the relation of the relativistic precession (RP) QPOs model

$$\left.\frac{\nu_{\rm u}}{\nu_{\rm l}}\right|_{\rm RP} = \frac{\nu_{\rm K}}{\nu_{\rm K}-\nu_r}. \tag{36}$$

The RP model was proposed in a series of papers by Stella & Vietri (1998, 1999, 2002), Morsink & Stella (1999) and explains the QPOs as a direct manifestation of relativistic epicyclic motion of radiating blobs (Stella & Vietri 1999). In the case of slow rotation, the frequency relation (35) still almost coincides with the ratio of twin peaks HP QPOs frequencies predicted by the relation (36) (Török et al. 2012). Such an approach can be understood as a redefinition of the modulation mechanism of RP model, but it preserves the predictive power of the model.

4. Numerical modelling of radiation emission, propagation, and detection

4.1. Ray-tracing in the Kerr spacetime

Relativistic ray-tracing is a key ingredient of proper models of relativistic imaging, lightcurves of accretion structures, related power spectra, as well as relativistic spectral line profiles.

[3] Investigated torus model does not consider the presence of the resonant coupling of oscillation modes, which can cause amplification or excitation of QPOs for the preferred values of the radial coordinate (Horák 2008).

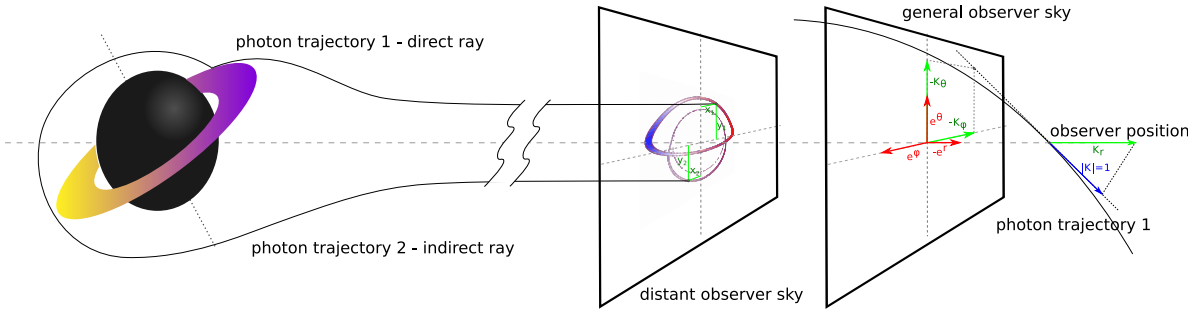

Fig. 1. Schematic ray-tracing geometry for the cases of a general observer and distant observer ($r_{\rm obs} \to \infty$).

Different ray-tracing techniques were developed using direct numerical integration, transfer functions, and elliptic integrals (see e.g. Cunningham & Bardeen 1972; Karas et al. 1992; Viergutz 1993; Schnittman 2006; Rauch & Blandford 1994; Beckwith & Done 2005; Broderick & Loeb 2005; Bakala et al. 2007; Dexter & Agol 2009; Vincent et al. 2011; Schee & Stuchlík 2013; Chan et al. 2013; Yang & Wang 2014). Our parallel code LSDplus uses reverse ray-tracing implemented by a direct numerical integration of the null geodesics.

Components of the four-momentum of a photon in the Kerr spacetime are given by

$$\begin{aligned} p^r &= \dot{r} = s_r \Sigma^{-2} \sqrt{R_{\lambda,q}(r)}, \\ p^\theta &= \dot{\theta} = s_\theta \Sigma^{-2} \sqrt{\Theta_{\lambda,q}(\theta)}, \\ p^\phi &= \dot{\phi} = \Sigma^{-2}\Delta^{-1}\left[2ar + \lambda\left(\Sigma^2 - 2r\right)\mathrm{cosec}^2\theta\right], \\ p^t &= \dot{t} = \Sigma^{-2}\Delta^{-1}\left(\Sigma^2 - 2ar\lambda\right), \end{aligned} \tag{37}$$

where the dotted quantities denote differentiation with respect to some affine parameter, and the sign pair $s_{\rm r}$,s_θ describes orientation of radial and latitudinal evolution, respectively (see e.g. Carter 1968; Misner et al. 1973; Chandrasekhar 1983). Radial and latitudial effective potentials read as

$$\begin{aligned} R_{\lambda,q}(r) &= \left[\left(r^2 + a^2\right) - a\lambda\right]^2 - \Delta\left[q - (\lambda - a)^2\right], \\ \Theta_{\lambda,q}(\theta) &= q + a^2\cos^2\theta - \lambda^2\cot^2\theta. \end{aligned} \tag{38}$$

Here, λ and q are constants of motion related to the photons covariant angular and linear momenta. The LSDplus code performs a time-reverse integration of the package of null geodesics falling on a virtual detector of a distant observer with the screen resolution 1000 × 1000 pixels located at ($\theta_{\rm obs}$, r = 1000 M, φ = 0) and traces the intersection of the geodesics with the disk surface corresponding to the emission events.

The code LSDplus enables modelling relativistic optical effects in the sky of the observer located anywhere above the event horizon of a Kerr black hole. In the local reference frame related to such an observer, the components of the four-momentum of photons with energy normalized to one, falling on the pixel with coordinates x, y, can be written as follows (see the right side of Fig. 1):

$$k_t = -1, \quad k_r = \sqrt{1 - x^2 - y^2}, \quad k_\theta = -y, \quad k_\varphi = -x. \tag{39}$$

Then one can obtain the coordinate covariant components of the four-momentum by transforming the local components (39), using appropriate frame tetrads of one-form by relation

$$p_\mu = e^{\langle\alpha\rangle}_\mu k_{\langle\alpha\rangle}. \tag{40}$$

The frame tetrad of one-form related to static observer in the Kerr spacetime is given as

$$\begin{aligned} e^{(t)} &= \left\{\sqrt{1 - \frac{2r}{\Sigma}}, 0, 0, \frac{2ar\sin^2\theta}{\sqrt{\Sigma^2 - 2r\Sigma)}}\right\}, \\ e^{(r)} &= \left\{0, \sqrt{\Sigma/\Delta}, 0, 0\right\}, \\ e^{(\theta)} &= \left\{0, 0, \sqrt{\Sigma}, 0\right\}. \\ e^{(\varphi)} &= \left\{0, 0, 0, \sqrt{\frac{\Delta\Sigma}{\Sigma - 2r}}\sin\theta\right\}. \end{aligned} \tag{41}$$

The constants of motion $\lambda(x, y)$ and $q(x, y)$ can be easily obtained by straightforward calculation from the components of the four-momentum (40), using the relations (see e.g. Chandrasekhar 1983)

$$\begin{aligned} \lambda &= -\frac{p_\phi}{p_t}, \\ q^2 &= \left(\frac{p_\theta}{p_t}\right)^2 + \left(\lambda\tan\left(\frac{\pi}{2} - \theta\right)\right)^2 - a^2\cos^2\theta. \end{aligned} \tag{42}$$

However, in the investigated case of a distant static observer ($r_{\rm obs} \to \infty$), when the rays reaching the observer position are almost parallel (see Fig. 1), the relations between coordinates on the detector screen and constants of motion can be simply written as (e.g. Cunningham & Bardeen 1973)

$$x = -\frac{\lambda}{\sin\theta_{\rm obs}}, \qquad y = \Theta_{\lambda,q}(\theta_{\rm obs}). \tag{43}$$

In the event of detection, the constants $\lambda(x, y)$ and $q(x, y)$, together with the initial conditions (coordinates of observer and sign pair s_r, s_θ), fully determine the reverse temporal evolution of the zero geodesics of photons falling on a pixel of the detector screen with the coordinates x, y. The Runge Kutta method of the eighth order (Dorman-Prince method) (Press et al. 2002) used here, integrates the null geodesics and reaches the relative accuracy of 10^{-15}, which, in the case of a central black hole with stellar mass $M = 5\ M_\odot$, corresponds to an order of accuracy of 10^{-11} m on a radial coordinate. To determine the proper orientation of the radial and latitudinal component of the four-momentum (37), the code also analyses the positions of the radial and vertical turning point and sets the corresponding signs $s_{\rm r}$ and s_θ. The integration of Eq. (37) by the Runge Kutta method of the eighth order proceeds naturally with an adaptive step. However, the resulting null geodesic is then finally interpolated by the polynomials of the third order for the chosen equidistant time step ΔT, in the case of central black hole mass $M = 5\ M_\odot$, corresponding to 10^{-5} s.

A&A 581, A35 (2015)

4.2. Radiating surfaces and lightcurves

The surfaces of the tori are modelled by the grid with a resolution of 15 nodes in the radial direction and 75 nodes in the azimuthal one. The grid contains the time-dependent information about coordinates, local intensity, and the four-velocity in the nodes. The time resolution of the surface of the tori necessarily corresponds to the time resolution of the interpolation steps of the geodesics package ΔT. The code LSDplus traces the intersections of the geodesics and linearly interpolated surface of a torus between triads of the nodes of the grid. Assuming the normalized energy in the local observer's frame, the frequency ratio of the emitted and observed radiation from the torus can be expressed using projection of the four-momentum of a photon p^μ to the four-velocity of the surface of the torus $u^{\rm sur}_\mu$ in the event of the emission as follows:

$$g = \frac{1}{p^\mu u^{\rm sur}_\mu}. \tag{44}$$

Radial and vertical components of the surface four-velocity are given by equations (25) and (29). The remaining components $u^{\rm sur}_\varphi$, $u^{\rm sur}_{\rm t}$ can easily be obtained using the normalisation condition $u^\mu u_\mu = -1$, together with the assumption of constant specific angular momentum (Vincent et al. 2014). Then the instantaneous bolometric intensity detected by each pixel of the screen of a small virtual detector is calculated as

$$I_{\rm obs}(t_{\rm obs}) = I_{\rm em}(t_{\rm obs} - t_{\rm delay})g^4, \tag{45}$$

where $t_{\rm delay}$ corresponds to the time delay (the change of a time coordinate) along the appropriate photon trajectory connecting the event of detection of a photon on a pixel with the event of emission on the surface of the torus. Here, $I_{\rm em}$ is local intensity on the surface in the comoving frame given by the Eq. (33). The total instantaneous detected bolometric flux $F(t_{\rm obs})$ is a sum of intensities (45) detected by individual pixels multiplied by the solid angle $\Delta\Pi$ subtended by the pixel in the observer sky

$$F(t_{\rm obs}) = \sum_{i=1}^{1000}\sum_{j=1}^{1000} I_{ij}(t_{\rm obs})\,\Delta\Pi, \tag{46}$$

where i is the index of a pixel column and where j is the index of a pixel row[4]. Since we are using relative units, we can simply set $\Delta\Pi = 1$. The resulting lightcurves are generated in the time resolution ΔT that corresponds to 20 time samples per characteristic vertical oscillation period of the analysed dual oscillation mode.

4.3. Power spectra

To calculate power spectral densities (PSD), the resulting lightcurves are processed by fast Fourier transform (FFT). The PSD at frequency $f_k = k/(N\Delta t)$ is given as the square of the modulus of the FFT of the signal as

$$\mathrm{PSD}(f_k) = \left|\frac{1}{N}\sum_{j=0}^{N-1} F(t_j)\exp(2\pi i jk/N)\right|^2, \tag{47}$$

where $F(t_j)$ is the observed flux (46) at observation time $t_j = j\Delta t$, and N is the total number of time samples in the lightcurve.

[4] We assume tiny angular size of the torus image in the observer sky and therefore constant $\Delta\Pi$.

Table 1. Most prominent peaks observed in power density spectra of simulated lightcurves.

Frequency scaled in $\nu_{\rm l}$	Peak origin
1/2	$\nu_{\rm u} - \nu_{\rm l}$
1	$\nu_{\rm l} = \lvert\Omega_{\rm r}/2\pi\rvert$
3/2	$\nu_{\rm u} = \lvert\Omega_\theta/2\pi\rvert$
2	$2\nu_{\rm l}$
5/2	$\nu_{\rm u} + \nu_{\rm l}$
3	$3\nu_{\rm l}$, $2\nu_{\rm u}$

4.4. Iron Kα line profiles

The fluorescent iron Kα line consists of two components with $FWHM \approx 3.5$ eV and separation ≈13 eV (see Basko 1978, for details). Considering the energy resolution $\Delta E = 10$ eV of the simulation code, we approximated the rest iron Kα line profile by Lorentzian peak with the scale factor $\gamma = 20$ eV located at $E_0 = 6.4$ keV. The instantaneous observed flux per pixel in the energy bin with the central energy $E_{\rm c}$ is given as

$$\Phi(t_{\rm obs}, E_{\rm c}) = I_{\rm em}(t_{\rm obs} - t_{delay})g^3 f(E_{\rm c}/g, \gamma, E_0)\,\Delta\Pi, \tag{48}$$

where Lorentzian function f reads as

$$f(x, \gamma, x_0) = \frac{1}{\pi\gamma\left[1 + \left(\frac{x-x_0}{\gamma}\right)^2\right]}. \tag{49}$$

Then the observed instantaneous iron Kα line profile is constructed by summing energy bin fluxes per pixels (48) over all pixels of the virtual detector in the given time sample. The final integrated line profile is obtained by summing instantaneous line profiles over all time samples.

5. Methods

Applying ray-tracing methods described in the previous section, we performed simulations of lightcurves of the model discussed above of a slender accretion torus oscillating in the dual-mode regime. To obtain closed trajectories of the torus surface and corresponding closed lightcurves, we simulated the behaviour of emitted radiation during three periods of vertical oscillation considering the fixed ratio of oscillation frequencies $\nu_{\rm u}/\nu_{\rm l} = 3{:}2$. Then we calculated power spectra of obtained lightcurves by relation (47). We studied the impact of the central black hole spin using its three representative values $a \in (0,\ 0.5,\ 0.96)$. The upper limit of the investigated spin value is almost the highest one, for which the location of equilibrium torus centre r_0 can be found by the RP-like frequency relation (35). The impact of the observer inclination (polar angle) i is analysed using the following set of inclination values:

$$i \in \left(0.01,\ \frac{\pi}{12},\ \frac{\pi}{6},\ \frac{\pi}{4},\ \frac{\pi}{3},\ \frac{5}{12}\pi,\ \frac{5.5}{12}\pi,\ \frac{5.75}{12}\pi,\ \frac{\pi}{2}\right).$$

We analyse the magnitude relations of five prominent PSD peaks corresponding to two main dual-mode oscillation frequencies, their higher harmonics, and their sum or difference, particularly summarised in the Table 1. Power spectra are calculated for all combinations of investigated values for the spin and the inclination. We plot the magnitudes of these peaks as linearly interpolated functions of the inclination for all the investigated values of the spin and for both investigated torus setups separately (see left panels of Figs. 3 and 4).

Table 2. Values of parameters describing the investigated slender torus model for ER axisymmetric setup.

Spin	0.0	0.5	0.96
β	0.04	0.04	0.04
Central radial coordinate r_0	10.80	7.92	4.35
Torus radial extent	1.08	0.79	0.44
Torus vertical extent	0.80	0.61	0.38
Max. radial displacement	0.27	0.20	0.11
Max. vertical displacement	0.20	0.15	0.09

Table 3. Values of parameters describing the investigated slender torus model for RP-like non-axisymmetric setup.

Spin	0.0	0.5	0.96
β	0.02	0.02	0.002
Central radial coordinate r_0	6.75	4.66	1.85
Torus radial extent	0.68	0.47	0.18
Torus vertical extent	0.27	0.18	0.02
Max. radial displacement	0.17	0.12	0.05
Max. vertical displacement	0.07	0.05	0.004

Moreover, the integrated iron Kα line profiles emitted from the torus surface are modelled for inclination values $i \in \left(\frac{\pi}{12}, \frac{\pi}{6}, \frac{\pi}{4}, \frac{\pi}{3}, \frac{\pi}{2}\right)$. The geometry of the torus's optical projection is illustrated in Fig. 2 by the frequency shift maps on the virtual detector screen drawn in false colours related to the frequency shift values[5]. The maps clearly show that the simulation parameters are sufficient for distinguishing the first three relativistic images. The iron Kα line profiles that were also computed display significant secondary blueshifted horns related to secondary (first indirect) relativistic images (see right panels of Figs. 3 and 4).

6. Results

6.1. Results for the ER axisymmetric setup

Table 2 summarises the parameters of the slender torus that oscillates in the pure epicyclic axisymmetric dual mode ($m_r = 0$, $m_\theta = 0$) for three investigated values of the spin. The radial coordinate of equilibrium torus centre r_0 given by relation (34) remains above both the black hole photosphere[6] and the ergosphere for all such configurations.

The lightcurve waveforms are influenced by a complex interplay of the general relativistic frequency shift, the time variation of the emitting torus surface area, and the time variation of the apparent torus area on the virtual detector screen (Bakala et al. 2015). All these effects strongly depend on the radial coordinate of the emission event, the inclination of the distant observer i, and the central black hole spin a. Nevertheless, the magnitude relations depicted in the left-hand panels of Fig. 3 exhibit certain identical qualitative features for all investigated spin values. The pair of peaks corresponding to radial ν_l and vertical ν_u torus oscillation frequency is dominant on a wide range of i. For this inclination range, the examined ER axisymmetric setup predicts twin peaks HF QPOs frequency ratio equal to 3:2 in accordance with expectations. The ν_l peak remains most prominent for low and medium values of distant observer inclination i. The magnitude of the ν_u peak grows with i becoming the most prominent for relatively high inclinations, but it rapidly falls for exact or almost exact equatorial observers. At the same time, the magnitude of the peak corresponding to $3\nu_l$, $2\nu_u$ rapidly grows. Therefore, in the case of such observers, the examined torus configuration predicts a frequency ratio equal to $1/3$ for the pair of the most distinguishable HF QPO peaks. In the case of zero or moderate spins ($a = 0$, $a = 0.5$) and small inclinations ($i \leq \frac{\pi}{12}$), the magnitude of the $2\nu_l$ peak slightly exceeds the ν_l peak magnitude, and the predicted twin peaks HF QPOs frequency ratio value is equal to 1:2. As illustrated in the plots of magnitude relations (see left panels of Fig. 3), the spectral content of less distinct PSD peaks varies depending on values of i and a.

Like the power spectra behaviour, the iron Kα line profiles keep some identical qualitative features for all investigated spin values. Naturally, the energy span of line profiles is expanded and shifted down with decreasing r_0. The dependence of the height of the primary blueshifted horns on i is the only qualitative difference observable for different spin values (see right panels of Fig. 3).

6.2. Results for the RP-like non-axisymmetric setup

Table 3 summarizes parameters of the slender torus oscillating in the RP-like non-axisymmetric dual mode ($m_r = -1$, $m_\theta = -2$) for three investigated values of the spin. In the case of zero or moderate spin ($a = 0$, $a = 0.5$), the radial coordinate of equilibrium torus centre r_0 given by relation (35) remains located above the black hole photosphere, as well as the ergosphere, while in the case of high spin ($a = 0.96$), the torus is located inside the ergopshere and therefore also deeply inside the photosphere. Moreover, in the case of high spin, the radial extent of the torus obtained as $r_0/10$ exceeds the location of the cusp of equipotential surfaces (Blaes et al. 2006; Straub & Šrámková 2009). Such a torus configuration becomes unstable. Unfortunately, a surface area of the high spin stable configuration with maximum possible $\beta = 7.0 \times 10^{-5}$ is almost negligible, and emitted flux is comparable to the numerical error of the simulation. Therefore, we keep the torus radial extent equal to $r_0/10$ and choose the unstable high spin configuration with $\beta = 0.002$.

In the case of zero or moderate spin ($a = 0$, $a = 0.5$), the qualitative picture of power spectra and iron Kα line profiles behaviour is very similar to the case of the ER axisymmetric setup discussed in the previous section (see Fig. 4). The prediction for low inclination represents the main difference. In the Schwarzschild case, the pair of peaks corresponding to radial ν_l and vertical ν_u oscillation frequency also remains dominant for $i \leq \frac{\pi}{12}$, predicting the twin peaks HF QPOs frequency ratio equal to 3:2, as depicted in the top left panel of Fig. 4. In the case of $a = 0.5$ and a very small inclination, the magnitude of the $\nu_u - \nu_l$ peak (instead of the $2\nu_l$ peak acting the same way in the case of the ER axisymmetric setup) slightly exceeds the ν_l peak magnitude, and the predicted twin peaks HF QPOs frequency ratio is equal to 1:2 (see the middle left panel of Fig. 4).

The unstable high-spin configuration exhibits an entirely different picture, as shown in the bottom panels of Fig. 4. In the whole range of inclination, the pair of dominant PSD peaks corresponds to the radial ν_l frequency and its second harmonic $2\nu_l$. Therefore, in the unstable high spin case, the examined RP-like non-axisymmetric setup surprisingly predicts the twin peaks HF

[5] The frequency shift maps displayed in Fig. 2 are not zoomed and not positioned identically with respect to the projection of the whole observer sky.

[6] Kerr black hole photosphere – a region of spherical unstable photon orbits reaches maximum extent in the equatorial plane between corotating and counter-rotating circular photon orbits, while it becomes infinitesimally thin on the polar axis (see e.g. Teo 2003, for details)

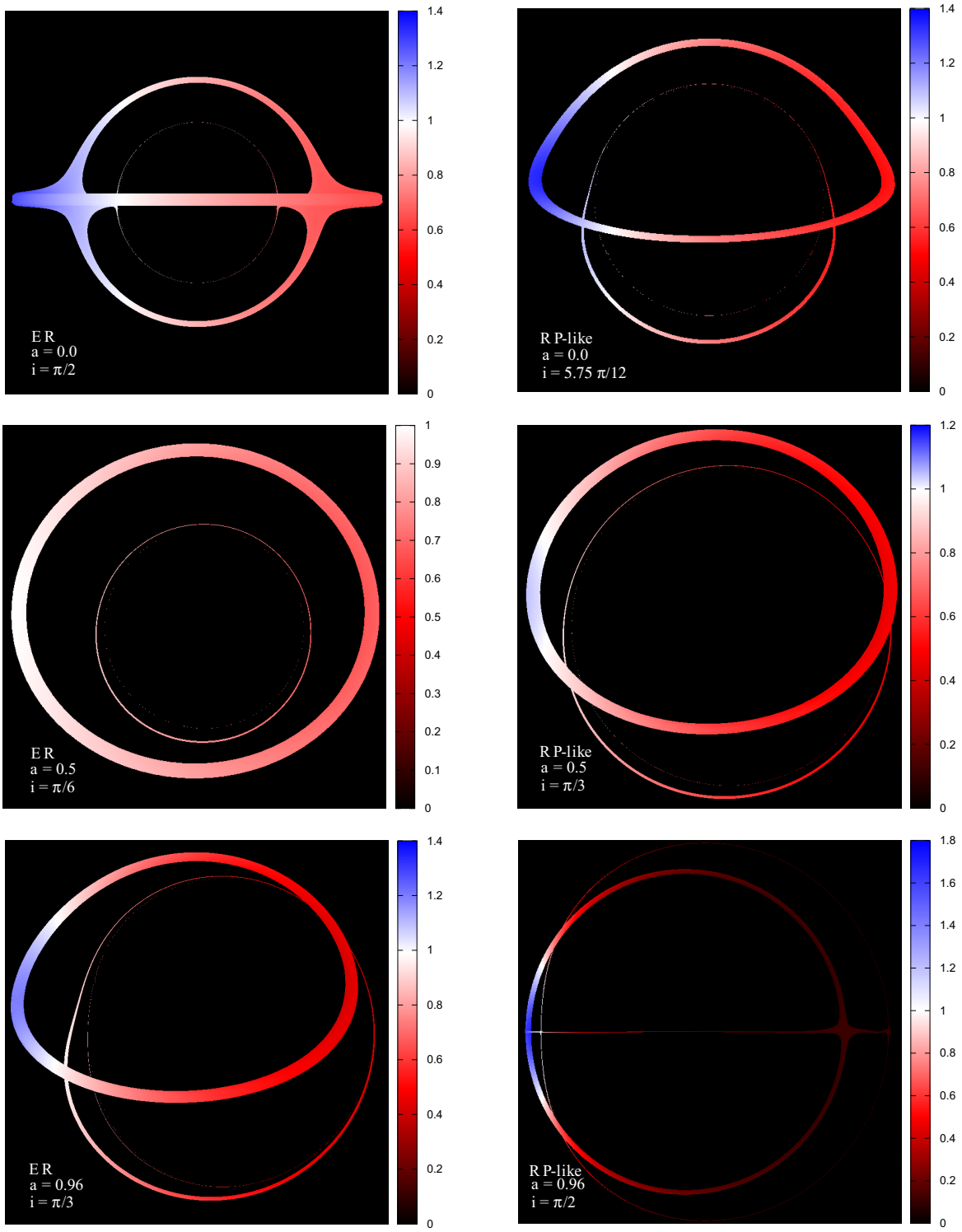

Fig. 2. Examples of the frequency shift maps for different distant views of the oscillating slender torus. The colour boxes on the right display the false colours scale of frequency shift values. The *left column* corresponds to the case of the ER axisymmetric dual mode. The *right column* corresponds to the case of the RP-like non-axisymmetric dual mode. The rows of the figure correspond to spin values $a = 0$, $a = 0.5$ and $a = 0.96$, respectively.

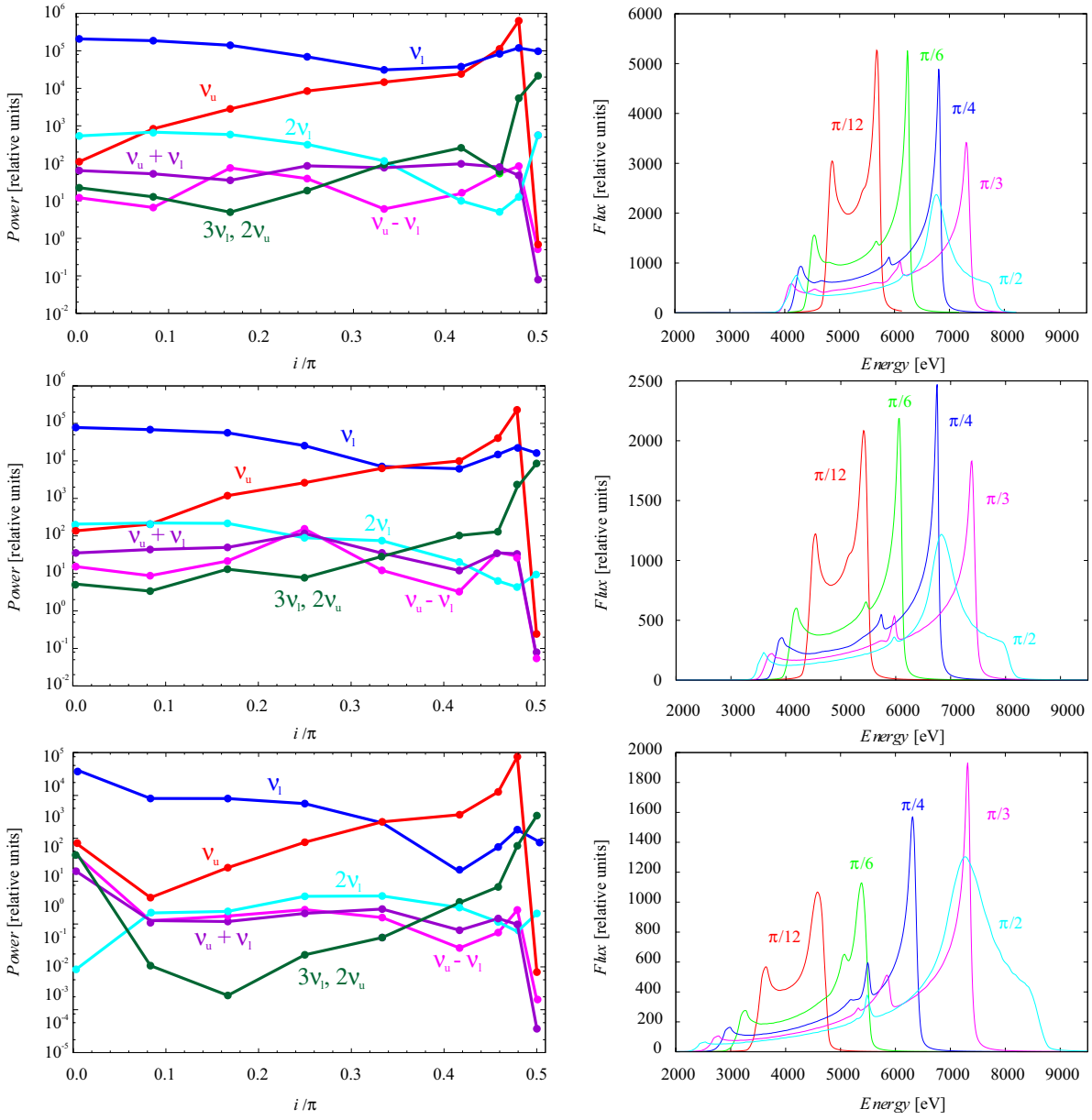

Fig. 3. Simulations outputs in the case of the ER axisymmetric dual mode. *Left panels*: the amplitudes of prominent PSD peaks (see Table 1) as a function of distant observer inclination i. *Right panels*: iron Kα line profiles constructed for $i \in \left(\frac{\pi}{12}, \frac{\pi}{6}, \frac{\pi}{4}, \frac{\pi}{3}, \frac{\pi}{2}\right)$. The rows of the picture correspond to the cases of spin values $a = 0, a = 0.5$, and $a = 0.96$, respectively (see Table 2).

QPOs frequency ratio value that is only equal to 1:2. The dramatic change of the optical projection properties is documented by iron Kα line profiles in the bottom right-hand panel of Fig. 4. The energy span is significantly shifted down, and both primary and secondary blueshifted horns have comparable heights. The computed profiles also display numerical instabilities caused by a small emitting surface area of the unstable high spin torus configuration. The line profile related to $i = \frac{\pi}{2}$ exhibits exceptional behaviour, because its extremely wide energy span reaches 11 keV and its primary blueshifted horn is absolutely dominant. The corresponding frequency shift map in the bottom right-hand panel of Fig. 2 also illustrates the equatorial optical projection of the torus located in the close vicinity of the Kerr black hole event horizon. It is clearly visible that the angular size of both secondary and tertiary relativistic images exceeds the angular size of the primary image. Moreover, despite the significant gravitational redshift, the high Keplerian orbital velocity causes a high Doppler blueshift for the left side of the torus projection corresponding to the extreme height of the primary blueshifted horn in the iron Kα line profile.

A&A 581, A35 (2015)

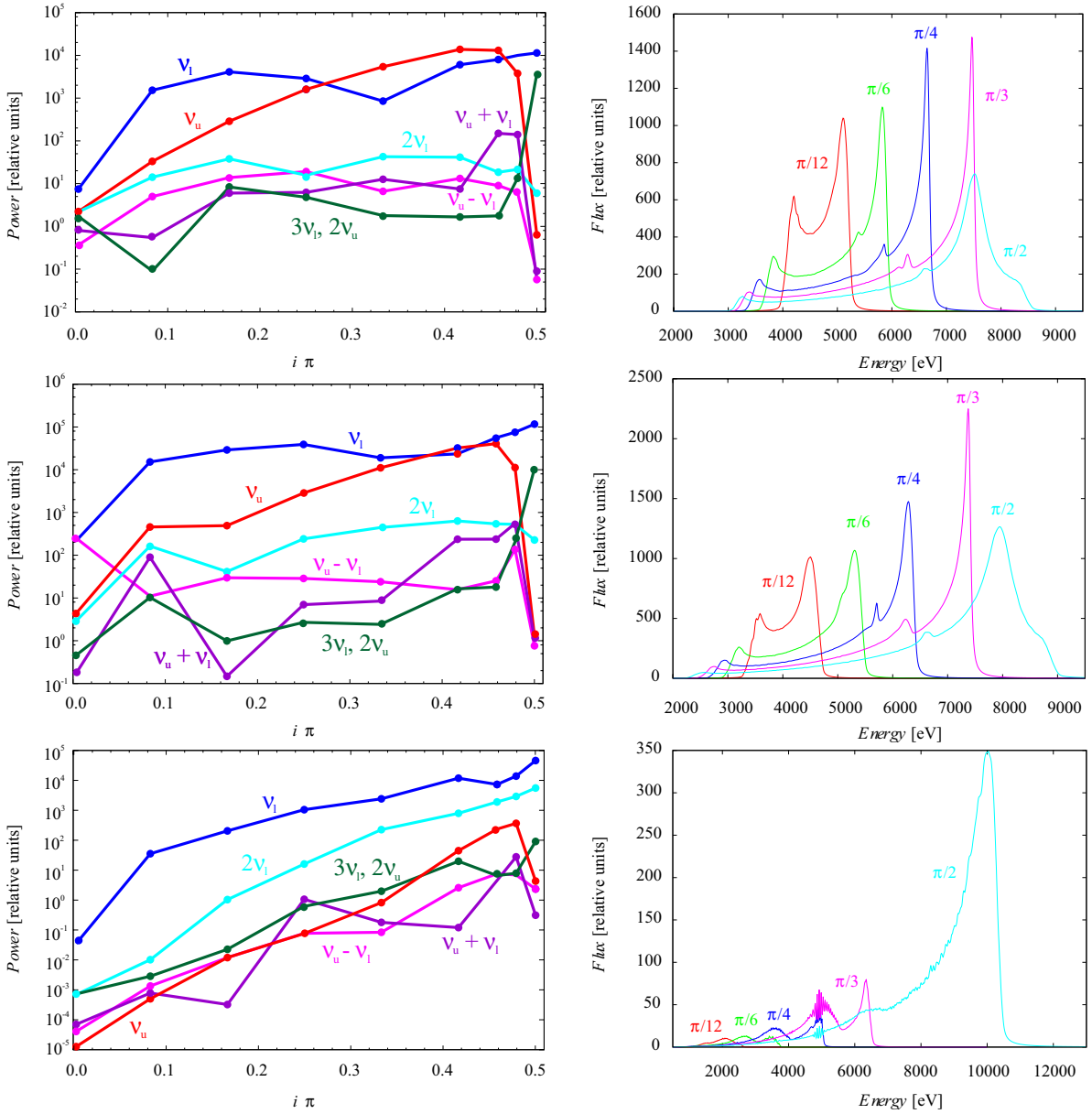

Fig. 4. Simulations outputs in the case of the RP-like non-axisymmetric dual mode. *Left panels*: the amplitudes of prominent PSD peaks (see Table 1) as a function of distant observer inclination i. *Right panels*: iron Kα line profiles constructed for $i \in \left(\frac{\pi}{12}, \frac{\pi}{6}, \frac{\pi}{4}, \frac{\pi}{3}, \frac{\pi}{2}\right)$. The rows of the picture correspond to the cases of spin values $a = 0, a = 0.5$, and $a = 0.96$, respectively (see Table 3).

7. Conclusions and perspectives

The aim of this article has been to model twin peaks HF QPOs as a spectral impact of isotropically radiating slender tori oscillating in a dual mode regime in the close vicinity of Kerr black holes. Vincent et al. (2014) show that a significant fraction of the observed flux is regulated by the torus motion described by the lowest oscillation modes. We therefore examined two configurations of the dual oscillation regime based on the lowest radial and vertical oscillation modes with different azimuthal wave numbers. Appropriate frequency relations correspond to the two competing QPOs models, the epicyclic resonance (ER) HF QPOs model (Abramowicz & Kluźniak 2001) and a slightly modified relativistic precession (RP) QPOs model (Stella & Vietri 1999). We model twin peaks HF QPOs by the pair of the most prominent peaks in the obtained power spectra. Our results show that independently of the spin, the ER axisymmetric setup yields power spectra with the pair of dominant PSD peaks corresponding to the frequencies of radial and vertical oscillation modes with a proper ratio equal to 3:2, except some

special cases of very high or very low distant observer inclinations, where higher harmonics becomes prominent. The predictions of the RP-like non-axisymmetric setup are almost identical to the ER case for zero or moderate spin configurations. An unstable high-spin RP-like configuration with the torus located in the ergosphere exhibits dominant PSD peaks pair corresponding to the frequency of radial oscillation modes and its second harmonics in the whole range of inclinations, so it predicts a constant frequency ratio equal to 1:2. The entire change of the optical projection is also documented by the different iron Kα line profiles with respect to the previous cases.

The analysis presented in the article primarily focused on the relative ratios of the amplitudes of the most prominent frequency peaks in the modelled power spectra. However, the absolute fractional rms of the amplitudes of HF QPOs peaks in the detected signal depends not only on the amplitudes of perturbation $A_{\mathrm{r},\theta}$, but also on the relations of individual components of the whole total source flux. In Bakala et al. (2014) we defined an empirical model of total source flux, which mimics the so-called high steep power-law (HSPL) state in GRS 1905+105, including steep spectrum and power-law-dominated variability with an additional broad Lorentzian component at low frequencies (McClintock & Remillard 2006). Then we used this background to analyse the resolution of HF QPO peaks for a similar but simpler model of oscillating slender torus in the Schwarzschild geometry (Bursa et al. 2004), slowly passing the resonant orbit r_0. Considering the capabilities of the RXTE and LOFT instruments simulated by their response matrices, we showed that the presently available observational technology enables a good detection of the pair of the most prominent peaks in such a modelled signal. Nevertheless, the behaviour of spectral content of less distinct PSD peaks probably remains the key task for the data analysis of future sensitive space observatory missions for X-ray timing, such as the proposed LOFT mission (see Bakala et al. 2014; Feroci et al. 2014; Karas et al. 2014, for details).

Our simulation yields iron Kα line profiles that are very different from the line profile integrated over the entire accretion disk. Therefore, the next related topic for future space X-ray missions can be sensitive frequency-resolved spectroscopy, which will be able to isolate the spectral component oscillating on the QPO frequency (see e.g. Axelsson et al. 2014; Revnivtsev et al. 1999). Phase-resolved spectroscopy that traces the iron line profile changes throughout an oscillation cycle could be another potentially interesting diagnostic tool. This idea has already been suggested for the case of low-frequency QPOs (e.g. Ingram & Done 2012b; Tsang & Butsky 2013), but its application for the studied model of HF QPO driven by slender torus oscillations will require a more detailed future study.

We assume an optically thick slender torus, and thus the influence of the torus opacity can also be the subject for our future research. It is possible to generalise the examined slender torus model by considering the pressure effects on the mode frequencies and the torus shape (Straub & Šrámková 2009). In our study, the location of the torus centre is empirically chosen using the observed twin peaks HF QPOs ratio. The resonant coupling of oscillation modes can prefer particular values of radial coordinate for amplification or excitation of QPOs (Horák 2008). Therefore, further important improvements in the simulations can incorporate mode-resonant coupling. Future implementation of improved models of non-slender tori into the used LSDplus code can be the next step towards more realistic results. A future detailed comparative study of spectral harmonic content can also be devoted to the possibility of distinguishing between QPOs models based on either accretion tori oscillations or the orbital motion of radiating blobs.

Acknowledgements. We acknowledge the Czech research grant GAČR 209/12/P740, Polish NCN UMO-2011/01/B/ST9/05439 grant and the internal grants of Silesian University in Opava IGS/11/2015 and SGS/11/2013.

References

Abramowicz, M. A., & Fragile, P. C. 2013, Liv. Rev. Relativity, 16, 1
Abramowicz, M. A., & Kluźniak, W. 2001, A&A, 374, L19
Abramowicz, M. A., & Kluźniak, W. 2004, in X-ray Timing 2003: Rossi and Beyond, eds. P. Kaaret, F. K. Lamb, & J. H. Swank, AIP Conf. Ser., 714, 21
Abramowicz, M. A., & Kluźniak, W. 2005, Ap&SS, 300, 127
Abramowicz, M. A., Bulik, T., Bursa, M., & Kluźniak, W. 2003a, A&A, 404, L21
Abramowicz, M. A., Karas, V., Kluźniak, W., Lee, W. H., & Rebusco, P. 2003b, PASJ, 55, 467
Abramowicz, M. A., Blaes, O. M., Horák, J., Kluźniak, W., & Rebusco, P. 2006, Classical and Quantum Gravity, 23, 1689
Aliev, A. N. 2008, in The Eleventh Marcel Grossmann Meeting On Recent Developments in Theoretical and Experimental General Relativity, Gravitation and Relativistic Field Theories, ed. H. Kleinert, R. T. Jantzen, & R. Ruffini, 1057
Aliev, A. N., & Galtsov, D. V. 1981, General Relativity Gravitation, 13, 899
Alpar, M. A., & Shaham, J. 1985, Nature, 316, 239
Axelsson, M., Done, C., & Hjalmarsdotter, L. 2014, MNRAS, 438, 657
Bakala, P., Čermák, P., Hledík, S., Stuchlík, Z., & Truparová, K. 2007, Centr. Eur. J. Phys., 5, 599
Bakala, P., Török, G., Karas, V., et al. 2014, MNRAS, 439, 1933
Bakala, P., Goluchová, K., Šrámková, E., et al. 2015, in IAU Symp. 313, eds. F. Massaro, C. C. Cheung, E. Lopez, & A. Siemiginowska, 380
Bambi, C. 2013, Phys. Rev. D, 87, 023007
Basko, M. M. 1978, ApJ, 223, 268
Beckwith, K., & Done, C. 2005, MNRAS, 359, 1217
Belloni, T. M., Sanna, A., & Méndez, M. 2012, MNRAS, 426, 1701
Blaes, O. M., Arras, P., & Fragile, P. C. 2006, MNRAS, 369, 1235
Broderick, A. E., & Loeb, A. 2005, MNRAS, 363, 353
Bursa, M., Abramowicz, M. A., Karas, V., & Kluźniak, W. 2004, ApJ, 617, L45
Čadež, A., & Calvani, M. 2005, MNRAS, 363, 177
Čadež, A., Calvani, M., & Kostić, U. 2008, A&A, 487, 527
Carter, B. 1968, Phys. Rev., 174, 1559
Chan, C.-k., Psaltis, D., & Özel, F. 2013, ApJ, 777, 13
Chandrasekhar, S. 1983, The mathematical theory of black holes (Oxford: Clarendon Press)
Cunningham, C. T., & Bardeen, J. M. 1972, ApJ, 173, L137
Cunningham, C. T., & Bardeen, J. M. 1973, ApJ, 183, 237
Dexter, J., & Agol, E. 2009, ApJ, 696, 1616
Done, C., Gierliński, M., & Kubota, A. 2007, A&ARv, 15, 1
Fabian, A. C., Rees, M. J., Stella, L., & White, N. E. 1989, MNRAS, 238, 729
Feroci, M., den Herder, J. W., Bozzo, E., et al. 2014, in SPIE Conf. Ser., 9144, 2
Germanà, C. 2013, MNRAS, 430, L1
Germanà, C., Kostić, U., Čadež, A., & Calvani, M. 2009, in AIP Conf. Ser. 1126, eds. J. Rodriguez & P. Ferrando, 367
Horák, J. 2008, A&A, 486, 1
Ingram, A., & Done, C. 2012a, MNRAS, 419, 2369
Ingram, A., & Done, C. 2012b, MNRAS, 427, 934
Ingram, A., & Motta, S. 2014, MNRAS, 444, 2065
Karas, V., Vokrouhlicky, D., & Polnarev, A. G. 1992, MNRAS, 259, 569
Karas, V., Bakala, P., Torok, G., et al. 2014, Acta Polytechnica, 54, 191
Kato, S. 2001, PASJ, 53, 1
Kato, S. 2007, PASJ, 59, 451
Kluźniak, W., & Abramowicz, M. A. 2001, ArXiv e-prints [arXiv:astro-ph/0105057]
Kostić, U., Čadež, A., Calvani, M., & Gomboc, A. 2009, A&A, 496, 307
Lai, D., Fu, W., Tsang, D., Horák, J., & Yu, C. 2013, in IAU Symp. 290, eds. C. M. Zhang, T. Belloni, M. Méndez, & S. N. Zhang, 57
Lamb, F. K., Shibazaki, N., Alpar, M. A., & Shaham, J. 1985, Nature, 317, 681
Mazur, G. P., Vincent, F. H., Johansson, M., et al. 2013, A&A, 554, A57
McClintock, J. E., & Remillard, R. A. 2006, Black hole binaries, eds. W. H. G. Lewin & M. van der Klis, 157
Miller, M. C., Lamb, F. K., & Psaltis, D. 1998, ApJ, 508, 791
Misner, C. W., Thorne, K. S., & Wheeler, J. A. 1973, Gravitation (San Francisco: Freeman)
Morsink, S. M., & Stella, L. 1999, ApJ, 513, 827

Motta, S. E., Belloni, T. M., Stella, L., Muñoz-Darias, T., & Fender, R. 2014, MNRAS, 437, 2554
Mukhopadhyay, B. 2009, ApJ, 694, 387
Papaloizou, J. C. B., & Pringle, J. E. 1984, MNRAS, 208, 721
Pecháček, T., Karas, V., & Czerny, B. 2008, A&A, 487, 815
Pecháček, T., Goosmann, R. W., Karas, V., Czerny, B., & Dovčiak, M. 2013, A&A, 556, A77
Pétri, J. 2005, A&A, 439, L27
Press, W. H., Teukolsky, S. A., Vetterling, W. T., & Flannery, B. P. 2002, Numerical recipes in C++: the art of scientific computing (New York: Cambridge University Press)
Psaltis, D., Wijnands, R., Homan, J., et al. 1999, ApJ, 520, 763
Rauch, K. P., & Blandford, R. D. 1994, ApJ, 421, 46
Remillard, R. A., & McClintock, J. E. 2006, ARA&A, 44, 49
Revnivtsev, M., Gilfanov, M., & Churazov, E. 1999, A&A, 347, L23
Rezzolla, L., Yoshida, S., & Zanotti, O. 2003, MNRAS, 344, 978
Schee, J., & Stuchlík, Z. 2013, J. Cosmology Astropart. Phys., 4, 5
Schnittman, J. D. 2006, Ph.D. Thesis, Massachusetts Institute of technology
Schnittman, J. D., & Bertschinger, E. 2004, ApJ, 606, 1098
Schnittman, J. D., & Rezzolla, L. 2006, ApJ, 637, L113
Šrámková, E. 2005, Astron. Nachr., 326, 835
Šrámková, E., Torkelsson, U., & Abramowicz, M. A. 2007, A&A, 467, 641
Stella, L., & Vietri, M. 1998, ApJ, 492, L59
Stella, L., & Vietri, M. 1999, Phys. Rev. Lett., 82, 17
Stella, L., & Vietri, M. 2002, in The Ninth Marcel Grossmann Meeting, eds. V. G. Gurzadyan, R. T. Jantzen, & R. Ruffini (Singapore: World Scientific), 426
Straub, O., & Šrámková, E. 2009, Classical and Quantum Gravity, 26, 055011
Stuchlík, Z., Konar, S., Miller, J. C., & Hledík, S. 2008, A&A, 489, 963
Tagger, M., & Varnière, P. 2006, ApJ, 652, 1457
Teo, E. 2003, General Relativity and Gravitation, 35, 1909
Titarchuk, L., & Wood, K. 2002, ApJ, 577, L23
Török, G. 2005, Astron. Nachr., 326, 856
Török, G., & Stuchlík, Z. 2005, A&A, 437, 775
Török, G., Abramowicz, M. A., Kluźniak, W., & Stuchlík, Z. 2005, A&A, 436, 1
Török, G., Stuchlík, Z., & Bakala, P. 2007, Centr. Eur. J. Phys., 5, 457
Török, G., Abramowicz, M. A., Bakala, P., et al. 2008a, Acta Astron., 58, 15
Török, G., Abramowicz, M. A., Bakala, P., et al. 2008b, Acta Astron., 58, 113
Török, G., Bakala, P., Stuchlík, Z., & Čech, P. 2008c, Acta Astron., 58, 1
Török, G., Bakala, P., Šrámková, E., Stuchlík, Z., & Urbanec, M. 2010, ApJ, 714, 748
Török, G., Bakala, P., Šrámková, E., et al. 2012, ApJ, 760, 138
Tsang, D., & Butsky, I. 2013, MNRAS, 435, 749
Urbanec, M., Miller, J. C., & Stuchlík, Z. 2013, MNRAS, 433, 1903
van der Klis, M. 2004, ArXiv e-prints [arXiv:astro-ph/0410551]
Viergutz, S. U. 1993, A&A, 272, 355
Vincent, F. H., Paumard, T., Gourgoulhon, E., & Perrin, G. 2011, Classical and Quantum Gravity, 28, 225011
Vincent, F. H., Mazur, G. P., Straub, O., et al. 2014, A&A, 563, A109
Yang, X.-L., & Wang, J.-C. 2014, A&A, 561, A127
Zhang, C.-M. 2005, Chin. J. Astron. Astrophys. Suppl., 5, 21

Paper IV

6.4. Equations of State in the Hartle-Thorne Model of Neutron Stars Selecting Acceptable Variants of the Resonant Switch Model of Twin HF QPOs in the Atoll Source 4U 1636-53

Stuchlík Zdeněk, Urbanec Martin, Kotrlová Andrea,
Török Gabriel & Goluchová Kateřina

Acta Astronomica, 2015,
Volume 65, no 2, p. 169-195

ACTA ASTRONOMICA
Vol. **65** (2015) pp. 169–195

Equations of State in the Hartle–Thorne Model of Neutron Stars Selecting Acceptable Variants of the Resonant Switch Model of Twin HF QPOs in the Atoll Source 4U 1636–53

Z. Stuchlík, M. Urbanec, A. Kotrlová,
G. Török and K. Goluchová

Institute of Physics, Faculty of Philosophy and Science, Silesian University in Opava,
Bezručovo nám. 13, CZ-74601 Opava, Czech Republic
e-mail: andrea.kotrlova@fpf.slu.cz

Received October 9, 2014

ABSTRACT

The Resonant Switch (RS) model of twin high-frequency quasi-periodic oscillations (HF QPOs) observed in neutron star binary systems, based on switch of the twin oscillations at a resonant point, has been applied to the atoll source 4U 1636–53 under assumption that the neutron star exterior can be approximated by the Kerr geometry. Strong restrictions of the neutron star parameters M (mass) and a (spin) arise due to fitting the frequency pairs admitted by the RS model to the observed data in the regions related to the resonant points. The most precise variants of the RS model are those combining the relativistic precession frequency relations with their modifications. Here, the neutron star mass and spin estimates given by the RS model are confronted with a variety of equations of state (EoS) governing structure of neutron stars in the framework of the Hartle–Thorne theory of rotating neutron stars applied for the observationally given rotation frequency $f_{\rm rot} \approx 580$ Hz (or alternatively $f_{\rm rot} \approx 290$ Hz) of the neutron star in 4U 1636–53. It is shown that only two variants of the RS model based on the Kerr approximation are compatible with two EoS applied in the Hartle–Thorne theory for $f_{\rm rot} \approx 580$ Hz, while no variant of the RS model is compatible for $f_{\rm rot} \approx 290$ Hz. The two compatible variants of the RS model are those giving the best fits of the observational data. However, a self-consistency test by fitting the observational data to the RS model with oscillation frequencies governed by the Hartle–Thorne geometry described by three spacetime parameters M, a and (quadrupole moment) q related by the two available EoS puts strong restrictions. The test admits only one variant of the RS model of twin HF QPOs for the Hartle–Thorne theory with the EoS predicting the parameters of the neutron star $M \approx 2.10\,\mathrm{M}_\odot$, $a \approx 0.208$, and $q/a^2 \approx 1.77$.

Key words: *Accretion, accretion disks – Stars: neutron – X-rays: binaries*

1. Introduction

The high-frequency quasi-periodic oscillations (HF QPOs) in the Galactic Low Mass X-Ray Binaries (LMXBs) containing neutron (quark) stars are often demonstrated as two simultaneously observed pairs of peaks (twin peaks) in the Fourier

power spectra corresponding to oscillations at the upper and lower frequencies (ν_U, ν_L) that substantially change over time (even in one observational sequence). Most of the twin HF QPOs in the so-called atoll sources (van der Klis 2006) have been detected at lower frequencies 600–800 Hz *vs.* upper frequencies 900–1200 Hz, demonstrating a clustering of the twin HF QPOs frequency ratio around 3 : 2 (Abramowicz *et al.* 2003, 2005, Belloni *et al.* 2007, Török *et al.* 2008ab, Montero and Zanotti 2012, Wang *et al.* 2013, Stefanov 2014).[1]

For some atoll neutron star sources the upper and lower HF QPO frequencies can be traced along the whole observed range, but the probability to detect both QPOs simultaneously increases when the frequency ratio is close to ratio of small natural numbers, namely 3 : 2, 4 : 3, 5 : 4 (Török 2009). The analysis of root-mean-squared-amplitude evolution in the group of six atoll sources (4U 1636–53, 4U 1608–52, 4U 0614+09, 4U 1728–34, 4U 1820–30, 4U 1735–44) shows that the upper and lower HF QPO amplitudes equal each other and alter their dominance while passing rational frequency ratios $(3:2$ or $4:3)$ corresponding to the datapoints clustering (Török 2009). Such an "energy switch effect" can be well explained in the framework of non-linear resonant orbital models as shown in Horák *et al.* (2009). Another interesting phenomenon related to energy of the twin HF QPOs has been recently demonstrated in Mukherjee and Bhattacharyya (2012). Further, analysis of the twin peak HF QPO amplitudes in the atoll sources (4U 1636–53, 4U 1608–52, and 4U 1820–30, 4U 1735–44) indicates a cut-off at resonant radii corresponding to the frequency ratios 5 : 4 and 4 : 3 respectively, implying a possibility that the accretion disk inner edge is located at the innermost resonant radius rather than at the innermost stable circular geodesic (ISCO, Stuchlík *et al.* 2011). The situation is different for some of the Z-sources where the twin peak frequency ratios are clustered close to 2 : 1, and 3 : 1 ratios as demonstrated in the case of Circinus X-1 (Boutloukos *et al.* 2006). Then the resonant radii could be expected at larger distance from the ISCO than in the atoll sources (Török *et al.* 2010).

The evolution of the lower and upper twin HF QPOs frequencies in the atoll and Z sources suggests a rough agreement of the data distribution with the so-called hot spot models of HF QPOs, *e.g.,* the Relativistic Precession (RP) model prescribing the evolution of the upper frequency by the Keplerian frequency $\nu_U = \nu_K$ and the lower frequency by the precession frequency $\nu_L = \nu_K - \nu_r$ (Stella and Vietri 1998, 1999) governed by the radial epicyclic frequency of geodetical circular motion. In rough agreement with the data are other models based on the assumption of the oscillatory motion of hot spots, or accretion disk oscillations, with oscillatory frequencies given by the geodetical orbital and epicyclic motion. They include

[1] In the black hole sources, twin peaks with fixed pair of frequencies at the ratio 3 : 2 are usually observed and can be explained by the internal non-linear resonance of oscillations with radial and vertical epicyclic frequencies (Török *et al.* 2005).

the modified RP1 model (Bursa 2005), the Total Precession (TP) model (Stuchlík *et al.* 2007), the Tidal Disruption (TD) model (Kostić *et al.* 2009), or the Warp Disk oscillations (WD) model (Kato 2008). In all of them the frequency difference $\nu_U - \nu_L$ decreases with increasing magnitude of the lower and upper frequencies, in accord with the observational data (Belloni *et al.* 2007, Barret *et al.* 2005a, Török *et al.* 2012). This property of the observational data excludes the epicyclic oscillations model assuming $\nu_U = \nu_\theta$ and $\nu_L = \nu_r$ (Urbanec *et al.* 2010b) that works well in the case of HF QPOs in black hole LMXBs (Török *et al.* 2005).[2]

The ν_U/ν_L frequency relations, given by the models mentioned above, can be compared to the observational data found for neutron star LMXBs, *e.g.*, data of the atoll source 4U 1636–53 (Barret *et al.* 2005a, Török *et al.* 2008ab), or the Z-source Circinus X-1 (Boutloukos *et al.* 2006). The parameters of the neutron star spacetime can be then determined due to the fits of the data to the frequency-relation models. The rotating neutron stars are described properly by the Hartle–Thorne geometry (Hartle and Thorne 1968) characterized by three parameters: mass M, internal angular momentum J and quadrupole moment Q, or by dimensionless parameters $a = J/M^2$ (spin) and $q = QM/J^2$. In the special case when $q/a^2 = 1$, the Hartle–Thorne external geometry reduces to the well known Kerr geometry if it is expanded up to the second order in a. The Kerr approximation is very convenient for calculations in strong gravity regime because of simplicity of relevant formulae. It has been recently shown that near-maximum-mass neutron (quark) star Hartle–Thorne models, constructed for any given equation of state (EoS), imply $q/a^2 \approx 1$ and the Kerr geometry is applicable with high precision in such situations instead of the Hartle–Thorne geometry (Urbanec *et al.* 2013, Török *et al.* 2010). Such high-mass neutron stars can be expected at the LMXB systems due to the mass increase caused by the accretion process.

Assuming the geodesic orbital and epicyclic frequencies related to the Kerr geometry, the fitting procedure applied to the RP model of the frequency-relation evolution implies mass–spin relation $M(a) = M_0\left[1 + k(a + a^2)\right]$ rather than concrete values of the neutron star parameters M and a. For the Z-source Circinus X-1 there is $M_0 \approx 2.2\ \mathrm{M}_\odot$ and $k \approx 0.5$ (Török *et al.* 2010). The same mass–spin relations, but with different values of the Schwarzschild (no-rotation) mass $M_0 \approx 1.8\ \mathrm{M}_\odot$ and the constant $k \approx 0.75$, were obtained for the atoll source 4U 1636–53 (Török *et al.* 2012). In the case of the models similar to the RP model (RP1, TP), the same $M(a)$ relations were found, while for the models TD and WD, the relations are different – for details see Török *et al.* (2012). Quality of the fits to the data obtained

[2]Note that quite recently a special frequency set of HF QPOs has been reported for the neutron star binary system XTE J1701–407 that is one of the least luminous atoll sources with $L_X \approx 0.01\,L_{\mathrm{Edd}}$ (Pawar *et al.* 2013). This frequency set resembles observations of the HF QPOs in the microquasars, *i.e.*, black hole binary systems, and it can be explained by the model of string loop oscillations (Stuchlík and Kološ 2015) that works quite well also in the case of Galactic microquasars GRS 1915 + 105, XTE 1550–564, GRO 1655–40 (Stuchlík and Kološ 2014).

for individual models is very poor for the atoll source 4U 1636–53. This fact is extensively discussed in Török *et al.* (2012). Bad fitting of observational data with the frequency-relation models was found also in Lin *et al.* (2011) for the atoll source 4U 1636–53 and the Z-source Sco X-1 for some models of the HF QPOs with the frequency relations given by some phenomena of non-geodesic origin (Miller *et al.* 1998, Zhang *et al*. 2006, Mukhopadhyay 2009, Shi 2011).

The bad fitting of the data distribution in the atoll sources by the frequency-relation models of HF QPOs based on the assumption of the geodesic character of the oscillatory frequencies invoked attempts to find a correction of a non-geodesic origin reflecting some important physical ingredients, as influence of the magnetic field of the neutron star onto slightly charged innermost parts of the disk (Bakala *et al.* 2010, Kovář *et al.* 2008), of thickness of non-slender oscillating tori (Straub and Šrámková 2009), or of oscillating string loop model (Stuchlík and Kološ 2012, 2014, Cremaschini and Stuchlík 2013). Such modifications of the frequency-relation models could make the fitting procedure better as shown for a simple toy model in Török *et al.* (2012). However, in all these cases, some additional free parameter has to be introduced along with the spacetime parameters of the neutron star. Some relevant modifications can be also obtained in the framework of models related to the braneworld compact objects (Stuchlík and Kotrlová 2009, Schee and Stuchlík 2009).

Therefore, the Resonant Switch (RS) model of twin peak HF QPOs has been recently proposed modifying the standard orbital frequency relation models in a way that allows keeping the assumption of the relevant frequencies being combinations of the geodesic orbital and epicyclic frequencies. No non-geodesic corrections are necessary in the RS model, although these are not excluded (Stuchlík *et al.* 2012, 2013) – the RS model considers only the spacetime parameters of the neutron star exterior as free parameters. The RS model has been applied in the case of the atoll source 4U 1636–53 (Stuchlík *et al.* 2012) and tested for this atoll source by fitting the observational data using the frequency relations predicted by the RS model as acceptable due to the neutron star structure theory (Stuchlík *et al.* 2014).

The fitting procedure predicts the mass and spin parameters of the 4U 1636–53 neutron star with relatively high precision (Stuchlík *et al.* 2014). Here we test the frequency relation pairs of the RS model giving the best fits for the corresponding values of the mass M and spin a of the neutron star, using variety of equations of state considered recently in modeling the rotating neutron stars in the framework of the Hartle–Thorne theory. Strong limits implied by the Hartle–Thorne models can be obtained due to the precise knowledge of the rotation velocity of the 4U 1636–53 neutron star (Strohmayer and Markwardt 2002). We are then able to put strong restrictions on validity of the acceptable frequency-relation variants of the RS model.

2. Resonant Switch Model of Twin HF QPOs in the 4U 1636–53 Atoll Source

2.1. The RS model

We briefly summarize the basic ideas of the RS model – for details see Stuchlík *et al.* (2012, 2013). According to the RS model a switch of twin oscillatory modes creating sequences of the lower and upper HF QPOs occurs at a resonant point. Non-linear resonant phenomena are able to excite a new oscillatory mode (or two new oscillatory modes) and damp one of the previously acting modes (or both the previous modes).[3] Switching from one pair of the oscillatory modes to some other pair will be relevant up to the following resonant point where the sequence of twin HF QPOs ends.

Here, two resonant points at the disk radii $x_{\rm out}$ and $x_{\rm in}$ are assumed ($x = r/(GM/c^2)$ is the dimensionless radius, expressed in terms of the gravitational radius), with observed frequencies $\nu_{\rm U}^{\rm out}$, $\nu_{\rm L}^{\rm out}$ and $\nu_{\rm U}^{\rm in}$, $\nu_{\rm L}^{\rm in}$, being in commensurable ratios $p^{\rm out} = n^{\rm out} : m^{\rm out}$ and $p^{\rm in} = n^{\rm in} : m^{\rm in}$. Observations of the twin HF QPOs in the atoll systems put the restrictions $\nu_{\rm U}^{\rm in} > \nu_{\rm U}^{\rm out}$ and $p^{\rm in} < p^{\rm out}$ (Török 2009). In the region related to the resonant point at $x_{\rm out}$, the twin oscillatory modes with the upper (lower) frequency are determined by the functions $\nu_{\rm U}^{\rm out}(x;M,a)$, ($\nu_{\rm L}^{\rm out}(x;M,a)$. In the region related to the inner resonant point at $x_{\rm in}$ different oscillatory modes given by the frequency functions $\nu_{\rm U}^{\rm in}(x;M,a)$ and $\nu_{\rm L}^{\rm in}(x;M,a)$ occur. All the frequency functions are assumed to be combinations of the orbital and epicyclic frequencies of the geodesic circular motion in the Kerr backgrounds. Such a simplification is correct with high accuracy for neutron (quark) stars with large masses, close to maximum allowed for a given equation of state (Török *et al.* 2010, Urbanec *et al.* 2013), that can be assumed in the known atoll or Z-sources because of mass increasing due to the accretion. Of course, for neutron stars having mass significantly lower than the maximal allowed mass, the Hartle–Thorne external geometry reflecting also the role of the quadrupole moments of the neutron star has to be taken into account (Urbanec *et al.* 2013, Gondek-Rosińska *et al.* 2014).

In the Kerr spacetime, the vertical epicyclic frequency ν_θ and the radial epicyclic frequency ν_r take the form (*e.g.*, Perez *et al.* 1997, Stella and Vietri 1998, Török and Stuchlík 2005)

$$\nu_\theta^2 = \alpha_\theta \nu_{\rm K}^2, \quad \nu_r^2 = \alpha_r \nu_{\rm K}^2 \tag{1}$$

where the Keplerian (orbital) frequency $\nu_{\rm K}$ and the dimensionless quantities deter-

[3] Note that the switch could occur for other reasons, *e.g.*, due to the phenomena related to the magnetic field of neutron stars (Zhang *et al.* 2006).

mining the epicyclic frequencies are given by the formulae

$$\nu_{\rm K} = \frac{1}{2\pi}\left(\frac{GM}{r_{\rm G}^3}\right)^{1/2}\left(x^{3/2}+a\right)^{-1} = \frac{1}{2\pi}\left(\frac{c^3}{GM}\right)\left(x^{3/2}+a\right)^{-1}, \tag{2}$$

$$\alpha_\theta = 1-\frac{4a}{x^{3/2}}+\frac{3a^2}{x^2}, \tag{3}$$

$$\alpha_r = 1-\frac{6}{x}+\frac{8a}{x^{3/2}}-\frac{3a^2}{x^2}. \tag{4}$$

Details of the properties of the orbital and epicyclic frequencies can be found in Török and Stuchlík (2005), Stuchlík and Schee (2012). We can see that any linear combination of the orbital and epicyclic frequencies depends on the mass parameter M in the same way, therefore, their frequency ratio becomes independent of M. Then the conditions

$$\begin{aligned} &\nu_{\rm U}^{\rm out}(x;M,a) : \nu_{\rm L}^{\rm out}(x;M,a) = p^{\rm out}, \\ &\nu_{\rm U}^{\rm in}(x;M,a) : \nu_{\rm L}^{\rm in}(x;M,a) = p^{\rm in} \end{aligned} \tag{5}$$

imply relations for the spin a in terms of the dimensionless radius x and the resonant frequency ratio p that can be expressed as $a_p^{\rm out}(x)$ and $a_p^{\rm in}(x)$, or in an inverse form $x_p^{\rm out}(a)$ and $x_p^{\rm in}(a)$.

The frequency relation functions have to meet the resonant frequencies that can be determined by the energy switch effect (Török 2009, Stuchlík *et al.* 2012). In the RS model applied here, two resonant points and two pairs of the frequency functions are assumed. This enables direct determination of the Kerr background parameters assumed to govern the exterior geometry of the neutron (quark) star. At the resonant radii the conditions

$$\nu_{\rm U}^{\rm out} = \nu_{\rm U}^{\rm out}(x;M,a)\,, \quad \nu_{\rm U}^{\rm in} = \nu_{\rm U}^{\rm in}(x;M,a) \tag{6}$$

are satisfied along the functions $M_{p_{\rm out}}^{\rm out}(a)$ and $M_{p_{\rm in}}^{\rm in}(a)$. The parameters of the neutron (quark) star are then given by the condition (Stuchlík *et al.* 2012)

$$M_{p_{\rm out}}^{\rm out}(a) = M_{p_{\rm in}}^{\rm in}(a). \tag{7}$$

This condition predicts M and a with precision implied by the error occurring in determination of the resonant frequencies by the energy switch effect that is rather high for the observational data obtained at present state of the observational devices (see Török 2009, Stuchlík *et al.* 2012). However, the fitting of the observational data by the frequency relations predicted by the RS model improves substantially the precision of determination of the neutron star parameters and, simultaneously, restricts the versions of the RS model that can be considered as realistic.

Starting from the results obtained in Stuchlík *et al.* (2012), we consider in the present paper pairs of the frequency relations given by the RP model (Stella and Vietri 1998, 1999), the TP model (Stuchlík *et al.* 2007), and their modifications RP1

(Bursa 2005), and TP1, combined also with the TD model (Kostić *et al.* 2009), and the WD model (Kato 2008). The frequency relations are summarized in Table 1. In the RS model applied to the source 4U 1636–53 the frequency relations are combined, and the switch of their validity occurs at the outer resonant point as described in Stuchlík *et al.* (2012). For each of the frequency relations under consideration the frequency resonance functions and the resonance conditions determining the resonant radii $x_{n:m}(a)$ are given in Stuchlík *et al.* (2012).

T a b l e 1

Frequency relations corresponding to individual HF QPO models

Model	Relations	
RP	$\nu_{\rm L} = \nu_{\rm K} - \nu_r$	$\nu_{\rm U} = \nu_{\rm K}$
RP1	$\nu_{\rm L} = \nu_{\rm K} - \nu_r$	$\nu_{\rm U} = \nu_\theta$
TP	$\nu_{\rm L} = \nu_\theta - \nu_r$	$\nu_{\rm U} = \nu_\theta$
TP1	$\nu_{\rm L} = \nu_\theta - \nu_r$	$\nu_{\rm U} = \nu_{\rm K}$
TD	$\nu_{\rm L} = \nu_{\rm K}$	$\nu_{\rm U} = \nu_{\rm K} + \nu_r$
WD	$\nu_{\rm L} = 2(\nu_{\rm K} - \nu_r)$	$\nu_{\rm U} = 2\nu_{\rm K} - \nu_r$

2.2. Application to the Source 4U 1636–53

The mass M and spin a ranges predicted by the RS model with resonant frequencies given by the energy switch effect are very large (see Table 1 in Stuchlík *et al.* 2012). However, the ranges can be strongly restricted by fitting the observational data near the resonant points by the pairs of the frequency relations corresponding to the twin oscillatory modes. We use the data of twin HF QPOs in the 4U 1636–53 source as presented and studied in Török *et al.* (2012), analyzed in the original papers by Barret *et al.* (2005a,b) – in this case it is immediately clear what is the extension of the data related to the resonant points with frequency ratio $3:2$ and $5:4$, respectively. In the fitting procedure, based on the formulae related to the Kerr spacetime, we applied those switched twin frequency relations predicted by the RS model that are acceptable due to the neutron (quark) star structure theory (Stuchlík *et al.* 2012, 2014). All the resulting twin frequency relations considered in our testing are presented in Table 2 where the values of the mass M and spin a of the neutron star predicted by the RS model and the related fitting procedure presented in Stuchlík *et al.* (2014) are explicitly given along with the corresponding errors. In fitting the observational data, the standard least-squares (χ^2) method (Press *et al.* 2007) has been applied. In the space of the lower and upper frequencies, $\nu_{\rm L}$ and $\nu_{\rm U}$, the χ^2-test represents the minimal (squared) distance of the frequency relation

curve $\nu_U(\nu_L)$ given by a model of the twin HF QPOs from the observed set of data points:

$$\chi^2 \equiv \sum_{n=1}^{m} \Delta_n^2, \qquad \Delta_n = \mathrm{Min}\left(\frac{l_{n,p}}{\sigma_{n,p}}\right)_{p_\infty}^{p_{\mathrm{ISCO}}} \tag{8}$$

where $l_{n,p}$ is the length of a line between the centroid values of the nth measured data point $[\nu_L(n), \nu_U(n)]$ and a point $[\nu_L(p(n)), \nu_U(p(n))]$ belonging to the relevant frequency curve of the model; the points are considered down to the point corresponding to the ISCO. The quantity $\sigma_{n,p}$ denotes the length of the part of this line located within the error ellipse around the data point (Press *et al.* 2007).

The χ^2-test has been applied solely for the RP, TP and TD frequency relations along the whole range of the observational data in Török *et al.* (2012). However, the results were quite unsatisfactory, giving $\chi^2 \approx 350$ and $\chi^2/\mathrm{dof} \approx 16$. On the other hand, the RS model enables increase of the fit precision by almost one order, giving in the best cases $\chi^2 \approx 55$ and $\chi^2/\mathrm{dof} \approx 2.6$ (Stuchlík *et al.* 2014).[4]

Table 2

The best fits of the observational data and the corresponding spin and mass parameters of the neutron star located in the 4U 1636–53 source, along with related errors in determining spin and mass of the neutron star due to the fitting procedure

Combination of models	χ^2_{min}	a	Δa	M [$M_\odot$]	ΔM [$M_\odot$]
RP1(3:2) + RP(5:4)	55	0.27	0.02	2.20	0.04
TP(3:2) + RP(5:4)	55	0.52	0.02	2.87	0.06
RP1(3:2) + TP1(5:4)	61	0.20	0.01	2.12	0.03
RP1(3:2) + TP(5:4)	62	0.45	0.03	2.46	0.06
TP(3:2) + TP1(5:4)	68	0.31	0.02	2.39	0.05
RP(3:2) + TP1(5:4)	72	0.46	0.03	2.81	0.09
WD(3:2) + TD(5:4)	113	0.34	0.08	2.84	0.21

The results are taken, as the most promising ones, from Stuchlík *et al.* (2014). The two cases of the neutron star parameters that are in agreement with the Hartle–Thorne model of the neutron stars are shaded. They are those corresponding to the best fits of the observational data of twin HF QPOs.

The mass M and spin a ranges determined by the fitting procedure in Stuchlík *et al.* (2014) for acceptable combinations of frequency-relation pairs are illustrated

[4]The fitting procedure has been realized in the ranges of M and a predicted by the RS model with data given by the energy switch effect, but we convinced ourselves that outside these ranges the fits are worse than inside of them.

in Figs. 1 and 2 and summarized in Table 2. The best fit is obtained for the combination of frequency pairs RP1+RP.

The results of the fitting procedure will be further tested by confrontation with detailed Hartle–Thorne theoretical models (Hartle and Thorne 1968, Chandrasekhar and Miller 1974, Miller 1977) describing slowly rotating neutron stars that are constructed under the observationally given constraint of the rotation frequency 580 Hz (or 290 Hz) relevant for the 4U 1636–53 neutron star (Strohmayer and Markwardt 2002), using the variety of widely accepted equations of state that were studied in Urbanec *et al.* (2013). We assume a detailed test of a much more extended family of acceptable equations of state in a future paper.

The results of the RS model have to be related in future to the limits on the 4U 1636–53 neutron star parameters indicated by other possible observational phenomena. In fact, a preliminary result of simultaneous treatment of the twin peak HF QPOs and profiled (X-ray) spectral lines indicates the neutron star mass to be $M \approx 2.4\ \mathrm{M}_\odot$ (Sanna *et al.* 2012) that gives an important restriction on the results of the RS model and restricts substantially the variety of allowed combinations of frequency relations used in the RS model. However, we clearly need more detailed study of the profiled spectral lines based on the precise predictions of the character of the external spacetime of the neutron star.

3. Hartle–Thorne Model of Rotating Neutron Stars

The Hartle–Thorne theory represents a standard approximate method of constructing models of compact stars (neutron stars, quark stars, white dwarfs) within general relativity, assuming rigid and slow rotation of the stars (Hartle 1967, Hartle and Thorne 1968). It is treating deviations away from the spherical symmetry as perturbations with terms up to a specified order of the rotational angular velocity Ω of the compact star. Going up to second order in Ω, the theory gives the lowest order expressions for the frame dragging ω, the moment of inertia $I = J/\Omega$, with J denoting the angular momentum of the star, the shape distortion caused by centrifugal effects, the quadrupole moment Q and the change in the gravitational mass due to rotation δM. Recent results indicate that the slow rotation approach is quite correct for all the observed rotating neutron stars, even in the case of the fastest observed pulsar PSR J1748–2446ad with rotational frequency ≈ 716 Hz (Urbanec *et al.* 2013). For very fast rotation only, near to that giving centrifugal break-up, we have to solve numerically the full set of the Einstein equations rather than using the approximate approach of Hartle–Thorne theory – see models presented in Bonazzola *et al.* (1998) and Stergioulas (2003).

For our purposes, the second-order slow-rotation Hartle–Thorne approximate theory developed in Hartle and Thorne (1968) and Chandrasekhar and Miller (1974) is quite appropriate because of the rotation frequency observed for the neutron star in 4U 1636–53. Then the Hartle–Thorne geometry describing both the internal and

external spacetime takes in the geometric units with $c = G = 1$ the form

$$\begin{aligned} ds^2 = & -e^{2\nu_0}\left[1+2h_0(r)+2h_2(r)P_2(\theta)\right]dt^2 \\ & +e^{2\lambda_0}\left\{1+\frac{e^{2\lambda_0}}{r}\left[2m_0(r)+2m_2(r)P_2(\theta)\right]\right\}dr^2 \\ & +r^2\left[1+2k_2(r)P_2(\theta)\right]\left\{d\theta^2+\left[d\phi-\omega(r)\,dt\right]^2\sin^2\theta\right\} \end{aligned} \tag{9}$$

where ν_0, λ_0 and the coordinates are identical with corresponding spherical non-rotating solution, $\omega(r)$ is a perturbation of order Ω, representing the frame dragging, and $h_0(r)$, $h_2(r)$, $m_0(r)$, $m_2(r)$, $k_2(r)$ are perturbations of order Ω^2. All of these perturbations are functions of the radial coordinate only. The non-spherical angular dependence is determined by the second-order Legendre polynomial $P_2(\theta) = \frac{1}{2}\left(3\cos^2\theta - 1\right)$.

All the perturbation functions have to be calculated under appropriate boundary conditions at the center and at the surface of the compact star. The second-order perturbations are labeled with a subscript indicating their multipole order: $l = 0$ for spherical perturbations, $l = 2$ for the quadrupole perturbations representing the deviation away from the spherical symmetry. By matching the internal and external solution at the star surface, the external parameters of the compact star as measured by distant observers can be calculated: the mass M, angular momentum J and quadrupole moment Q that fully characterize the external gravitational field in the slow-rotation approximation, if one is retaining only perturbations up to the second order.

To construct the internal solution, the Einstein equations are solved with the source term given by the energy momentum of a perfect fluid. Rigid rotation of an axisymmetric configuration means that the four velocity has components

$$U^t = \left[-\left(g_{tt} - 2\Omega g_{t\phi} + \Omega^2 g_{\phi\phi}\right)\right]^{1/2}, \quad U^\phi = \Omega U^t. \tag{10}$$

The derivation of the equations for the perturbation quantities together with boundary conditions was given in detail in Hartle and Thorne (1968), Chandrasekhar and Miller (1974), Miller (1977). We will not repeat this in the present paper. We use the same procedures as those presented in Miller (1977).

4. Equations of State

The crucial ingredient of the compact star models is the equation of state describing properties of matter constituting them. Neutron stars are expected to consist of neutrons closely packed in β-equilibrium with protons, electrons and at high densities also muons, hyperons, kaons and possibly other particles. Their central densities correspond to microphysics that is not well understood, therefore, they serve as laboratories of nuclear matter under extreme conditions, giving complementary information to those obtained in the collider experiments.

A wide range of approaches for nucleon-nucleon interactions and their role in modeling of the structure of neutron stars has been used – see the review by Lattimer and Prakash (2007). An alternative to the standard neutron star picture is represented by quark stars consisting partially or fully from deconfined quarks. The most radical version of this approach is represented by strange stars consisting entirely from deconfined quarks (Farhi and Jaffe 1984, Haensel *et al.* 1986, Colpi and Miller 1992). It is based on the suggestion of Witten (1984) that matter consisting of equal numbers of up, down and strange quarks represent the absolute ground state of strongly interacting matter. It is important to mention that the strange stars have to be bound together by a combination of the strong and gravitational forces, in contrast to neutron stars where only the gravity is responsible for the binding. Here we restrict attention on the equations of state governing the neutron stars only.

We consider a set of neutron-star matter equations of state that are based on various approaches – following the recent study of the neutron star properties related to the behavior of the quadrupole moment (Urbanec *et al.* 2013). We give a brief review of these equations of state, details can be found in Urbanec *et al.* (2013) and the original literature.

We choose relatively wide set of Skyrme parameterizations, whose labels are starting with S; see Stone *et al.* (2003) for details of Skyrme potential and differences between various parameterizations. We use two variants of APR model based on the variational theory reflecting the three body forces and the relativistic boost corrections (Akmal *et al.* 1998). APR corresponds to $A18+\delta v+\mathrm{UIX}^{*}$, while APR2 corresponds to $A18+\mathrm{UIX}$, where relativistic boost corrections are not included. The UBS equation of state is based on the relativistic Dirac–Brueckner–Hartree–Fock mean field theory (Urbanec *et al.* 2010a) and corresponds to model originally labeled as H. The non-relativistic Brueckner–Hartree–Fock theory is represented by the equation of state labeled as BBB2 (Baldo *et al.* 1997). We also use GlendNH3 (Glendenning 1985) and BalbN1H1 (Balberg and Gal 1997) equation of state including the hyperons at high densities. FPS is the very well know EoS and has been used very often in the past (Lorenz *et al.* 1993) and BPAL12 is very soft EoS giving very low maximum mass (Bombaci 1995). Stiff equations of state were recently constructed in the framework of the auxiliary field diffusion Monte Carlo technique and are labeled as Gandolfi (Gandolfi *et al.* 2010). Our selection of EoS represents wide range of possible models. However, some of these do not meet current observations (Steiner *et al.* 2010, Demorest *et al.* 2010, Antoniadis *et al.* 2013). Here, we focus on the selection of the acceptable variants of the RS model of QPOs using the Hartle–Thorne theory of neutron stars that is properly applied to the restricted set of the equations of state.

It is useful to give the maximal values of the neutron star parameters M and a obtained in the framework of different approaches to the equation of state. It follows from general relativistic restrictions that mass of a neutron star cannot exceed $M_{\mathrm{max}} \approx 3\ \mathrm{M}_{\odot}$ (Rhoades and Ruffini 1974). The realistic equations of state

put limit on the maximal mass of neutron stars $M_{\rm maxN} \approx 2.8\ {\rm M}_\odot$ (Postnikov *et al.* 2010) – the extremal maximum $M_{\rm maxN} \approx 2.8\ {\rm M}_\odot$ is predicted by the field theory (Müller and Serot 1996). The limit of $M_{\rm maxN} \approx 2.5\ {\rm M}_\odot$ is predicted by the Dirac–Brueckner–Hartree–Fock approach in some special case (Müther *et al.* 1987) or by some Skyrme models. The variational approaches (Akmal and Pandharipande 1997, Akmal *et al.* 1998) and other approaches (Urbanec *et al.* 2010a) allow for $M_{\rm maxN} \approx 2.25\ {\rm M}_\odot$.

On the neutron star dimensionless spin the limit of $a < a_{\rm maxN} = 0.7$ has been recently reported on the basis of numerical, non-approximate methods, independently of the equation of state (Lo and Lin 2011). The Hartle–Thorne theory can be well applied up to the spin $a \approx 0.4$ (Urbanec *et al.* 2013).

In the Hartle–Thorne models of rotating neutron stars the spin of the star is linearly related to its rotation frequency. The rotation frequency of the neutron star at the atoll source 4U 1636–53 has been observed at $f_{\rm rot} \approx 580$ Hz (or $f_{\rm rot} \approx 290$ Hz if we observe doubled radiating structure, Strohmayer and Markwardt 2002). Such a rotation frequency is sufficiently low in comparison with the mass shedding frequency, and the Hartle–Thorne theory can be applied quite well, predicting spins much lower than the maximally allowed spin. The theory of neutron star structure then implies for a wide variety of realistic equations of state the spin in the range (Stergioulas 2003, Urbanec *et al.* 2013)

$$0.1 < a < 0.4. \tag{11}$$

Of course, the upper part of the allowed spin range corresponds to the rotation frequency $f_{\rm rot} \approx 580$ Hz, while the lower part corresponds to $f_{\rm rot} \approx 290$ Hz. The related restriction on the neutron star (near-extreme) mass reads

$$M < 2.8\ {\rm M}_\odot. \tag{12}$$

Detailed comments on the precision of the Kerr geometry approximating the Hartle–Thorne geometry in dependence on the spacetime parameters a and q/a^2 can be found in Stuchlík and Kološ (2015). For the HF QPO models the differences induced by the Kerr approximation could be smaller than five percent for the dimensionless spin $a < 0.4$.

5. Testing the RS Model by Equations of State Applied in the Hartle–Thorne Model of the Neutron Star in the Source 4U 1636–53

5.1. Selection of the Relevant Variants of the RS Model

The resulting limits on the mass M and spin a of the 4U 1636–53 neutron star implied by the data fitting procedure realized in the framework of the RS model of HF QPOs are presented in Table 2 taken from Stuchlík *et al.* (2014) and reflected in Figs. 1 and 2. The precision of the mass and spin estimates is also reflected in Figs. 1 and 2. The Hartle–Thorne models are constructed for a variety of acceptable

equations of state discussed above (and studied in Urbanec *et al.* 2013) for both possible rotational frequencies of the 4U 1636–53 neutron star. We use nine parameterizations of the Skyrme equation of state (SkT5, Sk0', Sk0, SLy4, Gs, SkI2, SkI5, SGI, SV) and other nine equations of state (UBS, APR, FPS, BBB2, BPAL12, BalbN1H1, GlendNH3, Gandolfi, APR2) that well represent the variety of equations of state. The results of the Hartle–Thorne model that are calculated for the equations of state under consideration are illustrated in the $M-a$ plane in Fig. 1 for both the assumed neutron star rotation frequencies $f_{\rm rot} \approx 290$ Hz and $f_{\rm rot} \approx 580$ Hz. Clearly, all the mass-spin dependencies constructed for $f_{\rm rot} \approx 290$ Hz can be excluded. In Fig. 2 we give detailed picture of fitting the mass and spin range implied by the acceptable variants of the RS model by the $a(M)$ curves constructed for the acceptable EoS with the rotation frequency $f_{\rm rot} \approx 580$ Hz.

We immediately see that no equation of state allows to construct a Hartle–Thorne model that can fit the RS model data, if we assume the rotational frequency

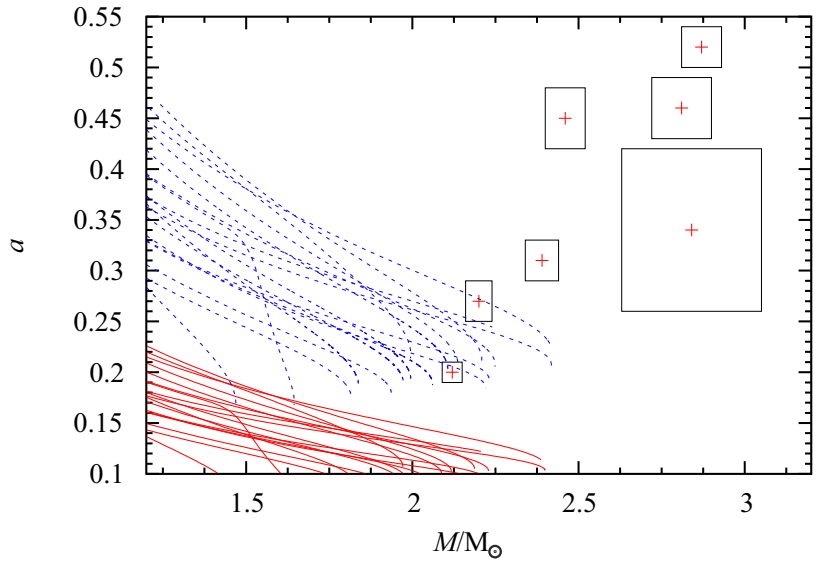

Fig. 1. Hartle–Thorne models of neutron stars with rotation frequency $f_{\rm rot} \approx 290$ Hz (red) and $f_{\rm rot} \approx 580$ Hz (blue), for a variety of EoS considered in Urbanec *et al.* (2013): SkT5, Sk0', Sk0, SLy4, Gs, SkI2, SkI5, SGI, SV – Skyrme equations (Stone *et al.* 2003), UBS equation (Urbanec *et al.* 2010a), FPS equation (Lorenz *et al.* 1993), APR (Akmal *et al.* 1998), BBB2 equation (Baldo *et al.* 1997), BPAL12 equation (Bombaci 1995), BalbN1H1 equation (Balberg and Gal 1997), GlendNH3 equation (Glendenning 1985), APR2 equation (Akmal *et al.* 1998), Gandolfi equation (Gandolfi *et al.* 2010). Each equation of state applied in the Hartle–Thorne model predicts for a fixed rotational frequency a sequence of stable states represented by a curve in the $M-a$ plane. Its final point indicates an instability. Clearly, all predicted values of the 4U 1636–53 neutron star spacetime parameters M, a related to $f_{\rm rot} \approx 290$ Hz are located outside the predictions of the Hartle–Thorne models.

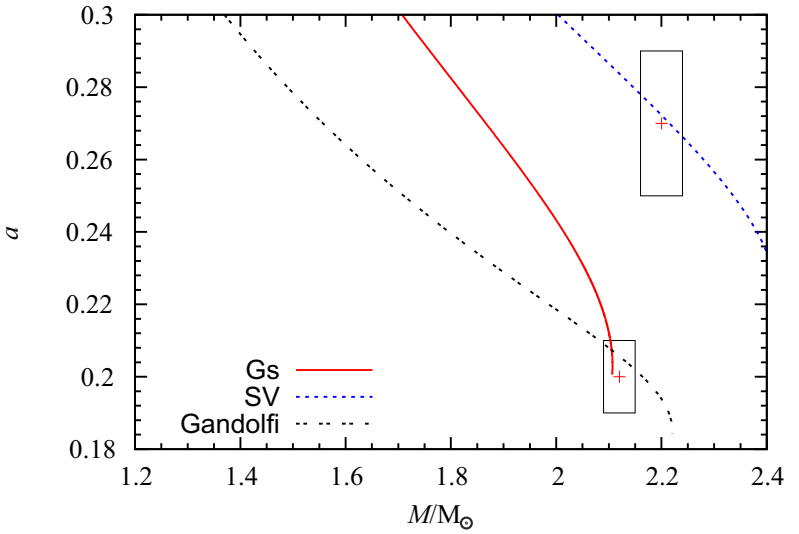

Fig. 2. Hartle–Thorne models of neutron stars with rotation frequency $f_{\rm rot} \approx 580$ Hz are illustrated for the $a(M)$ dependencies related to the two best fits of the observational data by the RS model. The acceptable sequences of equilibrium configurations predicted by the Hartle–Thorne model are constructed for two equations of state (Skyrme SV EoS for RP1+RP variant, and Gandolfi EoS for the RP1+TP1 variant). Notice that the variant of the RS model predicting the lower parameters of $M = 2.12$ M$_\odot$ and $a = 0.20$ is also very close to the final state given by the sequence of equilibrium states predicted by the Skyrme Gs EoS, indicating possibility of an instability of the neutron star in the 4U 1636–53 system in near future.

of the 4U 1636–53 neutron star $f_{\rm rot} \approx 290$ Hz. For the rotational frequency $f_{\rm rot} \approx 580$ Hz, the Hartle–Thorne models give very interesting restrictions that are in significant agreement with results of the fitting the HF QPO data in the framework of the RS model. The Hartle–Thorne model based on the Skyrme equation of state SV meets with high precision the prediction of the RP1+RP version of the RS model that gives the best fit to the twin peak HF QPO data observed in the 4U 1636–53 source for the neutron star parameters $M \approx 2.20$ M$_\odot$ and $a \approx 0.27$.[5] The Hartle–Thorne model based on the Gandolfi equation of state meets with high precision the prediction of the RP1+TP1 version of the RS model that gives the second best fit to the observational data of the twin HF QPOs in 4U 1636–53 for a neutron star having parameters $M \approx 2.12$ M$_\odot$ and $a \approx 0.20$. Notice that the variant of the RS model giving the second best fit is in accord with another version of the Skyrme equation of state (Gs) which predicts the neutron star with parameters $M \approx 2.11$ M$_\odot$ and $a \approx 0.20$. Such a result demonstrates that the 4U 1636–53

[5]The same precision of the fit, namely $\chi^2 \approx 55$, is obtained for the TP+RP version of the RS model. However, in this case the predicted mass and spin, $M \approx 2.87$ M$_\odot$ and $a \approx 0.52$, are outside the values acceptable by the neutron star models.

neutron star could be in a state very close to an instability, as the neutron star mass and spin indicated by the HF QPO data fitting procedure can correspond to the final state of the evolution of the neutron stars rotating with the frequency $f_{\rm rot} \approx 580$ Hz and governed by the Skyrme equation of state Gs – see Fig. 2. Predictions of all the other variants of the RS model are located in the $M-a$ plane at positions that are evidently out of the scope of all the equations of state considered in the present paper. We can expect that this is true also for all other variants of the presently known equations of state.

5.2. Parameters and the Shape of the Neutron Star

Shape of isobaric surfaces $P = \text{const}$ and the shape of the neutron star surface $P = 0$ are given by

$$r(P = \text{const}, \theta) = r_0(P) + \xi_0(r_0) + \xi_2(r_0) P_2(\cos\theta) \tag{13}$$

where r_0 is the spherical coordinate and functions ξ_0 and ξ_2 are given by the relations (Miller 1977)

$$\xi_0(r) = \frac{r[r-2m(r)]p_0}{4\pi r^3 P + m(r)}, \tag{14}$$

$$\xi_2(r) = \frac{r[r-2m(r)]p_2}{4\pi r^3 P + m(r)} \tag{15}$$

and

$$p_2(r) = -h_2(r) - \frac{1}{3} r^2 \mathrm{e}^{-2\nu_0} \omega^2. \tag{16}$$

The calculations were performed using the detailed set of equations presented in Miller (1977). Then equatorial and polar radii governing the surface shape of the rotating neutron star read

$$R_{\rm eq} = R_0(P) + \xi_0(R_0) - \frac{1}{2}\xi_2(R_0), \tag{17}$$

$$R_{\rm pol} = R_0(P) + \xi_0(R_0) + \xi_2(R_0). \tag{18}$$

The agreement of the Hartle–Thorne neutron star models based on the Skyrme and Gandolfi equations of state with two best fits of the observational data of twin HF QPOs observed in the source 4U 1636–53 enables to predict in detail properties of the neutron star in this source. Namely, we are able to find along with the two known parameters, mass M and spin a, also the radius in the equatorial plane $R(\theta = \pi/2)$ and along the symmetry axis $R(\theta = 0)$ and whole the shape of the neutron star surface, the moment of inertia I, and quadrupole moment Q and its dimensionless form $q = QM/J^2$. Then we can calculate also the parameter representing compactness of the neutron stars in dependence on the latitude

$$C_\theta = \frac{R(\theta)}{2M}. \tag{19}$$

We can consider the characteristic values of the compactness parameter related to the equatorial plane $\theta = \pi/2$ and the symmetry axis $\theta = 0$. Here we give for simplicity the compactness parameter related to the basic, spherically symmetric model that is a starting point of the Hartle–Thorne models, given by

$$C_0 = \frac{R_0}{2M_0}. \tag{20}$$

The results of the Hartle–Thorne model calculations for all three equations of state giving acceptable agreement with the data predicted by the RS model are presented in Table 3. For the Skyrme equation of state SV, and the Gandolfi equation of state, the neutron star parameters are given for the mass parameter corresponding to the mean value of the data fitting (Stuchlík *et al*. 2014). In the case of the Skyrme equation of state Gs, the mass parameter of the neutron star ($M \approx 2.11$ M$_\odot$) corresponds to the maximal value predicted by this equation of state, *i.e.*, it gives the instability point of the neutron stars governed by this equation of state. This mass parameter is lower than the related mean value given by the data fitting, but it falls into the allowed range of the mass parameter.

T a b l e 3

Parameters of neutron stars predicted by the selected equations of state giving Hartle–Thorne models compatible with the fitting of the twin HF QPOs observed in 4U 1636–53

EoS	M [M$_\odot$]	$R_{\rm eq}$ [km]	a	q	q/a^2	$R_0/(2M_0)$
Gandolfi	2.12	10.75	0.205	0.0723	1.71	1.72
Gs	2.11	10.84	0.201	0.0676	1.68	1.75
SV	2.20	13.41	0.272	0.1940	2.60	2.07

The mass is fixed to the mean value given by the fitting procedure with exception of the Skyrme equation of state Gs where it corresponds to the final state indicating an instability. The spin predicted by the Hartle–Thorne model fits the range given by the error determined by the data fitting. All models predict very compact neutron stars with low value of the parameter q/a^2.

6. Self-Consistency Test by the Hartle–Thorne Geometry

Assuming that the external geometry of the 4U 1636–53 neutron star can be approximated by the Kerr geometry, we have found that the two most precise variants of the RS model can be fitted by realistic EoS applied in the Hartle–Thorne model of slowly rotating neutron stars. For the RP1+RP variant, the Skyrme SV EoS predicts $M \approx 2.20$ M$_\odot$, $a \approx 0.272$, $q/a^2 \approx 2.60$. For the RP1+TP1 variant, the Gandolfi EoS predicts $M \approx 2.12$ M$_\odot$, $a \approx 0.205$, $q/a^2 \approx 1.71$. For this RS variant, also the Skyrme Gs EoS gives acceptable values of $M \approx 2.11$ M$_\odot$, $a \approx 0.201$,

$q/a^2 \approx 1.68$, however, this estimated mass parameter is at the maximum allowed mass for the EoS.

We have to perform now a self-consistency test of the Kerr geometry approximation applied in fitting the observational data. We have to check, if fitting the observational data by the χ^2-test using the orbital and epicyclic frequencies related to the Hartle–Thorne geometry with parameters M, a, q governed by the acceptable EoS gives results comparable or better than the fitting based on the assumption of the Kerr geometry approximation. We carry out the self-consistency test in the following three steps.

First, we characterize the sequence of configurations given by the Hartle–Thorne model for the acceptable EoS and the rotational frequency of the neutron star $f_{\rm rot} = 580$ Hz – see Fig. 3. The free parameter is the mass M and we represent the sequence by the functions $a(M)$ and $q/a^2(M)$. For each considered EoS we show the Hartle–Thorne model for $M > 1.2$ M$_\odot$, and we follow the sequence of allowed neutron stars to the limiting values of the parameters $M, a, q/a^2$ corresponding to the maximal allowed mass for the considered EoS. For each of the EoS, the closest approach of the Hartle–Thorne model to the Kerr geometry occurs for the maximal mass allowed by given EoS. We can see that closest approach to the Kerr geometry is allowed for the Hartle–Thorne model based on the Gandolfi EoS, enabling the lowest value of $q/a^2 \approx 1.5$ for $M_{\rm max} \approx 2.24$ M$_\odot$. On the other hand, the largest difference from the Kerr geometry approximation are expected for the Skyrme SV model with the lowest value of $q/a^2 \approx 1.9$. The maximal mass is highest for this EoS, reaching $M_{\rm max} \approx 2.4$ M$_\odot$.

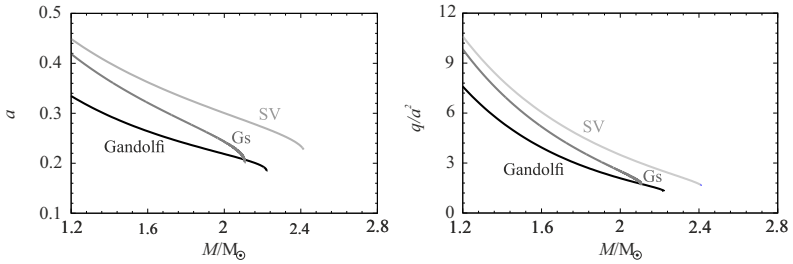

Fig. 3. Sequence of the Hartle–Thorne spacetime parameters implied by the Gandolfi, Skyrme Gs and Skyrme SV EoS for the rotational frequency $f_{\rm rot} = 580$ Hz. *Left*: Spin (a) as a function of mass (M). *Right*: Reduced quadrupole moment (q/a^2) as a function of mass (M). All sequences are constructed for the mass interval 1.2 M$_\odot < M < M_{\rm max}$.

Second, we define the orbital and epicyclic radial and vertical frequencies of the quasicircular geodesic motion in the Hartle–Thorne geometry, $\nu_{\rm K}(r;M,a,q)$, $\nu_r(r;M,a,q)$, $\nu_\theta(r;M,a,q)$ (Abramowicz *et al.* 2003, Török *et al.* 2008b). For completeness, we give the explicit expressions for the frequencies in the Appendix.

Third, using the Hartle–Thorne orbital and epicyclic frequencies, we repeat the least-square (χ^2-test) fitting procedure for the same sample of the observational

data in the 4U 1636–53 atoll source as those considered in our previous paper (Stuchlík *et al.* 2014). For the self-consistency test, we study only the two selected variants of the RS model, RP1+RP and RP1+TP1, along the sequences of the neutron star parameters M, a, q related to the allowed EoS and the rotational frequency of the neutron star.[6]

The results of the fitting procedure are given in Fig. 4 for the RP1+RP variant of the RS model and the Skyrme SV EoS. Along with the fitting based on the Hartle–Thorne geometry, we repeat for comparison also the results obtained under the Kerr approximation of the neutron star external spacetime. The fitting procedure implies the best fit $\chi^2 = 101$. In comparison to the best fit based on the Kerr approximation ($\chi^2 = 55$, $M \approx 2.20\ \mathrm{M}_\odot$, $a \approx 0.272$), the mass parameter is shifted to lower value of $M \approx 2.11\ \mathrm{M}_\odot$, and higher value of spin $a \approx 0.286$. Moreover, at the values of mass and spin predicted by the Kerr approximation when $\chi^2 = 55$, Stuchlík *et al.* 2014), the Hartle–Thorne geometry implies $\chi^2 > 1000$. Such a large discrepancy is caused by relatively large value of the parameter $q/a^2 \approx 3$ when large errors of the Kerr approximation are expected. The resulting value of the Hartle–Thorne best fit, $\chi^2 = 101$, is too high in comparison with the Kerr approximation value, $\chi^2 = 55$, and we can conclude that the RP1+RP variant of the RS model is not satisfying the self-consistency test.

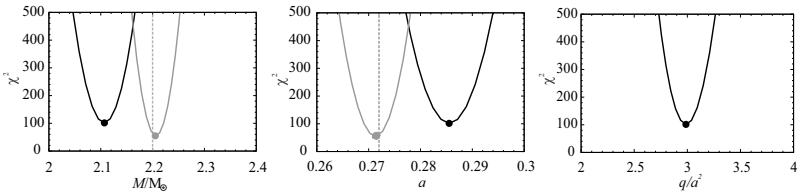

Fig. 4. Results of the fitting procedure for the RP1+RP variant of the RS model and the Skyrme SV EoS. χ^2 dependency on M (*left*), a (*middle*), and q/a^2 (*right*). The gray curves correspond to the Kerr approximation. Dashed lines correspond to values of M and a from Table 3.

For the RP1+TP1 variant of the RS model and the Gandolfi EoS, the results of the fitting procedure are presented in Fig. 5. We again give for comparison the results of the best fit obtained for the Kerr geometry approximation ($\chi^2 = 61$, $M \approx 2.12\ \mathrm{M}_\odot$, $a \approx 0.205$). The best fit based on the Hartle–Thorne geometry gives for the Gandolfi EoS $\chi^2 = 64$, a slight decrease of the mass parameter to $M = 2.10\ \mathrm{M}_\odot$ and a very slight increase of the spin parameter to $a = 0.208$. Therefore, we can conclude that the RP1+TP1 model with the Gandolfi EoS satisfies the self-consistency test, as both precision of the fit and the estimate of the neutron star

[6]The fitting of the data can be done for the Hartle–Thorne geometry by considering the neutron star parameters M, a, q as free parameters. However, such a fitting is extremely time consuming. We use the fitting tied to the EoS and the rotation frequency of the neutron star, along the curve characterized by the functions $a(M)$, $q(M)$ in the space of spacetime parameters. This is much faster procedure, being quite relevant for our self-consistency test.

parameters are in very good agreement with the predictions of the Kerr approximation used in the fitting procedure. The precision of the mass estimate is on the level of one percent. The best fit parameter $q/a^2 = 1.77$ is low enough to enable the high coincidence of predictions of the Hartle–Thorne geometry and the Kerr approximation.

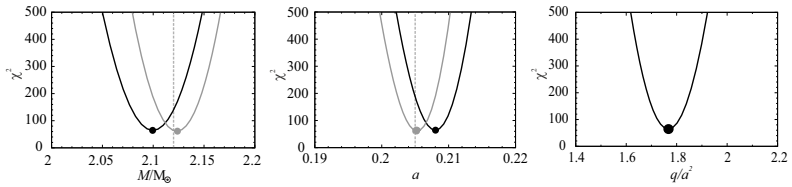

Fig. 5. Results of the fitting procedure for the RP1+TP1 variant of the RS model and the Gandolfi EoS. χ^2 dependency on M (*left*), a (*middle*) and q/a^2 (*right*). The gray curves correspond to the Kerr approximation. Dashed lines correspond to values of M and a from Table 3.

For the RP1+TP1 variant of the RS model and the Skyrme Gs EoS, the results of the fitting procedure are presented in Fig. 6. We again give for comparison the results of the best fit obtained for the Kerr geometry approximation ($\chi^2 = 61$, $M \approx 2.12\ \mathrm{M}_\odot$, $a \approx 0.201$). However, for this EoS the maximal allowed mass ($M \approx 2.11\ \mathrm{M}_\odot$) is slightly lower than the Kerr approximation estimate. The best fit based on the Hartle–Thorne geometry gives for the Skyrme Gs EoS $\chi^2 = 64$, and a slight decrease of the mass parameter to $M = 2.10\ \mathrm{M}_\odot$, still very close to the maximal allowed mass for this EOS, and a slight increase of the spin parameter to $a = 0.211$. Therefore, we can conclude that the RP1+TP1 model with the Skyrme Gs EoS satisfies the self-consistency test, as both precision of the fit and the estimate of the neutron star parameters are in very good agreement with the predictions of the Kerr approximation. The precision of the mass estimate is on the level of one percent again. At the best fit, the parameter $q/a^2 = 1.83$ is still low enough to enable the high coincidence of predictions of the Hartle–Thorne geometry and the Kerr approximation. However, the predicted mass of the neutron star is very close to the maximum related to the Skyrme Gs EoS, bringing some doubts on the applicability of this EoS for the source 4U 1636–53. If the Skyrme Gs EoS is the proper one, than we could expect some strong instability of this source in near future.

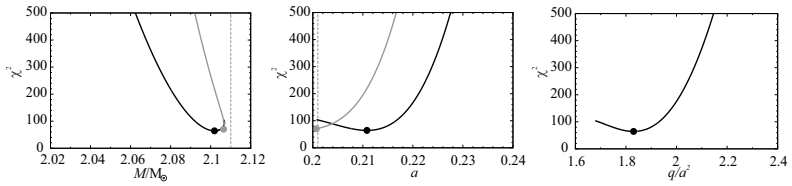

Fig. 6. Results of the fitting procedure for the RP1+TP1 variant of the RS model and the Gs EoS. χ^2 dependency on M (*left*), a (*middle*) and q/a^2 (*right*). The gray curves correspond to the Kerr approximation. Dashed lines correspond to values of M and a from Table 3.

The results of the χ^2-test realized for the external Hartle–Thorne geometry with parameters governed by the acceptable EoS are summarized in Table 4. These results give the self-consistency test of the results obtained due to the assumption of Kerr approximation of the neutron star external spacetime. We can see that only the RP1+TP1 variant of the RS model can be considered as surviving the self-consistency test. Moreover, the Gandolfi EoS can be considered as the most plausible one in explaining the fitting of observational data related to the twin HF QPOs observed in the 4U 1636–53 source. Notice that the best fits implied by the Hartle–Thorne geometry give in all considered cases χ^2 value that is higher (worse fit) than in the case of the fits based on the Kerr approximation. Of course, we could obtain better fits by the Hartle–Thorne geometry for other values of the neutron star parameters. But in such a case, the fits have to be related to the parameters M, a, q considered as free parameters, while in our case the spacetime parameters were confined by the chosen EoS and the observed rotation frequency of the source. Therefore, we cannot exclude that in future an EoS will be discovered that will enable to obtain better fit to the observational data than those presented in our paper. However, we can note that all EoS considered in our paper give fits worse than those implied by the Gandolfi EoS.

T a b l e 4

Results of the χ^2-test realized for the external Hartle–Thorne geometry with parameters governed by the acceptable EoS

EoS	Models	M [$M_\odot$]	a	q/a^2	χ^2
Gandolfi	RP1+TP1	2.10	0.208	1.77	64
Gs	RP1+TP1	2.10	0.211	1.83	64
SV	RP1+RP	2.11	0.286	2.99	101

7. Discussion

The atoll source 4U 1636–53 seems to be one of the best test beds for both the models of strong gravity phenomena and the microphysics determining equations of state governing the internal structure and exterior of neutron stars. This is due to simultaneous availability of relatively good observational data of the HF QPOs occurring in the innermost parts of the accretion disk where the extremely strong gravity is relevant, enabling thus to put precise restrictions on the neutron star external spacetime parameters in the framework of the RS model, and the knowledge of the rotational frequency of the neutron star that enables a precise modeling of the internal and external structure of rotating neutron stars in the framework of the Hartle–Thorne theory, for the whole variety of the equations of state. Strong restrictions on the acceptable versions of the RS model can be obtained, because the

precise knowledge of the rotational frequency of the neutron star implies a narrow evolution line for the Hartle–Thorne models in the $M-a$ plane that has to be adjusted to relatively precisely determined points in the $M-a$ plane predicted by the acceptable variants of the RS model of the observed HF QPOs.

The RS model can be well tested for the atoll source 4U 1636–53 since this source demonstrates two resonant radii in the observational data. For all relevant pairs of the oscillatory frequency relations of the RS model, the range of allowed values of the mass and dimensionless spin of the neutron star at 4U 1636–53 has been given in Stuchlík *et al.* (2012). The most promising frequency pairs predicting the range of the 4U 1636–53 neutron star mass and spin in accord with neutron star structure theory were tested by fitting the frequency relation pairs to the observational data on the HF QPOs separated into two parts related to the pair of frequency relations. Only the frequency relations containing geodesic orbital and epicyclic frequencies, or some combinations of these frequencies, were considered (Stuchlík *et al.* 2014). Nevertheless, it should be noted that the cause of the switch of the pairs of the oscillatory modes is not necessarily tied to the resonant phenomena related to the oscillations governed by the frequencies of the geodesic motion. The switch can be related, *e.g.*, to the influence of the magnetic field of the neutron star and after the switch the Alfvén wave model can be relevant (Zhang *et al.* 2006). However, limiting the study to the resonant phenomena and frequencies of the geodesic origin, the number of free parameters of the model is restricted to the mass M and dimensionless spin a of the neutron star, as we are able to demonstrate that the predicted mass of the neutron star is large enough to guarantee with high precision independence of the geodesic frequencies on the quadrupole moment of the neutron star and applicability of the Kerr approximation in describing the neutron star external geometry (Urbanec *et al.* 2013). Inclusion of the non-geodesic oscillation modes and non-resonant causes of the switch is postponed to future studies and could be relevant for some other sources containing neutron stars.

The fitting procedure performed in the framework of the RS model is shown to be more precise by almost one order in comparison to the standard fitting based on the individual frequency relations that were used in pairs in the RS model (Stuchlík *et al.* 2014). For example, the fitting by the standard RP model predicts the best fit along the mass–spin relation $M(a) = M_0\left[1+0.75(a+a^2)\right]$ with rather poor maximal precision of the χ^2 test given by $\chi^2 \approx 350$ and $\chi^2/\mathrm{dof} \approx 16$. The other frequency relations give comparable poor precision (Török *et al.* 2012). Similar results with poor precision were obtained also for models with frequency relations of non-geodesic origin (Lin *et al.* 2011). On the other hand, the best fit obtained for the RS model with frequency relation pair RP1+RP gives $\chi^2 \approx 55$ and $\chi^2/\mathrm{dof} \approx 2.6$ that is quite acceptable due to the character of the data distribution (Török *et al.* 2012). The RP1+TP1 version of the RS model predicts the second best fit with precision that is given by $\chi^2 \approx 61$ and $\chi^2/\mathrm{dof} \approx 2.9$.

Testing the RS model using the Hartle–Thorne theory with fixed rotation fre-

quency and a variety of equations of state brings another efficient selection of the variants of the RS model. The results are illustrated in Figs. 1 and 2 and clearly demonstrate that only the two variants of the RS model giving the best results of the data fitting are acceptable by the Hartle–Thorne models of the neutron star structure, if the rotation frequency is $f_{\rm rot} \approx 580$ Hz. The RP1+RP version of the RS model predicts mean values of mass $M \approx 2.20$ M$_\odot$ and spin $a \approx 0.27$ and these are the data that can be met precisely by the Hartle–Thorne models – namely for the Skyrme equation of state SV. The RP1+TP1 version of the RS model predicts the mean values of mass $M \approx 2.12$ M$_\odot$ and spin $a \approx 0.20$. This mass and spin can be explained by the Hartle–Thorne model with the Gandolfi equation of state. It is interesting that the prediction of the Hartle–Thorne model based on the Skyrme equation of state Gs enters the allowed range of the mass and spin parameters given by the RP1+TP1 version of the RS model, although it does not reach the mean value of the mass parameter, as demonstrated in Fig. 2. If this equation of state is the real one, the neutron star in the source 4U 1636–53 has to be in a state very close to instability leading to some form of collapse and dramatic observational phenomena. Mass and spin of the neutron star predicted by the other versions of the RS model acceptable due to the data fitting are completely out of the range of the $M-a$ dependencies predicted by the Hartle–Thorne model for the whole variety of available equations of state.

In the special situations related to accreting neutron stars with near-maximum masses, the Kerr metric can be well applied in calculating the orbital and epicyclic geodesic frequencies, as has been done in the present paper. It should be stressed that the neutron star mass and spin parameters predicted by the two relevant findings of frequency pairs are in agreement with the assumption of near-maximum masses of the neutron stars – see Fig. 2. For each acceptable equation of state and the observed rotation frequency of the neutron star, the Hartle–Thorne model has been constructed, giving thus not only mass M and spin a, but also the dimensionless quadrupole moment q and other characteristics as the equatorial radius and the compactness. The detailed results of the Hartle–Thorne model obtained for the three equations of state that can be in the play are shown in Table 3. The results clearly demonstrate that in all three cases we obtain a very compact neutron star, especially for the Gandolfi and Skyrme Gs equations of state, related to the second best fit with mass parameter $M \approx 2.12$ M$_\odot$ and spin $a = 0.2$, having radius $R \approx 3.5M$. The spin exactly predicted by the Hartle–Thorne model is slightly overcoming the mean value of the spin of the data fitting of the RS model, but it belongs to the allowed range. The parameter $q/a^2 \approx 1.7$ corresponds to the external Hartle–Thorne spacetime that is very close to the Kerr spacetime.

The self-consistency test of the RP1+TP1 variant of the RS model using the Hartle–Thorne geometry, related to the Gandolfi EoS, confirms this choice, since the results of the χ^2-test are very close to those obtained due to the test in the Kerr geometry approximation – both for the value of χ^2 at the best fit, and the close

values of the mass and spin spacetime parameters. Similar results are obtained by the self-consistency test for the Hartle–Thorne model related to the Skyrme Gs EoS. However, the test confirms also the conclusion that the estimated mass has to be very close to the maximum allowed by the EoS, lowering thus the potential relevance of this EoS for the 4U 1636–53 neutron star.

For the RP1+RP variant of the RS model, the Hartle–Thorne model using the Skyrme SV EoS, related to the neutron star with mass $M \approx 2.20\ \mathrm{M}_\odot$, the spin is also predicted with the high precision $a = 0.272$, but the neutron star is not so extremely compact, having radius $R \approx 4.1M$. The parameter $q/a^2 \approx 2.6$ is too high to approve the application of the Kerr geometry in description of the Hartle–Thorne external spacetime. In fact, the self-consistency test using the Hartle–Thorne geometry predicts the best fit with χ^2 being too high (twice the estimate due to the fitting procedure using the Kerr approximation) to imply relevance of this variant for the chosen EoS. For this reason the RP1+RP variant of the RS model can be considered to be excluded by the self-consistency test.

8. Conclusions

We can conclude that there is a strong synergy effect of our approach. As expected, the equations of state applied in the Hartle–Thorne model of neutron stars fully exclude a lot of variants of the RS model that could be acceptable due to the fitting procedure to the HF QPO data observed in the 4U 1636–53 source. Moreover, the results of the RS model allow the rotation frequency of the 4U 1636–53 neutron star $f_{\mathrm{rot}} = 580$ Hz, but fully exclude the possibility of $f_{\mathrm{rot}} = 290$ Hz.

The restrictions work effectively in the opposite direction too – the results of the RS model put significant restrictions on the relevance of the equations of state. The crucial point is that the self-consistency test by fitting the observational data by the RS model with the orbital and epicyclic frequencies in the Hartle–Thorne geometry related to the acceptable EoS excludes one of the variants of the RS model predicted by the fitting under the Kerr approximation of the neutron star external geometry, and also the corresponding EoS. In fact, we have shown that the RP1+RP variant of the RS model along with the Skyrme SV EoS connected to this variant are excluded by the self-consistency test giving high value of χ^2 at the best fit. It is interesting that this happens for the variant of the RS model giving the best fit to the data of twin HF QPOs when the Kerr approximation of the oscillatory frequencies has been used.

On the other hand, the RP1+TP1 variant of the RS model related to a very stiff Gandolfi EoS goes successfully through the self-consistency test by the Hartle–Thorne geometry. In this case, the resulting best fit gives $\chi^2 = 64$ that is well comparable to the result obtained for the Kerr approximation ($\chi^2 = 61$). The resulting neutron star parameters ($M \approx 2.10\ \mathrm{M}_\odot$, $a \approx 0.208$, and $q/a^2 \approx 1.77$) are also very close to those obtained in the Kerr approximation, demonstrating errors

of one percent. Moreover, the Skyrme Gs EoS used in the self-consistency test by the Hartle–Thorne geometry gives also acceptable results, implying a possibility of the 4U 1636–53 neutron star being near the marginally stable state with mass $M \approx 2.11\ \mathrm{M}_{\odot}$. Of course, the vicinity of an instability of the neutron star puts some doubts on the applicability of the Skyrme Gs EoS.

We can conclude that in the framework of the Hartle–Thorne theory the EoS imply strong restriction on the RS model of the twin HF QPOs observed in the atoll source 4U 1636–53. In fact only the RP1+TP1 variant of the RS model satisfies the self-consistency test. Moreover, it seems that there is only one EoS, namely the Gandolfi EoS that can be considered as a fully realistic choice in the framework of the modeling the twin HF QPOs. The self-consistency test also demonstrates that the Kerr approximation of the neutron star external geometry gives very precise estimates for very compact neutron stars having sufficiently low values of the parameter $q/a^2 < 2$.

It was shown that observations of the twin HF QPOs provide tests on equation of state that put limits on the gravitational mass, and the spin that is linearly related to the moment of inertia of the neutron star. This could provide another test of the equations of state that allow for existence of neutron stars with $M > 2.0\ \mathrm{M}_{\odot}$.

For the equations of state acceptable by the RS model we can determine also the quadrupole moment and the shape of the neutron star surface governed by the equatorial and polar radii. These quantities have to enter other strong gravity tests of the 4U 1636–53 neutron star spacetime parameters predicted by the twin HF QPOs, *e.g.*, the profiled spectral lines generated at the neutron star surface or at its accretion disk. We believe that such tests could confirm or exclude one of the two EoS implied by the acceptable variant of the RS model.

Of course, it will be very important to test the RS model of the twin HF QPOs and all its consequences for some other neutron star system. We have to check, if the same variant of the RS model, and the same EoS in the Hartle–Thorne theory of the neutron stars could be relevant. However, no source similar to the 4U 1636–53 neutron star system has been observed. Such sources have to demonstrate sufficiently extended range of the twin HF QPOs and an indication of two clusters of the observational data that could be related to different models of twin HF QPOs that could be switched at a resonant point. Simultaneously, we have to know the rotation frequency of the neutron star.

Acknowledgements. The authors acknowledge the internal grants of the Silesian University in Opava FPF SGS/11,23/2013. ZS acknowledges the Albert Einstein Center for Gravitation and Astrophysics supported by the Czech Science Foundation grant No. 14-37086G. MU and GT acknowledge the support of the Czech grant GAČR 209/12/P740.

REFERENCES

Abramowicz, M.A., Almergren, G.J.E., Kluzniak, W., and Thampan, A.V. 2003, arXiv:gr-qc/0312070.

Abramowicz, M.A., Barret, D., Bursa, M., Kluzniak, W., Rebusco, P., and Török, G. 2005, *Astron. Nachr.*, **326**, 864.

Akmal, A., and Pandharipande, V.R. 1997, *Phys. Rev. C*, **56**, 2261.

Akmal, A., Pandharipande, V.R., and Ravenhall, D.G. 1998, *Phys. Rev. C*, **58**, 1804.

Antoniadis, J., *et al.* 2013, *Science*, **340**, 448.

Bakala, P., Šrámková, E., Stuchlík, Z., and Török, G. 2010, *Classical Quantum Gravity*, **27**, 045001.

Balberg, S., and Gal, A. 1997, *Nuclear Physics A*, **625**, 435.

Baldo, M., Bombaci, I., and Burgio, G.F. 1997, *A&A*, **328**, 274.

Barret, D., Olive, J.-F., and Miller, M.C. 2005a, *MNRAS*, **361**, 855.

Barret, D., Olive, J.-F., and Miller, M.C. 2005b, *Astron. Nachr.*, **326**, 808.

Belloni, T., Homan, J., Motta, S., Ratti, E., and Méndez, M. 2007, *MNRAS*, **379**, 247.

Bombaci, I. 1995, in: "Perspectives on Theoretical Nuclear Physics", Ed. I. Bombaci, *et al.* , p. 223–237.

Bonazzola, S., Gourgoulhon, E., and Marck, J.-A. 1998, *Phys. Rev. D*, **58**, 104020.

Boshkayev, K., Bini, D., Rueda, J., Geralico, A., Muccino, M., and Siutsou, I. 2014, *Gravitation and Cosmology*, **20**, 233.

Boutloukos, S., van der Klis, M., Altamirano, D., Klein-Wolt, M., Wijnands, R., Jonker, P. G., and Fender, R. P. 2006, *ApJ*, **653**, 1435.

Bursa, M. 2005, in: "Proceedings of RAGtime 6/7: Workshops on black holes and neutron stars", Opava, 16–18/18–20 September 2004/2005, Ed. S.Hledík and Z.Stuchlík (Opava: Silesian University in Opava), p. 39–45.

Chandrasekhar, S., and Miller, J.C. 1974, *MNRAS*, **167**, 63.

Colpi, M., and Miller, J.C. 1992, *ApJ*, **388**, 513.

Cremaschini, C., and Stuchlík, Z. 2013, *Phys. Rev. E*, **87**, 043113.

Demorest, P.B., Pennucci, T., Ransom, S.M., Roberts, M.S.E., and Hessels, J.W.T. 2010, *Nature*, **467**, 1081.

Farhi, E., and Jaffe, R.L. 1984, *Phys. Rev. D*, **30**, 2379.

Gandolfi, S., Illarionov, A.Y., Fantoni, S., Miller, J.C., Pederiva, F., and Schmidt, K.E 2010, *MNRAS*, **404**, L35.

Glendenning, N.K. 1985, *ApJ*, **293**, 470.

Gondek-Rosińska, D., Kluźniak, W., Stergioulas, N., and Wiśniewicz, M. 2014, *Phys. Rev. D*, **89**, 104001.

Haensel, P., Zdunik, J.L., and Schaefer, R. 1986, *A&A*, **160**, 121.

Hartle, J.B. 1967, *ApJ*, **150**, 1005.

Hartle, J.B., and Thorne, K. 1968, *ApJ*, **153**, 807.

Horák, J., Abramowicz, M.A., Kluźniak, W., Rebusco, P., and Török, G. 2009, *A&A*, **499**, 535.

Kato, S. 2008, *PASJ*, **60**, 111.

Kostić, U., Čadež, A., Calvani, M., and Gomboc, A. 2009, *A&A*, **496**, 307.

Kovář, J., Stuchlík, Z., and Karas, V. 2008, *Classical Quantum Gravity*, **25**, 095011.

Lattimer, J.M., and Prakash, M. 2007, *Physics Reports*, **442**, 109.

Lin, Y.-F., Boutelier, M., Barret, D., and Zhang, S.-N. 2011, *ApJ*, **726**, 74.

Lo, K.-W., and Lin, L.-M. 2011, *ApJ*, **728**, 12.

Lorenz, C.P., Ravenhall, D.G., and Pethick, C.J. 1993, *Phys. Rev. Lett.*, **70**, 379.

Miller, J.C. 1977, *MNRAS*, **179**, 483.

Miller, M.C., Lamb, F.K., and Psaltis, D. 1998, *ApJ*, **508**, 791.

Montero, P.J. and Zanotti, O. 2012, *MNRAS*, **419**, 1507.

Mukherjee, A. and Bhattacharyya, S. 2012, *ApJ*, **756**, 55.

Mukhopadhyay, B. 2009, *ApJ*, **694**, 387.

Müller, H., and Serot, B.D. 1996, *Nuclear Physics A*, **606**, 508.
Müther, H., Prakash, M., and Ainsworth, T.L. 1987, *Physics Letters B*, **199**, 469.
Pawar, D.D., Kalamkar, M., Altamirano, D., Linares, M., Shanthi, K., Strohmayer, T., Bhattacharya, D., van der Klis, M. 2013, *MNRAS*, **433**, 2436.
Perez, C.A., Silbergleit, A.S., Wagoner, R.V., and Lehr, D.E. 1997, *ApJ*, **476**, 589.
Postnikov, S., Prakash, M., and Lattimer, J.M. 2010, *Phys. Rev. D*, **82**, 024016.
Press, W.H., Teukolsky, S.A., Vetterling, W.T., and Flannery, B.P. 2007, "Numerical Recipes: The Art of Scientific Computing", Cambridge University Press, p. 1256.
Rhoades, C.E., and Ruffini, R. 1974, *Phys. Rev. Lett.*, **32**, 324.
Sanna, A., Méndez, M., Belloni, T., and Altamirano, D. 2012, Poster presentation at *IAU General Assembly XXVIII*, 20–31 August 2012, Beijing, China.
Schee, J., and Stuchlík, Z. 2009, *General Relativity and Gravitation*, **41**, 1795.
Shi, C. 2011, *Research in Astronomy and Astrophysics*, **11**, 1327.
Stefanov, I.Z. 2014, *MNRAS*, **444**, 2178.
Steiner, A.W., Lattimer, J.M., and Brown, E.F. 2010, *ApJ*, **722**, 33.
Stella, L., and Vietri, M. 1998, *ApJ*, **492**, L59.
Stella, L., and Vietri, M. 1999, *Phys. Rev. Lett.*, **82**, 17.
Stergioulas, N. 2003, *Living Reviews in Relativity*, **6**, 3.
Stone, J.Ř., Miller, J.C., Koncewicz, R., Stevenson, P.D., and Strayer, M.R. 2003, *Phys. Rev. C*, **68**, 034324.
Straub, O. and Šrámková, E. 2009, *Classical Quantum Gravity*, **26**, 055011.
Strohmayer, T.E., and Markwardt, C.B. 2002, *ApJ*, **577**, 337.
Stuchlík, Z., Török, G., and Bakala, P. 2007, arXiv:0704.
Stuchlík, Z., and Kotrlová, A. 2009, *General Relativity and Gravitation*, **41**, 1305.
Stuchlík, Z., Kotrlová, A., and Török, G. 2011, *A&A*, **525**, A82.
Stuchlík, Z., Kotrlová, A., and Török, G. 2012, *Acta Astron.*, **62**, 389.
Stuchlík, Z., and Kološ, M. 2012, *Journal of Cosmology and Astroparticle Physics*, **10**, 008.
Stuchlík, Z., and Schee, J. 2012, *Classical Quantum Gravity*, **29**, 065002.
Stuchlík, Z., Kotrlová, A., and Török, G. 2013, *A&A*, **552**, A10.
Stuchlík, Z., Kotrlová, A., and Török, G., and Goluchová, K. 2014, *Acta Astron.*, **64**, 45.
Stuchlík, Z., and Kološ, M. 2014, *Phys. Rev. D*, **89**, 065007.
Stuchlík, Z., and Kološ, M. 2015, *General Relativity and Gravitation*, **47**, 27.
Török, G. 2009, *A&A*, **497**, 661.
Török, G., Abramowicz, M.A., Kluźniak, W., and Stuchlík, Z. 2005, *A&A*, **436**, 1.
Török, G., and Stuchlík, Z. 2005, *A&A*, **437**, 775.
Török, G., Abramowicz, M.A., Bakala, P., Bursa, M., Horák, J., Kluzniak, W., Rebusco, P., and Stuchlík, Z. 2008a, *Acta Astron.*, **58**, 15.
Török, G., Bakala, P., Stuchlík, Z., and Čech, P. 2008b, *Acta Astron.*, **58**, 1.
Török, G., Bakala, P., Šrámková, E., Stuchlík, Z., and Urbanec, M. 2010, *ApJ*, **714**, 748.
Török, G., Bakala, P., Šrámková, E., Stuchlík, Z., Urbanec, M., and Goluchová, K. 2012, *ApJ*, **760**, 138.
Török, G., *et al.* 2015, in: "Proceedings of RAGtime: Workshops on black holes and neutron stars", Opava, 2015, (Opava: Silesian University in Opava).
Urbanec, M., Bělták, E., and Stuchlík, Z. 2010a, *Acta Astron.*, **60**, 149.
Urbanec, M., Török, G., Šrámková, E., Čech, P., Stuchlík, Z., and Bakala, P. 2010b, *A&A*, **522**, A72.
Urbanec, M., Miller, J.C., and Stuchlík, Z. 2013, *MNRAS*, **433**, 1903.
van der Klis, M. 2006, in: "Compact Stellar X-Ray Sources", Ed. W.H.G. Lewin and M. van der Klis (Cambridge: Cambridge University Press), p. 39–112.
Wang, D.H., Chen, L., Zhang, C.M., Lei, Y.J., and Qu, J.L. 2013, *MNRAS*, **435**, 3494.
Witten, E. 1984, *Phys. Rev. D*,, **30**, 272.
Zhang, C.M., Yin, H.X., Zhao, Y.H., Zhang, F., and Song, L.M. 2006, *MNRAS*, **366**, 1373.

Appendix. Orbital and Epicyclic Frequencies in Hartle–Thorne Geometry

Circular and epicyclic geodesic motion in the Hartle–Thorne geometry has been studied in Abramowicz *et al.* (2003), Török *et al.* (2008b, 2015). Here we only present the expressions for the orbital (Keplerian) frequency and the radial and vertical epicyclic frequencies as given in Török *et al.* (2008b). Alternative, but equivalent, expressions can be found in Boshkayev *et al.* (2014).

The Keplerian frequency is determined by the relations

$$\nu_{\rm K}(r;M,a,q) = \frac{c^3}{2\pi GM}\frac{1}{r^{3/2}}\left[1-\frac{a}{r^{3/2}}+a^2E_1(r)+qE_2(r)\right] \tag{21}$$

where

$$\begin{aligned} E_1(r) &= [48-80r+4r^2-18r^3+40r^4+10r^5+15r^6-15r^7] \\ &\quad (16(r-2)r^4)^{-1}+\frac{15(r^3-2)}{32}\ln\left(\frac{r}{r-2}\right), \\ E_2(r) &= \frac{5(6-8r-2r^2-3r^3+3r^4)}{16(r-2)r}-\frac{15(r^3-2)}{32}\ln\left(\frac{r}{r-2}\right). \end{aligned} \tag{22}$$

The radial epicyclic frequency ν_r and the vertical epicyclic frequency ν_θ are given by the relations

$$\nu_r^2(r;M,a,q) = \left(\frac{c^3}{2\pi GM}\right)^2\frac{(r-6)}{r^4}[1+aF_1(r)-a^2F_2(r)-qF_3(r)], \tag{23}$$

$$\nu_\theta^2(r;M,a,q) = \left(\frac{c^3}{2\pi GM}\right)^2\frac{1}{r^3}[1-aG_1(r)+a^2G_2(r)+qG_3(r)] \tag{24}$$

where

$$\begin{aligned} F_1(r) &= \frac{6(r+2)}{r^{3/2}(r-6)}, \\ F_2(r) &= [8r^4(r-2)(r-6)]^{-1}[384-720r-112r^2-76r^3 \\ &\quad -138r^4-130r^5+635r^6-375r^7+60r^8]+A(r), \\ F_3(r) &= \frac{5(48+30r+26r^2-127r^3+75r^4-12r^5)}{8r(r-2)(r-6)}-A(r), \\ A(r) &= \frac{15r(r-2)(2+13r-4r^2)}{16(r-6)}\ln\left(\frac{r}{r-2}\right), \\ G_1(r) &= \frac{6}{r^{3/2}}, \\ G_2(r) &= [8r^4(r-2)]^{-1}[48-224r+28r^2+6r^3-170r^4+295r^5 \\ &\quad -165r^6+30r^7]-B(r), \\ G_3(r) &= \frac{5(6+34r-59r^2+33r^3-6r^4)}{8r(r-2)}+B(r), \\ B(r) &= \frac{15(2r-1)(r-2)^2}{16}\ln\left(\frac{r}{r-2}\right). \end{aligned}$$

Paper V

6.5. Constraining Models of Twin-Peak Quasi-periodic Oscillations with Realistic Neutron Star Equations of State

Török Gabriel, Goluchová Kateřina, Urbanec Martin, Šrámková Eva, Adámek Karel, Urbancová Gabriela, Pecháček Tomáš, Bakala Pavel, Stuchlík Zdeněk, Horák Jiří & Juryšek Jakub

The Astrophysical Journal, 2016,
Volume 833, Issue 2, article id. 273, 11 pp.

The Astrophysical Journal, 833:273 (11pp), 2016 December 20 doi:10.3847/1538-4357/833/2/273

CONSTRAINING MODELS OF TWIN-PEAK QUASI-PERIODIC OSCILLATIONS WITH REALISTIC NEUTRON STAR EQUATIONS OF STATE

Gabriel Török[1], Kateřina Goluchová[1,2], Martin Urbanec[1], Eva Šrámková[1], Karel Adámek[1,2,3], Gabriela Urbancová[1], Tomáš Pecháček[1], Pavel Bakala[1], Zdeněk Stuchlík[2], Jiří Horák[4], and Jakub Juryšek[1,5]
[1] Research Centre for Computational Physics and Data Processing, Institute of Physics, Faculty of Philosophy & Science, Silesian University in Opava, Bezručovo nám. 13, CZ-746, 01 Opava, Czech Republic; gabriel.torok@gmail.com, katka.g@seznam.cz, martin.urbanec@physics.cz, eva.sramkova@fpf.slu.cz, karel.adamek@fpf.slu.cz, gabi.urbancova@gmail.com, pechacek_t@seznam.cz, pavel.bakala@fpf.slu.cz, jakubjurysek@astronomie.cz
[2] Research Centre for Theoretical Physics and Astrophysics, Institute of Physics, Faculty of Philosophy & Science, Silesian University in Opava, Bezručovo nám. 13, CZ-746, 01 Opava, Czech Republic; zdenek.stuchlik@fpf.slu.cz
[3] University of Oxford, Oxford e-Research Centre, 7 Keble Road, Oxford, OX1 3QG
[4] Astronomical Institute, Bocni II 1401/2a, CZ-14131 Praha 4 - Sporilov, Czech Republic; hjirkoun@gmail.com
[5] Astronomical Institute, Charles University Prague, Faculty of Mathematics and Physics, V Holešovičkách 2, Praha 8, CZ-180 00, Czech Republic.
Received 2016 January 11; revised 2016 October 26; accepted 2016 October 26; published 2016 December 21

ABSTRACT

Twin-peak quasi-periodic oscillations (QPOs) are observed in the X-ray power-density spectra of several accreting low-mass neutron star (NS) binaries. In our previous work we have considered several QPO models. We have identified and explored mass–angular-momentum relations implied by individual QPO models for the atoll source 4U 1636-53. In this paper we extend our study and confront QPO models with various NS equations of state (EoS). We start with simplified calculations assuming Kerr background geometry and then present results of detailed calculations considering the influence of NS quadrupole moment (related to rotationally induced NS oblateness) assuming Hartle–Thorne spacetimes. We show that the application of concrete EoS together with a particular QPO model yields a specific mass–angular-momentum relation. However, we demonstrate that the degeneracy in mass and angular momentum can be removed when the NS spin frequency inferred from the X-ray burst observations is considered. We inspect a large set of EoS and discuss their compatibility with the considered QPO models. We conclude that when the NS spin frequency in 4U 1636-53 is close to 580 Hz, we can exclude 51 of the 90 considered combinations of EoS and QPO models. We also discuss additional restrictions that may exclude even more combinations. Namely, 13 EOS are compatible with the observed twin-peak QPOs and the relativistic precession model. However, when considering the low-frequency QPOs and Lense–Thirring precession, only 5 EOS are compatible with the model.

Key words: accretion, accretion disks – equation of state – stars: neutron – X-rays: binaries

1. INTRODUCTION

Accreting neutron stars (NS) are believed to be the compact component in more than 20 low-mass X-ray binaries (LMXBs). In these systems, the mass is transferred from the companion by overflowing the Roche lobe and forming an accretion disk that surrounds the NS. The disk contributes significantly to the high X-ray luminosity of these objects, while most of the radiation comes from its inner parts and the disk–NS boundary layer. According to their X-ray spectral and timing properties, the NS LMXBs have been further classified into Z and atoll sources, whose names have been inspired by the shapes of the tracks they trace in the color–color diagram (e.g., van der Klis 2005). While the Z sources are generally more stable and brighter, the atoll sources are weaker and show significant changes in the X-ray luminosity. Both classes exhibit a variability over a wide range of frequencies. Except for irregular changes, their power spectra also contain relatively coherent features known as quasi-periodic oscillations (QPOs).

The so-called low-frequency QPOs have frequencies in the range of 1–100 Hz. In the case of Z sources they have been further classified into horizontal, flaring, and normal branch oscillations (HBO, FBO, and NBO, respectively) depending on the position of the source in the color–color diagram. Oscillations of properties similar to HBOs have also been observed in several atoll sources (see van der Klis 2006, p. 39, for a review). Much attention among theoreticians is attracted to the kilohertz QPOs (100–1000 Hz), however, because their high frequencies are comparable to the orbital timescale in the vicinity of a NS. It is believed that this coincidence represents a strong indication that the corresponding signal originates in the innermost parts of the accretion disks or close to the surface of the NS itself. This belief has also been supported by means of the Fourier-resolved spectroscopy (e.g., Gilfanov et al. 2000).

The kHz QPOs have similar properties in both Z and atoll sources. They are frequently observed in pairs and are often called twin-peak QPOs. Their "upper" and "lower" QPO frequencies (ν_U and ν_L, respectively) exhibit a strong and remarkably stable positive correlation and clustering around the rational ratios. These ratios are emphasized either by the intrinsic source clustering, or by a weakness of the two QPOs outside the limited frequency range (suggesting a possible resonant energy exchange between two physical oscillators, Abramowicz et al. 2003a; Belloni et al. 2005, 2007; Barret & Boutelier 2008; Török et al. 2008a, 2008b, 2008c; Horák et al. 2009; Boutelier et al. 2010). Other properties of each oscillation (e.g., the rms-amplitude and the quality factor) seem to mostly depend on its frequency, and the way in which they vary is different for the upper and lower oscillation. These differences often help to identify the type of kHz QPO in cases when only one peak is present in the power spectra (Barret et al. 2005, 2006; Méndez 2006; Török 2009).

Many models have been proposed to explain the rich phenomenology of twin-peak QPOs (Alpar & Shaham 1985; Lamb et al. 1985; Miller et al. 1998; Psaltis et al. 1999;

Table 1
Models Examined in this Work

Model	Relations	ν_L–ν_U Relation
RP	$\nu_L = \nu_K - \nu_r$, $\nu_U = \nu_K$	$\nu_L = \nu_U\left\{1 - \left[1 + \frac{8j\nu_U}{\mathcal{F}-j\nu_U} - 6\left(\frac{\nu_U}{\mathcal{F}-j\nu_U}\right)^{2/3} - 3j^2\left(\frac{\nu_U}{\mathcal{F}-j\nu_U}\right)^{4/3}\right]^{1/2}\right\}$
TD	$\nu_L = \nu_K$, $\nu_U = \nu_K + \nu_r$	$\nu_U = \nu_L\left\{1 + \left[1 + \frac{8j\nu_L}{\mathcal{F}-j\nu_L} - 6\left(\frac{\nu_L}{\mathcal{F}-j\nu_L}\right)^{2/3} - 3j^2\left(\frac{\nu_L}{\mathcal{F}-j\nu_L}\right)^{4/3}\right]^{1/2}\right\}$
WD	$\nu_L = 2(\nu_K - \nu_r)$,	$\nu_U = 2\nu_K - \nu_r$
RP1	$\nu_L = \nu_K - \nu_r$,	$\nu_U = \nu_\theta$
RP2	$\nu_L = \nu_K - \nu_r$,	$\nu_U = 2\nu_K - \nu_\theta$

Wagoner 1999; Abramowicz & Kluźniak 2001; Kato 2001, 2007, 2008; Kluźniak & Abramowicz 2001; Wagoner et al. 2001; Titarchuk & Wood 2002; Abramowicz et al. 2003b, 2003c; Rezzolla et al. 2003; Kluźniak et al. 2004; Bursa 2005; Pétri 2005; Zhang 2005; Török et al. 2007, 2016; Čadež et al. 2008; Stuchlík et al. 2008; Germanà et al. 2009; Kostić et al. 2009; Mukhopadhyay 2009; Stuchlík et al. 2013, 2014, 2015; Wang et al. 2015, and several others). While any acceptable model should address both the excitation mechanism and subsequent modulation of the resulting X-ray signal as well as their overall observational properties, most of the theoretical effort has so far been devoted to the observed frequencies. Clearly, their correlations serve as a first test of the model viability.

1.1. Aims and Scope of this Paper

Comparison between the observed and the expected frequencies can reveal the mass and angular momentum of the NS. These can be confronted with models of rotating NS based on a modern equation of state (EoS, e.g., Urbanec et al. 2010b). In Török et al. (2012) we have identified and explored mass–angular-momentum relations implied in Kerr spacetimes by individual QPO models. We have also discussed that the degeneracy in mass and angular momentum can be removed when the NS spin frequency is known.

Here we extend our study and confront QPO models with a large set of NS EoS while focusing on the influence of NS quadrupole moment that is related to its rotationally induced oblateness. The paper is arranged as follows. In Section 2 we very briefly recall individual QPO models that we consider together with previously obtained results. We present here the completed simplified calculations that assume Kerr background geometry and the atoll source 4U 1636-53. These follow previous comparison between predictions of the relativistic precession (RP) model and 5 EoS. The consideration is extended to other models and a large set of 18 EoS. Sections 3.1 and 4 bring detailed consequent calculations of RP model predictions considering the influence of the NS quadrupole moment within Hartle–Thorne spacetimes. We show here that the application of concrete Sly 4 EoS within the model in Hartle–Thorne spacetime brings a specific mass-spin relation. This relation is confronted with the NS spin frequency inferred from the X-ray burst observations. In Section 5 we present analogical results for the whole set of 5 QPO models and 18 EoS and outline their implications. We also discuss here the implications of the consideration of low-frequency QPOs.

2. TWIN-PEAK QPO MODELS APPROXIMATED IN KERR SPACETIMES

Within the framework of many QPO models, the observable frequencies can be expressed directly in terms of epicyclic frequencies. Formulae for the geodesic Keplerian and radial and vertical epicyclic frequencies in Kerr spacetimes were first derived by Aliev & Galtsov (1981). In a commonly used form (e.g., Török & Stuchlík 2005) they read

$$\Omega_K = \frac{\mathcal{F}}{j + x^{3/2}}, \quad \nu_r = \Gamma\Omega_K, \quad \nu_\theta = \Delta\Omega_K, \tag{1}$$

where

$$\Gamma = \sqrt{\frac{-3j^2 + 8j\sqrt{x} + (-6+x)x}{x^2}},$$
$$\Delta = \sqrt{1 + \frac{j(3j - 4\sqrt{x})}{x^2}}, \tag{2}$$

$x \equiv r/M$, and the "relativistic factor" $\mathcal{F}$ reads $\mathcal{F} \equiv c^3/(2\pi GM)$. We note that Kerr geometry represents an applicable approximation of NS spacetimes when the mass of the compact object is high (Török et al. 2010; Urbanec et al. 2013).

The above formulae are valid for Kerr spacetimes and describe (epicyclic) slightly perturbed circular geodesic motion well. This description of epicyclic motion of test particles that is relevant to standard thin accretion disks may also well approximate epicyclic motion in fluid accretion flow provided that the pressure effects in the fluid are negligible and linear quasi-incompressible modes are considered. Formulae for geodesic epicyclic oscillations are often assumed within several QPO models based on accretion disk hot-spot as well as global fluid motion (e.g., Stella & Vietri 1999, 2001; Abramowicz & Kluźniak 2001; Kluźniak & Abramowicz 2002). Here we investigate a subset of models that have previously been considered in the study of Török et al. (2012).

2.1. Individual Models of QPOs and their Predictions

The RP model explains the kHz QPOs as a direct manifestation of modes of relativistic epicyclic motion of blobs at various radii r in the inner parts of the accretion disk (Stella & Vietri 1999). For the RP model, one can easily solve relations defining the upper and lower QPO frequencies in terms of the orbital frequencies and arrive at an explicit formula that relates the upper and lower QPO frequencies in units of

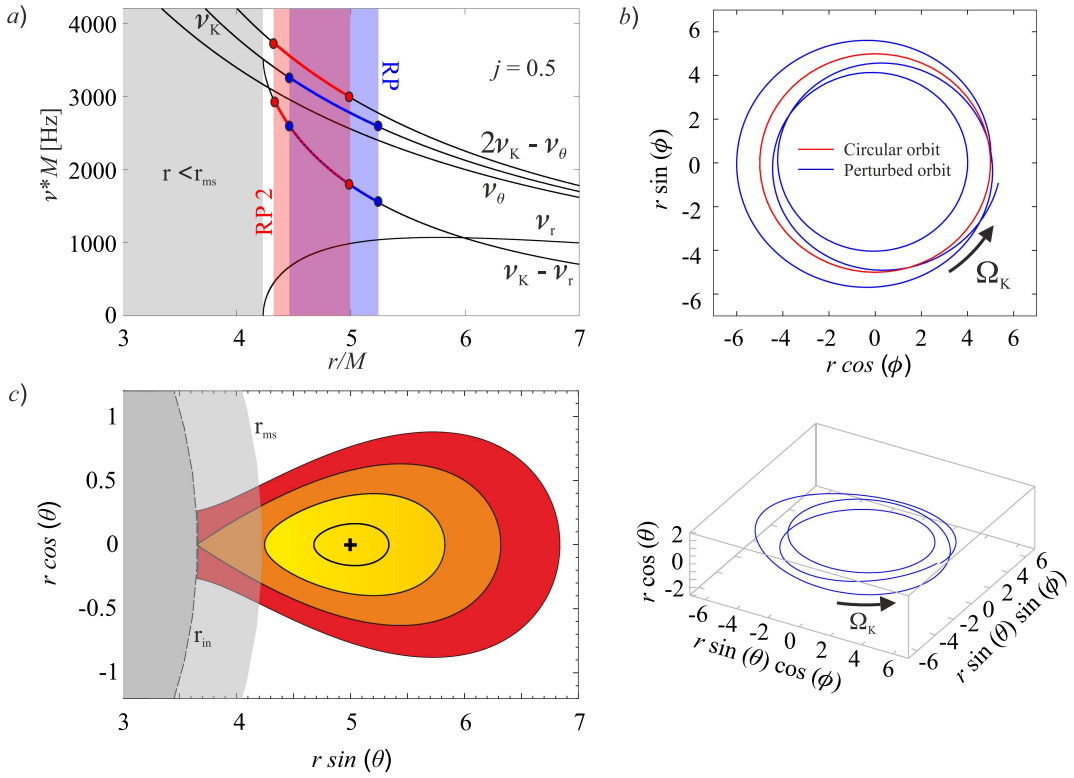

Figure 1. Frequencies of orbital motion and illustration of models of QPOs in the atoll source 4U 1636-53. (a) Behavior of characteristic orbital frequencies in Kerr spacetimes. The blue area denotes a radial region associated with the RP model, i.e., the region where orbital and periastron precession frequencies can be identified with the frequencies observed in the atoll source 4U 1636-53. The red area denotes the same, but for the RP2 model frequencies. The gray area corresponds to the region below the marginally stable circular orbit, $r < r_{ms}$. (b) Example of a free test particle trajectory and its projection onto the equatorial plane. The figure corresponds to the situation drawn in panel (a) and the RP model ($r = 5\,M$). The red circle indicates an unperturbed circular trajectory. (c) Equipotencial surfaces determining the shape of the torus located at $r = 5\,M$ drawn for different values of torus thickness β. The slender torus limit ($\beta = 0$) is denoted by the black cross. In this limit, and when the RP2 model is assumed, the torus oscillates with frequencies $\nu_K(r) - \nu_r(r)$ and $2\nu_K(r) - \nu_\theta(r)$. In the limit of $j = 0$, these frequencies coincide with the RP model frequencies $\nu_K(r) - \nu_r(r)$ and $\nu_K(r)$. Although the two models predict the same frequencies in the limit of non-rotating NS, the associated physical mechanisms are not the same.

Hertz (Török et al. 2010). We show this relation in Table 1. The concept of the tidal disruption (TD) model is similar to the RP model, but the QPOs are atributed to a disruption of large accreting inhomogenities (Germanà et al. 2009). The explicit relation between the two observed QPO frequencies can be evaluated in a way similar to the case of the RP model (Török et al. 2012), and we also include this relation in Table 1.

While the former two models assume motion of a hot-spot propagating within the accretion disk, the warp disk (WD) model assumes non-axisymmetric oscillation modes in a thick disk (Kato 2001). The two other considered models, RP1 and RP2, also deal with non-axisymmetric disk-oscillation modes. The frequencies of these modes coincide with the frequencies predicted by the RP model in the limit of $j = 0$ (Bursa 2005; Török et al. 2010). Although the relevant frequencies coincide in the case of non-rotating NS, they correspond to a different physical situation (see Figure 1 for an illustration). We include the expressions for lower and upper QPO frequency for all the three disk-oscillation models in Table 1.

Török et al. (2010, 2012) assumed a high-mass (Kerr) approximation of NS spacetimes and relations from Table 1. We have demonstrated that for each twin-peak QPO model and a given source, the model consideration results in a specific relation between the NS mass M and angular momentum j rather than in their single preferred combination. We payed special attention to the atoll source 4U 1636-53 and evaluated mass–angular-momentum relations for all discussed QPO models.[6]

2.2. Twin-Peak QPO Models versus NS EoS

Török et al. (2012) compared a χ^2 map describing the quality of the RP model fit of the 4U 1636-53 data to the $M - j$ relations implied by five specific NS EoS. These $M - j$ relations were calculated assuming that the NS spin frequency ν_S is 580 Hz (Strohmayer & Markwardt 2002; Galloway et al. 2008; Watts 2012). In these calculations we used the approach

[6] Lin et al. (2011) have performed a similar analysis assuming a different set of twin-peak QPO frequency data points for the atoll source 4U 1636-53. The data points in their study have been obtained via common processing of a large amount of data, while the data points used by Török et al. (2012) correspond to individual continuous observations of the source. It was shown in Török et al. (2012) that the results of the two studies are consistent (see also the NS parameteres resulting within the two studies denoted in Figure 2 and in Török et al. 2016).

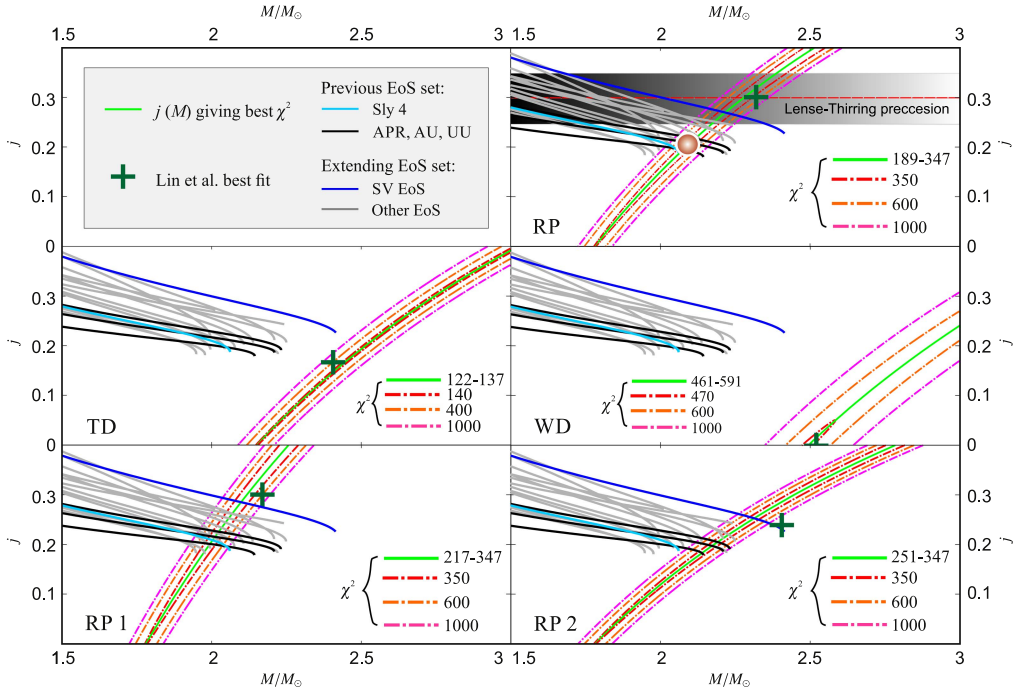

Figure 2. χ^2 maps (20d.o.f.) calculated from data of the atoll source 4U 1636-53 and individual QPO models within Kerr spacetimes vs. mass–angular-momentum relations predicted by NS EoS. For the calculations we consider 14 more EOS in addition to 4 EoS (SLy 4, APR, AU-WFF1, and UU-WFF2) assumed in Török et al. (2012). The full set of 18 EoS is listed in Table 2. In each panel the green line indicates the best χ^2 for a fixed M, while the dashed green line denotes its quadratic approximation. The white lines indicate the corresponding 1σ and 2σ confidence levels. The NS EoS are assumed for the rotational frequency of 580 Hz inferred from the X-ray burst observations. The green crosses denote the mass and angular momentum combinations reported for 4U 1636-53 and individual QPO models by Lin et al. (2011). The red spot roughly indicates the combination of mass and spin inferred from the common consideration of the RP model, NS spin frequency of 580 Hz, and 4 EoS as discussed by Török et al. (2012). The horizontal dashed red line together with the horizontal shaded bar indicate additional restrictions on the RP model that follow from consideration of Lense–Thirring precession, as discussed in Török et al. (2012).

of Hartle (1967), Hartle & Thorne (1968), Chandrasekhar & Miller (1974), Miller (1977), and Urbanec et al. (2010a).

In the top panel of Figure 2 we show a comparison between predictions of the RP model and 4 EoS carried out in Török et al. (2012). We note that the choice of concrete EoS used within that paper was motivated by low values of a scaled quadrupole moment $\tilde{q} \equiv q/j^2$ of the assumed NS configurations.[7] Although QPO model predictions are drawn for simplified calculations assuming Kerr background geometry, in following we do not restrict ourselves to high-mass (compactness) NS. We thus add 14 more EoS, which are indicated within the figure. The full set of 18 EoS considered hereafter is listed in Table 2. In the other panels of Figure 2 we make the same comparison, but for the other four considered QPO models.

Török et al. (2012) directly compared (a few) EoS and the RP model. Inspecting our overall extended Figure 2, we can expect that QPO models place strong restrictions on NS parameters and EoS, or vice versa. For instance, a direct confrontation of EoS and TD model predictions strongly suggests that the model (favored within the study of Lin et al. 2011) entirely fails to meet the requirements given by the consideration of NS EoS. Moreover, by comparing overlaps between the RP model relation and curves denoting the requirements of individual EoS, other interesting information can be obtained: there is a difference between overlaps considered in Török et al. (2012), which are denoted here by the red spot in Figure 2, and overlaps given by the newly considered EoS. Clearly, the high quadrupole moment of NS configurations related to the latter set of EoS increases the required NS angular momentum. For instance, there is $j \doteq 0.19$ for Sly 4 versus $j \doteq 0.28$ for SV EoS. It is also apparent that this effect can be important for the consideration of Lense–Thirring precession and low-frequency QPOs within the framework of the RP model.

Motivated by these findings, below we explore restrictions on QPO models in detail and perform consistent calculations in Hartle–Thorne spacetimes.

3. CALCULATIONS IN HARTLE–THORNE SPACETIMES

So far, we have considered only a Kerr approximation of the rotating NS spacetime assuming that the star is very compact. In this case the NS quadrupole moment q related to its rotationally induced oblateness reaches low values, and we have $\tilde{q} \approx 1$. In a more general case of $\tilde{q} > 1$, one should

[7] Török et al. (2012) also assumed one more EOS (WS, Wiringa et al. 1988; Stergioulas & Friedman 1995). We do not consider this EOS here since it does not fulfill the requirements of the current observational tests.

Table 2
EoS Examined in this Work

EoS	M_{max}	R (km)	n_c ($[fm]^{-3}$)	References
Sly 4	2.04	9.96	1.21	1
SkI5	2.18	11.3	0.97	1
SV	2.38*	11.9	0.80	1
SkO	1.97	10.3	1.19	1
Gs	2.08	10.8	1.07	1
SkI2	2.11	11.0	1.03	1
SGI	2.22	10.9	1.01	1
APR	2.21	10.2	1.12	2
AU	2.13	9.39	1.25	3
UU	2.19	9.81	1.16	3
UBS	2.20*	12.1	0.68	4
GLENDNH3	1.96	11.4	1.05	5
Gandolfi	2.20	9.82	1.16	6
QMC700	1.95	12.6	0.61	7
KDE0v1	1.96	9.72	1.29	8
NRAPR	1.93	9.85	1.29	9
PNM L80	2.02	10.4	1.16	10
J35 L80	2.05	10.5	1.14	10

Note. The individual columns indicate the maximum mass and corresponding radius, and the central baryon number density for each EoS along with the relevant references. The asterisks mark three EoS whose maximum mass corresponds to the maximum density allowed by the available EoS table, and not to a marginally stable star.
References. (1) Rikovska Stone et al. (2003), (2) Akmal et al. (1998), (3) Wiringa et al. (1988), (4) Urbanec et al. (2010a), (5) Glendenning (1985), (6) Gandolfi et al. (2010), (7) Rikovska Stone et al. (2007), (8) Agrawal et al. (2005), (9) Steiner et al. (2005), (10) Newton et al. (2013).

assume NS spacetime approximated by the Hartle–Thorne geometry (Hartle 1967; Hartle & Thorne 1968).[8]

Based on the Hartle–Thorne approximation, the Keplerian orbital frequency can be expressed as (Abramowicz et al. 2003a)

$$\Omega_K = \frac{\mathcal{F}}{x^{3/2}}\left[1 - \frac{j}{x^{3/2}} + j^2 F_1(x) + qF_2(x)\right], \quad (3)$$

where

$$F_1(x) = [48 - 80x + 4x^2 - 18x^3 + 40x^4 + 10x^5 + 15x^6 - 15x^7](16(x-2)x^4)^{-1} + A(x),$$
$$F_2(x) = \frac{5(6 - 8x - 2x^2 - 3x^3 + 3x^4)}{16(x-2)x} - A(x),$$
$$A(x) = \frac{15(x^3-2)}{32}\ln\left(\frac{x}{x-2}\right).$$

The radial and vertical epicyclic frequencies are then described by the following terms

$$\nu_r^2 = \frac{\mathcal{F}^2(x-6)}{x^4}[1 + jH_1(x) - j^2 H_2(x) - qH_3(x)], \quad (4)$$

$$\nu_\theta^2 = \frac{\mathcal{F}^2}{x^3}[1 - jG_1(x) + j^2 G_2(x) + qG_3(x)], \quad (5)$$

where

$$H_1(x) = \frac{6(x+2)}{x^{3/2}(x-6)},$$
$$H_2(x) = [8x^4(x-2)(x-6)]^{-1}[384 - 720x - 112x^2 - 76x^3 - 138x^4 - 130x^5 + 635x^6 - 375x^7 + 60x^8] + C(x),$$
$$H_3(x) = \frac{5(48 + 30x + 26x^2 - 127x^3 + 75x^4 - 12x^5)}{8x(x-2)(x-6)} - C(x),$$
$$C(x) = \frac{15x(x-2)(2 + 13x - 4x^2)}{16(x-6)}\ln\left(\frac{x}{x-2}\right),$$
$$G_1(x) = \frac{6}{x^{3/2}},$$
$$G_2(x) = [8x^4(x-2)]^{-1}[48 - 224x + 28x^2 + 6x^3 - 170x^4 + 295x^5 - 165x^6 + 30x^7] - B(x),$$
$$G_3(x) = \frac{5(6 + 34x - 59x^2 + 33x^3 - 6x^4)}{8x(x-2)} + B(x),$$
$$B(x) = \frac{15(2x-1)(x-2)^2}{16}\ln\left(\frac{x}{x-2}\right).$$

3.1. Results for the RP Model

Assuming the above formulae, we have calculated 3D-χ^2 maps for the RP model. In the left panel of Figure 3 we show the behavior of the best χ^2 as a function of M and j for several color-coded values of $\tilde{q}$. For each value of $\tilde{q}$ there is a preferred $M - j$ relation. We find that, although such a relation has a global minimum, the gradient of χ^2 along the relation is always much lower than the gradient in the perpendicular direction. In other words, χ^2 maps for a fixed $\tilde{q}$ are of the same type as the maps calculated in the Kerr spacetime. It then follows that there is a global $M - j - \tilde{q}$ degeneracy in the sense discussed by Török et al. (2012); see their Figure 3.

As emphasized by Urbanec et al. (2010b), Török et al. (2010), Kluźniak & Rosińska (2013), Török et al. (2014), Rosińska et al. (2014), and Boshkayev et al. (2015), Newtonian effects following from the influence of the quadrupole moment act on the orbital frequencies in a way opposite to that which is related to relativistic effects following from the increase of the angular momentum. The behavior of the relations shown in the left panel of Figure 3 is determined by this interplay. Because of this, we can see that the increased NS quadrupole moment can compensate for the increase in estimated mass given by a high angular momentum.

4. CONSIDERATION OF NS MODELS GIVEN BY CONCRETE EOS

The relations for the RP model drawn in the left panel of Figure 3 result from fitting of the 4U 1636-53 data points considering the general Hartle–Thorne spacetime. The consideration does not include strong restrictions on spacetime properties following from NS modeling based on present EoS. It can be shown that a concrete NS EoS covers only a 2D

[8] The adopted approximation represents a convenient alternative to a (more precise) numerical approach (discussed in the same context by Stella et al. 1999) or other spacetime descriptions (e.g., Manko et al. 2000; Stute & Camenzind 2002; Pappas 2015), see also Bonazzola et al. (1993, 1998), Stergioulas & Friedman (1995), Nozawa et al. (1998), Ansorg et al. (2003), and Berti et al. (2005).

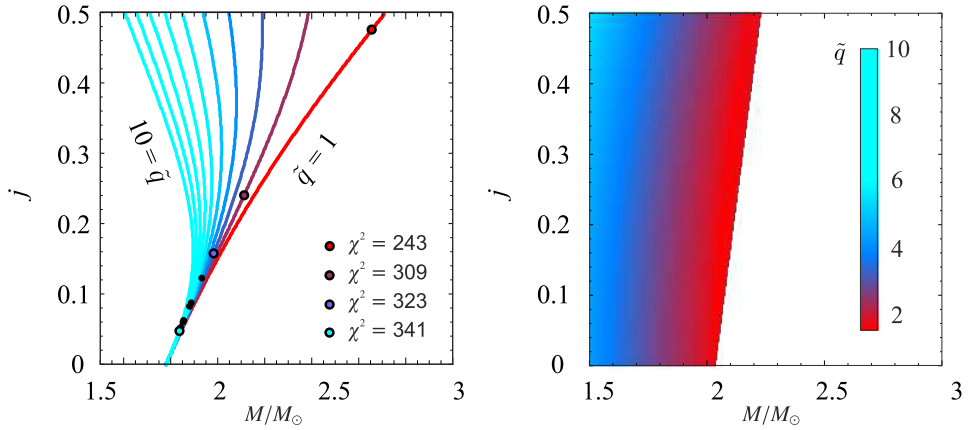

Figure 3. Left: behavior of the best χ^2 as a function of M and j for several values of $\tilde{q}$. The dots denote global minima for each value of $\tilde{q}$ (see, however, the main text, Section 3.1, for a comment on this). Right: the 2D surface in the 3D $M - j - \tilde{q}$ space given by the SLy 4 EoS.

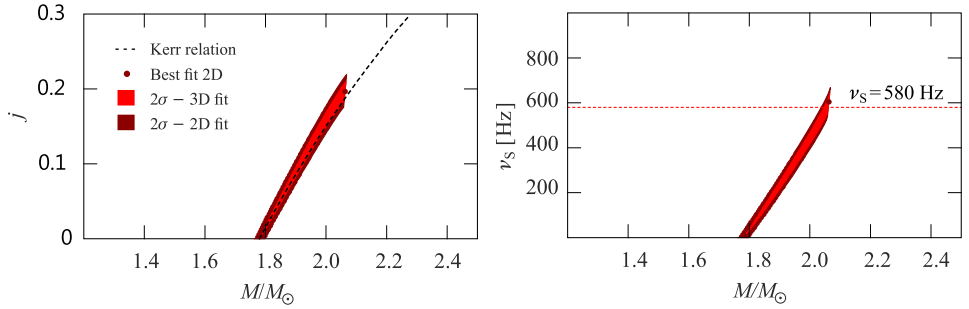

Figure 4. Left: the final $M - j$ map implied by the RP model and the Sly 4 EoS. The light color area denotes an intersection between the 2D surface given by the Sly 4 EoS and 3D volume corresponding to the 2σ confidence level given by the RP best-fit model found in the intervals of $M \in [1M_\odot, 4M_\odot]$, $j \in [0.0, 0.5]$, and $\tilde{q} \in [1, 10]$. The χ^2 minimum of 303/20d.o.f. at the 2D surface is denoted by the dark marker. The dark color area denotes the 2σ confidence level calculated when this local minimum is assumed as a global minimum, provided that the QPO frequency error bars are underestimated by a corresponding factor $\xi_{2D} = 3.9$. We can see that in this particular case, there is almost no difference between the two areas. The dashed curve indicates the $M - j$ relation obtained from the simplified consideration of Kerr spacetimes (see Section 2). Right: the same map, but drawn for the NS spin frequency ν_S. The horizontal dashed red line denotes the spin frequency measured from the X-ray bursts (i.e., $\nu_S = 580$ Hz). The minimum of χ^2 for the spin $\nu_S = 580$ Hz corresponds to $\chi^2 = 305/21$d.o.f.

surface in the 3D $M - j - \tilde{q}$ space since the quadrupole moment is determined by rotationally induced NS oblateness. Thus, when a given EoS is assumed, only the corresponding 2D surface is relevant for fitting data points by a given QPO model. Following Urbanec et al. (2013), we illustrate such a surface in the right panel of Figure 3 for the SLy 4 EoS. The color-coding of the plot is the same as the one in the left panel of the same figure.

The final $M - j$ map for the RP model and Sly 4 EoS, i.e., the values of M and j implied by the common consideration of the two panels of Figure 3, is shown in the left panel of Figure 4. The right panel of this figure then shows an equivalent map drawn for the NS mass and spin frequency ν_S.

4.1. NS Mass Inferred Assuming X-Ray Burst Measurements

The left panel of Figure 4 shows that the concrete EoS, SLy 4, considered for the RP model implies a clear $M - j$ relation. This relation exhibits only a shallow χ^2 minimum. The right panel of the same figure shows the equivalent relation between the NS mass and the spin frequency as well as its shallow minimum. Taking into account the spin frequency inferred from the X-ray bursts, 580 Hz, we can find from Figure 4 that the NS mass and angular momentum have to take values of

$$M = (2.06 \pm 0.01)M_\odot, \quad j \doteq 0.2. \tag{6}$$

These values are in a good agreement with those inferred from the simplified consideration using Kerr spacetimes (see Figure 2). Considering the shallow χ^2 minima denoted in Figure 4, it may be interesting that its frequency value almost coincides with the measured spin frequency of 580 Hz.

5. DISCUSSION AND CONCLUSIONS

In addition to the Sly 4 EoS, we have investigated a wide set of 17 other EoS that are based on different theoretical models. All these EoS are listed in Table 2, where we show the maximum NS mass allowed by each EoS as well as the corresponding NS radius and the central number density. All these EoS are compatible with the highest observed NS masses

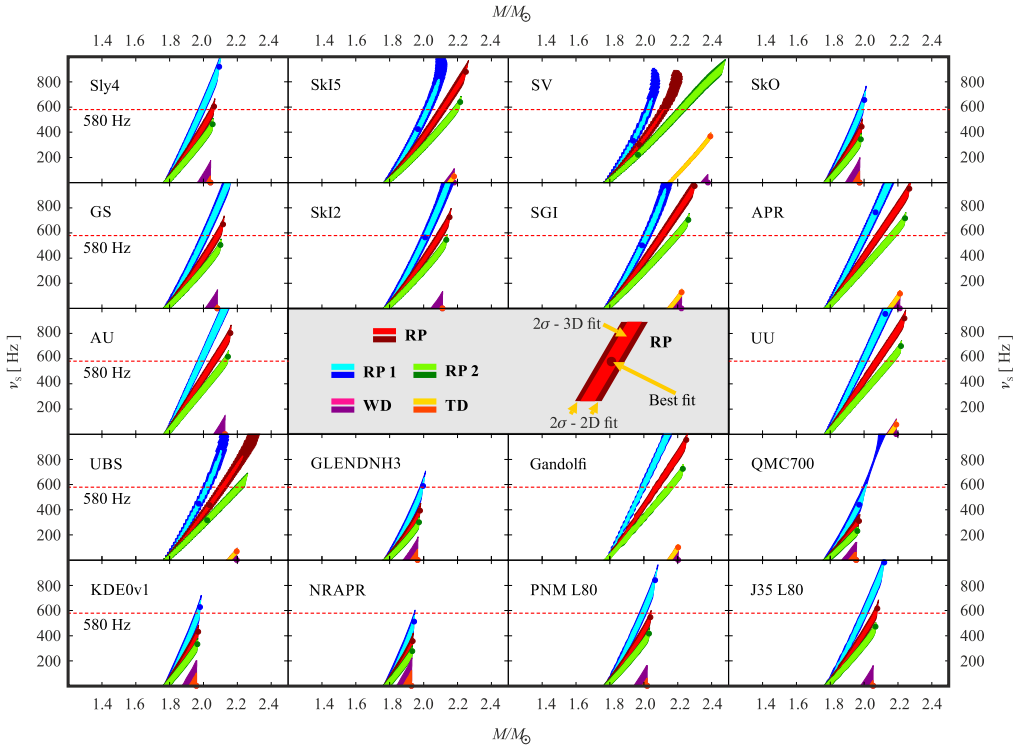

Figure 5. Mass-spin maps for the considered QPO models and 18 different EoS. The light color area denotes an intersection between the 2D surface given by the EoS and 3D volume corresponding to 2σ confidence level associated to the best fit for a given model and the intervals of $M \in [1M_{\odot}, 4M_{\odot}]$, $j \in [0.0, 0.5]$, and $\tilde{q} \in [1, 10]$. The χ^2 minimum at the 2D surface is denoted by the dark marker. The dark color area denotes the 2σ confidence level calculated when this local minimum is assumed as a global one providing that the QPO frequency error bars are underestimated by a corresponding factor ξ_{2D}. The horizontal dashed red lines denote spin frequency measured from the X-ray bursts (i.e., $\nu_S = 580$ Hz).

(see, e.g., Klähn et al. (2006), Steiner et al. (2010, 2015), Klähn et al. (2007), Dutra et al. (2012), and Dutra et al. (2014) for various tests of EoS and their applications, and Demorest et al. (2010) and Antoniadis et al. (2013) for the highest observed NS masses).

In Figure 5 we show several relations between the mass and spin frequency obtained for the RP model and our large set of EoS. These relations are similar to those implied by the Sly 4 EoS discussed above. However, we can see that in several cases, a given EoS does not provide any match for the NS spin of 580 Hz. This can rule out the combination of the considered RP model and given specific EoS. The selection effect comes from the correlation between the estimated mass and angular momentum and the limits on maximal mass allowed by the individual EoS.

5.1. Selecting Combinations of QPO Models and EoS

We also found an analogical selection effect for the other four examined QPO models. The corresponding $M - j$ maps are shown in Figure 5. The results for all considered models are summarized in Table 3. The table shows which of the models and EoS are compatible, and which of them are not. Overall, there are 39 matches from the 90 investigated cases for the NS spin frequency of 580 Hz. We can therefore conclude that for the NS spin frequency in 4U 1636-53 to be close to 580 Hz, we can exclude 51 of the 90 considered combinations of EoS and QPO models. This result follows from the requirement of the relatively high masses implied by the individual QPO models and from the increase in these masses with the NS spin.

5.2. Implications for QPO Models

When we assume that the Hartle–Thorne geometry is restricted to the range of angular momentum and scaled quadrupole moment $\{j, \tilde{q}\} \in \{[0, 0.4], [1, 10]\}$, the four investigated QPO models imply a relatively broad range of NS mass, $M \in [1.6, 3.4]\, M_{\odot}$ ($M \in [1.8, 2.5]\, M_{\odot}$ when $j = 0$). In Figure 6 we illustrate a corresponding comparison between the data and some individual fits. From inspecting Figure 6, we can see that the quality of the fits is rather poor (represented by $\chi^2/\text{d.o.f.} \sim 10$, see Table 3). The comparison between data and curves drawn for the RP model indicates the possible presence of systematic errors within the model. This also holds for the RP1, RP2, and WD model. The trend is somewhat better only in the case of the TD model. This has also been noted by Lin et al. (2011). However, when we take into account requirements given by present EoS and the NS spin of 580 Hz, the TD model is ruled out (see the green curve in the bottom right panel of Figure 6). The range of NS mass that corresponds to the considered models is then reduced to $M \in [2.0, 2.2]\, M_{\odot}$.

Remarkably, the consideration of Hartle–Thorne spacetime does not improve the quality of the fits. For instance, the deviation of the RP model curve from the data discussed by Lin

Table 3
Results for the Considered EoS and QPO Models

	RP Model			RP1 Model			RP2 Model		
	$\xi_{H+T}=3.6$, $\xi_{\rm Kerr}=3.1$			$\xi_{H+T}=3.6$, $\xi_{\rm Kerr}$=3.3			$\xi_{H+T}=3.9$, $\xi_{\rm Kerr}=3.5$		
EoS	M	j	$\chi^2_{\rm min}$	M	j	$\chi^2_{\rm min}$	M	j	$\chi^2_{\rm min}$
SLy 4	2.06 ± 0.01	0.19	305	1.99 ± 0.02	0.21	302	X	X	X
SkI5	2.11 ± 0.01	0.25	323	2.02 ± 0.01	0.27	321	2.19 ± 0.02	0.23	327
SV	2.12 ± 0.01	0.28	345	2.03 ± 0.01	0.30	334	2.22 ± 0.02	0.27	355
SkO	X	X	X	1.98 ± 0.01	0.20	302	X	X	X
Gs	2.08 ± 0.01	0.22	309	2.01 ± 0.02	0.24	307	X	X	X
SkI2	2.10 ± 0.01	0.23	313	2.01 ± 0.02	0.25	311	2.14 ± 0.01	0.21	395
SGI	2.11 ± 0.01	0.25	319	2.02 ± 0.02	0.26	314	2.19 ± 0.02	0.23	328
APR	2.09 ± 0.01	0.22	309	2.00 ± 0.02	0.23	304	2.17 ± 0.02	0.21	320
AU	2.06 ± 0.01	0.20	305	1.98 ± 0.02	0.20	301	2.13 ± 0.02	0.19	315
UU	2.08 ± 0.01	0.21	306	1.99 ± 0.02	0.22	302	2.16 ± 0.02	0.20	317
UBS	2.11 ± 0.01	0.26	325	2.02 ± 0.01	0.27	317	2.21 ± 0.02	0.25	338
GLENDNH3	X	X	X	2.00 ± 0.01	0.22	303	X	X	X
Gandolfi	2.08 ± 0.01	0.21	307	1.99 ± 0.01	0.22	303	2.15 ± 0.02	0.20	318
QMC700	X	X	X	2.01 ± 0.01	0.27	332	X	X	X
KDE0v1	X	X	X	1.97 ± 0.01	0.19	301	X	X	X
NRAPR	X	X	X	$1.95\pm0.01^*$	0.18^*	7196	X	X	X
PNM L80	2.04 ± 0.01	0.19	340	2.00 ± 0.01	0.22	303	X	X	X
J35 L80	2.07 ± 0.01	0.21	306	2.00 ± 0.01	0.23	304	X	X	X

Note. Values of $\xi=\sqrt{\chi^2_{\rm min}/{\rm dof}}$ corresponding to global minima of $\chi^2_{\rm min}$ in Hartle–Thorne spacetime are compared to values obtained for Kerr spacetimes in Török et al. (2012). Asterisks denote that the indicated values of M and j are connected to the dark color area in Figures 4 and 5. In this case there is no intersection between the spin frequency curve in the 2D EoS plane and the 2σ level 3D volume around the global minima of the QPO model fit in the Hartle–Thorne spacetime. The local minimum, $\chi^2_{\rm 2Dmin}$, at the 2D EoS plane is then assumed as a global minimum provided that the QPO frequency error bars are underestimated by a corresponding factor, $\xi_{\rm 2D}=\sqrt{\chi^2_{\rm 2Dmin}/{\rm dof}}$. The *X*-symbol indicates that the spin frequency 580 Hz is not reached even in this case. For the TD and WD models, the spin frequency is not reached.

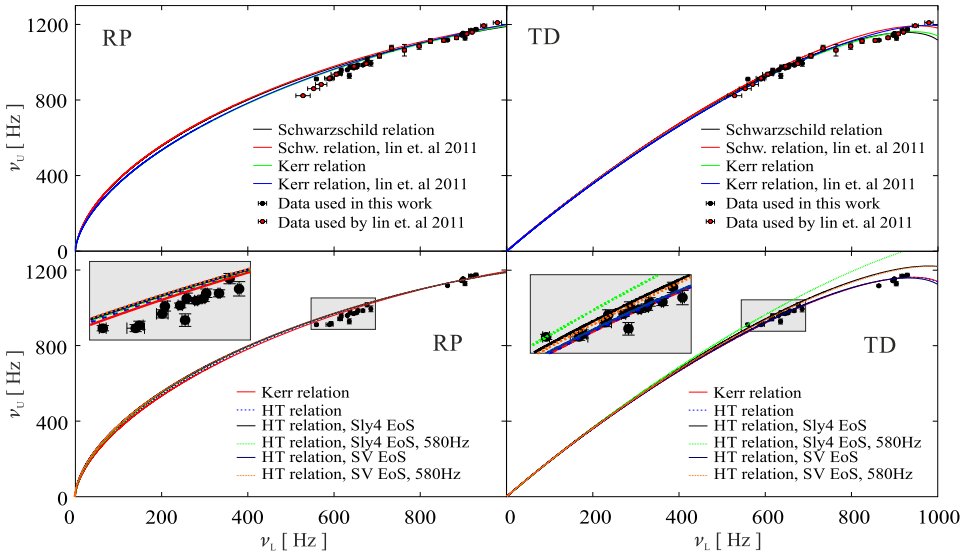

Figure 6. Twin-peak QPO data and examples of their individual fits. Top: best fits of data used in this work (black dots) vs. best fits of data (red dots) used by Lin et al. (2011). Bottom: best fits assuming Kerr spacetime denoted by red lines ($\chi^2_{\rm min,RP}=189/20$d.o.f., $\chi^2_{\rm min,TD}=122/20$d.o.f). Best fits in Hartle–Thorne spacetimes are denoted by blue lines ($\chi^2_{\rm min,RP}=243/19$d.o.f, $\chi^2_{\rm min,TD}=123/19$d.o.f.). Best fits in Hartle–Thorne spacetimes restricted to the parametric 2D surface given by SLy 4 EoS are denoted by black lines ($\chi^2_{\rm min,RP}=303/20$d.o.f, $\chi^2_{\rm min,TD}=2514/20$d.o.f). Best fits in Hartle–Thorne spacetimes restricted to the parametric 2D surface given by SV EoS are denoted by dark blue lines ($\chi^2_{\rm min,RP}=327/20$d.o.f, $\chi^2_{\rm min,TD}=129/20$d.o.f). Best fits in Hartle–Thorne spacetimes restricted by SLy 4 Eos and NS spin 580 Hz are denoted by green lines ($\chi^2_{\rm min,RP}=305/21$d.o.f, $\chi^2_{\rm min,TD}=15725/21$d.o.f). Best fits in Hartle–Thorne spacetimes restricted by SV EoS and NS spin 580 Hz are denoted by orange lines ($\chi^2_{\rm min,RP}=344/21$d.o.f, $\chi^2_{\rm min,TD}=2233/21$d.o.f).

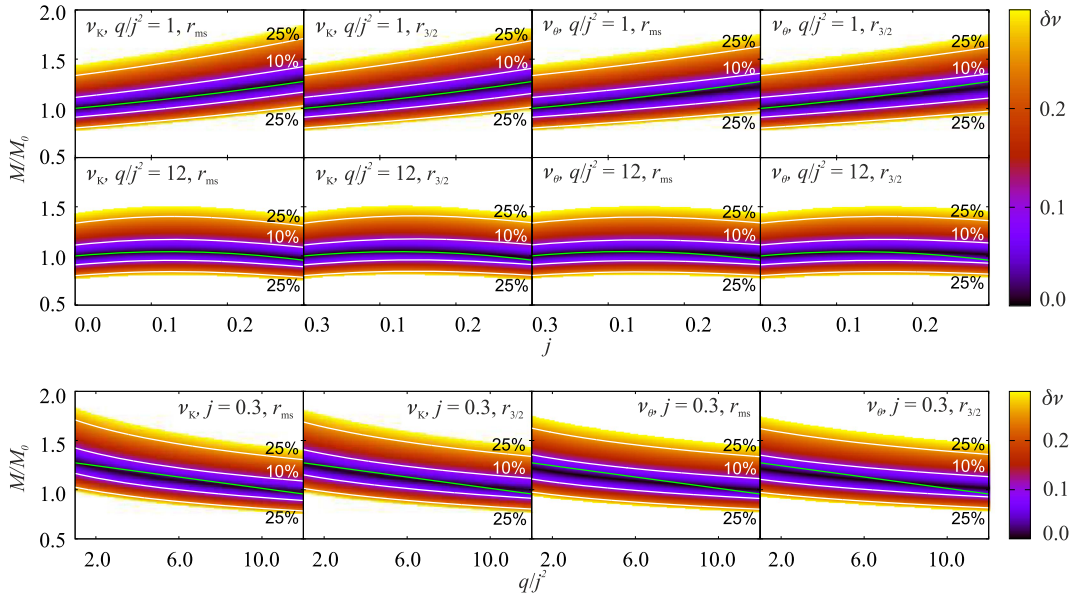

Figure 7. Color-coded maps indicating values of the dimensionless difference between the characteristic frequencies of orbital motion $\delta\nu \equiv (\nu(M_0) - \nu(M, j, q))/\nu(M_0)$ calculated assuming the Schwarzschild spacetimes ($M = M_0$) and Hartle–Thorne spacetimes. Individual panels assume the chosen fixed values of parameters j and $\tilde{q}$. Combinations of parameters indicated by green curves are given by relation (7), $M = M_0(1 + 0.7j + 1.02j^2 - 0.32q)$. Frequencies are calculated at characteristic radii $r_{3:2}$ and r_{ms}, where the Keplerian and periastron precession frequencies are in a 3:2 and 1:1 ratio.

et al. (2011) is present when we assume Hartle–Thorne as well as Kerr spacetime. There is $\Delta\chi \equiv \sum \mathrm{sign}(\chi_i)\chi_i^2 \sim -150$ for the bottom part of the curve ($i \in \{1 \ldots 14\}$), while it is $\Delta\chi \sim +20$ for the top part of the curve ($i \in \{15 \ldots 22\}$). The possibly required non-geodesic corrections discussed by Török et al. (2012) and Lin et al. (2011) therefore do not depend on the chosen spacetime description (see also Török et al. 2016, in this context). This conclusion is in a good agreement with the suggestion of Török et al. (2012), who implied that the parameters of RP model fits within Hartle–Thorne spacetime should exhibit a degeneracy approximated as

$$M = M_0(1 + 0.7j + 1.02j^2 - 0.32q), \qquad (7)$$

where $M_0 = 1.78M_\odot$ for 4U 1636-53. This degeneracy is illustrated in Figures 7 and 8, where we also quantify its validity for the other models discussed here.

5.3. Consideration of Low-frequency QPOs

Strong restrictions to the model and implied NS mass may be obtained when low-frequency QPOs are considered. This can be clearly illustrated for the RP model, which associates the observed low-frequency QPOs with the Lense–Thirring precession that occurs at the same radii as the periastron precession. Within the framework of the model, the Lense–Thirring frequency ν_{LT} represents a sensitive spin indicator (Stella & Vietri 1998a, 1998b; Morsink & Stella 1999; Stella et al. 1999). In our previous paper (Török et al. 2012) we carried out a simplified estimate of the underlying NS angular momentum and mass assuming Kerr spacetimes, arriving at values of $j \sim 0.25 \div 0.35$ and $M \sim (2.2 \div 2.4)M_\odot$. These values appeared too high when confronted with the

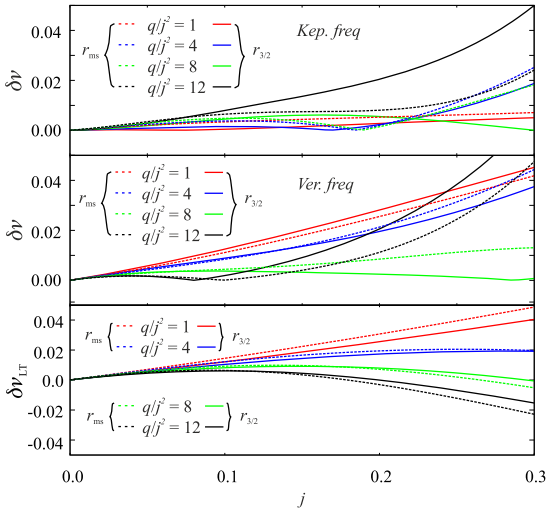

Figure 8. Dimensionless quantity $\delta\nu$ plotted for different values of q/j^2 and relation (7). We do not include panels for radial and periastron precession frequencies here because the values are the same as for the Keplerian frequency.

implications of the set of 5 EoS assumed within the paper. As discussed here in Section 2, the extended set of EoS can be more compatible with the expectations based on the consideration of Lense–Thirring precession. It is straightforward to extend our previous estimate to Hartle–Thorne spacetime and all 18 EoS. The results of such an extension are included in

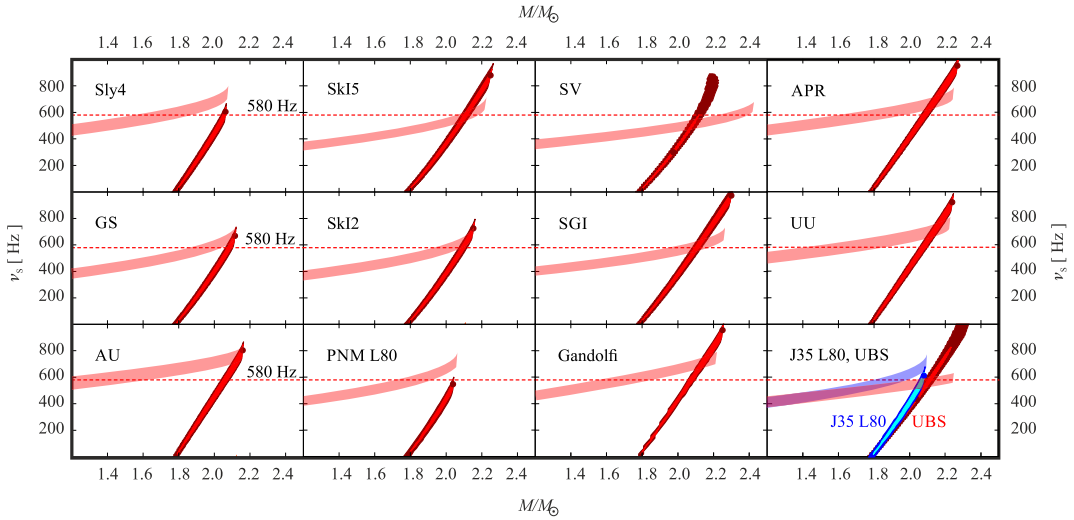

Figure 9. Consideration of RP model assuming both low- and high-frequency QPOs and 13 EoS. The RP model mass-spin maps from Figure 5 are confronted with requirements following from the identification of low-frequency QPOS with the Lense–Thirring precession frequency. The last panel includes the consideration of two different EoS.

Figure 9. We show there 13 EoS that are compatible with the observed twin-peak QPOs and RP model, and demonstrate that 8 of these EoS do not meet the requirements that are based on the consideration of Lense–Thirring preccession. Only 5 EoS are therefore compatible with the model.

We would like to acknowledge the Czech grant GAČR 209/12/P740, and internal grants of the Silesian University in Opava, SGS/11,23/2013, SGS/14,15/2016 and IGS/12/2015. Z.S. acknowledges the Albert Einstein Center for Gravitation and Astrophysics supported by the Czech Science Foundation grant No. 14-37086G. We are grateful to Marek Abramowicz, Wlodek Kluzniak (CAMK), John Miller (University of Oxford), Will Newton (Texas A&M University-Commerce), Luigi Stella (INAF), and Jiřina Stone (Oak Ridge National Laboratory) for many useful discussions. We also thank to the anonymous referee for the comments and suggestions that greatly helped us to improve the paper. Furthermore, we would like to acknowledge the hospitality of the University of Oxford and the Astronomical Observatory in Rome. Last but not least, we express our sincere thanks to the concierges of the Mlýnská hotel in Uherské Hradiště for their kind help and participation in organizing frequent workshops of the Silesian university and the Astronomical institute.

REFERENCES

Abramowicz, M. A., Almergren, G. J. E., Kluźniak, W., & Thampan, A. V. 2003a, arXiv:gr-qc/0312070
Abramowicz, M. A., Bulik, T., Bursa, M., & Kluźniak, W. 2003b, A&A, 404, L21
Abramowicz, M. A., Karas, V., Kluźniak, W., Lee, W. H., & Rebusco, P. 2003c, PASJ, 55, 467
Abramowicz, M. A., & Kluźniak, W. 2001, A&A, 374, L19
Agrawal, B. K., Shlomo, S., & Au, V. K. 2005, PhRvC, 72, 014310
Akmal, A., Pandharipande, V. R., & Ravenhall, D. G. 1998, PhRvC, 58, 1804
Aliev, A. N., & Galtsov, D. V. 1981, GReGr, 13, 899
Alpar, M. A., & Shaham, J. 1985, Natur, 316, 239
Ansorg, M., Kleinwächter, A., & Meinel, R. 2003, A&A, 405, 711
Antoniadis, J., Freire, P. C. C., Wex, N., et al. 2013, Sci, 340, 448
Barret, D., & Boutelier, M. 2008, NewAR, 51, 835
Barret, D., Olive, J.-F., & Miller, M. C. 2005, MNRAS, 361, 855
Barret, D., Olive, J.-F., & Miller, M. C. 2006, MNRAS, 370, 1140
Belloni, T., Homan, J., Motta, S., Ratti, E., & Méndez, M. 2007, MNRAS, 379, 247
Belloni, T., Méndez, M., & Homan, J. 2005, A&A, 437, 209
Berti, E., White, F., Maniopoulou, A., & Bruni, M. 2005, MNRAS, 358, 923
Bonazzola, S., Gourgoulhon, E., & Marck, J.-A. 1998, PhRvD, 58, 104020
Bonazzola, S., Gourgoulhon, E., Salgado, M., & Marck, J. A. 1993, A&A, 278, 421
Boshkayev, K., Quevedo, H., Abutalip, M., Kalymova, Z., & Suleymanova, S. 2015, arXiv:1510.02016
Boutelier, M., Barret, D., Lin, Y., & Török, G. 2010, MNRAS, 401, 1290
Bursa, M. 2005, in Proc. RAGtime 6/7, Workshops on Black Holes and Neutron Stars, ed. S. Hledík & Z. Stuchlík (Opava: Silesian Univ.), 39
Čadež, A., Calvani, M., & Kostić, U. 2008, A&A, 487, 527
Chandrasekhar, S., & Miller, J. C. 1974, MNRAS, 167, 63
Demorest, P. B., Pennucci, T., Ransom, S. M., Roberts, M. S. E., & Hessels, J. W. T. 2010, Natur, 467, 1081
Dutra, M., Louren co, O., Avancini, S. S., et al. 2014, PhRvC, 90, 055203
Dutra, M., Louren co, O., Sá Martins, J. S., et al. 2012, PhRvC, 85, 035201
Galloway, D. K., Muno, M. P., Hartman, J. M., Psaltis, D., & Chakrabarty, D. 2008, ApJS, 179, 360
Gandolfi, S., Illarionov, A. Y., Fantoni, S., et al. 2010, MNRAS, 404, L35
Germanà, C., Kostić, U., Čadež, A., & Calvani, M. 2009, in AIP Conf. Ser. 1126, SIMBOL-X: Focusing on the Hard X-Ray Universe, ed. J. Rodriguez & P. Ferrando (Melville, NY: AIP), 367
Gilfanov, M., Churazov, E., & Revnivtsev, M. 2000, MNRAS, 316, 923
Glendenning, N. K. 1985, ApJ, 293, 470
Hartle, J. B. 1967, ApJ, 150, 1005
Hartle, J. B., & Thorne, K. S. 1968, ApJ, 153, 807
Horák, J., Abramowicz, M. A., Kluźniak, W., Rebusco, P., & Török, G. 2009, A&A, 499, 535
Kato, S. 2001, PASJ, 53, 1
Kato, S. 2007, PASJ, 59, 451
Kato, S. 2008, PASJ, 60, 111
Klähn, T., Blaschke, D., Sandin, F., et al. 2007, PhLB, 654, 170
Klähn, T., Blaschke, D., Typel, S., et al. 2006, PhRvC, 74, 035802
Kluźniak, W., & Abramowicz, M. A. 2001, arXiv:astro-ph/0105057
Kluźniak, W., & Abramowicz, M. A. 2002, arXiv:astro-ph/0203314
Kluźniak, W., Abramowicz, M. A., Kato, S., Lee, W. H., & Stergioulas, N. 2004, ApJL, 603, L89

Kluźniak, W., & Rosińska, D. 2013, MNRAS, 434, 2825
Kostić, U., Čadež, A., Calvani, M., & Gomboc, A. 2009, A&A, 496, 307
Lamb, F. K., Shibazaki, N., Alpar, M. A., & Shaham, J. 1985, Natur, 317, 681
Lin, Y.-F., Boutelier, M., Barret, D., & Zhang, S.-N. 2011, ApJ, 726, 74
Manko, V. S., Mielke, E. W., & Sanabria-Gómez, J. D. 2000, PhRvD, 61, 081501
Méndez, M. 2006, MNRAS, 371, 1925
Miller, J. C. 1977, MNRAS, 179, 483
Miller, M. C., Lamb, F. K., & Psaltis, D. 1998, ApJ, 508, 791
Morsink, S. M., & Stella, L. 1999, ApJ, 513, 827
Mukhopadhyay, B. 2009, ApJ, 694, 387
Newton, W. G., Gearheart, M., & Li, B.-A. 2013, ApJS, 204, 9
Nozawa, T., Stergioulas, N., Gourgoulhon, E., & Eriguchi, Y. 1998, A&AS, 132, 431
Pappas, G. 2015, MNRAS, 454, 4066
Pétri, J. 2005, A&A, 439, L27
Psaltis, D., Wijnands, R., Homan, J., et al. 1999, ApJ, 520, 763
Rezzolla, L., Yoshida, S., & Zanotti, O. 2003, MNRAS, 344, 978
Rikovska Stone, J., Guichon, P. A. M., Matevosyan, H. H., & Thomas, A. W. 2007, NuPhA, 792, 341
Rikovska Stone, J., Miller, J. C., Koncewicz, R., Stevenson, P. D., & Strayer, M. R. 2003, PhRvC, 68, 034324
Rosińska, D., Kluźniak, W., Stergioulas, N., & Wiśniewicz, M. 2014, PhRvD, 89, 104001
Steiner, A. W., Gandolfi, S., Fattoyev, F. J., & Newton, W. G. 2015, PhRvC, 91, 015804
Steiner, A. W., Lattimer, J. M., & Brown, E. F. 2010, ApJ, 722, 33
Steiner, A. W., Prakash, M., Lattimer, J. M., & Ellis, P. J. 2005, PhR, 411, 325
Stella, L., & Vietri, M. 1998a, in Abstracts of the XIX Texas Symp. on Relativistic Astrophysics and Cosmology, ed. J. Paul, T. Montmerle, & E. Aubourg (Saclay, France: CEA)
Stella, L., & Vietri, M. 1998b, ApJL, 492, L59
Stella, L., & Vietri, M. 1999, PhRvL, 82, 17
Stella, L., & Vietri, M. 2001, in ASP Conf. Ser. 2000, X-ray Astronomy, ed. R. Giacconi, S. Serio, & L. Stella (San Francisco, CA: ASP), 213
Stella, L., Vietri, M., & Morsink, S. M. 1999, ApJL, 524, L63
Stergioulas, N., & Friedman, J. L. 1995, ApJ, 444, 306
Strohmayer, T. E., & Markwardt, C. B. 2002, ApJ, 577, 337
Stuchlík, Z., Konar, S., Miller, J. C., & Hledík, S. 2008, A&A, 489, 963
Stuchlík, Z., Kotrlová, A., & Török, G. 2013, A&A, 552, A10
Stuchlík, Z., Kotrlová, A., Török, G., & Goluchová, K. 2014, AcA, 64, 45
Stuchlík, Z., Urbanec, M., Kotrlová, A., Török, G., & Goluchová, K. 2015, AcA, 65, 169
Stute, M., & Camenzind, M. 2002, MNRAS, 336, 831
Titarchuk, L., & Wood, K. 2002, ApJL, 577, L23
Török, G. 2009, A&A, 497, 661
Török, G., Abramowicz, M. A., Bakala, P., et al. 2008a, AcA, 58, 15
Török, G., Abramowicz, M. A., Bakala, P., et al. 2008b, AcA, 58, 113
Török, G., Bakala, P., Stuchlik, Z., & Čech, P. 2008c, AcA, 58, 1
Török, G., Bakala, P., Šrámková, E., et al. 2012, ApJ, 760, 138
Török, G., Bakala, P., Šrámková, E., Stuchlík, Z., & Urbanec, M. 2010, ApJ, 714, 748
Török, G., Goluchová, K., Horák, J., et al. 2016, MNRAS, 457, L19
Török, G., & Stuchlík, Z. 2005, A&A, 437, 775
Török, G., Stuchlík, Z., & Bakala, P. 2007, CEJPh, 5, 457
Török, G., Urbanec, M., Adámek, K., & Urbancová, G. 2014, A&A, 564, L5
Urbanec, M., Běták, E., & Stuchlík, Z. 2010a, AcA, 60, 149
Urbanec, M., Miller, J. C., & Stuchlík, Z. 2013, MNRAS, 433, 1903
Urbanec, M., Török, G., Šrámková, E., et al. 2010b, A&A, 522, A72
van der Klis, M. 2005, AN, 326, 798
van der Klis, M. 2006, in Compact stellar X-ray sources, ed. W. Lewin & M. van der Klis (Cambridge: Cambridge Univ. Press), 39
Wagoner, R. V. 1999, PhR, 311, 259
Wagoner, R. V., Silbergleit, A. S., & Ortega-Rodríguez, M. 2001, ApJL, 559, L25
Wang, D. H., Chen, L., Zhang, C. M., et al. 2015, MNRAS, 454, 1231
Watts, A. L. 2012, ARA&A, 50, 609
Wiringa, R. B., Fiks, V., & Fabrocini, A. 1988, PhRvC, 38, 1010
Zhang, C.-M. 2005, ChJAS, 5, 21

Paper VI

6.6. Twin peak quasi-periodic oscillations as signature of oscillating cusp torus

Török Gabriel, Goluchová Kateřina, Horák Jiří, Šrámková Eva, Urbanec Martin, Pecháček Tomáš, & Bakala, Pavel

Monthly Notices of the Royal Astronomical Society: Letters, 2016, Volume 457, Issue 1, p.L19-L23

Monthly Notices of the ROYAL ASTRONOMICAL SOCIETY

MNRAS **457,** L19–L23 (2016) doi:10.1093/mnrasl/slv196

Twin peak quasi-periodic oscillations as signature of oscillating cusp torus

G. Török,[1]★ K. Goluchová,[1] J. Horák,[2] E. Šrámková,[1] M. Urbanec,[1] T. Pecháček[1] and P. Bakala[1]

[1] *Institute of Physics, Faculty of Philosophy and Science, Silesian University in Opava, Bezručovo nám. 13, CZ-746 01 Opava, Czech Republic*
[2] *Astronomical Institute, Boční II 1401/2a, CZ-14131 Praha 4 - Spořilov, Czech Republic*

Accepted 2015 December 6. Received 2015 November 13; in original form 2015 August 25

ABSTRACT

Serious theoretical effort has been devoted to explain the observed frequencies of twin-peak quasi-periodic oscillations (HF QPOs) observed in low-mass X-ray neutron star binaries. Here we propose a new model of HF QPOs. Within its framework we consider an oscillating torus with cusp that changes location r_0 of its centre around radii very close to innermost stable circular orbit. The observed variability is assigned to global modes of accreted fluid motion that may give strong modulation of both accretion disc radiation and the accretion rate. For a given space–time geometry, the model predicts that QPO frequencies are function of single parameter r_0. We illustrate that the model can provide fits of data comparable to those reached by other models, or even better. In particular, it is compared to relativistic precession model. Moreover, we also illustrate that the model consideration is compatible with consideration of models of a rotating neutron star in the atoll source 4U 1636−53.

Key words: accretion, accretion discs – equation of state – stars: neutron – X-rays: binaries.

1 INTRODUCTION

Many models have been proposed to explain a phenomenon of high-frequency quasi-periodic oscillations (QPOs) observed in neutron-star low-mass X-ray binaries (HF QPOs in LMXBs). It is believed that HF QPOs are carrying signatures of strong gravity and dense matter composition. Serious theoretical effort has been devoted to explain the observed frequencies and their correlations (see e.g. Török et al. 2012, for further information and a large list of references to various individual models of HF QPOs). In this section, we only briefly recall two particular outstanding theoretical frameworks.

One of the first QPO models, the so-called relativistic-precession model (RP model) identifies the twin-peak kHz QPO frequencies ν_U and ν_L with two fundamental frequencies of a nearly circular geodesic motion: the Keplerian orbital frequency and the periastron-precession frequency,

$$\nu_U = \nu_{\rm K}, \quad \nu_L = \nu_{\rm per} = \nu_{\rm K} - \nu_{\rm r}\,, \tag{1}$$

where $\nu_{\rm r}$ denotes the radial epicyclic frequency. The correlations among them is then obtained by varying the radius of the underlying circular orbit in a reasonable range. Within this framework it is usually assumed that the variable component of the observed X-ray signal originates in a bright localized spot or blob orbiting the neutron star on a slightly eccentric orbit. The observed radiation is then periodically modulated due to the relativistic effects. It has been shown that the model is roughly matching the observed $\nu_U(\nu_L)$ correlations (Stella & Vietri 1999; Belloni, Méndez & Homan 2007; Török et al. 2012). Nevertheless, the RP model also suffers some theoretical difficulties. It is not clear whether the modulation of a radiation from a small localized spot can produce sufficiently strong signal modulation to explain a relatively large observed HF QPO amplitudes. It is then expected that larger spots (giving higher amount of modulated photons) can undergo a serious shearing due to the differential rotation in the surrounding accretion disc. This does not agree with a high coherence of the HF QPO signal which is often observed. The model also lacks an explanation of inferred existence of preferred orbits which should be responsible for appearance of HF QPO pairs (twin peaks) and clustering of their frequencies.

Only slightly later, Abramowicz & Kluźniak (2001) and Kluzniak & Abramowicz (2001) proposed the concept of orbital resonance models. Within this concept, HF QPOs originate in resonances between oscillation modes of the accreted fluid. The most quoted, so-called 3:2 epicyclic resonance model, identifies the resonant eigenfrequencies with frequencies ν_θ and $\nu_{\rm r}$ of radial and vertical epicyclic axisymmetric modes of disc (or torus) oscillations. It is assumed that

$$\nu_U = \nu_\theta,\ \nu_L = \nu_{\rm r} \Leftrightarrow \nu_U/\nu_L = 3/2\,, \tag{2}$$

while the correlation $\nu_U(\nu_L)$ arises from resonant corrections to the eigenfrequencies (Abramowicz et al. 2005). We stress that the model

★E-mail: gabriel.torok@physics.cz

deals with a collective motion of the accreted matter.[1] Moreover, the oscillation modes of innermost region of the accretion flow can modulate the amount of matter transferred to NS surface through the boundary layer (Paczynski 1987; Horák 2005; Abramowicz, Horák & Kluzniak 2007). Therefore, it may naturally explain both high amplitudes and coherence of the HF QPOs. Nevertheless, it is questionable whether the resonant corrections to the eigenfrequencies can be large enough to explain the whole observed range of ν_U and ν_L. Furthermore, it has been shown that the model implies large range of NS masses and has difficulties when confronted to models of rotating NS based on up-to-date equations of state (EoS; see Urbanec et al. 2010b; Török et al. 2012).

Motivated by partial success of the above models and their complementary difficulties, we present a modified framework for interpreting the HF QPOs.

2 OSCILLATING CUSP TORI

Our model is largely based on the theoretical work of Straub & Šrámková (2009). We adopt Kerr geometry to describe slowly rotating compact NS. We assume that the innermost region of accretion flow is hot enough to form a pressure supported torus of a moderate thickness. Assuming a non-relativistic polytropic EoS and neglecting the poloidal components of the fluid velocity (so that the fluid follows circular orbits), the equilibrium torus shape and its structure are completely determined by the Lane–Embden function, which is given by a simple analytic formula (Abramowicz et al. 2006; Straub & Šrámková 2009)

$$f = 1 - \frac{1}{nc_{s0}^2} \ln \frac{\mathcal{E}}{\mathcal{E}_0}. \tag{3}$$

In this equation, $\mathcal{E}$ denotes the energy of a particle on a (non-geodesic) circular orbit having the specific angular momentum ℓ. We assume that the angular momentum is constant in the whole volume of the torus, $\ell = \ell_0 = \text{const}$. Since we assume that the torus is located in the vicinity of the innermost stable circular orbit (ISCO, $r = r_{ms}$), where also Keplerian angular momentum is nearly constant, we believe it is a reasonable approximation. Meaning of other symbols in equation (3) is straightforward: n is the polytropic index ($n = 3$ for a radiation-pressure-dominated fluid) and c_{s0} is the sound speed at the centre of the torus located at radius r_0 in the equatorial plane, where the pressure gradient vanishes and energy $\mathcal{E}$ takes the value $\mathcal{E}_0$. Vanishing of the pressure forces at the torus centre implies the streamline $r = r_0$, $\theta = \pi/2$ to be a geodesic line because of which the fluid angular momentum takes Keplerian value at that radius, $\ell_0 = \ell_K(r_0)$.

2.1 Torus size

The surfaces of constant density and pressure coincide with those of constant f and their values can be calculated from f by $\rho = \rho_0 f^n$ and $p = p_0 f^{n+1}$, where ρ_0 and p_0 refer to the values at the torus centre that corresponds to $f = 1$. On the other hand, the surface of the torus, where both pressure and density vanishes, is given by the condition $f = 0$. It is also worth to note that the position of the centre r_0 and the shape of these surfaces are entirely given by the value of ℓ_0 and the space–time geometry, while the particular values of p and ρ and consequently the location of the overall surface of the torus are set by the central value of the sound speed c_{s0}.

Straub & Šrámková (2009) introduce a dimensionless parameter β that characterizes the size of the torus,

$$\beta = \frac{\sqrt{2n}c_{s0}}{r_0\mathcal{E}_0\left(\ell_0\, g_0^{\phi\phi} - g_0^{t\phi}\right)}. \tag{4}$$

This parameter is roughly proportional to the Mach number of the flow at the torus centre as can be seen from its Newtonian limit $\beta = \sqrt{2n}(c_s/r\Omega)_0$ (see also Blaes 1985). In addition, it is also roughly proportional to the ratio of the radial (or vertical) extension of the torus to its central radius r_0. Hence, the sound-crossing time and the dynamical time-scale of the torus are roughly similar.

2.2 Marginally overflowing tori (cusp tori)

The stationary solution does not exist for an arbitrary large value of β (Abramowicz, Jaroszynski & Sikora 1978). In addition to the obvious limit $\beta \leq \beta_\infty$ corresponding to tori whose outer edge extends to infinity, there is a much stronger constrain coming from general relativity that significantly limits the torus size close to ISCO. Large enough tori that extend below the ISCO radius, may be terminated there by a 'cusp', where the rotation of the flow becomes Keplerian again. This is a consequence of the fact that the Keplerian angular momentum reaches its minimum at ISCO.

The cusp corresponds to a saddle point of the Lane–Embden function and the corresponding self-crossing equipotential limits the surface of any stationary rotating fluid configuration with given angular momentum ℓ_0. Fluid that appear outside this surface, is accreted on to the central star on the dynamical time-scale driven by gravity and pressure forces without need of viscosity (Paczynski 1977). Abramowicz et al. (1978) calculated analytically the accretion rate from a slightly overflowing torus, their result agrees very well with numerical simulations.

The critical value of β giving a marginally overflowing torus follows from equations (3) and (4),

$$\beta_c(r_0) = \frac{\sqrt{2\ln(\mathcal{E}_c/\mathcal{E}_0)}}{r_0\mathcal{E}_0\left(\ell_0\, g_0^{\phi\phi} - g_0^{t\phi}\right)}, \tag{5}$$

where $\mathcal{E}_c = \mathcal{E}(r_c)$ is the particle energy at the cusp. Its location $r = r_c$ can be found by equating the Keplerian angular momentum to the fluid angular momentum ℓ_0. This procedure leads to the third-order algebraic equation (in $\sqrt{r_c}$), giving the position of the cusp in terms of the location of the torus centre.

If the stellar spin is neglected ($j = 0$), the equation is reduced to the quadratic one and its solution can be expressed as

$$r_c = r_0\left(\frac{M + \sqrt{(2r_0 - 3M)M}}{r_0 - 2M}\right)^2, \quad r_0 \geq 6M \tag{6}$$

and the critical β-parameter reads

$$\beta_c = \frac{(r_0 - r_c)(r_0 - 2M)^2[r_0 r_c - 2M(r_0 + 2r_c)]^{1/2}}{r_c r_0 (r_c - 2M)^{1/2}(r_0 - 3M)^{1/2}}. \tag{7}$$

This can be used for $r_0 \lesssim 10.47\,M$, where $\beta = \beta_\infty$.

2.3 Frequencies of epicyclic oscillations

Abramowicz et al. (2006) pointed out the existence of the radial and vertical epicyclic modes that describes a global motion of the

[1] A different class of models dealing with collective motion of accreted matter considers normal modes of accretion disc oscillations, referred to as discoseismology (e.g. Kato 2001; Wagoner, Silbergleit & Ortega-Rodríguez 2001).

torus. They have found that, in the limit of infinitesimally slender tori $\beta \to 0$, frequencies of these modes $\nu_{\rm R}$ and $\nu_{\rm V}$ measured in the fluid reference frame coincide with the epicyclic frequencies of test particles,

$$\nu_r = \left(1 - \frac{6M}{r} + \frac{8jM^{3/2}}{r^{3/2}} - \frac{3j^2M^2}{r^2}\right)^{1/2} \nu_{\rm K}, \tag{8}$$

$$\nu_\theta = \left(1 - \frac{4jM^{3/2}}{r^{3/2}} + \frac{3j^2M^2}{r^2}\right)^{1/2} \nu_{\rm K}, \tag{9}$$

while at fixed azimuth their frequencies are given by $\nu_{\rm R,\,m} = \nu_{\rm r} + m\nu_{\rm K}$ and $\nu_{\rm V,\,m} = \nu_\theta + m\nu_{\rm K}$ with m being the integer azimuthal wavenumber. In particular, the $m = -1$ radial and vertical modes give the frequencies of the periastron and nodal precession of a weakly eccentric and tilted torus. It is also worth to note that they describe a collective motion of the fluid, rather than a motion of individual particles.

In a more realistic case, when $\beta > 0$, the pressure gradient contributes to the restoring force of the perturbed torus shifting their frequencies to new 'corrected' values,

$$\nu_{\rm R,m}(r_0, \beta) = \nu_{\rm r}(r_0) + m\nu_{\rm K}(r_0) + \Delta\nu_{\rm R,m}(r_0, \beta), \tag{10}$$

$$\nu_{\rm V,m}(r_0, \beta) = \nu_\theta(r_0) + m\nu_{\rm K}(r_0) + \Delta\nu_{\rm V,m}(r_0, \beta). \tag{11}$$

The pressure corrections $\Delta\nu_{\rm R,\,m}$ and $\Delta\nu_{\rm R,\,m}$ have been calculated by Straub & Šrámková (2009) using perturbation expansion in β-parameter. They found that the first non-zero corrections are of the order of β^2.

3 FREQUENCY IDENTIFICATION

We identify the observed HF QPO frequencies with frequencies of the epicyclic modes of torus oscillations. We propose that the upper kilohertz QPO frequency is the Keplerian orbital frequency of the fluid at the centre of the torus, where both pressure and density peaks and from which most of the torus radiation emerges. The lower kilohertz QPO corresponds to the frequency of the non-axisymmetric $m = -1$ radial epicyclic mode. Overall, there is

$$\nu_U \equiv \nu_{\rm K}(r_0), \quad \nu_L \equiv \nu_{\rm R,-1}(r_0, \beta). \tag{12}$$

The QPO frequencies are then strong functions of the position of the centre of the torus r_0 and its thickness β. Obviously, the choice of $\beta = 0$ (slender tori) recovers the RP model frequencies. In the case of a finite thickness $\beta > 0$, they also weakly depend on the value of the polytropic index n. In next, we fix $n = 3$ as the inner parts of the accretion flow are believed to be radiation-pressure-dominated.

We assume the cusp configuration

$$\beta(r_0) \doteq \beta_{\rm c}(r_0). \tag{13}$$

In other words, we expect that for given r_0 the torus is always close to its maximal possible size, just filling its 'Roche-like' lobe. Thus, for a given accreting central compact object, our model predicts that the QPO frequencies are functions of a single parameter r_0,

$$\nu_{\rm u} \equiv \nu_{\rm K}(r_0), \quad \nu_{\rm l} \equiv \nu_{\rm R,-1}\left[r_0, \beta_{\rm c}(r_0)\right]. \tag{14}$$

Therefore, one obtains a unique correlation among them by changing this parameter in a physically reasonable range.

3.1 Applicability of the adopted approximation

The above equations are exact for Kerr space–times and represent an acceptable approximation for high-mass neutron stars (Urbanec, Miller & Stuchlík 2013). Another restriction on their applicability follows from the adopted description of torus dynamics assuming a second order expansion in $\beta_{\rm c}$. Consequently we can assume only $\beta_{\rm c} \lesssim 0.3$. For $j = 0$, this corresponds to tori with radial extension $r_{\rm out} - r_{\rm c} \equiv \Delta r \lesssim 10M$. Neglecting the effects of neutron star rotation, equation (14) implies a relation between torus thickness $\beta_{\rm c}$ and frequency ratio $R \equiv \nu_{\rm u}/\nu_{\rm l}$. We show this relation in Fig. 1a. From this figure we can see that our approximation can be well applied when $R \lesssim 1.7$, while for $R > 2$ it is not sufficient.

4 APPLICATION TO OBSERVED TWIN PEAK QPOS

Lin et al. (2011) and Török et al. (2012) have confronted several HF QPO models with data of the atoll source 4U 1636−53 displaying twin peak QPOs mostly within the range of $R \in [1.25–1.7]$. They have outlined comparison between individual matches of the model to the data as well as quantitative estimates of the inferred NS parameters. The data points assumed in the former study come from a common processing of a large amount of data while the data points used in the latter study correspond to individual continuous observations of the source. As discussed in Török et al. (2012), results of both studies are consistent.

Here, we confront the cusp torus model with the previously examined data. We primarily assume the data points of Lin et al. (2011) that span a larger range of frequencies but we also check the results for the data points corresponding to continuous segments of observation.

4.1 Non-rotating approximation

First, we investigate the case of a simple one-parametric fit assuming non-rotating NS. This way we can obtain comparison with the RP model and a rough estimate of the NS mass implied by our cusp torus model. In Fig. 1b, we plot the sequence of equipotential contours of cusp tori that provide the best match to the 4U 1636−53 data. In Fig. 1c, we show this best fit. The best fit of the RP model is included for the sake of comparison. Clearly, the cusp torus model matches the observed trend better than the RP model. We have $\chi^2/{\rm dof} = 2.3$ for the torus model while it is $\chi^2/{\rm dof} = 16.4$ for the RP model. The NS mass inferred from the cusp torus model, within 2σ confidence level, reads

$$M_0 = 1.69[\pm 0.02]\,{\rm M}_\odot\,. \tag{15}$$

For the data points corresponding to continuous segments of observation we obtain the same mass, $M_0 = 1.69[\pm 0.01]\,{\rm M}_\odot$.

4.2 Consideration of NS rotation

In analogy to results of Török et al. (2012), we may expect that the mass (15) belongs to a mass–angular-momentum relation implied by the cusp torus model. The result of the two-dimensional fitting of the parameters M and j is shown in Fig. 2a. Indeed, the best fits are reached when M and j are related through the specific relation. This relation can be approximated by a quadratic form, $M = M_0(1 + 0.68(j + j^2))$, which results for each of the two data sets.

5 DISCUSSION AND CONCLUSIONS

There is good evidence on the NS spin frequency of 4U 1636−53 based on X-ray burst measurements. Depending on the hotspot

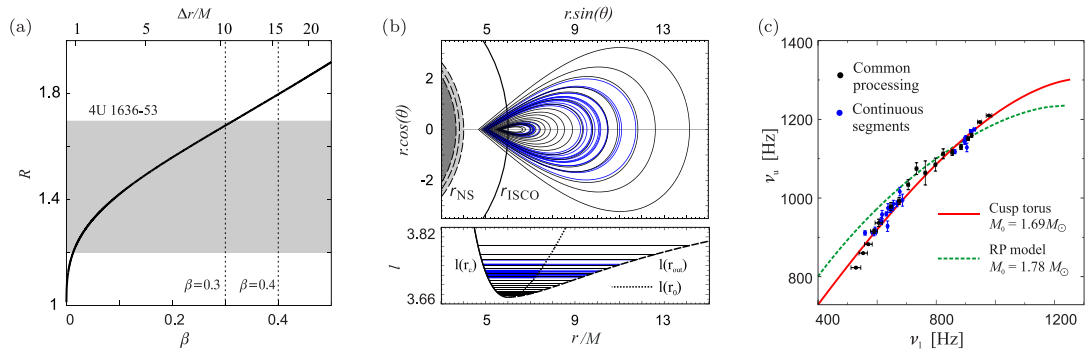

Figure 1. (a) Relation between the thickness of cusp torus and the expected frequency ratio R. The vertical shadow region indicates the interval of R corresponding to most of the available data of the atoll source 4U 1636−53. (b) Sequence of cusp tori corresponding to a one-parametric fit ($j = 0$). The colour-coding is the same as in panel (c). Neutron star radii $r_{\rm NS}$ are drawn for three particular NS EoS (Gle, APR, and GAN) that are further assumed within Fig. 2. The bottom panel indicates angular momentum behaviour together with positions of the torus centre r_0 and both inner and outer edge $r_{\rm c}$ and $r_{\rm out}$. (c) Corresponding frequency relation plotted together with the data points. For the sake of comparison we also present the best fit implied by the RP model ($j = 0$).

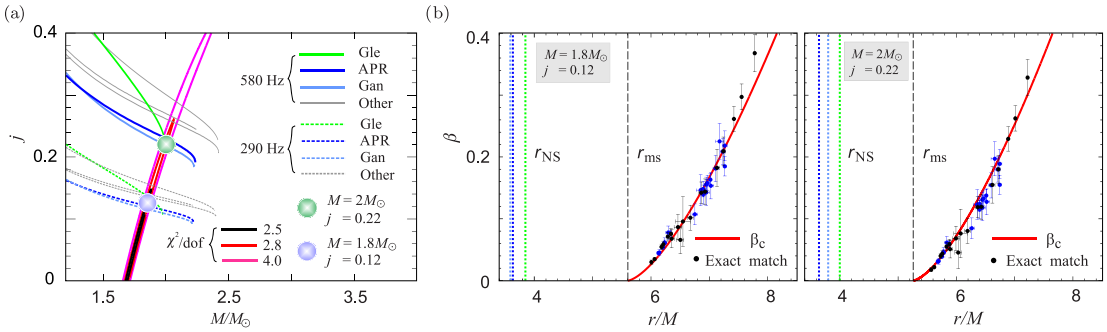

Figure 2. (a) The mass-angular momentum countours resulting from fitting of data points by the cusp torus model vs. mass–angular-momentum relations predicted by models of rotating NS. These are drawn for several NS EoS and spin 290Hz or 580 Hz inferred from the X-ray burst measurements. The two spots indicate chosen combinations of angular momentum where the QPO model and EoS relations overlap. (b) Consideration of combinations of β and r exactly matching individual data points for the two chosen combinations of mass and angular momentum. The colour-coding is the same as in Fig. 1c. The red line denotes the numerically calculated cusp torus relation.

model consideration, the spin $\nu_{\rm S}$ reads either $\nu_{\rm S} \doteq 290$ Hz or $\nu_{\rm S} \doteq 580$ Hz (Strohmayer & Markwardt 2002). The value of 580Hz is usually preferred. We can therefore roughly compare the cusp torus model predictions to predictions of models of rotating NS.

5.1 Neutron star equation of state and radius

In Fig. 2a, we include several mass-angular momentum relations expected from models of rotating NS. We assume the following set of EoS - SLy 4, APR, AU-WFF1, UU-WFF2 and WS-WFF3 (Wiringa, Fiks & Fabrocini 1988; Stergioulas & Friedman 1995; Akmal, Pandharipande & Ravenhall 1998; Rikovska Stone et al. 2003).[2]

Inspecting Fig. 2a, we can see that there are overlaps between the relations given by models of rotating stars and the relation inferred from the cusp torus model. In the figure we denote two particular values of angular momentum together with corresponding masses that roughly represent these overlaps. Assuming the two chosen combinations of mass and angular momentum, we attempted in Fig. 2 b to fit the data by the torus frequencies considering *any* torus thickness, not only $\beta_{\rm c}$. We searched for the combinations of β and r exactly matching each individual data point. Clearly, the obtained values are distributed very close to the cusp relation (13), $\beta = \beta_{\rm c}(r)$, where we have $r > r_{\rm NS}$.

5.2 Model perspectives

A more careful and computationally demanding investigation of the spin influence following the work of Straub & Šrámková (2009) and assuming the Hartle–Thorne space–time should be applied in a consequent work following our study assuming high-mass NS approximation. Nevertheless, we can conclude that there is a very strong indication that twin peak QPOs can be identified with a particular non-axisymmetric $m = -1$ radial epicyclic mode and Keplerian orbital motion associated with the cusp torus. These modes may naturally give strong modulation of both emerging radiation and the accretion rate and their eigenfunctions change only weakly on the spatial scale of the turbulent motion. They are therefore very good candidates for explaining high amplitudes of HF QPOs.

[2] In our calculations we follow the approach of Hartle & Thorne (1968), Chandrasekhar & Miller (1974), Miller (1977), and Urbanec et al. (2013).

5.2.1 Low frequency QPOs

The presented concept has the potential to explain also the observed low-frequency QPOs. As noticed by Kluźniak & Rosińska (2013) and Rosińska et al. (2014) the frequencies of vertical modes seem to be very sensitive to the NS quadrupole moment. Their consideration thus may exceed the framework of Kerr space–time approximation adopted here. However, we roughly investigated also the frequencies of non-axisymmetric $m = 1$ vertical epicyclic mode of cusp tori. This mode corresponds to a low-frequency global precession of inclined torus and is analogical to the 'tilted hot flow precession' discussed by Ingram & Done (2010). Assuming the same mass, angular momentum and radii as those in Fig. 2 we obtained values of tens of Hertz that are of the same order as the observed frequencies. The $m = -1$ vertical epicyclic mode may therefore play the same role in the framework of cusp torus model as the Lense–Thirring precession in the framework of RP model.

ACKNOWLEDGEMENTS

GT, ES and MU would like to acknowledge the Czech grant GAČR 209/12/P740. JH was supported by the grant LH14049. We also acknowledge the internal grants of SU Opava, SGS/11/2013 and IGS/12/2015. We thank to the anonymous referee for his/her comments and suggestions that have significantly helped to improve the Letter. We are grateful to Marek Abramowicz, Wlodek Kluzniak (CAMK), John Miller (University of Oxford), and Luigi Stella (INAF) for many useful discussions. Furthermore we would like to acknowledge the hospitality of the University of Oxford and the Astronomical Observatory in Rome.

REFERENCES

Abramowicz M. A., Kluźniak W., 2001, A&A, 374, L19
Abramowicz M., Jaroszynski M., Sikora M., 1978, A&A, 63, 221
Abramowicz M. A., Barret D., Bursa M., Horák J., Kluźniak W., Rebusco P., Török G., 2005, Astron. Nachr., 326, 864
Abramowicz M. A., Blaes O. M., Horák J., Kluźniak W., Rebusco P., 2006, Class. Quantum Gravity, 23, 1689
Abramowicz M. A., Horák J., Kluzniak W., 2007, Acta Astron., 57, 1
Akmal A., Pandharipande V. R., Ravenhall D. G., 1998, Phys. Rev. C, 58, 1804
Belloni T., Méndez M., Homan J., 2007, MNRAS, 376, 1133
Blaes O. M., 1985, MNRAS, 216, 553
Chandrasekhar S., Miller J. C., 1974, MNRAS, 167, 63
Hartle J. B., Thorne K. S., 1968, AJ, 153, 807
Horák J., 2005, Astron. Nachr., 326, 845
Ingram A., Done C., 2010, MNRAS, 405, 2447
Kato S., 2001, PASJ, 53, 1
Kluzniak W., Abramowicz M. A., 2001, Acta Phys. Pol. B, 32, 3605
Kluźniak W., Rosińska D., 2013, MNRAS, 434, 2825
Lin Y.-F., Boutelier M., Barret D., Zhang S.-N., 2011, AJ, 726, 74
Miller J. C., 1977, MNRAS, 179, 483
Paczynski B., 1977, AJ, 216, 822
Paczynski B., 1987, Nature, 327, 303
Rikovska Stone J., Miller J. C., Koncewicz R., Stevenson P. D., Strayer M. R., 2003, Phys. Rev. C, 68, 034324
Rosińska D., Kluźniak W., Stergioulas N., Wiśniewicz M., 2014, Phys. Rev. D, 89, 104001
Stella L., Vietri M., 1999, Phys. Rev. Lett., 82, 17
Stergioulas N., Friedman J. L., 1995, AJ, 444, 306
Straub O., Šrámková E., 2009, Class. Quantum Gravity, 26, 055011
Strohmayer T. E., Markwardt C. B., 2002, AJ, 577, 337
Török G., Bakala P., Šrámková E., Stuchlík Z., Urbanec M., Goluchová K., 2012, AJ, 760, 138
Urbanec M., Török G., Šrámková E., Čech P., Stuchlík Z., Bakala P., 2010b, A&A, 522, A72
Urbanec M., Miller J. C., Stuchlík Z., 2013, MNRAS, 433, 1903
Wagoner R. V., Silbergleit A. S., Ortega-Rodríguez M., 2001, AJ, 559, L25
Wiringa R. B., Fiks V., Fabrocini A., 1988, Phys. Rev. C, 38, 1010

This paper has been typeset from a TEX/LATEX file prepared by the author.

Paper VII

6.7. On one-parametric formula relating the frequencies of twin-peak quasi-periodic oscillations

Török Gabriel, Goluchová Kateřina, Šrámková Eva, Horák Jiří, Bakala Pavel & Urbanec Martin

Monthly Notices of the Royal Astronomical Society: Letters, 2018
Volume 473, Issue 1, p.L136-L140

Monthly Notices of the ROYAL ASTRONOMICAL SOCIETY

MNRAS **473,** L136–L140 (2018) doi:10.1093/mnrasl/slx177
Advance Access publication 2017 October 31

On one-parametric formula relating the frequencies of twin-peak quasi-periodic oscillations

Gabriel Török,[1]★ Kateřina Goluchová,[1] Eva Šrámková,[1] Jiří Horák,[2] Pavel Bakala[1] and Martin Urbanec[1]

[1] *Institute of Physics and Research Centre for Computational Physics and Data Processing, Faculty of Philosophy & Science, Silesian University in Opava, Bezručovo nám. 13, CZ-746 01 Opava, Czech Republic*
[2] *Astronomical Institute, Boční II 1401/2a, CZ-14131 Praha 4-Spořilov, Czech Republic*

Accepted 2017 October 26. Received 2017 October 19; in original form 2017 June 16

ABSTRACT

Twin-peak quasi-periodic oscillations (QPOs) are observed in several low-mass X-ray binary systems containing neutron stars. Timing the analysis of X-ray fluxes of more than dozen of such systems reveals remarkable correlations between the frequencies of two characteristic peaks present in the power density spectra. The individual correlations clearly differ, but they roughly follow a common individual pattern. High values of measured QPO frequencies and strong modulation of the X-ray flux both suggest that the observed correlations are connected to orbital motion in the innermost part of an accretion disc. Several attempts to model these correlations with simple geodesic orbital models or phenomenological relations have failed in the past. We find and explore a surprisingly simple analytic relation that reproduces individual correlations for a group of several sources through a single parameter. When an additional free parameter is considered within our relation, it well reproduces the data of a large group of 14 sources. The very existence and form of this simple relation support the hypothesis of the orbital origin of QPOs and provide the key for further development of QPO models. We discuss a possible physical interpretation of our relation's parameters and their links to concrete QPO models.

Key words: accretion, accretion discs – stars: neutron – X-rays: binaries.

1 INTRODUCTION

Black holes (BHs) and neutron stars (NSs) represent the accreting compact component in several tens of X-ray binaries. In low-mass X-ray binary systems (LMXBs), the mass transfer from the companion on to the compact object occurs due to the Roche lobe's overflow. An accretion disc is formed enhancing these objects through high X-ray luminosity coming from its innermost parts. In NS systems, additional strong radiation arises from the disc–NS boundary layer (e.g. Lewin, van Paradijs & van den Heuvel 1997).

The LMXBs exhibit a variability over a large range of frequencies. Their power density spectra contain relatively coherent features known as quasi-periodic oscillations (QPOs; van der Klis 2000; Belloni, Psaltis & van der Klis 2002; McClintock & Remillard 2006; van der Klis 2006, and references therein). Apart from strong, the so-called low-frequency (LF) QPOs observed in the range of 0.1–100 Hz, there are also the high-frequency (HF) QPOs observed in the range of 40–1300 Hz. Commonly, for BH and NS sources, HF QPOs attract large attention of theoreticians since their frequencies correspond to orbital time-scales in the vicinity of the compact object. The strong indication that the corresponding signal originates in the innermost parts of the disc is also supported by the results of the Fourier-resolved spectroscopy (Gilfanov, Churazov & Revnivtsev 2000). In this context, a large variety of models of the observed fast variability has been proposed (Alpar & Shaham 1985; Lamb et al. 1985; Miller et al. 1998; Psaltis et al. 1999; Kato 2001; Kluźniak & Abramowicz 2001; Wagoner et al. 2001; Stella & Vietri 2001; Titarchuk & Wood 2002; Abramowicz et al. 2003b; Rezzolla, Yoshida & Zanotti 2003; Kluźniak et al. 2004; Zhang 2004; Bursa 2005; Pétri 2005; Čadež et al. 2008; Mukhopadhyay 2009; Stuchlík et al. 2013, and several others).

The NS LMXBs reveal characteristic pairs of HF QPOs, the so-called twin-peak QPOs. More than a dozen of systems exhibit remarkable correlations between their 'upper' and 'lower' frequencies, ν_U and ν_L. In this letter, we focus on these frequencies. We remind the reader that other properties of each oscillation, such as the rms amplitude $\mathcal{A}$ and quality factor Q, strongly vary reaching values of up to $Q \sim 250$ and $\mathcal{A} \sim 20$ which are much higher than those associated to HF QPOs in BH systems. The variations of the quantities are correlated also with the two QPO frequencies (e.g. van Straaten et al. 2002; Barret, Olive & Miller 2005a,b,

★ E-mail: gabriel.torok@gmail.com

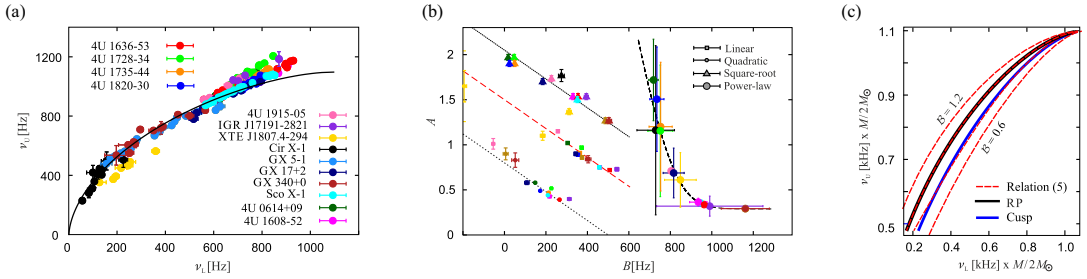

Figure 1. The expected and observed correlations between the frequencies of twin-peak QPOs. (a) Frequencies of twin-peak QPOs in 14 sources. The black curve indicates the prediction of the RP model assuming a non-rotating NS with $M = 2M_\odot$. (b) Parameters of various relations fitting the frequencies displayed in panel (a) and the slope intercept anticorrelation found by Abramowicz et al. (2005b,a) (red line). For the clarity of drawing, we rescale the parameters of the individual relations as follows. Linear: $A = a$, $B = b$; quadratic: $A = 694\,a + 0.06$, $B = b - 500$; square-root: $A = a/30 + 0.2$, $B = b + 400$; power law: $A = 42.86\,a + 0.29$, $B = 500\,b$. The units of coefficients are chosen such that A is dimensionless and B is given in the units of Hz. In two cases, the parameters resulting for Circinus X-1 exceed the displayed range. There is $A = 8.36$ and $B = -298$ for the quadratic relation, and $A = 1.57$ and $B = 273$ for the square-root relation. (c) A comparison between the shape of $\nu_U(\nu_L)$ curves predicted by the RP model (black line), CT model (blue line) and relation (5) for $\mathcal{B} \in \{0.6, 0.8, 1.0, 1.2\}$ (dashed red lines). Note that the RP model curve coincides with those given by relation (5) for $\mathcal{B} = 1$ while the CT model curve nearly overlaps with those given by relation (5) for $\mathcal{B} = 0.8$.

Table 1. List of sources, references and parameters obtained through data matching. Goodness of fits is formally characterized by χ^2 values (we use the same procedure as Török et al. 2012, displayed errors correspond to standard errors). The individual columns displaying χ^2 values correspond to relation (5) in its one- and two-parametric form, RP model and CT model. For these two models, we assume a non-rotating NS (as discussed in Török et al. 2016a, the spin consideration almost does not improve the fits). References: (1)–(3), (10)–(12) - Barret et al. (2005a,b, 2006), (4) - Boirin et al. (2000), (5) - Altamirano et al. (2010), (6) - Homan et al. (2002), (7) - van der Klis et al. (1997), (8) - Boutloukos et al. (2006), (9) - Linares et al. (2005), (13) - Jonker et al. (2000) and (14) - Jonker et al. (2002).

Source No./ Type[a]	Name	$\mathcal{M}$	$\frac{\chi^2}{d.o.f.}$	$\mathcal{M}(\mathcal{B})$	$\mathcal{B}$	$\frac{\chi^2_{\mathcal{M}(\mathcal{B})}}{d.o.f.}$	$\frac{M_{RP}}{M_\odot}$	$\frac{\chi^2_{RP}}{d.o.f.}$	$\frac{M_{CUSP}}{M_\odot}$	$\frac{\chi^2_{CUSP}}{d.o.f.}$	Data points
1/A	4U 1608-52	$1.80^{\pm0.01}$	1.6	$1.79^{\pm0.04}$	$0.79^{\pm0.03}$	1.7	1.94	10.1	$1.74^{\pm0.01}$	1.9	12
2/A	4U 1636-53	$1.70^{\pm0.01}$	2.0	$1.70^{\pm0.01}$	$0.8^{\pm0.01}$	2.1	1.79	17.4	$1.69^{\pm0.01}$	3.4	22
3/A	4U 1735-44	$1.69^{\pm0.01}$	2.1	$1.48^{\pm0.10}$	$0.61^{\pm0.06}$	1.0	1.81	5.1	$1.66^{\pm0.01}$	1.4	8
4/A	4U 1915-05	$1.58^{\pm0.03}$	0.8	$1.65^{\pm0.03}$	$0.82^{\pm0.01}$	0.2	2.09	28.6	–[b]	–[b]	5
5/A	IGR J17191-2821	$1.58^{\pm0.02}$	0.6	$1.63^{\pm0.20}$	$0.85^{\pm0.2}$	0.8	1.76	0.6	$1.52^{\pm0.02}$	0.6	4
6/Z	GX 17+2	$1.89^{\pm0.02}$	1.2	$1.77^{\pm0.07}$	$0.72^{\pm0.04}$	0.8	2.08	5.5	$1.83^{\pm0.02}$	0.9	10
7/Z	Sco X-1	$1.82^{\pm0.01}$	1.0	$1.81^{\pm0.01}$	$0.8^{\pm0.01}$	1.0	2.0	24.2	$1.76^{\pm0.01}$	2.3	39
8/Z	Cir X-1	$0.74^{\pm0.10}$	1.2	$1.42^{\pm0.5}$	$0.89^{\pm0.06}$	1.1	2.23	1.3	–[b]	–[b]	11
9/P	XTE J1807.4-294	$2.61^{\pm0.11}$	0.8	$2.85^{\pm0.25}$	$0.86^{\pm0.07}$	0.8	3.27	1.4	–[b]	–[b]	7
10/A	4U 1728-34	$1.57^{\pm0.01}$	3.2	$1.35^{\pm0.12}$	$0.65^{\pm0.06}$	2.5	1.74	5.7	$1.51^{\pm0.01}$	2.8	15
11/A	4U 0614+09	$1.71^{\pm0.02}$	5.1	$1.39^{\pm0.06}$	$0.62^{\pm0.02}$	1.1	1.90	14.7	$1.65^{\pm0.01}$	3.4	13
12/A	4U 1820-30	$1.81^{\pm0.01}$	9.3	$1.53^{\pm0.07}$	$0.58^{\pm0.03}$	3.2	1.93	24.2	$1.78^{\pm0.01}$	6.4	23
13/Z	GX 340+0	$1.62^{\pm0.08}$	4.2	$2.23^{\pm0.10}$	$1.10^{\pm0.08}$	1.6	2.07	1.8	–[b]	–[b]	12
14/Z	GX 5-1	$1.65^{\pm0.10}$	16.7	$2.31^{\pm0.04}$	$1.11^{\pm0.02}$	1.5	2.13	3.1	–[b]	–[b]	21

[a] A - atoll, Z - Z, P - pulsar. [b] The observed frequencies extend below the expected range of physical applicability of CT model discussed by Török et al. (2016b).

2006; Méndez 2006; van der Klis 2006; Török 2009; Wang et al. 2014).

2 BEHAVIOUR AND FITS OF THE FREQUENCY CORRELATIONS

The frequency correlations observed in the individual sources clearly differ, but they roughly follow a common individual pattern. This is illustrated in Fig. 1a that displays twin-peak QPOs observed in 14 different sources. These include eight atoll sources, five Z-sources and a millisecond X-ray pulsar. Detailed X-ray timing studies of these objects which have been carried out over the last two decades reveal a large amount of information. A list of individual sources along with a dozen of related references is given in Table 1. Apart from the data points, we include in Fig. 1a a curve that indicates the trend predicted by the relativistic precession model of HF QPOs – hereafter RP model (see, e.g. Stella & Vietri 1999; Stella & Vietri 2001; Belloni, Méndez & Homan 2005; Török et al. 2016a).

Several attempts to model the individual observed correlations with simple geodesic orbital models or phenomenological relations have failed in the past (e.g. Lin et al. 2011; Török et al. 2012, 2016a, and references therein). In several particular cases, fits are reliable when two free parameters specific for each source are considered (e.g. Psaltis et al. 1998; Abramowicz et al. 2005b,a; Zhang 2006), although there are still numerous clear deviations of data from

the expected trend. For instance, fitting by straight lines typically provides a reasonable match (but deviation from linear trend is apparent, e.g. in a large amount of data available for the atoll source 4U 1636-53; Lin et al. 2011; Török et al. 2012).

It has been noticed by Abramowicz et al. (2005b,a) that the slope a and intercept b of the linear fits obtained for several sources are roughly related as

$$a \approx 1.5 - 0.0015b \,(\text{assuming } \nu_U = a\nu_L + b)\,. \tag{1}$$

In Fig. 1b, we illustrate the coefficients a and b obtained for each of the sources listed in Table 1. Within the figure, we furthermore illustrate the coefficients obtained for the other two-parametric fitting relations. These are namely the quadratic relation, $\nu_U = a\nu_L^2 + b$, the square-root relation, $\nu_U = a\sqrt{\nu_L} + b$, and the power-law relation, $\nu_U = b(1\nu_L)^a$. For each of these relations, including relation (1), the units of coefficients are chosen such that a is dimensionless while b is given in the units of Hz. Inspecting Fig. 1b, one can speculate that the frequency correlations within a large group of sources can be described by the means of a single parameter.

3 A SIMPLE FORMULA REPRODUCING THE INDIVIDUAL CORRELATIONS

In the series of works (Török et al. 2010, 2012, 2016a), the effective degeneracy between various parameters of several orbital QPO models has been discussed. Within this degeneracy, each combination of NS mass M, angular momentum j and quadrupole moment q corresponds to a certain value of a single generalized parameter $\mathcal{M}$, e.g. non-rotating NS mass. It follows that, when these parameters dominate and only non-geodesic effects that do not much vary across different systems are assumed within a given QPO model, one may expect that the correlations can be described by a one-parametric relation,

$$\nu_{L,U} \propto (\mathrm{r},\, \mathcal{M}) \Rightarrow \nu_L = \nu_L\,(\nu_U,\, \mathcal{M})\,,\ \nu_U = \nu_U\,(\nu_L,\, \mathcal{M})\,, \tag{2}$$

where the common internal parameter r does not appear in the function $\nu_U(\nu_L)$. This expectation is in good agreement with the possible degeneracy of the two-parametric frequency relations mentioned in Section 2.

3.1 Frequency scaling

Motivated by the above mentioned findings, we attempt to model the observed correlations with the following relation:

$$\nu_L = \nu_U \left(1 - \mathcal{B}\sqrt{1 - (\nu_U/\nu_0)^{2/3}}\right), \tag{3}$$

where ν_0 represents the highest possible QPO frequency, $\nu_0 \geq \nu_U \geq \nu_L$. In the specific case when it is assumed that ν_0 equals the Keplerian orbital frequency at the innermost stable circular orbit around a non-rotating NS with gravitational mass M, it can be expressed in the units of Hz as (e.g. Kluzniak & Wagoner 1985; Kluzniak, Michelson & Wagoner 1990)

$$\nu_0 = \nu_{ISCO} = \frac{1}{6^{3/2}}\frac{c^3}{2\pi G}\frac{1}{M} = 2198\,\frac{M_\odot}{M} = 2198\,\frac{1}{\mathcal{M}}. \tag{4}$$

Consequently, relation (3) can be written in the form

$$\nu_L = \nu_U \left(1 - \mathcal{B}\sqrt{1 - 0.0059\,(\nu_U\mathcal{M})^{2/3}}\right). \tag{5}$$

Considering $\mathcal{B} = 1$, relation (5) coincides with the frequency relation implied by the RP model. Moreover, for any constant value of $\mathcal{B}$, relation (5) implies $1/\mathcal{M}$ scaling of the QPO frequencies. This means that the $[\nu_L,\ \nu_U]$ frequency pairs calculated for a certain value of $\mathcal{M} = \mathcal{M}_1$ can be recalculated for another value, $\mathcal{M} = \mathcal{M}_2$, using a simple multiplication,

$$[\nu_L,\ \nu_U]_2 = [\nu_L,\ \nu_U]_1 \times (\mathcal{M}_1/\mathcal{M}_2). \tag{6}$$

In Fig. 1c, we illustrate the shape of $\nu_U(\nu_L)$ curves given by relation (5) and compare them to the predictions of two previously proposed models of QPOs. We assume in this section for relation (5) to have either one-parametric or two-parametric form, and in both cases we make a comparison with the data of the individual sources. We then provide a more detailed discussion on the motivation for our choice of the form of relation (5) in Section 4.

3.2 The one-parametric relation (pure $1/\mathcal{M}$ scaling)

Taking into account expectation (2), we attempt to reproduce the data of the 14 sources listed in Table 1 assuming relation (5) for a fixed value of $\mathcal{B} = 0.8$. The particular choice of $\mathcal{B} = 0.8$ stems from the results of Török et al. (2012). At the same time, it links relation (5) to a QPO model introduced by Török et al. (2016b) which deals with marginally overflowing inner accretion tori. See Fig. 1c for illustration and Section 4 for a more detailed discussion on this matter.

The results obtained for the whole set of sources are presented in Table 1 and illustrated in Fig. 2a. Remarkably, for the sources 1–9 good agreement is obtained. For each of these sources, there is $0.5 < \chi^2/\text{d.o.f.} \lesssim 2$. These sources span (approximately) the range of $\nu_L \in (200, 900)$Hz and include the atoll source 4U 1915-05 that itself covers a large range of frequencies, $\nu_L \in (200, 800)$Hz. We can also see from Fig. 2a that the trend observed in each of the sources 10–12 is still matched.

The two sources, GX 5-1 and GX 340+0, reveal clear deviations of data from the expected trend (see the last sub-panel of Fig. 2a). In Table 1, we include relevant χ^2 values along with the values of the $\mathcal{M}$ parameter obtained for each of the considered 14 sources. The obtained $\mathcal{M}$ parameter values range from $\mathcal{M} = 0.7$ to $\mathcal{M} = 2.6$ while in most cases there is $\mathcal{M} \in (1.6,\ 1.9)$.

3.3 The consideration of the $\mathcal{B}$ parameter as a free parameter

As a second step, using relation (5), we attempt to reproduce the data assuming two free parameters ($\mathcal{M}$ and $\mathcal{B}$). The results are again presented in Table 1 and illustrated in Fig. 2a.

Clearly, for each of the 14 sources including GX 5-1 and GX 340+0 (no. 13 and 14), the observed trend is well matched (although there is some scatter of data points around the expected curves). In Table 1, we summarize the relevant χ^2 values along with the obtained values of $\mathcal{M}$ and $\mathcal{B}$. The values of $\mathcal{M}$ range from $\mathcal{M} = 1.39$ to $\mathcal{M} = 2.85$ while the values of $\mathcal{B}$ range from $\mathcal{B} = 0.61$ to $\mathcal{B} = 1.11$ [in most cases, there is $\mathcal{B} \in (0.1, 0.4)$].

4 PHYSICAL INTERPRETATION

We begin this section by briefly recalling the RP model that is most often discussed in relation to the possibility of hotspots arising in the innermost accretion region. This model relates the frequencies of the two observed QPOs to the Keplerian frequency $\nu_U = \nu_K$ and the relativistic precession frequency $\nu_L = \nu_P$ of a slightly perturbed circular geodesic motion that occurs at an arbitrary orbital radius r. The precession frequency ν_P equals to a difference between the Keplerian and the radial epicyclic frequency, $\nu_P = \nu_K - \nu_\mathrm{r}$.

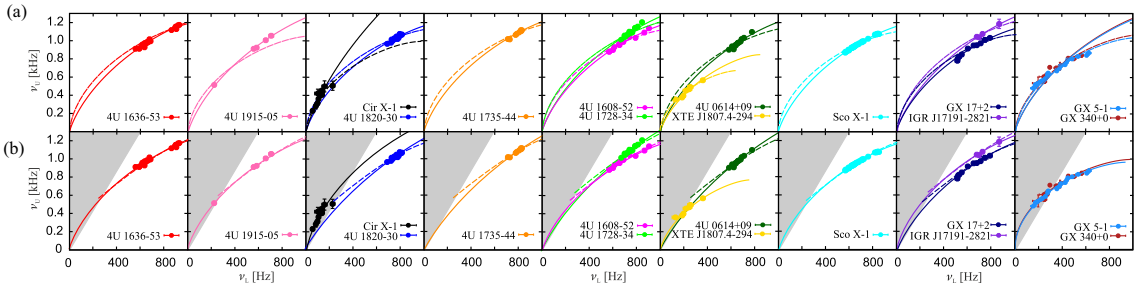

Figure 2. Correlations between the twin-peak QPO frequencies in the individual sources versus fitting relations. (a) A comparison between relation (5) assuming $\mathcal{B} = 0.8$ (solid lines) and the RP model (dashed lines). (b) A comparison between relation (5) assuming $\mathcal{B}$ parameter as a free parameter (solid lines) and the CT model (dashed lines). The shaded areas denote the range in which the CT model is not applicable. For both panels of this figure, the parameters of the individual fits are summarized in Table 1.

Török et al. (2012) have suggested a toy non-geodesic modification of the RP model. In their paper, it is assumed that ν_r decreases due to non-geodesic effects by a constant $\mathcal{B}^*$ factor. The expected lower QPO frequency is then given as

$$\nu_L = \nu_L^* + \mathcal{B}^* \left(\nu_U^* - \nu_L^*\right), \tag{7}$$

where ν_L^* and ν_U^* denote the frequencies implied by the non-modified RP model. The authors attempt to model the correlation of QPO frequencies observed in the atoll source 4U 1636-53 and find that there is good agreement between the model and the data for the NS mass $M = 1.7 M_\odot$ and $\mathcal{B}^* = 0.2$.

Assuming relation (7), formulae for the orbital frequencies around a non-rotating NS, and $\mathcal{B}^* = 1 - \mathcal{B}$, we obtain relation (5).

4.1 Global modes of fluid motion

Oscillations of tori have been studied in the context of QPOs in a large number of works over the past decade (see, e.g. Rezzolla, Yoshida & Zanotti 2003; Abramowicz et al. 2006; Šrámková, Torkelsson & Abramowicz 2007; Ingram & Done 2010; Fragile, Straub & Blaes 2016; Parthasarathy, Kluzniak & Cemeljic 2017; Mishra et al. 2017; de Avellar et al. 2017). The recent work of Török et al. (2016b) explores the model of an oscillating torus (in next CT model). In this model, the torus is assumed to fill up the critical equipotential volume forming a cusp. It is suggested by the model that the twin-peak QPOs are assigned to global modes of cusp–torus fluid motion that may give rise to strong modulation of both the accretion disc radiation and the accretion rate.[1] The observed frequency variations are given by the changes of the location r of the torus centre radii very close to the innermost stable circular orbit. In the paper of Török et al. (2016b), the model predictions are compared to the data of the atoll source 4U 1636-53 obtaining a good match.

For a fixed j and a given torus location, the frequencies predicted by the model depend solely on the NS mass. Although the related exact dependence $\nu_U(\nu_L)$ has to be evaluated numerically, we find it can be well approximated by relation (5) for $\mathcal{B} \approx 0.8$. The one-parametric form of relation (5) investigated in Section 3.2 therefore represents the prediction of the CT model (see Fig. 1c).

In Fig. 2b, we directly compare the predictions of the CT model with the data of the individual sources. For sources no. 1–3, 5–7 and 10–12, the CT model allows fits comparable to those obtained for relation (5) and $\mathcal{B} = 0.8$. In Table 1, we present relevant χ^2 values along with the required values of NS mass. In the case of sources no. 4, 8, 9, 13 and 14 (4U 1915-05, Circinus X-1, XTE J1807.4-294, GX 5-1 and GX 340+0), the correlation however cannot be modelled since the observed frequencies ν_L extend below the range of applicability of the approximation of the torus model discussed by Török et al. (2016b) (see the shaded areas in Fig. 2b).

5 CONCLUSIONS

The simple formula (5) well fits the frequencies of twin-peak QPOs within a large group of 14 sources. This match might be of high importance for the twin-peak QPO model identification. The frequency scaling (6), $\nu \propto \mathcal{M}^{-1}$, further supports the hypothesis of the orbital origin of NS HF QPOs since the frequencies of orbital motion scale with the NS mass M as $\nu \propto M^{-1}$. It is of a particular interest that already the one-parametric form of our relation assuming $\mathcal{B} = 0.8$ describes several of these sources. We suggest that this finding represents the NS analogy of the $1/M$ scaling of the 3:2 BH HF QPO frequencies (Abramowicz et al. 2004; McClintock & Remillard 2006; Zhou et al. 2015).

A detailed physical explanation of the origin of relation (5) is not yet clear. The recently suggested CT model reproduces the data of nine sources. For other five sources, however, the data cannot be firmly reproduced within the approximation developed so far. The results obtained for relation (5) and the $\mathcal{B}$ free parameter can help improve the model. Larger deviations from the case of $\mathcal{B} = 0.8$ can have a direct physical interpretation. The cause of these deviations may be due to a torus thickness different from the cusp value, or, more likely, by further non-geodesic effects acting on the torus formation, such as NS magnetic field.

The above hypothesis agrees with a more general interpretation of relation (5) in which the $\mathcal{M}$ parameter represents the main parameter reflecting the space–time geometry given by the NS mass and spin, while the $\mathcal{B}$ parameter reflects the additional stable factors. In this context, we note that we have not been able to reproduce the data for any significant group of sources assuming $\mathcal{B}$ as a free and $\mathcal{M}$ as a fixed parameter.

[1] The resulting total observed flux is given by the composition of the emissivity of the boundary layer (radial mode) and the disc (radial and Keplerian mode). Detailed modelling of contributions of particular modulation mechanisms can be important in relation to the recent findings of Ribeiro et al. (2017) (see also Méndez 2006; Gilfanov et al. 2003). In this context, we note that the considered oscillatory modes can, in principle, cause also oscillation of the accretion disc corona.

ACKNOWLEDGEMENTS

We would like to acknowledge the Czech Science Foundation grant no. 17-16287S, the INTER-EXCELLENCE project no. LTI17018 supporting collaboration between the Silesian University in Opava (SU) and Astronomical Institute in Prague (ASU), and the internal SU grant no. SGS/15/2016. We thank to the anonymous referee for his/her comments and suggestions that have significantly helped to improve the letter. We are grateful to Marek Abramowicz (SU) and Omer Blaes (University of California in Santa Barbara – UCSB) for useful discussions. Last but not least, we would like to acknowledge the hospitality of UCSB, and to express our thanks to concierges of Mlýnská hotel in Uherské Hradiště, Czech Republic for their participation in organizing frequent workshops of SU and ASU.

REFERENCES

Abramowicz M. A., Karas V., Kluźniak W., Lee W. H., Rebusco P., 2003b, PASJ, 55, 467
Abramowicz M. A., Kluźniak W., McClintock J. E., Remillard R. A., 2004, ApJ, 609, L63
Abramowicz M. A., Barret D., Bursa M., Horák J., Kluźniak W., Rebusco P., Török G., 2005a, in S. Hledík, Z. Stuchlík, eds, RAGtime 6/7: Workshops on black holes and neutron stars. Vol. 1, Silesian University Opava, Opava, p. 1
Abramowicz M. A., Barret D., Bursa M., Horák J., Kluzniak W., Rebusco P., Török G., 2005b, Astron. Nachr., 326, 864
Abramowicz M. A., Blaes O. M., Horák J., Kluźniak W., Rebusco P., 2006, CQG, 23, 1689
Alpar M. A., Shaham J., 1985, Nature, 316, 239
Altamirano D. et al., 2010, MNRAS, 401, 223
Barret D., Olive J.-F., Miller M. C., 2006, MNRAS, 370, 1140
Barret D., Olive J.-F., Miller M. C., 2005a, MNRAS, 361, 855
Barret D., Olive J.-F., Miller M. C., 2005b, Astron. Nachr., 326, 808
Belloni T., Psaltis D., van der Klis M., 2002, A&A, 572, 392
Belloni T., Méndez M., Homan J., 2005, A&A, 437, 209
Boirin L., Barret D., Olive J. F., Bloser P. F., Grindlay J. E., 2000, A&A, 361, 121
Boutloukos S., van der Klis M., Altamirano D., Klein-Wolt M., Wijnands R., Jonker P. G., Fender R. P., 2006, ApJ, 653, 1435
Bursa M., 2005, in S. Hledík, Z. Stuchlík, eds, RAGtime 6/7: Workshops on black holes and neutron stars. Vol. 1, Silesian University in Opava, Opava, pp. 39-45
Čadež A., Calvani M., Kostić U., 2008, A&A, 487, 527
de Avellar M. G., Porth O., Younsi Z., Rezzolla L., 2017, preprint (arXiv:1709.07706)
Fragile P. C., Straub O., Blaes O., 2016, MNRAS, 461, 1356
Gilfanov M., Churazov E., Revnivtsev M., 2000, MNRAS, 316, 923
Gilfanov M., Revnivtsev M., Molkov S., 2003, A&A, 410, 217
Homan J., van der Klis M., Jonker P. G., Wijnands R., Kuulkers E., Méndez M., Lewin W. H. G., 2002, ApJ, 568, 878
Ingram A., Done C., 2010, MNRAS, 405, 2447
Jonker P. G. et al., 2000, ApJ, 537, 374
Jonker P. G. et al., 2002, MNRAS, 333, 665
Jonker P. G., van der Klis M., Homan J., Méndez M., Lewin W. H. G., Wijnands R., Zhang W., 2002, MNRAS, 333, 665
Kato S., 2001, PASJ, 53, 1
Kluzniak W., Wagoner R. V., 1985, ApJ, 297, 548
Kluzniak W., Michelson P., Wagoner R. V., 1990, ApJ, 358, 538
Kluźniak W., Abramowicz M. A., Kato S., Lee W. H., Stergioulas N., 2004, ApJ, 603, L89
Lamb F. K., Shibazaki N., Alpar M. A., Shaham J., 1985, Nature, 317, 681
Lin Y.-F., Boutelier M., Barret D., Zhang S.-N., 2011, ApJ, 726, 74
Linares M., van der Klis M., Altamirano D., Markwardt C. B., 2005, ApJ, 634, 1250
McClintock J. E., Remillard R. A., 2006, in Lewin W., van der Klis M., eds, Black Hole Binaries. Cambridge Univ. Press, Cambridge, p. 157
Méndez M., 2006, MNRAS, 371, 1925
Miller M. C., Lamb F. K., Psaltis D., 1998, ApJ, 508, 791
Mishra B., Vincent F. H., Manousakis A., Fragile P. C., Paumard T., Kluzniak W., 2017, MNRAS, 467, 4036
Mukhopadhyay B., 2009, ApJ, 694, 387
Parthasarathy V., Kluzniak W., Cemeljic M., 2017, MNRAS, 470, 34
Psaltis D. et al., 1998, ApJ, 501, L95
Lewin W. H. G., van Paradijs J., van den Heuvel E. P. J., 1997, Formation and evolution of neutron stars and black holes in binaries. Cambridge Univ. Press, Cambridge
Pétri J., 2005, A&A, 439, L27
Psaltis D. et al., 1999, ApJ, 520, 763
Rezzolla L., Yoshida S., Zanotti O., 2003, MNRAS, 344, 978
Ribeiro E. M., Méndez M., Zhang G., Sanna A., 2017, MNRAS, 471, 1208
Šrámková E., Torkelsson U., Abramowicz M. A., 2007, A&A, 467, 641
Stella L., Vietri M., 1999, PhRvL, 82, 17
Stella L., Vietri M., 2001, in Giacconi R., Serio S., Stella L., eds, ASP Conf. Ser. Vol. 234, X-ray Astronomy 2000. Astron. Soc. Pac., San Francisco, p. 213
van Straaten S., van der Klis M., di Salvo T., Belloni T., 2002, ApJ, 568, 912
Stuchlík Z., Kotrlová A., Török G., 2013, A&A, 552, 41
Titarchuk L., Wood K., 2002, ApJ, 577, L23
Török G., 2009, A&A, 497, 661
Török G., Bakala P., Šrámková E., Stuchlík Z., Urbanec M., 2010, ApJ, 714, 748
Török G., Bakala P., Šrámková E., Stuchlík Z., Urbanec M., Goluchová K., 2012, ApJ, 760, 138
Török G. et al., 2016a, ApJ, 833, 273
Török G., Goluchová K., Horák J., Šrámková E., Urbanec M., Pecháček T., Bakala P., 2016b, MNRAS, 457, L19
van der Klis M., 2000, Annu. Rev. Astron. Astrophys., 38, 717
van der Klis M., 2006, in Lewin W., van der Klis M., eds, Rapid X-ray Variability. Cambridge Univ. Press, Cambridge, pp. 39–112.
van der Klis M., Wijnands R. A. D., Horne K., Chen W., 1997, ApJ, 481, L97
Wang D. H., Chen L., Zhang C. M., Lei Y. J., Qu J. L., 2014, Astron. Nachr., 335, 168
Wagoner R. V., Silbergleit A. S., Ortega-Rodríguez M., 2001, ApJ, 559, L25
Zhang C., 2004, A&A, 423, 401
Zhang C. M., Yin H. X., Zhao Y. H., Zhang F., Song L. M., 2006, MNRAS, 366, 1373
Zhou X.-L., Yuan W., Pan H.-W., Liu Z., 2015, ApJ, 798, L5

This paper has been typeset from a TEX/LATEX file prepared by the author.

Paper VIII

6.8. Simple analytic formula relating the mass and spin of accreting compact objects to their rapid X-ray variability

Gabriel Török, Andrea Kotrlová, Monika Matuszková, Kateřina Klimovičová, Debora Lančová, Gabriela Urbancová & Eva Šrámková

Submitted to the Astrophysical Journal

Simple analytic formula relating the mass and spin of accreting compact objects to their rapid X-ray variability

Gabriel Török, Andrea Kotrlová, Monika Matuszková, Kateřina Klimovičová, Debora Lančová, Gabriela Urbancová, Eva Šrámková

Research Centre for Computational Physics and Data Processing, Institute of Physics, Silesian University in Opava, Bezručovo nám. 13, CZ-746 01 Opava, Czech Republic

gabriel.torok@gmail.com

ABSTRACT

Following the previous extensive research on epicyclic oscillations of accretion disks around black holes (BHs) and neutron stars (NSs), a new model of high-frequency quasi-periodic oscillations (QPOs), which deals with oscillations of fluid in marginally overflowing accretion tori predicted by general relativity (tori terminated by cusps), has been proposed (CT model). According to preliminary investigations based on Kerr spacetimes, the model provides overall better fits of the NS QPO data compared to the relativistic precession (RP) model often considered in the context of NS and BH parameters estimations. It also implies a significantly higher upper limit on the Galactic microquasars BH spin. A short analytic formula has been noticed to well reproduce the model's predictions on the QPO frequencies in Schwarzschild spacetimes. Here we derive an extended version of this formula that applies to rotating compact objects. We start with the consideration of Kerr spacetimes and derive a formula that is not restricted to a particular specific angular momentum distribution of the inner accretion flow, such as Keplerian or constant. Finally, we consider Hartle-Thorne spacetimes and include corrections implied by the oblateness of rotating neutron stars. For a particular choice of a single parameter, our relation with high accuracy provides frequencies predicted by the CT model. For another value, it provides frequencies predicted by the RP model. We conclude that the formula is well applicable for rotating oblateness NSs and both models. We briefly illustrate application of our simple formula on several NS sources and confirm the expectation that the CT model is compatible with realistic values of the NS mass and provides better fits of data than the RP model.

Subject headings: X-ray binary stars, Black hole physics, Accretion

1. Introduction

Accreting compact sources such as low-mass X-ray binaries (LMXBs) and active galactic nuclei (AGN) provide a unique opportunity to explore the effects associated with strong gravity in black hole (BH) and

neutron star (NS) systems where they may also serve as a good tool for the exploration of supra-dense matter (van der Klis 2006; Lewin & van der Klis 2010). There is a common aim within the large astrophysical community to relate the mass and spin of the compact objects to their spectral and timing behaviour. In this paper, we focus on the rapid X-ray variability and its models.

The high-frequency part of the power density spectra of many sources reveals more or less sharp peaks that are called the high-frequency quasi-periodic oscillations (HF QPOs). Commonly, the HF QPOs seem to have frequencies close to those of the orbital motion in the innermost part of a given accreting system. Detections of elusive HF QPO peaks in BH LMXB sources have been reported at rather constant frequencies, which tend to appear in ratios of small natural numbers (Abramowicz & Kluźniak 2001; Remillard et al. 2002; McClintock & Remillard 2006). The observed HF QPOs are however very weak and the overall picture can be more complex (Belloni et al. 2012; Belloni & Altamirano 2013; Varniere & Rodriguez 2018). In NS sources, HF QPOs are commonly referred to as twin-peak QPOs because they often appear in pairs observed simultaneously at the upper and lower QPO frequency, $\nu_{\rm U} > \nu_{\rm L}$. Notably, robust correlations are observed between the frequencies of twin-peak QPOs. Each source reveals its specific frequency correlation, $\nu_{\rm U} = \nu_{\rm U}(\nu_{\rm L})$, although the sources roughly follow a common pattern (Psaltis et al. 1999a; Abramowicz et al. 2005b,a; Zhang et al. 2006). This is illustrated in Figure 1a where we show the frequencies of 3:2 QPOs observed in Galactic microquasars along with the HF QPO correlations in a group of 14 NS sources.[1] The data used in the figure come from the works of Barret et al. (2005b,c); Boirin et al. (2000); Altamirano et al. (2010); Linares et al. (2005); van der Klis et al. (1997); Boutloukos et al. (2006); Homan et al. (2002); Jonker et al. (2000, 2002) - NSs, and Strohmayer (2001); Remillard et al. (2002); Homan et al. (2003); Remillard et al. (2003) - BHs.

At present, there is no commonly accepted model for the observed QPOs. Based on various strong arguments, it is nevertheless usually expected that the QPOs are related to orbital motion in the vicinity of NSs. Miscellaneous concepts have been proposed to explain the phenomenon (e.g., Alpar & Shaham 1985; Lamb et al. 1985; Miller et al. 1998; Psaltis et al. 1999b; Stella et al. 1999; Wagoner et al. 2001; Kluźniak & Abramowicz 2001; Abramowicz & Kluźniak 2001; Kato 2001; Titarchuk & Wood 2002; Abramowicz et al. 2003; Rezzolla et al. 2003; Kluźniak et al. 2004; Zhang 2004; Pétri 2005; Bursa 2005; Čadež et al. 2008; Wang et al. 2008; Mukhopadhyay 2009; Bachetti et al. 2010; Dönmez et al. 2011; Stuchlík & Kološ 2014; Huang et al. 2016; Le et al. 2016; Germanà 2017; Stuchlík et al. 2020; Wang & Zhang 2020; Smith et al. 2021, and references therein).

In this short paper, we follow our previous work (Török et al. 2016a,b, 2018, 2019) and derive a simple analytic formula relating the QPO frequencies to the parameters of the rotating compact objects. We also apply this formula to the data of several NS sources.

---

[1]For the sake of simplicity, we often use the shorter term "QPOs" instead of "HF QPOs" or "twin-peak QPOs" throughout the paper.

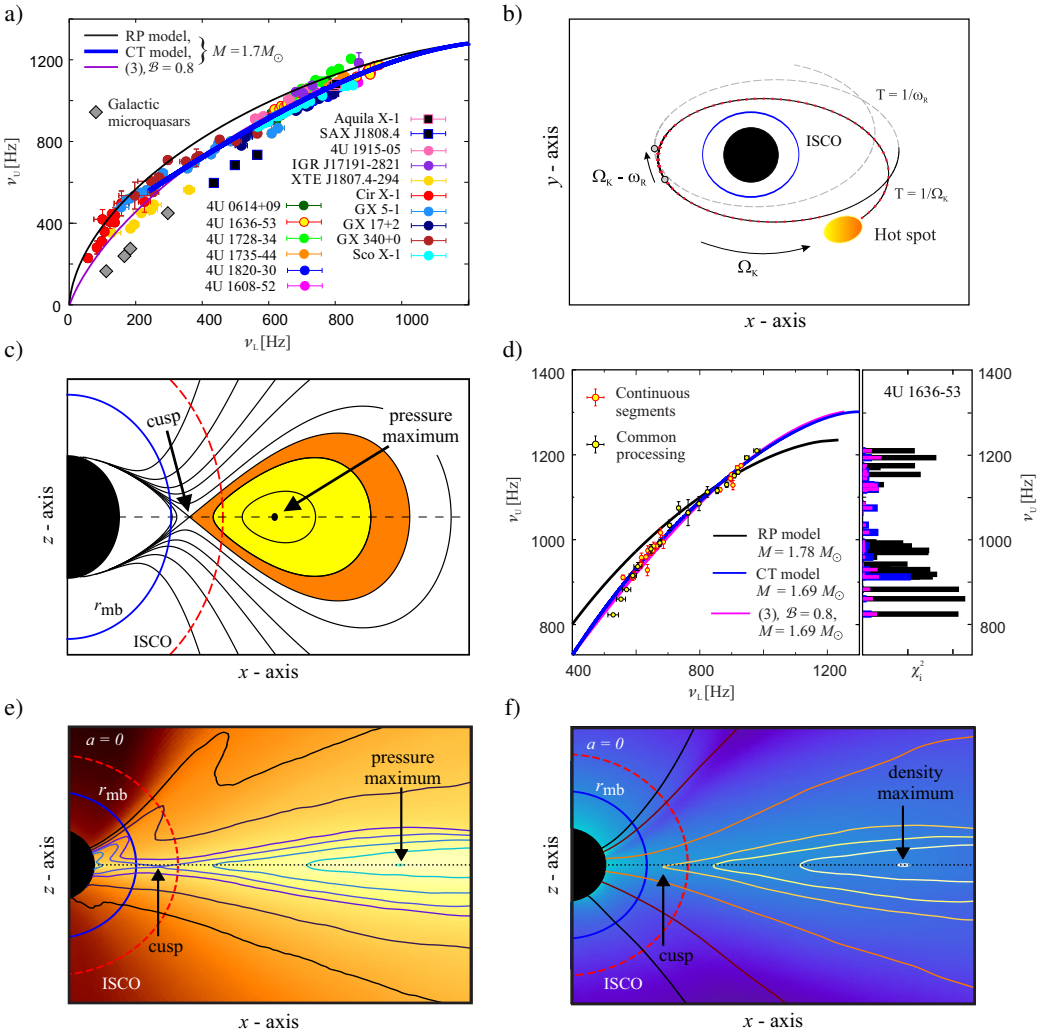

Fig. 1.— a) The data of several sources and examples of the expected frequency relations that are drawn for $M = 1.7M_\odot$. The expected frequency relations are drawn for a non-rotating NS. b) Sketch of the trajectory of a test particle on slightly eccentric orbit which plays cruial role in the hot-spot interpretation of QPOs. c) Topology of equipotential surfaces that determine the spatial distribution of fluid in thick disks. The orange (along with yellow) region corresponds to a torus with a cusp. d) The data of the atoll source 4U 1636-53 and their best fits for non-rotating NS. For the sake of clarity, the data-set which corresponds to the individual continuous observations is compared to the data-set associated with the common processing of all observations (see Török et al. 2016a, for details). e) The equipressure contours seen within general relativistic three-dimensional global radiative magnetohydrodynamic simulation of Lančová et al. (2019) who have reported on a new class of realistic solutions of black hole accretion flows – the so-called puffy accretion disks. f) Equidensity profiles corresponding to panel e.

– 4 –

2. QPO models under consideration

We focus on two particular QPO models that deal with orbital motion of the accreted fluid. First is the so-called relativistic precession (RP) model, which in its usual form incorporates the assumption that the observed rapid X-ray variability originates in the local orbital motion of hot inhomogeneities orbiting in the innermost parts of the accretion disk, such as blobs or vortices (see Abramowicz et al. 1992; Stella & Vietri 1998, 1999). The frequencies of the two observed QPOs are in this model represented by the Keplerian frequency $\nu_{\rm K}$ and the relativistic precession frequency ν_P of a slightly perturbed circular geodesic motion occuring at an arbitrary QPO excitation orbital radius r_0 (see Figure 1b),

$$\nu_{\rm U}(r_0) = \nu_{\rm K}(r_0), \quad \nu_{\rm L}(r_0) = \nu_P(r_0)\,. \tag{1}$$

The precession frequency equals to a difference between the Keplerian and the radial epicyclic frequency,

$$\nu_P(r_0) = \nu_{\rm K}(r_0) - \nu_{\rm r}(r_0)\,. \tag{2}$$

The RP model has been used and quoted in numerous studies. It frequently serves as a rough tool for estimation of compact object mass based on its variability (e.g., Boutloukos et al. 2006; Barret et al. 2006; Boutloukos et al. 2007; Barret et al. 2008; Boutloukos et al. 2008; Török et al. 2010; Lin et al. 2011; Motta et al. 2014; du Buisson et al. 2019; Maselli et al. 2020, and references therein). Relation (1) has been shown to roughly match the NS sources data (e.g., Morsink & Stella 1999; Stella & Vietri 1998, 1999; Belloni et al. 2007; Lin et al. 2011; Török et al. 2012, 2016b). It is however questionable whether the local motion of hot spots can be responsible for the observed QPOs high amplitudes and coherence times (e.g., Barret et al. 2005a; Méndez 2006; Barret & Vaughan 2012).

The other QPO model under consideration, which was proposed recently by Török et al. (2016a), assumes marginally overflowing accretion tori (see the works of Abramowicz & Kluźniak 2001; Kluźniak & Abramowicz 2001; Rezzolla et al. 2003; de Avellar et al. 2018, for a broader context). This concept, to which we in next refer as the CT model, was suggested as a disk-oscillation-based alternative to the RP model. It utilizes the expectation that toroidal structures and cusps are likely to appear in real accretion flows, in which case the overall accretion rate through the inner edge of the disk could be strongly modulated by the torus oscillations (Kozlowski et al. 1978; Abramowicz et al. 1978; Paczynski & Abramowicz 1982; Abramowicz et al. 2006; Parthasarathy et al. 2017). A sketch of the marginally overflowing acretion torus geometry is shown in Figure 1c.

The CT model provides generally better fits of the NS data than the RP model. This is depicted in Figure 1d. This finding is rather independent on the NS spin (Török et al. 2016a,b). The model also likely predicts a lower NS mass compared to the RP model, which, in some cases, implies a mass estimate that is too high (Török et al. 2016a, 2018, 2019). Moreover, the upper limit on the Galactic microquasars spin given by this model is significantly higher than in the RP model's case, namely $j \sim 0.75$ vs. $j \sim 0.55$. This is in better agreement with the spectral spin estimates (Kotrlová et al. 2020).

An overview of the physical assumptions of the model, as well as all appropriated references, can be found in the studies of Török et al. (2016a) and Kotrlová et al. (2020). Similarly to the RP model, the

currently applied concept of inner torus displaying a cusp is very simplified compared to real accretion flows. Nevertheless, it assumes a global motion of the disk fluid instead of the local motion approximated by the test particle description within the RP model. Moreover, the structure of the inner accretion flow observed in GRRMHD simulations often resembles those assumed within the model (see Figures 1e and f).

3. Formulae for QPO frequencies in Schwarzschild spacetimes

For a non-rotating relativistic compact star, the relation between the QPO frequencies implied by the RP model, i.e. by Equation (1), can be written as

$$\nu_{\rm L} = \nu_{\rm U}\left(1 - \mathcal{B}\sqrt{1-(\nu_{\rm U}/\nu_0)^{2/3}}\right), \tag{3}$$

where $\mathcal{B} = 1$ and ν_0 equal to the Keplerian frequency at the innermost stable circular orbit (ISCO). The ISCO frequency is given solely by the gravitational mass M,

$$\nu_0 = \mathcal{F}\frac{1}{6^{3/2}}, \quad \mathcal{F} \equiv {\rm c}^3/(2\pi {\rm G}M)\,. \tag{4}$$

For the CT model, the relation between the QPO frequencies also depends purely on M and can be written in the following implicit form:

$$\nu_{\rm U}(r_0) = \nu_{\rm K}(r_0), \quad \nu_{\rm L}(r_0) = \nu_{{\rm r},\,m=-1}\,, \tag{5}$$

where r_0 denotes the torus centre, $\nu_{\rm K}$ determines the torus corotation mode frequency, and $\nu_{\rm r,\,m=-1}$ equals to the frequency of the first non-axisymmetric radial epicyclic mode calculated for the marginally overflowing torus (i.e., the torus that forms a cusp). There is no explicit analytical evaluation of $\nu_{\rm U}(\nu_{\rm L})$ function and the relation (5) must be solved numerically. It has been however noticed by Török et al. (2018) that there is a solid analytic approximation – the numerical solution nearly coincides with relation (3) when $\mathcal{B} = 0.8$. This is illustrated in Figure 1b.

4. Rotating compact stars

It has been noticed by Török et al. (2010) that in Kerr spacetimes characterized by the $j \equiv {\rm c}J/({\rm G}M^2)$ rotational parameter, the relation between the QPO frequencies implied by the RP model can be expressed as

$$\nu_{\rm L} = \nu_{\rm U}\left\{1 - \mathcal{B}\left[1 + \frac{8j\nu_{\rm U}}{\mathcal{F}-j\nu_{\rm U}} - 6\left(\frac{\nu_{\rm U}}{\mathcal{F}-j\nu_U}\right)^{2/3} - 3j^2\left(\frac{\nu_{\rm U}}{\mathcal{F}-j\nu_{\rm U}}\right)^{4/3}\right]^{1/2}\right\}, \tag{6}$$

when one sets $\mathcal{B} = 1$.

Based on the analogy to non-rotating stars, relation (6) for a particular choice of $\mathcal{B}(j)$ can be expected to reproduce the numerically calculated frequency relation given by the CT model. Having this intention in mind, we presume a simple linear prescription,

$$\mathcal{B}(j) = \mathrm{k}\, j + 0.8 \tag{7}$$

which results in $\mathcal{B} = 0.8$ for the $j = 0$ limit.

We made a comparison between the predictions of relation (6) and numerically obtained CT model predictions. The whole set of formulae necessary for the numerical calculations is given by fairly long expressions, we therefore provide their explicit form in a Wolfram Mathematica notebook.[2] A good match between the analytical prescription and the numerically calculated predictions is found for $\mathrm{k} = -0.2$ and illustrated in Figure 2.

We note that the applicability of our result to rapidly rotating BHs is limited. The so far performed numerical calculations of frequencies given by the CT model utilize a perturbative approach valid within the second-order accuracy in torus thickness. Within this approach, the calculations are for high spins very sensitive to small changes in the torus thickness and the rotational parameter. Full numerical investigation of the Papaloizou–Pringle equation, which determines the epicyclic mode frequencies, will be needed for rapidly rotating BHs.

5. QPO frequencies and accretion flow angular momentum distribution

Following the previous studies of Straub & Šrámková (2009), Török et al. (2016a), Fragile et al. (2016) and Kotrlová et al. (2020), our simple formula relating the QPO frequencies and the cmpact objects mass and spin was derived under the specific consideration of tori with constant distribution of angular momentum ℓ of the accreted fluid. Nevertheless, it can be easily shown that the formula is of a more general importance since its validity is not limited to this particular ℓ-prescription.

5.1. Range of QPO frequencies

If we replace the $\mathcal{B}$ factor in equation (6) by unity, we obtain exactly the prediction based on the test particle motion. This case also describes the scenario in which the angular momentum distribution of the accreted fluid is Keplerian. It is a limit case, in which the cross-section of the oscillating torus is infinitely small (a parameter determining the torus thickness, β, goes to zero).

When the $\mathcal{B}$ factor is taken into account, we come up with a scenario in which the torus has its maximal possible size ($\beta = \beta_{\mathrm{cusp}}$). As shown by Straub & Šrámková (2009), the $\mathrm{m} = -1$ radial mode frequency evolves as a monotonic function of the torus thickness (see Figure 3a for illustration). Accordingly, the

[2] https://github.com/Astrocomp/Torus_oscillations

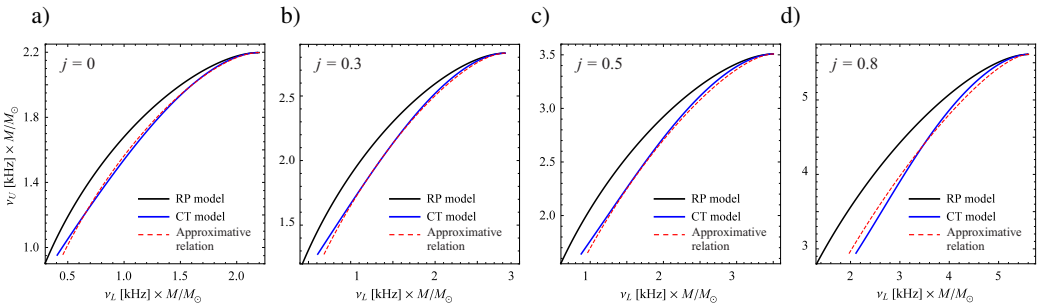

Fig. 2.— Comparison between expected QPO frequencies (Kerr spacetimes). The individual curves denote frequencies given by analytical prescription for RP model, numerically calculated for CT model, and those given by relation (6) for k = −0.2.

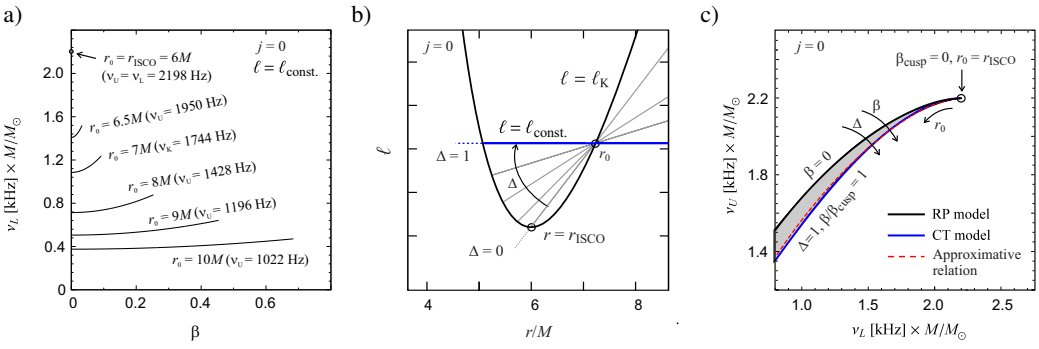

Fig. 3.— a) Behaviour of the m = −1 radial oscillation mode frequency $\nu_{\mathrm{r,\,m=-1}}$. Frequency values quoted in the labels are evaluated for one solar mass star. b) Sketch of various angular momentum distributions of the accreted fluid represented by Keplerian distribution and a family of linear distributions characterized by a Δ-parameter. c) The expected QPO frequencies. Shaded area denotes frequency range corresponding to all combinations of Δ-parameter, $\Delta \in [0,\ 1]$, and torus thickness β, $\beta \in [0,\ \beta_{\mathrm{cusp}}]$.

black curve (marked as the RP model) and the coloured curves (CT model) in Figure 2 describe the two extreme predictions of the QPO frequencies given by equation (6). The area between these curves covers the whole range of the QPO frequencies determined under the consideration of constant ℓ and any β. When we put

$$\mathcal{B} = 1 - 0.2(1 + a)\frac{\beta}{\beta_{\rm cusp}}, \tag{8}$$

we obtain a continuous set of curves that cover the area between the limiting curves given by $\beta = 0$ and $\beta = \beta_{\rm cusp}$.

5.2. Generalization for non-constant angular momentum distributions

The above consideration can be extended to a more general picture. In panel a) of Figure 3, we show the behaviour of the m $= -1$ radial frequency (the expected lower QPO frequency) for the particular case of $\ell = \ell_{\rm const}$. One should note the increasing monotonic behaviour of the curves. When β increases, the $m = 0$ mode frequency decreases and the $m = -1$ mode frequency increases getting closer to the Keplerian frequency. The trend of the $m = -1$ mode frequency rising with growing size of the oscillating structure persists for less simplified situations as well. In panels b) and c) of Figure 3, we show a sketch of a possible parametrization of linear angular momentum distributions and its projection in the plane of the expected QPO frequencies. Clearly, taking into account the presumption of a monotonic behaviour of the $\nu_{\rm r,\,m=-1}(\beta)$ function, any linear prescription for the angular momentum distribution, and all possible torus thicknesses from the $\beta \in [0, \beta_{\rm cusp}]$ range, the expected QPO frequencies should fall into the range denoted by the shaded area. An analogical consideration also applies to non-linear distributions.

Overal, the narrow range between the two extremal curves given by equation (11), which is indicated by the shaded area in Figure 3b, represents a rather general limit on the QPO frequencies valid for a variety of plausible angular momentum distributions.

6. NSs and their oblatness

Formula (6) is valid for Kerr spacetimes relevant for black hole sources. Within a reasonable accuracy, it can be applied to neutron star sources as well provided that the NS mass is high. Considering the restrictions on NS quadrupole moment $q \equiv QM_0/J^2$ given by present NS equations of state and consequent implications on the orbital frequencies (Urbanec et al. 2013; Urbancová et al. 2019), we can estimate the uncertainty in our formula valid for most of the available NS data. For high NS masses (typically $M \gtrsim 2M_\odot$) and spins corresponding up to $j \sim 0.3$, the uncertainty in NS mass induced within our formula by the quadrupole moment should not be higher than 3%. On the other hand, for low NS masses ($M \lesssim 1.4M_\odot$), this uncertainty may exceed the value of 10%.

A modification of the formula that would be sufficiently valid for such less compact NS sources can be obtained assuming the Hartle-Thorne geometry (Hartle 1967; Hartle & Thorne 1968), which applies to

slowly rotating neutron stars. One may expect that the impact of the quadrupole moment consideration on the relation between the QPO frequencies can be roughly included substituting the (rotational) $3j^2$ term in formula (6) by a simple dependency on q, $\mathcal{Q} = \mathcal{Q}(j,\ q)$. In the limit of $q = j^2$, the Hartle-Thorne formula should coincide with those expressed in the Kerr spacetime (e.g., Urbancová et al. 2019) and there in

$$\mathcal{Q}(j,\ q = j^2) = 3j^2\,. \tag{9}$$

In analogy to Section 4, we attempt to find the best evaluation of the $\mathcal{Q}$ term performing numerical calculations of the CT model frequencies in Hartle-Thorne spacetimes. We utilize the results of Kotrlová et al. (2020) and their extension to Hartle-Thorne spacetimes. We find that the particular term

$$\mathcal{Q} = \frac{1}{3}(8a^2 - 17q) \tag{10}$$

well matches the numerical calculations. This is illustrated in Figure 4. It is also clear from the Figure that for $\mathcal{B} = 1$ we obtain the frequencies predicted by the RP model. We note that for high QPO frequencies, corresponding to radii close to ISCO, when $\nu_{\rm L}$ approaches $\nu_{\rm U}$, there are discrepancies between the examined relations. These follow from the limitations of the Hartle-Thorne approach, which is accurate up to the second-order terms in q. The inaccuracies however grow only when the difference between the two QPO frequencies, $\Delta\nu = (\nu_{\rm U} - \nu_{\rm L})/\nu_{\rm L}$, is smaller than 10%.

7. Discussion and conclusions

For practical purposes, taking into account the ISCO frequency term for non-rotating stars, $\nu_{\rm L} = \nu_{\rm U} = \nu_0$, equation (6) can be further rewritten into a final compact form,

$$\nu_{\rm L} = \nu_{\rm U}\left[1 - \mathcal{B}\sqrt{1 + 8j\mathcal{V}_0 - 6\mathcal{V}_0^{2/3} - \mathcal{Q}\mathcal{V}_0^{4/3}}\right], \tag{11}$$

where

$$\mathcal{B} = 0.8 - 0.2j\,, \quad \mathcal{V}_0 \equiv \frac{\nu_{\rm U}/\nu_0}{6^{3/2} - j\nu_{\rm U}/\nu_0}\,, \quad \nu_0 = 2198\frac{\mathrm{M}_\odot}{M}\,, \quad \mathcal{Q} = \frac{1}{3}(8j^2 - 17q)\,. \tag{12}$$

For the above choice of $\mathcal{B}$, our relation with high accuracy provides frequencies predicted by the CT model. Choosing a constant $\mathcal{B}$, $\mathcal{B} = 1$, it (almost exactly) provides frequencies predicted by the RP model. We therefore conclude it is applicable for both models in the case of rotating oblateness NSs. For $\mathcal{Q} = 3j^2$, the relation reduces to the case of Kerr spacetimes describing rotating BHs.

7.1. Application to the atoll source 4U 1636-53 and other NSs

Following Török et al. (2016a), we apply relation 11 to the data of the atoll source 4U 1636-53. The main outputs of our investigation are illustrated in Figure 5. Figure 5a includes examples of the best fits given by the CT model. Fits given by the RP model are shown as well for the sake of comparison. Figure 5b

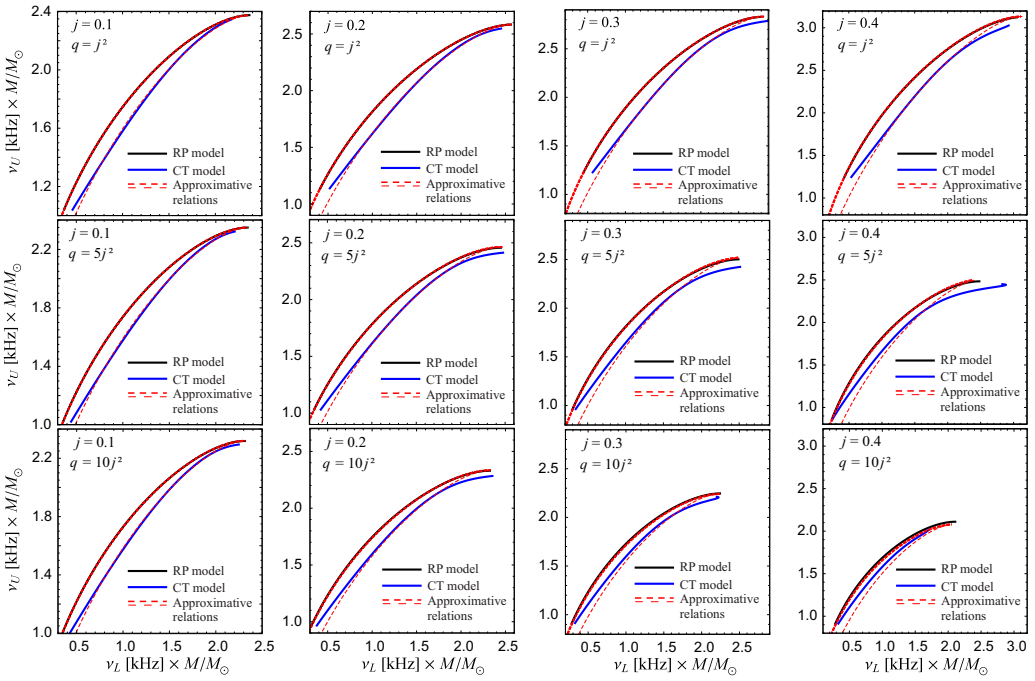

Fig. 4.— Comparison between the expected QPO frequencies (Hartle-Thorne spacetimes). The continuous curves denote frequencies calculated numerically for the CT and RP models. The dashed curves denote frequencies calculated using the approximative relation for the CT ($\mathcal{B} = 0.8 - 0.2j$) and RP ($\mathcal{B} = 1$) models.

depicts how the best fitting M depends on j and q/j^2. It shows that for very compact with $q/j^2 \sim 1$ the best fitting M increases with increasing j, reaching values of $M \in [2, 2.2]M_\odot$ for $j \in [0.2, 0.4]M_\odot$. This is in agreement with the investigation of Török et al. (2016a) limited to the case of Kerr spacetimes. On the other hand, for stars of high oblateness, $q/j^2 > 4$, the best fitting M decreases with increasing j. For stars of moderate oblateness, $q/j^2 \sim 3$, there is only a very weak dependency on j and the estimated mass is around $M = 1.75M_\odot$.

The same investigation was performed for the atoll source 4U 1735-44. The results are illustrated in Figure 5 showing a picture very similar to the 4U 1636-53 case. In analogy to the 4U 1636-53 case, we obtain fits better than those of the RP model and similar quadrupole moment dependence. For very compact stars, $q/j^2 \sim 1$, the best fitting M increases with increasing j, reaching values of $M \in [1.9, 2.2]M_\odot$ for $j \in [0.2, 0.4]M_\odot$, while for stars of high oblateness, $q/j^2 > 4$, the best fitting M decreases with increasing j. For stars of moderate oblateness, $q/j^2 \sim 3$, there is only a very weak dependency on j and the estimated mass is around $M = 1.9M_\odot$. In the same way, we investigated another four atoll sources with high amount

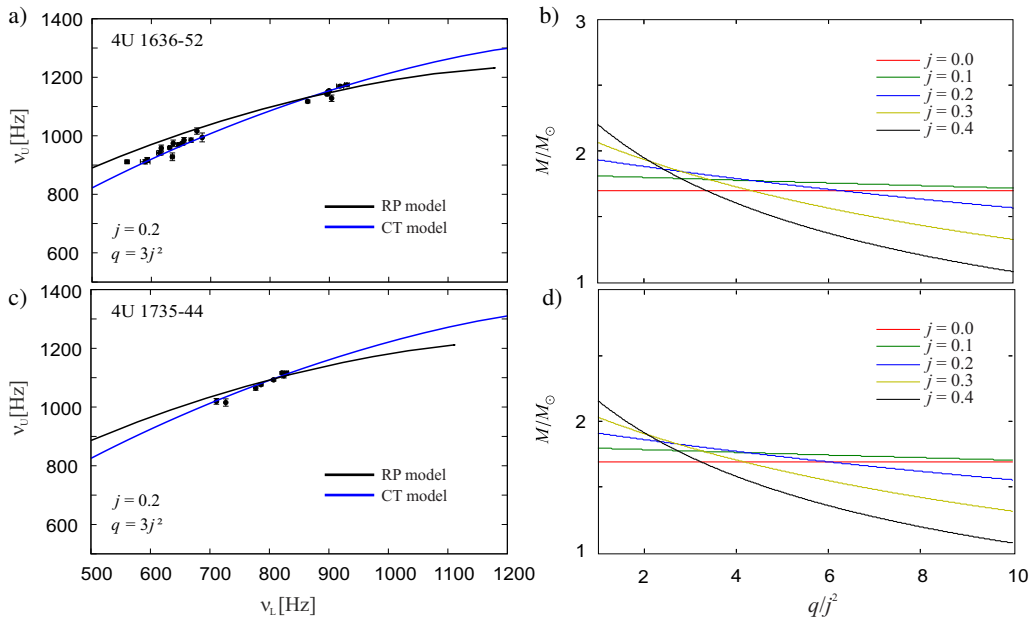

Fig. 5.— a) Best fits of the data of the 4U 1636-53 atoll source found for the RP and CT models and a particular choice of the NS spin and oblateness. For the other choices within the considered range of parameters, $j \in [0, 0.4]$ and $q/j^2 \in [1, 10]$, the resulting fits are similar. b) The best fitting mass corresponding to the CT model as it depends on q/j^2. c) The same as in panel a) but for the 4U 1735-44 atoll source. c) The same as in panel b) but for the 4U 1735-44 atoll source.

of available data (Barret et al. 2005b,c; Török et al. 2012). Overall, we find that for stars of moderate oblateness, $q/j^2 \sim 3$, the mass should be within the interval of $M \in [1.6, 1.9]M_\odot$.

These findings further confirm the expectation that the CT model not only fits the data better than the RP model, but is also compatible with realistic values of the NS mass.

7.2. Caveats

Our finding on the NS mass needs to be expanded to a larger set of sources, namely to a full confrontation of the parameters implied by the model and particular NS equations of state. It should be sufficient if this confrontation is carried out within the framework of the Hartle-Thorne spacetime for most sources and data except for very rapidly rotating sources and data with $\nu_U/\nu_L < 1.2$. It is questionable whether the present

relation can be applied to sources with very strong magnetic fields such as X-ray pulsars. The applicability of our result to rapidly rotating BHs has yet to be explored as well using the full numerical solution of the Papaloizou–Pringle equation.

Despite these facts, we conclude that the simple relation (11) can be useful for a brief estimation of mass and spin of accreting BHs and NSs.

Acknowledgments

We acknowledge the Czech Science Foundation (GAČR) grant No. 21-06825X. We wish to thank three internal grants of the Silesian University in Opava, SGS/12,13/2019. DL thanks the Student Grant Foundation of the Silesian University in Opava, Grant No. SGF/1/2020, which has been carried out within the EU OPSRE project entitled "Improving the quality of the internal grant scheme of the Silesian University in Opava", reg. number: CZ.02.2.69/0.0/0.0/18_054/0014696. KK was supported by the Czech grant LTC18058 and the COST Action PHAROS (CA 16124).

REFERENCES

Abramowicz, M., Jaroszynski, M., & Sikora, M. 1978, A&A, 63, 221

Abramowicz, M. A., Barret, D., Bursa, M., et al. 2005a, in RAGtime 6/7: Workshops on black holes and neutron stars, ed. S. Hledík & Z. Stuchlík, 1–9

Abramowicz, M. A., Barret, D., Bursa, M., et al. 2005b, Astronomische Nachrichten, 326, 864

Abramowicz, M. A., Blaes, O. M., Horák, J., Kluźniak, W., & Rebusco, P. 2006, CQG, 23, 1689

Abramowicz, M. A., Karas, V., Kluźniak, W., Lee, W. H., & Rebusco, P. 2003, PASJ, 55, 467

Abramowicz, M. A., & Kluźniak, W. 2001, A&A, 374, L19

Abramowicz, M. A., Lanza, A., Spiegel, E. A., & Szuszkiewicz, E. 1992, Nature, 356, 41

Alpar, M. A., & Shaham, J. 1985, Nature, 316, 239

Altamirano, D., Linares, M., Patruno, A., et al. 2010, MNRAS, 401, 223

Bachetti, M., Romanova, M. M., Kulkarni, A., Burderi, L., & di Salvo, T. 2010, MNRAS, 403, 1193

Barret, D., Boutelier, M., & Miller, M. C. 2008, MNRAS, 384, 1519

Barret, D., Kluźniak, W., Olive, J. F., Paltani, S., & Skinner, G. K. 2005a, MNRAS, 357, 1288

Barret, D., Olive, J.-F., & Miller, M. C. 2005b, MNRAS, 361, 855

—. 2005c, Astronomische Nachrichten, 326, 808

—. 2006, MNRAS, 370, 1140

Barret, D., & Vaughan, S. 2012, APJ, 746, 131

Belloni, T., Méndez, M., & Homan, J. 2007, MNRAS, 376, 1133

Belloni, T. M., & Altamirano, D. 2013, MNRAS, 432, 10

Belloni, T. M., Sanna, A., & Méndez, M. 2012, MNRAS, 426, 1701

Boirin, L., Barret, D., Olive, J. F., Bloser, P. F., & Grindlay, J. E. 2000, A&A, 361, 121

Boutloukos, S., van der Klis, M., Altamirano, D., Klein-Wolt, M., & Wijnands, R. 2008, in The Eleventh Marcel Grossmann Meeting On Recent Developments in Theoretical and Experimental General Relativity, Gravitation and Relativistic Field Theories, 1198–1200

Boutloukos, S., van der Klis, M., Altamirano, D., et al. 2006, APJ, 653, 1435

—. 2007, APJ, 664, 596

Bursa, M. 2005, in RAGtime 6/7: Workshops on black holes and neutron stars, ed. S. Hledík & Z. Stuchlík, 39–45

de Avellar, M. G. B., Porth, O., Younsi, Z., & Rezzolla, L. 2018, MNRAS, 474, 3967

Dönmez, O., Zanotti, O., & Rezzolla, L. 2011, MNRAS, 412, 1659

du Buisson, L., Motta, S., & Fender, R. 2019, MNRAS, 486, 4485

Fragile, P. C., Straub, O., & Blaes, O. 2016, MNRAS, 461, 1356

Germanà, C. 2017, PRD, 96, 103015

Hartle, J. B. 1967, APJ, 150, 1005

Hartle, J. B., & Thorne, K. S. 1968, APJ, 153, 807

Homan, J., Miller, J. M., Wijnands, R., et al. 2003, The Astronomer's Telegram, 162, 1

Homan, J., van der Klis, M., Jonker, P. G., et al. 2002, APJ, 568, 878

Huang, C.-Y., Ye, Y.-C., Wang, D.-X., & Li, Y. 2016, MNRAS, 457, 3859

Jonker, P. G., van der Klis, M., Homan, J., et al. 2002, MNRAS, 333, 665

Jonker, P. G., van der Klis, M., Wijnands, R., et al. 2000, APJ, 537, 374

Kato, S. 2001, PASJ, 53, 1

Kluźniak, W., & Abramowicz, M. A. 2001, Acta Phys. Polonica B, 32, 3605

Kluźniak, W., Abramowicz, M. A., Kato, S., Lee, W. H., & Stergioulas, N. 2004, APJ, 603, L89

Kotrlová, A., Šrámková, E., Török, G., et al. 2020, A&A, 643, arXiv:2008.12963

Kozlowski, M., Jaroszynski, M., & Abramowicz, M. A. 1978, A&A, 63, 209

Lamb, F. K., Shibazaki, N., Alpar, M. A., & Shaham, J. 1985, Nature, 317, 681

Lančová, D., Abarca, D., Kluźniak, W., et al. 2019, APJ, 884, L37

Le, T., Wood, K. S., Wolff, M. T., Becker, P. A., & Putney, J. 2016, APJ, 819, 112

Lewin, W., & van der Klis, M. 2010, Compact Stellar X-ray Sources

Lin, Y.-F., Boutelier, M., Barret, D., & Zhang, S.-N. 2011, APJ, 726, 74

Linares, M., van der Klis, M., Altamirano, D., & Markwardt, C. B. 2005, APJ, 634, 1250

Maselli, A., Pappas, G., Pani, P., et al. 2020, APJ, 899, 139

McClintock, J. E., & Remillard, R. A. 2006, Black hole binaries (Cambridge University Press), 157–213

Méndez, M. 2006, MNRAS, 371, 1925

Miller, M. C., Lamb, F. K., & Psaltis, D. 1998, APJ, 508, 791

Morsink, S. M., & Stella, L. 1999, APJ, 513, 827

Motta, S. E., Belloni, T. M., Stella, L., Muñoz-Darias, T., & Fender, R. 2014, MNRAS, 437, 2554

Mukhopadhyay, B. 2009, APJ, 694, 387

Paczynski, B., & Abramowicz, M. A. 1982, APJ, 253, 897

Parthasarathy, V., Kluźniak, W., & Čemeljić, M. 2017, MNRAS, 470, L34

Pétri, J. 2005, A&A, 439, L27

Psaltis, D., Belloni, T., & van der Klis, M. 1999a, ApJ, 520, 262

Psaltis, D., Wijnands, R., Homan, J., et al. 1999b, APJ, 520, 763

Remillard, R. A., Muno, M. P., McClintock, J. E., & Orosz, J. A. 2002, APJ, 580, 1030

Remillard, R. A., Muno, M. P., McClintock, J. E., & Orosz, J. A. 2003, in AAS/High Energy Astrophysics Division, Vol. 7, AAS/High Energy Astrophysics Division #7, 30.03

Rezzolla, L., Yoshida, S., & Zanotti, O. 2003, MNRAS, 344, 978

Smith, K. L., Tandon, C. R., & Wagoner, R. V. 2021, APJ, 906, 92

Stella, L., & Vietri, M. 1998, APJL, 492, L59

—. 1999, Phys. Rev. Lett., 82, 17

Stella, L., Vietri, M., & Morsink, S. M. 1999, ApJ, 524, L63

Straub, O., & Šrámková, E. 2009, CQG, 26, 055011

Strohmayer, T. E. 2001, APJL, 552, L49

Stuchlík, Z., & Kološ, M. 2014, PRD, 89, 065007

Stuchlík, Z., Kološ, M., Kovář, J., Slaný, P., & Tursunov, A. 2020, Universe, 6, 26

Titarchuk, L., & Wood, K. 2002, APJ, 577, L23

Török, G., Bakala, P., Šrámková, E., Stuchlík, Z., & Urbanec, M. 2010, APJ, 714, 748

Török, G., Bakala, P., Šrámková, E., et al. 2012, APJ, 760, 138

Török, G., Goluchová, K., Horák, J., et al. 2016a, MNRAS, 457, L19

Török, G., Goluchová, K., Šrámková, E., et al. 2018, MNRAS, 473, L136

Török, G., Goluchová, K., Šrámková, E., Urbanec, M., & Straub, O. 2019, MNRAS, 488, 3896

Török, G., Goluchová, K., Urbanec, M., et al. 2016b, APJ, 833, 273

Urbancová, G., Urbanec, M., Török, G., et al. 2019, APJ, 877, 66

Urbanec, M., Miller, J. C., & Stuchlík, Z. 2013, MNRAS, 433, 1903

Čadež, A., Calvani, M., & Kostić, U. 2008, A&A, 487, 527

van der Klis, M. 2006, Rapid X-ray Variability (Cambridge University Press), 39–112

van der Klis, M., Wijnands, R. A. D., Horne, K., & Chen, W. 1997, APJL, 481, L97

Varniere, P., & Rodriguez, J. 2018, APJ, 865, 113

Wagoner, R. V., Silbergleit, A. S., & Ortega-Rodríguez, M. 2001, APJ, 559, L25

Wang, D.-H., & Zhang, C.-M. 2020, MNRAS, 497, 2893

Wang, D.-X., Gan, Z.-M., Huang, C.-Y., & Li, Y. 2008, MNRAS, 391, 1332

Zhang, C. 2004, A&A, 423, 401

Zhang, C. M., Yin, H. X., Zhao, Y. H., Zhang, F., & Song, L. M. 2006, MNRAS, 366, 1373